

# Global Methane Budget 2000-2020

Marielle Saunio<sup>1</sup>, Adrien Martinez<sup>1</sup>, Benjamin Poulter<sup>2</sup>, Zhen Zhang<sup>3,4</sup>, Peter A. Raymond<sup>5</sup>, Pierre Regnier<sup>6</sup>, Josep G. Canadell<sup>7</sup>, Robert B. Jackson<sup>8</sup>, Prabir K. Patra<sup>9,10</sup>, Philippe Bousquet<sup>1</sup>, Philippe Ciais<sup>1</sup>, Edward J. Dlugokencky<sup>11</sup>, Xin Lan<sup>11,12</sup>, George H. Allen<sup>13</sup>, David Bastviken<sup>14</sup>, David J. Beerling<sup>15</sup>, Dmitry A. Belikov<sup>16</sup>, Donald R. Blake<sup>17</sup>, Simona Castaldi<sup>18</sup>, Monica Crippa<sup>19</sup>, Bridget R. Deemer<sup>20</sup>, Fraser Dennison<sup>21</sup>, Giuseppe Etiope<sup>22,23</sup>, Nicola Gedney<sup>24</sup>, Lena Höglund-Isaksson<sup>25</sup>, Meredith A. Holgerson<sup>26</sup>, Peter O. Hopcroft<sup>27</sup>, Gustaf Hugelius<sup>28</sup>, Akihiko Ito<sup>29</sup>, Atul K. Jain<sup>30</sup>, Rajesh Janardanan<sup>31</sup>, Matthew S. Johnson<sup>32</sup>, Thomas Kleinen<sup>33</sup>, Paul B. Krummel<sup>21</sup>, Ronny Lauerwald<sup>34</sup>, Tingting Li<sup>35</sup>, Xiangyu Liu<sup>36</sup>, Kyle C. McDonald<sup>37</sup>, Joe R. Melton<sup>38</sup>, Jens Mühle<sup>39</sup>, Jurek Müller<sup>40</sup>, Fabiola Murguía-Flores<sup>41</sup>, Yosuke Niwa<sup>31,42</sup>, Sergio Noce<sup>43</sup>, Shufen Pan<sup>44</sup>, Robert J. Parker<sup>45</sup>, Changhui Peng<sup>46,47</sup>, Michel Ramonet<sup>1</sup>, William J. Riley<sup>48</sup>, Gerard Rocher-Ros<sup>49</sup>, Judith A. Rosentreter<sup>50</sup>, Motoki Sasakawa<sup>31</sup>, Arjo Segers<sup>51</sup>, Steven J. Smith<sup>52,53</sup>, Emily H. Stanley<sup>54</sup>, Joël Thanwerdas<sup>55,\*</sup>, Hanqin Tian<sup>56</sup>, Aki Tsuruta<sup>57</sup>, Francesco N. Tubiello<sup>58</sup>, Thomas S. Weber<sup>59</sup>, Guido R. van der Werf<sup>60</sup>, Douglas E. J. Worthy<sup>61</sup>, Yi Xi<sup>1</sup>, Yukio Yoshida<sup>31</sup>, Wenxin Zhang<sup>62</sup>, Bo Zheng<sup>63,64</sup>, Qing Zhu<sup>48</sup>, Qian Zhu<sup>65</sup>, and Qianlai Zhuang<sup>36</sup>

<sup>1</sup>Laboratoire des Sciences du Climat et de l'Environnement, LSCE-IPSL (CEA-CNRS-UVSQ), Université Paris-Saclay 91191 Gif-sur-Yvette, France

<sup>2</sup>NASA Goddard Space Flight Center, Biospheric Science Laboratory, Greenbelt, MD 20771, USA

<sup>3</sup>National Tibetan Plateau Data Center (TPDC), State Key Laboratory of Tibetan Plateau Earth System, Environment and Resource (TPESER), Institute of Tibetan Plateau Research, Chinese Academy of Sciences, Beijing, 100101, China

<sup>4</sup>Earth System Science Interdisciplinary Center, University of Maryland, College Park, MD 20740, USA

<sup>5</sup>Yale School of the Environment, Yale University, New Haven, CT 06511, USA

<sup>6</sup>Department Geoscience, Environment & Society (BGEOSYS), Université Libre de Bruxelles, 1050 Bruxelles, Belgium

<sup>7</sup>Global Carbon Project, CSIRO Environment, Canberra, ACT 2601, Australia

<sup>8</sup>Department of Earth System Science, Woods Institute for the Environment, and Precourt Institute for Energy, Stanford University, Stanford, CA 94305-2210, USA

<sup>9</sup>Research Institute for Global Change, JAMSTEC, 3173-25 Showa-machi, Kanazawa, Yokohama, 236-0001, Japan

<sup>10</sup>Research Institute for Humanity and Nature, Kyoto 6038047, Japan

<sup>11</sup>NOAA Global Monitoring Laboratory, 325 Broadway, Boulder, CO 80305, USA

<sup>12</sup>Cooperative Institute for Research in Environmental Sciences, University of Colorado Boulder, CO 80303, USA

<sup>13</sup>Department of Geosciences, Virginia Polytechnic Institute and State University, Blacksburg, VA, USA

<sup>14</sup>Department of Thematic Studies – Environmental Change, Linköping University, 581 83 Linköping, Sweden

<sup>15</sup>School of Biosciences, University of Sheffield, UK

<sup>16</sup>Center for Environmental Remote Sensing, Chiba University, Chiba, 263-8522, Japan

<sup>17</sup>Department of Chemistry, University of California Irvine, 570 Rowland Hall, Irvine, CA 92697, USA

<sup>18</sup>Dipartimento di Scienze Ambientali, Biologiche e Farmaceutiche, Università degli Studi della Campania Luigi

42 Vanvitelli, via Vivaldi 43, 81100 Caserta, Italy  
 43 <sup>19</sup>European Commission, Joint Research Centre (JRC), Ispra, Italy  
 44  
 45 <sup>20</sup>U.S. Geological Survey, Southwest Biological Science Center, Flagstaff, AZ, USA  
 46 <sup>21</sup>CSIRO Environment, Aspendale, Victoria 3195, Australia  
 47 <sup>22</sup>Istituto Nazionale di Geofisica e Vulcanologia, Sezione Roma 2, via V. Murata 605 00143 Rome, Italy  
 48 <sup>23</sup>Faculty of Environmental Science and Engineering, Babes Bolyai University, Cluj-Napoca, Romania  
 49 <sup>24</sup>Met Office Hadley Centre, Joint Centre for Hydrometeorological Research, Maclean Building, Wallingford  
 50 OX10 8BB, UK  
 51 <sup>25</sup>Pollution Management Group (PM), International Institute for Applied Systems Analysis (IIASA), 2361  
 52 Laxenburg, Austria  
 53 <sup>26</sup>Department of Ecology & Evolutionary Biology, Cornell University, Ithaca, NY, USA  
 54 <sup>27</sup>School of Geography, Earth & Environmental Sciences, University of Birmingham, UK  
 55 <sup>28</sup>Department of Physical Geography and Bolin Centre for Climate Research, Stockholm University, 106 91  
 56 Stockholm, Sweden  
 57 <sup>29</sup>Graduate School of Agricultural and Life Sciences, The University of Tokyo, Tokyo, Japan  
 58 <sup>30</sup>Department of Atmospheric Sciences, University of Illinois, Urbana, IL 61821, USA  
 59 <sup>31</sup>Earth System Division, National Institute for Environmental Studies (NIES), Onogawa 16-2, Tsukuba, Ibaraki  
 60 305-8506, Japan  
 61 <sup>32</sup>Earth Science Division, NASA Ames Research Center, Moffett Field, CA USA.  
 62 <sup>33</sup>Max Planck Institute for Meteorology, Bundesstraße 53, 20146 Hamburg, Germany  
 63 <sup>34</sup>Université Paris-Saclay, INRAE, AgroParisTech, UMR EcoSys, Palaiseau, France  
 64 <sup>35</sup>LAPC, Institute of Atmospheric Physics, Chinese Academy of Sciences, Beijing, 100029, China  
 65 <sup>36</sup>Department of Earth, Atmospheric, and Planetary Sciences, Purdue University, West Lafayette, IN, USA  
 66 <sup>37</sup>Department of Earth and Atmospheric Sciences, City College of New York, City University of New York, NY,  
 67 USA  
 68 <sup>38</sup>Climate Research Division, Environment and Climate Change Canada, Victoria, BC, V8W 2Y2, Canada  
 69 <sup>39</sup>Scripps Institution of Oceanography, University of California San Diego, La Jolla, CA, 92037, USA  
 70 <sup>40</sup>Climate and Environmental Physics, Physics Institute and Oeschger Centre for Climate Change Research,  
 71 University of Bern, Sidlerstr. 5, 3012 Bern, Switzerland  
 72 <sup>41</sup>Instituto de Investigaciones en Ecología y Sustentabilidad, Universidad Nacional Autónoma de México,  
 73 Morelia, Mexico  
 74 <sup>42</sup>Department of Climate and Geochemistry Research, Meteorological Research Institute (MRI), Nagamine 1-1, Tsukuba,  
 75 Ibaraki 305-0052, Japan  
 76 <sup>43</sup>CMCC Foundation - Euro-Mediterranean Center on Climate Change, Italy  
 77 <sup>44</sup>Department of Engineering and Environmental Studies Program, Boston College, Chestnut Hill, MA 02467,  
 78 USA  
 79 <sup>45</sup>National Centre for Earth Observation, School of Physics and Astronomy, University of Leicester, Leicester,  
 80 LE1 7RH, UK  
 81 <sup>46</sup>Department of Biology Sciences, Institute of Environment Science, University of Quebec at Montreal,  
 82 Montreal, QC H3C 3P8, Canada  
 83 <sup>47</sup>School of Geographic Sciences, Hunan Normal University, Changsha 410081, China  
 84 <sup>48</sup>Climate and Ecosystem Sciences Division, Lawrence Berkeley National Lab, 1 Cyclotron Road, Berkeley, CA  
 85 94720, US  
 86 <sup>49</sup>Department of Forest Ecology and Management, Swedish University of Agricultural Sciences, 90183 Umeå,  
 87 Sweden  
 88 <sup>50</sup>Faculty of Science and Engineering, Southern Cross University, Lismore, NSW 2480, Australia  
 89 <sup>51</sup>TNO, dep. of Climate Air & Sustainability, P.O. Box 80015, NL-3508-TA, Utrecht, The Netherlands  
 90 <sup>52</sup>Joint Global Change Research Institute, Pacific Northwest National Lab, College Park, MD, USA

<sup>53</sup>Center for Global Sustainability, University of Maryland, College Park, MD, USA  
<sup>54</sup>Center for Limnology, University of Wisconsin-Madison, Madison, WI, USA  
<sup>55</sup>Empa, Swiss Federal Laboratories for Materials Science and Technology, Dübendorf, Switzerland  
<sup>56</sup>Center for Earth System Science and Global Sustainability, Schiller Institute for Integrated Science and  
Society, Department of Earth and Environmental Sciences, Boston College, Chestnut Hill, MA 02467, USA  
<sup>57</sup>Finnish Meteorological Institute, P.O. Box 503, FI-00101, Helsinki, Finland  
<sup>58</sup>Statistics Division, Food and Agriculture Organization of the United Nations (FAO), Viale delle  
Terme di Caracalla, Rome 00153, Italy  
<sup>59</sup>Department of Earth and Environmental Sciences, University of Rochester, Rochester, NY 14627,  
USA  
<sup>60</sup>Meteorology and Air Quality Group, Wageningen University and Research, Wageningen, the Netherlands  
<sup>61</sup>Environment and Climate Change Canada, 4905, Dufferin Street, Toronto, Canada  
<sup>62</sup>Department of Physical Geography and Ecosystem Science, Lund University, Sölvegatan 12, 223 62, Lund, Sweden  
<sup>63</sup>Institute of Environment and Ecology, Tsinghua Shenzhen International Graduate School, Tsinghua University,  
Shenzhen 518055, China  
<sup>64</sup>State Environmental Protection Key Laboratory of Sources and Control of Air Pollution Complex, Beijing 100084,  
China  
<sup>65</sup>College of Geography and Remote Sensing, Hohai University, Nanjing, 210098, China  
\*formerly at LSCE <sup>1</sup>  
*Correspondence to:* Marielle Saunois (marielle.saunois@lsce.ipsl.fr)

**Abstract.** Understanding and quantifying the global methane (CH<sub>4</sub>) budget is important for assessing realistic pathways to  
mitigate climate change. CH<sub>4</sub> is the second most important human-influenced greenhouse gas in terms of climate forcing  
after carbon dioxide (CO<sub>2</sub>) and both emissions and atmospheric concentrations of CH<sub>4</sub> continue to increase since 2007 after  
a temporary pause. The relative importance of CH<sub>4</sub> emissions compared to those of CO<sub>2</sub> for temperature change is related  
to its shorter atmospheric lifetime, stronger radiative effect, and acceleration in atmospheric growth rate over the past decade,  
the causes of which are still debated. Two major challenges in quantifying the factors responsible for the observed  
atmospheric growth rate arise from diverse, geographically overlapping CH<sub>4</sub> sources and from the uncertain magnitude and  
temporal change in the destruction of CH<sub>4</sub> by short-lived and highly variable hydroxyl radicals (OH). To address these  
challenges, we have established a consortium of multi-disciplinary scientists under the umbrella of the Global Carbon Project  
to improve, synthesise and update the global CH<sub>4</sub> budget regularly and to stimulate new research on the methane cycle.  
Following Saunois et al. (2016, 2020), we present here the third version of the living review paper dedicated to the decadal  
CH<sub>4</sub> budget, integrating results of top-down CH<sub>4</sub> emission estimates (based on in-situ and greenhouse gas observing satellite  
(GOSAT) atmospheric observations and an ensemble of atmospheric inverse-model results) and bottom-up estimates (based  
on process-based models for estimating land-surface emissions and atmospheric chemistry, inventories of anthropogenic  
emissions, and data-driven extrapolations). We present a budget for the most recent 2010-2019 calendar decade (the latest  
period for which full datasets are available), for the previous decade of 2000-2009 and for the year 2020.

129 The revision of the bottom-up budget in this 2024 edition benefits from important progress in estimating inland freshwater  
 130 emissions, with better accounting of emissions from lakes and ponds, reservoirs, and streams and rivers. This budget also  
 131 reduces double accounting across freshwater and wetland emissions and, for the first time, includes an estimate of the  
 132 potential double accounting that may exist (average of 23 Tg CH<sub>4</sub> yr<sup>-1</sup>). Bottom-up approaches show that the combined  
 133 wetland and inland freshwater emissions average 248 [159-369] Tg CH<sub>4</sub> yr<sup>-1</sup> for the 2010-2019 decade. Natural fluxes are  
 134 perturbed by human activities through climate, eutrophication, and land use. In this budget, we also estimate, for the first  
 135 time, this anthropogenic component contributing to wetland and inland freshwater emissions. Newly available gridded  
 136 products also allowed us to derive an almost complete latitudinal and regional budget based on bottom-up approaches.  
 137 For the 2010-2019 decade, global CH<sub>4</sub> emissions are estimated by atmospheric inversions (top-down) to be 575 Tg CH<sub>4</sub> yr<sup>-1</sup>  
 138 <sup>1</sup> (range 553-586, corresponding to the minimum and maximum estimates of the model ensemble). Of this amount, 369 Tg  
 139 CH<sub>4</sub> yr<sup>-1</sup> or ~65% are attributed to direct anthropogenic sources in the fossil, agriculture and waste and anthropogenic  
 140 biomass burning (range 350-391 Tg CH<sub>4</sub> yr<sup>-1</sup> or 63-68%). For the 2000-2009 period, the atmospheric inversions give a  
 141 slightly lower total emission than for 2010-2019, by 32 Tg CH<sub>4</sub> yr<sup>-1</sup> (range 9-40). The 2020 emission rate is the highest of  
 142 the period and reaches 608 Tg CH<sub>4</sub> yr<sup>-1</sup> (range 581-627), which is 12% higher than the average emissions in the 2000s. Since  
 143 2012, global direct anthropogenic CH<sub>4</sub> emission trends have been tracking scenarios that assume no or minimal climate  
 144 mitigation policies proposed by the Intergovernmental Panel on Climate Change (shared socio-economic pathways SSP5  
 145 and SSP3). Bottom-up methods suggest 16% (94 Tg CH<sub>4</sub> yr<sup>-1</sup>) larger global emissions (669 Tg CH<sub>4</sub> yr<sup>-1</sup>, range 512-849)  
 146 than top-down inversion methods for the 2010-2019 period. The discrepancy between the bottom-up and the top-down  
 147 budgets has been greatly reduced compared to the previous differences (167 and 156 Tg CH<sub>4</sub> yr<sup>-1</sup> in Saunio et al. (2016,  
 148 2020), respectively), and for the first time uncertainty in bottom-up and top-down budgets overlap. Although differences  
 149 have been reduced between inversions and bottom-up, the most important source of uncertainty in the global CH<sub>4</sub> budget is  
 150 still attributable to natural emissions, especially those from wetlands and inland freshwaters.  
 151 The tropospheric loss of methane, as the main contributor to methane lifetime, has been estimated at 563 [510-  
 152 663] Tg CH<sub>4</sub> yr<sup>-1</sup> based on chemistry climate models. These values are slightly larger than for 2000-2009 due to the impact  
 153 of the rise in atmospheric methane, and remaining large uncertainty (~25%). The total sink of CH<sub>4</sub> is estimated at 633  
 154 [507-796] Tg CH<sub>4</sub> yr<sup>-1</sup> by the bottom-up approaches and at 554 [550-567] Tg CH<sub>4</sub> yr<sup>-1</sup> by top-down approaches. Though,  
 155 most of the top-down models use the same OH distribution, which introduces less uncertainty to the global budget than is  
 156 likely justified.  
 157 For 2010-2019, agriculture and waste contributed an estimated 228 [213-242] Tg CH<sub>4</sub> yr<sup>-1</sup> in the top-down budget and 211  
 158 [195-231] Tg CH<sub>4</sub> yr<sup>-1</sup> in the bottom-up budget. Fossil fuel emissions contributed 115 [100-124] Tg CH<sub>4</sub> yr<sup>-1</sup> in the top-  
 159 down budget and 120 [117-125] Tg CH<sub>4</sub> yr<sup>-1</sup> in the bottom-up budget. Biomass and biofuel burning contributed 27 [26-  
 160 27] Tg CH<sub>4</sub> yr<sup>-1</sup> in the top-down budget and 28 [21-39] Tg CH<sub>4</sub> yr<sup>-1</sup> in the bottom-up budget.

We identify five major priorities for improving the CH<sub>4</sub> budget: i) producing a global, high-resolution map of water-saturated soils and inundated areas emitting CH<sub>4</sub> based on a robust classification of different types of emitting ecosystems; ii) further development of process-based models for inland-water emissions; iii) intensification of CH<sub>4</sub> observations at local (e.g., FLUXNET-CH<sub>4</sub> measurements, urban-scale monitoring, satellite imagery with pointing capabilities) to regional scales (surface networks and global remote sensing measurements from satellites) to constrain both bottom-up models and atmospheric inversions; iv) improvements of transport models and the representation of photochemical sinks in top-down inversions, and v) integration of 3D variational inversion systems using isotopic and/or co-emitted species such as ethane as well as information in the bottom-up inventories on anthropogenic super-emitters detected by remote sensing (mainly oil and gas sector but also coal, agriculture and landfills) to improve source partitioning.

The data presented here can be downloaded from <https://doi.org/10.18160/GKQ9-2RHT> (Martinez et al., 2024).

## 1 Introduction

The average surface dry air mole fraction of atmospheric methane (CH<sub>4</sub>) reached 1912 ppb in 2022 (Fig. 1; Lan et al., 2024), 2.6 times greater than its estimated pre-industrial value in 1750. This increase is attributable in large part to increased anthropogenic emissions arising primarily from agriculture (e.g., livestock production, rice cultivation, biomass burning), fossil fuel production and use, waste disposal, and alterations to natural CH<sub>4</sub> fluxes due to increased atmospheric CO<sub>2</sub> concentrations, land use (Woodward et al., 2010, Fluet-Chouinard et al., 2023) and climate change (Ciais et al., 2013; Canadell et al., 2021). An equal mass of CH<sub>4</sub> emissions have a stronger impact on climate than carbon dioxide (CO<sub>2</sub>), which is reflected by its global warming potential (GWP) relative to CO<sub>2</sub> on a given time horizon. For a 100-yr time horizon the GWP of CH<sub>4</sub> emitted by fossil sources is 29.8 (GWP of CH<sub>4</sub> emitted by microbial sources is 27), whereas the values reach 82.5 over a 20-year horizon for CH<sub>4</sub> emitted by fossil sources and 79.7 for CH<sub>4</sub> emitted by microbial sources (Forster et al., 2021). Although global anthropogenic emissions of CH<sub>4</sub> are estimated at around 359 Tg CH<sub>4</sub> yr<sup>-1</sup> (Saunio et al., 2020), representing around 2.5% of the global CO<sub>2</sub> anthropogenic emissions when converted to units of carbon mass flux for the recent decade, the emissions-based effective radiative forcing of CH<sub>4</sub> concentrations has contributed ~31% (1.19 W m<sup>-2</sup>) to the additional radiative forcing from anthropogenic emissions of greenhouse gases and their precursors (3.84 W m<sup>-2</sup>) over the industrial era (1750-2019) (Forster et al., 2021). Changes in other chemical compounds such as nitrogen oxides (NO<sub>x</sub>) or carbon monoxide (CO) also influence atmospheric CH<sub>4</sub> through changes to its atmospheric lifetime. Emissions of CH<sub>4</sub> contribute to the production of ozone, stratospheric water vapour, and CO<sub>2</sub>, and most importantly affect its own lifetime (Myhre et al., 2013; Shindell et al., 2012). CH<sub>4</sub> has a short lifetime in the atmosphere (about 9 years for the year 2010, Prather et al., 2012; Szopa et al., 2021). Hence a stabilisation or reduction of CH<sub>4</sub> emissions leads to the stabilisation or reduction of its atmospheric concentration (assuming no change in the chemical oxidants), and therefore its radiative forcing, in only a few decades. While reducing CO<sub>2</sub> emissions is necessary to stabilise long-term warming, reducing CH<sub>4</sub> emissions

192 is recognized as an effective option to limit climate warming in the near-term (Shindell et al., 2012; Jackson et al., 2020;  
193 Ocko et al., 2021; UNEP, 2021), because of its shorter lifetime compared to CO<sub>2</sub>.

194 The momentum around the potential of CH<sub>4</sub> to limit near-term warming has led to the launch of the Global Methane  
195 Pledge at the November 2021 Conference of the Parties (COP 26). Signed by 158 countries (update on October 2024), this  
196 collective effort aims at reducing global CH<sub>4</sub> anthropogenic emissions at least 30 percent from 2020 levels by 2030 (Global  
197 Methane Pledge, 2023). Given that global baseline CH<sub>4</sub> emissions are expected to grow through 2030 (by an additional 20-  
198 50 Million tons (Mt) of CH<sub>4</sub>, UNEP 2022), the CH<sub>4</sub> emission reductions currently needed to reach the Global Methane  
199 Pledge objective (UNEP, 2022) correspond to 36% of the projected baseline emissions in 2030 (ie. if no further emission  
200 reductions were implemented). This implies that large reductions of CH<sub>4</sub> emissions are needed to meet the Global Methane  
201 Pledge that is consistent also with the 1.5-2°C target of the Paris Agreement (UNEP, 2022). Moreover, because CH<sub>4</sub> is a  
202 precursor of important air pollutants such as ozone, CH<sub>4</sub> emissions reductions are required by two international conventions:  
203 the United Nations Framework Convention on Climate Change (UNFCCC) and the Convention on Long Range Transport  
204 of Air Pollution (CLRTAP), making this global CH<sub>4</sub> budget assessment all the more critical.

205 Changes in the magnitude and temporal variation (annual to interannual) of CH<sub>4</sub> sources and sinks over the past  
206 decades are characterised by large uncertainties (e.g., Kirschke et al., 2013; Sauniois et al., 2017; Turner et al., 2019). Also,  
207 the decadal budget suggests relative uncertainties (hereafter reported as min-max ranges) of 20-35% for inventories of  
208 anthropogenic emissions in specific sectors (e.g., agriculture, waste, fossil fuels (Tibrewal et al., 2024)), 50% for biomass  
209 burning and natural wetland emissions, and up to 100% for other natural sources (e.g., inland waters, geological sources).  
210 The uncertainty in the chemical loss of CH<sub>4</sub> by OH, the predominant sink of atmospheric CH<sub>4</sub>, has been estimated using  
211 Prather et al. (2012) and Rigby et al. (2017). The former study estimated this uncertainty at ~10% from the uncertainty in  
212 the reaction rate between CH<sub>4</sub> and OH, and the latter study was based on methyl-chloroform measurements. Bottom-up  
213 approaches (chemistry transport models) estimate the uncertainty of the chemical loss by OH at around 15-20% (Sauniois et  
214 al., 2016, 2020). This uncertainty on the OH induced loss translates, in the top-down methods, into the minimum relative  
215 uncertainty associated with global CH<sub>4</sub> emissions, as other CH<sub>4</sub> sinks (atomic oxygen and chlorine oxidations, soil uptake)  
216 are much smaller and the atmospheric growth rate is well-defined (Dlugokencky et al., 2009). Globally, the contribution of  
217 natural CH<sub>4</sub> emissions to total emissions can be quantified by combining lifetime estimates with reconstructed pre-industrial  
218 atmospheric CH<sub>4</sub> concentrations from ice cores (assuming natural emissions have not been perturbed during the  
219 anthropocene) (e.g., Ehhalt et al., 2001). Regionally or nationally, uncertainties in emissions may reach 40-60% (e.g., for  
220 South America, Africa, China, and India; see Sauniois et al., 2016). Another difficulty of the CH<sub>4</sub> budget lies in the necessity  
221 to also match the isotopic signal and in particular reflect the decreasing methane isotopic signal <sup>13</sup>C (Nisbet et al., 2016;  
222 2019). The previous budgets were tested against the isotopic observations (Sauniois et al., 2017) and follow an exhaustive  
223 assessment (Zhang et al., 2021b). To date only a couple of atmospheric inverse systems are able to assimilate both CH<sub>4</sub>  
224 mixing ratios and stable isotopic signal to retrieve fluxes at the global scale (Thanwerdas et al., 2024; Basu et al., 2022), but

these systems still need improvements in terms of configuration set-up and computing time resources, in addition to characterisation of source signatures and chemical kinetic effect (Chandra et al., 2024). We hope to be able to report isotopic constrained budgets in the coming years, or at least test the budget against the isotopic balance.

To monitor emission reductions, for example to help conduct the Paris Agreement's stocktake, sustained and long-term monitoring of anthropogenic emissions per sector is needed in particular for hotspots of emissions that may be missed in inventories (Bergamaschi et al., 2018a; Pacala, 2010; Lauvaux et al., 2022). At the same time, reducing uncertainties in all individual CH<sub>4</sub> sources, and thus in the overall CH<sub>4</sub> budget remains challenging for at least four reasons. First, CH<sub>4</sub> is emitted by multiple processes, including natural and anthropogenic sources, point and diffuse sources, and sources associated with at least three different production origins (i.e., microbial, thermogenic, and pyrogenic). These multiple sources and processes require the integration of data from diverse scientific communities and across multiple temporal and spatial scales. The production of accurate bottom-up estimates is complicated by the fact that anthropogenic emissions result from leakage from fossil fuel production with large differences between countries depending on technologies and practices, the fact that many large leak events are sporadic, and the location of many emissions hotspots is not well known, and from uncertain emission factors used to summarise complex microbial processes in the agriculture and waste sectors. For the latter, examples include difficulties in upscaling methane emissions from livestock without considering the variety of animal weight, diet and environment, and difficulties in assessing emissions from landfills depending on waste type and waste management technology. Second, atmospheric CH<sub>4</sub> is removed mainly by chemical reactions in the atmosphere involving OH and other radicals that have very short lifetimes (typically ~1s). Due to the short lifetime of OH, the spatial and temporal distributions of OH are highly variable. While OH can be measured locally, calculating global CH<sub>4</sub> loss through OH measurements requires high-resolution global OH measurements (typically half an hour to integrate cloud cover, and 1 km spatially to consider OH high reactivity and heterogeneity) which is impossible from direct OH observations. As a result, OH can only be calculated through large scale atmospheric chemistry modelling. Those simulated OH concentrations from transport-chemistry models prescribed with emissions of precursor species affecting OH still show uncertain spatio-temporal distribution from regional to global scales (Zhao et al., 2019). Third, only the net CH<sub>4</sub> budget (sources minus sinks) is well constrained by precise observations of atmospheric growth rates (Dlugokencky et al., 2009), leaving the sum of sources and the sum of sinks uncertain. One distinctive feature of CH<sub>4</sub> sources compared to CO<sub>2</sub> fluxes is that the oceanic contribution to the global CH<sub>4</sub> budget is small (~1-3%), making CH<sub>4</sub> source estimation predominantly a terrestrial endeavour (USEPA, 2010b). Finally, we lack comprehensive observations to constrain 1) the areal extent of different types of wetlands and inland freshwater (Kleinen et al., 2012, 2020, 2021, 2023; Stocker et al., 2014; Zhang et al., 2021), 2) models of wetland and inland freshwater emission rates (Melton et al., 2013; Poulter et al., 2017; Wania et al., 2013; Bastviken et al., 2011; Wik et al., 2016a; Rosentreter et al., 2021; Bansal et al., 2023; Lauerwald et al., 2023a; Stanley et al. 2023), 3) inventories of anthropogenic emissions (Höglund-Isaksson et al., 2020; Crippa et al., 2023; USEPA, 2019), and 4) atmospheric inversions, which aim to estimate CH<sub>4</sub> emissions from global to regional scales (Houweling et al., 2017; Jacob et al., 2022).

258 The global CH<sub>4</sub> budget inferred from atmospheric observations by atmospheric inversions relies on regional  
259 constraints from atmospheric sampling networks, which are relatively dense for northern mid-latitudes, with various high-  
260 precision and high-accuracy surface stations, but are sparser at tropical latitudes and in the Southern Hemisphere  
261 (Dlugokencky et al., 2011). Recently, the density of atmospheric observations has increased in the tropics due to satellite-  
262 based platforms that provide column-average CH<sub>4</sub> mixing ratios. Despite continuous improvements in the precision and  
263 accuracy of space-based measurements (e.g., Buchwitz et al., 2016), systematic errors greater than several ppb on total  
264 column observations can still limit the usage of such data to constrain surface emissions (e.g., Jacob et al., 2022). The  
265 development of robust bias corrections on existing data can help overcome this issue (e.g., Inoue et al., 2016, Lorente et al.,  
266 2023; Balasu et al., 2023) and satellite data are now widely used in atmospheric inversions where they provide more global  
267 information on the distribution of fluxes and highly complement the surface networks (e.g., Lu et al., 2021).

268 In this context, the Global Carbon Project (GCP) seeks to develop a complete picture of the carbon cycle by  
269 establishing common, consistent scientific knowledge to support policy development and actions to mitigate greenhouse gas  
270 emissions to the atmosphere ([www.globalcarbonproject.org](http://www.globalcarbonproject.org)). The objective of this paper is to analyse and synthesise the  
271 current knowledge of the global CH<sub>4</sub> budget, by gathering results of observations and models to better understand and  
272 quantify the main robust features of this budget, its remaining uncertainties, and to make recommendations for improvement.  
273 We combine results from a large ensemble of bottom-up approaches (e.g., process-based models for natural wetlands, data-  
274 driven approaches for other natural sources, inventories of anthropogenic emissions and biomass burning, and atmospheric  
275 chemistry models), and top-down approaches (including CH<sub>4</sub> atmospheric observing networks, atmospheric inversions  
276 inferring emissions and sinks from the assimilation of atmospheric observations into models of atmospheric transport and  
277 chemistry). The focus of this work is to update the previous assessment made for the period 2000-2017 (Saunois et al., 2020)  
278 to the more recent 2000-2020 period. More in-depth analyses of trends and year-to-year changes are left to future  
279 publications. Our current paper is a living review, published at about four-year intervals, to provide an update and new  
280 synthesis of available observational, statistical, and model data for the overall CH<sub>4</sub> budget and its individual components.

281 Kirschke et al. (2013) was the first CH<sub>4</sub> budget synthesis followed by Saunois et al. (2016) and Saunois et al.  
282 (2020), with companion papers by Stavert et al. (2021) on regional CH<sub>4</sub> budgets and Jackson et al. (2020) focusing on the  
283 last year of the budget (2017). Saunois et al. (2020) covered 2000-2017 and reported CH<sub>4</sub> emissions and sinks for three time  
284 periods: 1) the latest calendar decade at that time (2000-2009), 2) data for the latest available decade (2008-2017), and 3)  
285 the latest available year (2017) at the time. Here, the Global Methane Budget (GMB) covers 2000-2020 split into the 2000-  
286 2009 decade, the 2010-2019 decade (where data are available), the year 2020 affected by COVID induced changes in human  
287 activity, and briefly for 2021-2023 as per data availability (Section 6). The CH<sub>4</sub> budget is presented at global, latitudinal,  
288 and regional scales and data can be downloaded from <https://doi.org/10.18160/GKQ9-2RHT> (Martinez et al., 2024). A  
289 global, regional and sectoral assessment of methane emission changes over the last two decades is discussed in Jackson et  
290 al. (2024) based on the data of Martinez et al. (2024).



291 Six sections follow this introduction. Section 2 presents the methodology used in the budget: units, definitions of  
292 source categories, regions, data analysis; and discusses the delay between the period of study of the budget and the release  
293 date. Section 3 presents the current knowledge about CH<sub>4</sub> sources and sinks based on the ensemble of bottom-up approaches  
294 reported here (models, inventories, data-driven approaches). Section 4 reports atmospheric observations and top-down  
295 atmospheric inversions gathered for this paper. Section 5, based on Sections 3 and 4, provides the updated analysis of the  
296 global CH<sub>4</sub> budget by comparing bottom-up and top-down estimates and highlighting differences. Section 6 discusses the  
297 recent changes in atmospheric CH<sub>4</sub> in relation with changes in CH<sub>4</sub> sources and sinks. Finally, Section 7 discusses future  
298 developments, missing components, and the most critical remaining uncertainties based on our update to the global CH<sub>4</sub>  
299 budget. For easier reading, the list of Contents of this manuscript is presented in the first section of the Supplementary  
300 Material.

## 301 **2 Methodology**

### 302 **2.1 Units used**

303 Unless specified, fluxes are expressed in teragrams of CH<sub>4</sub> per year ( $1 \text{ Tg CH}_4 \text{ yr}^{-1} = 10^{12} \text{ g CH}_4 \text{ yr}^{-1}$ ), while atmospheric  
304 mixing ratios are expressed as dry air mole fractions, in parts per billion (ppb), with atmospheric CH<sub>4</sub> annual increases,  
305  $G_{\text{ATM}}$ , expressed in ppb yr<sup>-1</sup>. In the tables, we present mean values and ranges for the two decades 2000-2009 and 2010-  
306 2019, together with results for the most recent available year (2020). Results obtained from previous syntheses (i.e., Sauniois  
307 et al., 2020 and Sauniois et al., 2016) are also given for the decade 2000-2009. Following Sauniois et al. (2016) and  
308 considering that the number of studies is often relatively small for many individual source and sink estimates, uncertainties  
309 are reported as minimum and maximum values of the available studies, given in brackets. In doing so, we acknowledge that  
310 we do not consider the uncertainty of the individual estimates, and we express uncertainty as the range of available mean  
311 estimates, i.e., differences across measurements/methodologies considered. These minimum and maximum values are those  
312 presented in Section 2.5 and exclude identified outliers.

313 The CH<sub>4</sub> emission estimates are provided with up to three significant digits, for consistency across all budget flux  
314 components and to ensure the accuracy of aggregated fluxes. Nonetheless, given the values of the uncertainties in the CH<sub>4</sub>  
315 budget, we encourage the reader to consider not more than two digits as significant for the global total budget.

### 316 **2.2 Period of the budget and availability of data**

317 The bottom-up estimates rely on global anthropogenic emission inventories, an ensemble of process-based models for  
318 wetlands emissions, and published estimates in the literature for other natural sources. The global gridded anthropogenic  
319 inventories (see Section (3.1.1)) are updated irregularly, generally every 3 to 5 years. The last reported years of available  
320 inventories were 2018 or 2019 when we started the top-down modelling activity. In order to cover the period 2000-2020, it

was necessary to extrapolate the anthropogenic inventory EDGARv6 (Crippa et al., 2021) to 2020 to use it as prior information for the anthropogenic emissions in the atmospheric inversion systems as explained in the supplementary material. Though EDGARv7 (EDGAR, 2022; Crippa et al., 2023) spanning until 2021 was then released, and was used for the bottom-up budget. EDGARv8 (EDGAR, 2023 ; Crippa et al., 2023) spanning until 2022 and released in 2024, was used in Section 6 to discuss the post 2020 methane budget. The land surface (wetland) models were run over the full period 2000-2020 using dynamical wetland areas, derived by remote sensing data or other models of flooded area variability (Sect. 3.2.1). The atmospheric inversions run until mid-2021, but the last year of reported inversion results is 2020, which represents a three-year lag with the present. This is due to the long time period it takes to acquire atmospheric in-situ data and integrate models. Even though satellite observations are processed operationally and are generally available with a latency of days to weeks, by contrast surface observations can lag from months to years because of the time for flask analyses and data quality checks in (mostly) non-operational chains. In addition, the final six months of inversions must be generally ignored because the estimated fluxes are not constrained by as many observations as the previous periods. Lastly, this budget presents an extended synthesis of the most recent development regarding inland water emissions (Sect. 3.2.2) and corrections associated with double counting with wetlands.

### 2.3 Definition of regions

Geographically, emissions are reported globally and for three latitudinal bands (90°S-30°N, 30-60°N, 60-90°N, only for gridded products). When extrapolating emission estimates forward in time (see Sect. 3.1.1), and for the regional budget presented by Stavert et al. (2021), a set of 19 regions (oceans and 18 continental regions, see supplementary Fig. S3) were used. As anthropogenic emissions are often reported by country, we define these regions based on a country list (Table S1). This approach was compatible with all top-down and bottom-up approaches considered. The number of regions was chosen to be close to the widely used TransCom inter-comparison map (Gurney et al., 2004) but with subdivisions to separate the contribution from important countries or regions for the CH<sub>4</sub> cycle (China, South Asia, Tropical America, Tropical Africa, United States of America, and Russia). The resulting region definition is the same as that used for the Global Carbon Project (GCP) N<sub>2</sub>O budget (Tian et al., 2020). Compared to Saunio et al. (2020), the Oceania region has been replaced by Australasia including only Australia and New Zealand. Other territories formerly in Oceania were included in Southeast Asia.

### 2.4 Definition of source and sink categories

CH<sub>4</sub> is emitted by different processes (i.e., biogenic, thermogenic, or pyrogenic) and can be of anthropogenic or natural origin. Biogenic CH<sub>4</sub> is the final product of the decomposition of organic matter by methanogenic *Archaea* in anaerobic environments, such as water-saturated soils, swamps, rice paddies, marine and freshwater sediments, landfills, sewage and wastewater treatment facilities, or inside animal digestive systems. Thermogenic methane is formed on geological time

scales by the breakdown of buried organic matter due to heat and pressure deep in the Earth's crust. Thermogenic CH<sub>4</sub> reaches the atmosphere through marine and land geological gas seeps. These CH<sub>4</sub> emissions are increased by human activities, for instance, the exploitation and distribution of fossil fuels. Pyrogenic CH<sub>4</sub> is produced by the incomplete combustion of biomass and other organic materials. Peat fires, biomass burning in deforested or degraded areas, wildfires, and biofuel burning are the largest sources of pyrogenic CH<sub>4</sub>. CH<sub>4</sub> hydrates, ice-like cages of frozen CH<sub>4</sub> found in continental shelves and slopes and below sub-sea and land permafrost, can be of either biogenic or thermogenic origin. Each of these three process categories has both anthropogenic and natural components.

In the following, we present the different CH<sub>4</sub> sources depending on their anthropogenic or natural origin, which is relevant to climate policy. Compared to the previous budgets, marginal changes have been made regarding source categories (naming and grouping), to reflect the improved estimates for inland water sources and their indirect anthropogenic component. In the previous Global Methane Budgets (Saunio et al., 2016, 2020), natural and anthropogenic emissions were split in a way that did not correspond exactly to the definition used by the UNFCCC following the IPCC guidelines (IPCC, 2006), where, for pragmatic reasons, all emissions from managed land are typically reported as anthropogenic. For instance, we considered all wetlands as natural emissions, despite some wetlands being on managed land and their emissions being partly reported as anthropogenic in UNFCCC national communications. Separating natural from anthropogenic sources could be quite challenging, especially over regions where sources overlap, as over heavily human-dominated floodplain deltas for example. The human induced perturbation of climate, atmospheric CO<sub>2</sub>, and nitrogen and sulfur deposition may also cause changes in wetland sources we classified as natural. Following our previous definition, emissions from wetlands, inland freshwaters, thawing permafrost, or geological leaks are accountable for "natural" emissions, even though we acknowledge that climate change and other human perturbations (e.g., eutrophication) may cause changes in those emissions. CH<sub>4</sub> emissions from reservoirs were also considered as natural even though reservoirs are human-made. Indeed, since the 2019 refinement to the IPCC guidelines (IPCC, 2019) emissions from reservoirs and other flooded lands are considered to be anthropogenic by the UNFCCC and should be reported as such. However, these estimates are not provided by inventories and not systematically reported by all countries (especially non Annex-I countries). In this budget we rename "natural sources" to "natural and indirect anthropogenic sources" to acknowledge that CH<sub>4</sub> emissions from reservoirs, as well as from water bodies that were perturbed by agricultural activities (drainage, eutrophication, land use change) are indirect anthropogenic emissions. As a result, here, "natural and indirect anthropogenic sources" refer to "emissions that do not directly originate from fossil, agricultural, waste, and biomass burning sources" even if they are perturbed by anthropogenic activities and climate change. Natural and indirect anthropogenic emissions are split between "Wetlands and Inland Freshwaters" and "Other natural" emissions (e.g., wild animals, termites, land geological sources, oceanic geological and biogenic sources, and terrestrial permafrost). "Anthropogenic direct sources" are caused by direct human activities since pre-industrial/pre-agricultural time (3000-2000 BC, Nakazawa et al., 1993) including agriculture, waste management, fossil fuel-related activities and biofuel and biomass burning (yet we acknowledge that a small fraction of wildfires are naturally ignited). Direct anthropogenic

emissions are split between: “Agriculture and waste emissions”, “Fossil fuel emissions”, and “Biomass and biofuel burning emissions”, assuming that all types of fires are caused by anthropogenic activities. To conclude, this budget reports “direct anthropogenic”, and “natural and indirect anthropogenic” methane emissions for the five main source categories explained above for both bottom-up and top-down approaches.

The sinks of methane are split into the soil uptake that can be derived from land-surface models in the bottom-up budget, and the chemical sinks. The chemical sinks are estimated by either chemistry climate or chemistry transport models in the bottom-up budget, and are further detailed in terms of vertical distribution (troposphere and stratosphere) and oxidants.

Bottom-up estimates of CH<sub>4</sub> emissions for some processes are derived from process-oriented models (e.g., biogeochemical models for wetlands, models for termites), inventory models (agriculture and waste emissions, fossil fuel emissions, biomass and biofuel burning emissions), satellite-based models (large scale biomass burning), or observation-based upscaling models for other sources (e.g., inland water, geological sources). From these bottom-up approaches, it is possible to provide estimates for more detailed source subcategories inside each main category described above (see budget in Table 3). However, the total CH<sub>4</sub> emission derived from the sum of independent bottom-up estimates remains unconstrained.

For atmospheric inversions (top-down approach), atmospheric methane concentration observations provide a constraint on the global methane total source if we assume the global sink is known (OH and other oxidant prescribed), or inversions are optimising also for the chemical sink. OH estimates are constrained by methyl chloroform-inversion (Montzka et al., 2011; Rigby et al., 2017; Patra et al., 2021). The inversions reported in this work solve for the total net CH<sub>4</sub> flux at the surface (sum of sources minus soil uptake) (e.g., Pison et al., 2013), or a limited number of source categories (e.g., Bergamaschi et al., 2013). In most of the inverse systems the atmospheric oxidant concentrations were prescribed with pre-optimized or scaled OH fields, and thus the atmospheric sink is not optimised. The assimilation of CH<sub>4</sub> observations alone, as reported in this synthesis, can help to separate sources with different locations or temporal variations but cannot fully separate individual sources where they overlap in space and time in some regions. Top-down global and regional CH<sub>4</sub> emissions per source category were nevertheless obtained from gridded optimised fluxes, for the inversions that separated emissions into the five main GCP categories. Alternatively, for the inversion that only solved for total emissions (or for other categories other than the five described above), the prior contribution of each source category at the spatial resolution of the inversion was scaled by the ratio of the total (or embedding category) optimised flux divided by the total (or embedding category) prior flux (Kirschke et al., 2013). In other words, the prior relative mix of sources at model resolution is kept in each grid cell while total emissions are given by the atmospheric inversions. The soil uptake was provided separately to report total gross surface emissions instead of net fluxes (sources minus soil uptake).

In summary, bottom-up models and inventories emissions are presented for all relevant source processes and grouped if needed into the five main categories defined above. Top-down inversion emissions are reported globally and for the five main emission categories.

417       **2.5 Processing of emission maps and box-plot representation of emission budgets**

418       Common data analysis procedures have been applied to the different bottom-up models, inventories and atmospheric  
419       inversions whenever gridded products exist. Gridded emissions from atmospheric inversions, land-surface models for  
420       wetland or biomass burning were provided at the monthly scale. Emissions from anthropogenic inventories are usually  
421       available as yearly estimates. These monthly or yearly fluxes were provided on a 1°x1° grid or re-gridded to 1°x1°, then  
422       converted into units of Tg CH<sub>4</sub> per grid cell. Inversions with a resolution coarser than 1° were downscaled to 1° by each  
423       modelling group. Land fluxes in coastal pixels were reallocated to the neighbouring land pixel according to our 1° land-sea  
424       mask, and vice-versa for ocean fluxes. Annual and decadal means used for this study were computed from the monthly or  
425       yearly gridded 1°x1° maps.  
426       Budgets are presented as boxplots with quartiles (25%, median, 75%), outliers, and minimum and maximum values without  
427       outliers. Outliers were determined as values below the first quartile minus three times the interquartile range, or values above  
428       the third quartile plus three times the interquartile range. Mean values reported in the tables are represented as “+” symbols  
429       in the corresponding figures.

430       **3 Methane sources and sinks: bottom-up estimates**

431       For each source category, a short description of the relevant processes, original data sets (measurements, models) and related  
432       methodology are given. More detailed information can be found in original publication references, in Annex A2 where the  
433       sources of data used to estimate the different sources and sinks are summarised and compared with those used in Saunio et  
434       al. (2020) and in the Supplementary Material of this study when specified in the text. The emission estimates for each source  
435       category are compared with Saunio et al. (2020) in Table 3 and with Saunio et al. (2016) in Table S12 for the decade 2000-  
436       2009.

437       **3.1 Anthropogenic direct sources**

438       **3.1.1 Global inventories**

439       The main bottom-up global inventory datasets covering direct anthropogenic emissions from all sectors (Table 1) are from  
440       the United States Environmental Protection Agency (USEPA, 2019), the Greenhouse gas and Air pollutant Interactions and  
441       Synergies (GAINS) model developed by the International Institute for Applied Systems Analysis (IIASA) (Höglund-  
442       Isaksson et al., 2020) and the Emissions Database for Global Atmospheric Research (EDGARv6 and v7, Crippa et al., 2021,  
443       2023) compiled by the European Commission Joint Research Centre (EC-JRC) and Netherlands Environmental Assessment  
444       Agency (PBL). We also used the Community Emissions Data System for historical emissions (CEDS) (Hoesly et al., 2018)  
445       developed for climate modelling and the Food and Agriculture Organization (FAO) FAOSTAT emission database (Tubiello

et al., 2022), which covers emissions from agriculture and land use (including peatland fires and biomass fires). These inventories are not independent as they may use the same activity data or emission factors, as discussed below.

These inventory datasets report emissions from fossil fuel production, transmission, and distribution; livestock enteric fermentation; manure management and application; rice cultivation; solid waste and wastewater. Since the level of detail provided by country and by sector varies among inventories, the data were reconciled into common categories according to Table S2. For example, agricultural waste-burning emissions treated as a separate category in EDGAR, GAINS and FAO, are included in the biofuel sector in the USEPA inventory and in the agricultural sector in CEDS. The GAINS, EDGAR and FAO estimates of agricultural waste burning were excluded from this analysis (these amounted to 1-3 Tg CH<sub>4</sub> yr<sup>-1</sup> in recent decades) to prevent any potential overlap with separate estimates of biomass burning emissions (e.g., GFEDv4.1s; Giglio et al. (2013); van der Werf et al (2017)). In the inventories used here, emissions for a given region/country and a given sector are usually calculated following IPCC methodology (IPCC, 2006), as the product of an activity factor and its associated emission factor. An abatement coefficient may also be used, to account for any regulations implemented to control emissions (see e.g., Höglund-Isaksson et al., 2015). These datasets differ in their assumptions and data used for the calculation; however, they are not completely independent because they often use the same activity data and some of them follow the same IPCC guidelines (IPCC, 2006). While the USEPA inventory adopts emissions reported by the countries to the UNFCCC, other inventories (FAOSTAT, EDGAR and the GAINS model) produce their own estimates using a consistent approach for all countries, typically IPCC Tier 1 methods or deriving IPCC Tier 2 emission factors from country-specific information using a consistent methodology. These other inventories compile country-specific activity data and emission factor information or, if not available, adopt IPCC default factors (Tibrewal et al., 2024; Oreggioni et al., 2021; Höglund-Isaksson et al., 2020; Tubiello, 2019). CEDS takes a different approach (Hoesly et al., 2018) and combines data from GAINS, EDGAR and FAO depending on the sector. Then their first estimates are scaled to match other individual or region-specific inventory values when available. This process maintains the spatial information in the default emission inventories while preserving consistency with country level data. The FAOSTAT dataset (hereafter FAO-CH<sub>4</sub>) provides estimates at the country level and is limited to agriculture (CH<sub>4</sub> emissions from enteric fermentation, manure management, rice cultivation, energy usage, burning of crop residues, and prescribed burning of savannahs) and land-use (peatland fires and biomass burning). FAO-CH<sub>4</sub> uses activity data mainly from the FAOSTAT crop and livestock production database, as reported by countries to FAO (Tubiello et al., 2013), and applies mostly the Tier 1 IPCC methodology for emissions factors (IPCC, 2006), which depends on geographic location and development status of the country. For manure, the country-scale temperature was obtained from the FAO global agro-ecological zone database (GAEZv3.0, 2012). Although country emissions are reported annually to the UNFCCC by annex I countries, and episodically by non-annex I countries, data gaps of those national inventories do not allow the inclusion of these estimates in this analysis.

In this budget, we use the following versions of these inventories that were available at the start and during the analysis (see Table 1):

- EDGARv6 which provides yearly gridded emissions by sectors from 1970 to 2018 (Crippa et al., 2021; Oreggioni et al., 2021; EDGARv6 website [https://edgar.jrc.ec.europa.eu/dataset\\_ghg60](https://edgar.jrc.ec.europa.eu/dataset_ghg60); Monforti Ferrario et al., 2021),
- EDGARv7, which provides yearly gridded emissions by sectors from 1970 to 2020 (monthly for some sectors), but emissions from fossil fuel energy are not separated (oil and gas, and coal are lumped together - see Table S2) (EDGARv7 website [https://edgar.jrc.ec.europa.eu/dataset\\_ghg70](https://edgar.jrc.ec.europa.eu/dataset_ghg70); Crippa et al., 2023).
- GAINS model scenario version 4.0 (Höglund-Isaksson et al., 2020) which provides an annual sectorial gridded product from 1990 to 2020 both by country and gridded. USEPA (USEPA, 2019), which provides 5-year sectorial totals by country from 1990 to 2020 (estimates from 2015 onward are a projection), with no gridded distribution available. The USEPA dataset was linearly interpolated to provide yearly values from 1990-2020.
- CEDS version v\_2021\_04\_21 which provides gridded monthly and annual country-based emissions by sectors from 1970 to 2019 (Hoesly et al., 2018; O'Rourke et al., 2021). Fossil fuel emissions for 2020 have been updated using the methodology described for CO in Zheng et al. (2023).
- FAO-CH<sub>4</sub> (database accessed in December 2022, FAO, 2022) containing annual country level data for the period 1961-2020, for rice, manure, and enteric fermentation; and 1990-2020 for burning savannah, crop residue and non-agricultural biomass burning.

### 3.1.2 Total anthropogenic direct emissions

We calculated separately the total anthropogenic emissions for each inventory by adding its values for “Agriculture and waste”, “Fossil fuels” and “Biofuels” with additional large-scale biomass burning emissions data (Sect. 3.1.5). This method avoids double counting and ensures consistency within each inventory. This approach was used for the EDGARv6 and v7, CEDS and GAINS inventories, but we kept the USEPA inventory as originally reported because it includes its own estimates of biomass burning emissions. FAO-CH<sub>4</sub> was only included in the range reported for the “Agriculture and waste” category. For the latter, we calculated the range and mean value as the sum of the mean and range of the three anthropogenic subcategory estimates “Enteric fermentation and Manure”, “Rice”, and “Landfills and Waste”. The values reported for the upper-level anthropogenic categories (“Agriculture and waste”, “Fossil fuels” and “Biomass burning & biofuels”) are therefore consistent with the sum of their subcategories, although there might be small percentage differences between the reported total anthropogenic emissions and the sum of the three upper-level categories. This approach provides a more accurate representation of the range of emission estimates, avoiding an artificial expansion of the uncertainty attributable to subtle differences in the definition of sub-sector categorisations between inventories.

Based on the ensemble of databases detailed above, total direct anthropogenic emissions were 358 [329-387] Tg CH<sub>4</sub> yr<sup>-1</sup> for the decade 2010-2019 (Table 3, including biomass and biofuel burning) and 331 [305-365] Tg CH<sub>4</sub> yr<sup>-1</sup> for the decade 2000-2009. Our estimate for the 2000-2009 decade is within the range of Saunio et al. (2020) (334 [321-358]), Saunio et al. (2016) (338 Tg CH<sub>4</sub> yr<sup>-1</sup> [329-342]) and Kirschke et al. (2013) (331 Tg CH<sub>4</sub> yr<sup>-1</sup> [304-368]) for the same period. The

slightly larger range reported herein with respect to previous estimates is due to the USEPA lower estimate for agriculture, waste and fossil emissions associated with the lowest estimate of biomass burning.

Figure 2 (left) summarises or projects global CH<sub>4</sub> emissions of anthropogenic sources (including biomass and biofuel burning) by different datasets between 2000 and 2050. The datasets consistently estimate total anthropogenic emissions of ~300 Tg CH<sub>4</sub> yr<sup>-1</sup> in 2000. For the Sixth Assessment Report of the IPCC, seven main Shared Socioeconomic Pathways (SSPs) were defined for future climate projections in the Coupled Model Intercomparison Project 6 (CMIP6) (Gidden et al., 2019; O'Neill et al., 2016) ranging from 1.9 to 8.5 W m<sup>-2</sup> radiative forcing by the year 2100 (as shown by the number in the SSP names). For the 1970-2015 period, historical emissions used in CMIP6 (Feng et al., 2019) combine anthropogenic emissions from CEDS (Hoesly et al., 2018) and a climatological value from the GFEDv4.1s biomass burning inventory (van Marle et al., 2017). The harmonised scenarios used for CMIP6 activities start in 2015 at 388 Tg CH<sub>4</sub> yr<sup>-1</sup>, which corresponds to the higher range of our estimates. Since CH<sub>4</sub> emissions continue to track scenarios that assume no or minimal climate policies (SSP5 and SSP3), it may indicate that climate policies, when present, have not yet produced sufficient results to change the emissions trajectory substantially (Nisbet et al., 2019). After 2015, the SSPs span a range of possible outcomes, but current emissions appear likely to follow the higher-emission trajectories. given that over the past decade their trend has followed such trajectories, and because the peak emission year has not yet been reached. High or medium emission reduction rates as suggested by scenarios SSP1 and SSP2 have not yet happened. This illustrates the challenge of methane mitigation that lies ahead to help reach the goals of the Paris Agreement (Nisbet et al., 2020; Shindell et al., 2024). In addition, estimates of methane atmospheric concentrations (Meinshausen et al., 2017, 2020) from the harmonised scenarios (Riahi et al., 2017) indicate that observations of global CH<sub>4</sub> concentrations fall well within the range of scenarios in absolute values but their trend over the past few years is closest to those of scenario SSP5-8.5 (Fig. 2 right). The CH<sub>4</sub> concentrations are estimated using a simple exponential decay with inferred natural emissions (Meinshausen et al., 2011), and the emergence of any trend between observations and scenarios needs to be confirmed in the following years. However, the current observed concentrations and emissions estimates lie in the upper range of the former RCPs scenarios starting in 2005 (Fig. S1). In the future, it will be important to monitor the trends from 2015 (the Paris Agreement) and from 2020 (Global Methane Pledge) estimated in inventories and from atmospheric observations, and compare them to various scenarios.

**3.1.3 Fossil fuel production and use**

Most anthropogenic CH<sub>4</sub> emissions related to fossil fuels come from the exploitation, transportation, and usage of coal, oil, and natural gas. Additional emissions reported in this category include small industrial contributions such as the production of chemicals and metals, fossil fuel fires (e.g., underground coal mine fires and the Kuwait oil and gas fires), and transport (road and non-road transport). CH<sub>4</sub> emissions from the oil processing industry (e.g., refining) and production of charcoal are estimated to be a few Tg CH<sub>4</sub> yr<sup>-1</sup> only and are included in the transformation industry sector in the inventory. Fossil fuel fires are included in the subcategory “Oil & Gas”. Emissions from industries, road and, non-road transport are reported

Supprimé:

Supprimé: in terms of trend



545 apart from the two main subcategories “Oil & Gas” and “Coal”, as in Sauniois et al. (2020) and contrary to Sauniois et al.  
546 (2016); each of these amounts to about 2 to 5 Tg CH<sub>4</sub> yr<sup>-1</sup> (Table 3). The large range (1-9 Tg CH<sub>4</sub> yr<sup>-1</sup>) is attributable to  
547 difficulties in allocating some sectors to these sub-sectors consistently among the different inventories (See Table S2). The  
548 spatial distribution of CH<sub>4</sub> emissions from fossil fuels is presented in Fig. 3 based on the mean gridded maps provided by  
549 CEDS, EDGARv6, and GAINS for the 2010-2019 decade; USEPA lacks a gridded product.  
550 Global mean emissions from fossil fuel-related activities, other industries and transport are estimated from the four global  
551 inventories (Table 1) to be of 120 [117-125] Tg CH<sub>4</sub> yr<sup>-1</sup> for the 2010-2019 decade (Table 3), but with large differences in  
552 the rate of change during this period across inventories. The sector accounts on average for 34% (range 31-42%) of total  
553 global anthropogenic emissions in 2010-2019. This contribution has slightly increased from 32% on average in 2000-2009.  
554

#### 555 **Coal mining.**

556 During mining, CH<sub>4</sub> is emitted primarily from ventilation shafts, where large volumes of air are pumped in and out of the  
557 mine to keep the CH<sub>4</sub> mixing ratio below 0.5% to avoid accidental ignition, and from dewatering operations. In countries of  
558 the Organization for Economic Co-operation and Development (OECD), coalbed CH<sub>4</sub> is often extracted as fuel up to ten  
559 years before the coal mine starts operation, thereby reducing the CH<sub>4</sub> channelled through ventilation shafts during mining.  
560 In many countries, large quantities of ventilation air CH<sub>4</sub> are still released to the atmosphere or flared, despite efforts to  
561 extend coal mine gas recovery under the UNFCCC Clean Development Mechanisms (<http://cdm.unfccc.int>). CH<sub>4</sub> leaks also  
562 occur during post-mining handling, processing, and transportation. Some CH<sub>4</sub> is released from coal waste piles and  
563 abandoned mines; while emissions from these sources were believed to be low (IPCC, 2000), recent work has estimated  
564 these at 22 billion m<sup>3</sup> (compared to 103 billion m<sup>3</sup> from functioning coal mines) in 2010 with emissions projected to increase  
565 into the future (Kholod et al., 2020).

566 In 2020, more than 35% (IEA, 2023a) of the world’s electricity is still produced from coal. This contribution grew in the  
567 2000s at the rate of several percent per year, driven by Asian economic growth where large reserves exist, but global coal  
568 consumption declined between 2014 and 2020. In 2020, the top ten largest coal producing nations accounted for ~90% of  
569 total world CH<sub>4</sub> emissions from coal mining; among them, the top three producers (China, United States of America, and  
570 India) produced almost two-thirds (66%) of the world’s coal (IEA, 2021).

571 Global estimates of CH<sub>4</sub> emissions from coal mining show a reduced range of 37-44 Tg CH<sub>4</sub> yr<sup>-1</sup> for 2010-2019 (Table 3),  
572 compared to the previous estimate for 2008-2017 in Sauniois et al. (2020) reporting a range of 29-61 Tg CH<sub>4</sub> yr<sup>-1</sup> for 2008-  
573 2017. This reduced range probably results from using similar activity data (mostly from IEA statistics) in the different  
574 inventories. The highest value of the range in Sauniois et al. (2020) came from the CEDS inventory while the lowest came  
575 from USEPA. CEDS seems to have revised downward their estimate compared to the previous version used in Sauniois et  
576 al. (2020). There were previously large discrepancies in Chinese coal emissions, with a large overestimation from  
577 EDGARv4.2 on which CEDS was based. As highlighted by Liu et al. (2021a), a county-based inventory of Chinese methane

emissions also confirms the overestimation of previous EDGAR inventories and estimated total anthropogenic Chinese emissions at  $38.2 \pm 5.5 \text{ Tg CH}_4 \text{ yr}^{-1}$  for 2000-2008 (Liu et al., 2021a). Coal mining emission factors depend strongly on the type of coal extraction (underground mining emits up to 10 times more than surface mining), the geological underground structure (region-specific), history (basin uplift), and the quality of the coal (brown coal (lignite) emits **less** than hard coal (anthracite)). Finally, the different emission factors derived for coal mining is the main reason for the differences between inventories globally (Fig. 2).

For the 2010-2019 decade, methane emissions from coal mining represent 33% of total fossil fuel-related emissions of  $\text{CH}_4$  ( $40 [37-44] \text{ Tg CH}_4 \text{ yr}^{-1}$ , Table 3). An additional assumed very small source corresponds to fossil fuel fires, which are mostly underground coal fires. This source is estimated at around  $0.15 \text{ Tg yr}^{-1}$  in EDGARv7, though this value remains the same across EDGAR versions and for all years despite the changes in coal production, which could influence this estimate. However, to date, insufficient data is available to better estimate this largely unknown source.

**Oil and natural gas systems.**

This sub-category includes emissions from both conventional and shale oil and gas exploitation. Natural gas is composed primarily of  $\text{CH}_4$ , so both fugitive and planned emissions during the drilling of wells in gas fields, extraction, transportation, storage, gas distribution, end use, and incomplete combustion in gas flares emit  $\text{CH}_4$  (Lamb et al., 2015; Shorter et al., 1996). Persistent fugitive emissions (e.g., due to leaky valves and compressors) should be distinguished from intermittent emissions due to maintenance (e.g., purging and draining of pipes) or incidents. During transportation, fugitive emissions can occur in oil tankers, fuel trucks and gas transmission pipelines, attributable to corrosion, manufacturing, and welding faults. According to Lelieveld et al. (2005),  $\text{CH}_4$  fugitive emissions from gas pipelines should be relatively low, however, old distribution networks in some cities may have higher rates, especially those with cast-iron and unprotected steel pipelines (Phillips et al., 2013). Measurement campaigns in cities within the USA (e.g., McKain et al., 2015) and Europe (e.g., Defratyka et al., 2021) revealed that significant emissions occur in specific locations (e.g., storage facilities, city natural gas fueling stations, well and pipeline pressurisation/depressurisation points, sewage systems, and furnaces of buildings) along the distribution networks (e.g., Jackson et al., 2014a; McKain et al., 2015; Wunch et al., 2016). However,  $\text{CH}_4$  emissions vary significantly from one city to another depending, in part, on the age of city infrastructure and the quality of its maintenance, making urban emissions difficult to scale-up from measurement campaigns, although attempts have been made (e.g., Defratyka et al., 2021). In many facilities, such as gas and oil fields, refineries, and offshore platforms, most of the associated and other waste gas generated will be flared for security reasons with almost complete conversion to  $\text{CO}_2$ , however, due to the large quantities of waste gas generated, small fractions of gas still being vented make up relatively large quantities of methane. These two processes are usually considered together in inventories of oil and gas industries. In addition, single-point failure of natural gas infrastructure can leak  $\text{CH}_4$  at high rate for months, such as at the Aliso Canyon blowout in the Los Angeles, CA (Conley et al., 2016) or the shale gas well blowout in Ohio (Pandey et al., 2019), thus

Supprimé: more

hampering emission control strategies. Production of natural gas from the exploitation of hitherto unproductive rock formations, especially shale, began in the 1970s in the US on an experimental or small-scale basis, and then, from the early 2000s, exploitation started at a large commercial scale. The shale gas contribution to total dry natural gas production in the United States reached 82% in 2023, growing rapidly from 48% in 2013 (IEA, 2023b). The possibly larger emission factors from shale gas compared to conventional gas, have been widely debated (e.g., Cathles et al., 2012; Howarth, 2019; Lewan, 2020). The latest studies tend to infer emission factors from the oil gas production chain of about 1% to 6% (e.g., Schneising et al., 2020; Varon et al., 2023; Zhang et al., 2020), but loss rate could be as high as more than 10% in low producing well sites (e.g., Omara et al., 2022, Williams et al., 2024).

CH<sub>4</sub> emissions from oil and natural gas systems vary greatly in different global inventories (67 to 80 Tg yr<sup>-1</sup> in 2020, Table 3). The inventories generally rely on the same sources and magnitudes for activity data, with the derived differences therefore resulting primarily from different methodologies and parameters used, including emission factors. Those factors are country- or even site-specific and the few field measurements available often combine oil and gas activities (Brandt et al., 2014), resulting in high uncertainty in emission estimates for many major oil and gas producing countries. Depending on the region, the IPCC 2006 default emission factors may vary by two orders of magnitude for oil production and one order for gas production. For instance, the GAINSv4.0 estimate of CH<sub>4</sub> emissions from US oil and gas systems in 2015 is 16 Tg, which is almost twice as high as EDGARv8.0 (EDGAR, 2024) at 8.4 Tg and USEPA (UNFCCC, 2023) at 9.5 Tg. The difference can partly be explained by GAINS using a bottom-up methodology to derive country- and year-specific flows of associated petroleum gas and attributing these to recovery/reinjection, flaring or venting (Höglund-Isaksson, 2017), and partly to GAINS using a higher emission factor for unconventional gas production (Höglund-Isaksson et al., 2020). Recent quantifications using satellite observations and inversion estimate a relatively stable trend for US oil and gas systems emissions since 2010, with Lu et al. (2023) estimating 14.6 Tg for 2010, 15.9 Tg for 2014 and 15.6 Tg for 2019, Shen et al. (2022) estimating a mean of 12.6 Tg for 2018–2020, and Maasakkers et al (2021) a mean of 11.1 Tg for 2010 to 2015. The stable top-down trend for the US appears not well captured in the bottom-up inventories from GAINS and EDGAR, which tend to show an increasing trend driven by increase in production volumes.

Most recent studies (e.g., Zhang et al., 2020; Shen et al., 2023; Li et al., 2024; Tibrewal et al., 2024; Sherwin et al., 2024) still suggest that the methane emissions from oil and gas industry are underestimated by inventories, industries, and agencies, including the USEPA and UNFCCC reporting. Lauvaux et al. (2022) showed that emissions from a few high-emitting facilities, i.e., super-emitters (> 20 t hr<sup>-1</sup>), which are usually sporadic in nature, and not accounted for in the inventories, could represent 8–12% of global oil & gas emissions, or around 8 Tg CH<sub>4</sub> yr<sup>-1</sup>. These high emitting points, located on the conventional part of the facilities, could be avoided through better operating conditions and repair of malfunctions. Over the last decade, absolute CH<sub>4</sub> emissions almost certainly increased, since USA crude oil production doubled and natural gas production rose by about 50% (IEA, 2023a). However, global implications of the rapidly growing shale gas activity in the US remain to be determined precisely.

For the 2010-2019 decade, CH<sub>4</sub> emissions from upstream and downstream oil and natural gas sectors are estimated to represent about 56% of total fossil CH<sub>4</sub> emissions (67 [57-74] Tg CH<sub>4</sub> yr<sup>-1</sup>, Table 3) based on global inventories, with a lower uncertainty range than for coal emissions for most countries. However, it is worth noting that 8 Tg CH<sub>4</sub> yr<sup>-1</sup> should be added on top of this estimate to acknowledge the ultra-emitters contribution, as done in Tibrewal et al (2024).

#### 3.1.4 Agriculture and waste sectors

This main category includes CH<sub>4</sub> emissions related to livestock production (i.e., enteric fermentation in ruminant animals and manure management), rice cultivation, landfills, and wastewater handling. Of these activities, globally and in most countries, livestock is by far the largest source of CH<sub>4</sub>, followed by waste handling and rice cultivation. Conversely, field burning of agricultural residues is a minor source of CH<sub>4</sub> reported in emission inventories (a few Tg at the global scale). The spatial distribution of CH<sub>4</sub> emissions from agriculture and waste handling is presented in Fig. 3 based on the mean gridded maps provided by CEDS, EDGARv6 and GAINS over the 2010-2019 decade.

Global emissions from agriculture and waste for the period 2010-2019 are estimated to be 211 [195-231] Tg CH<sub>4</sub> yr<sup>-1</sup> (Table 3), representing 60% of total direct anthropogenic emissions. Agriculture emissions amount to 144 Tg CH<sub>4</sub> yr<sup>-1</sup>, 40% of the direct anthropogenic emissions, with the rest coming from the fossil fuel sector (34%), waste (19%) and biomass (5%) and biofuel (3%) burning .

**Livestock: Enteric fermentation and manure management.** Domestic ruminants such as cattle, buffalo, sheep, goats, and camels emit CH<sub>4</sub> as a by-product of the anaerobic microbial activity in their digestive systems (Johnson et al., 2002). The very stable temperatures (about 39°C) and pH (6.5-6.8) within the rumen of domestic ruminants, along with a constant plant matter flow from grazing (cattle graze many hours per day), allow methanogenic *Archaea* residing within the rumen to produce CH<sub>4</sub>. CH<sub>4</sub> is released from the rumen mainly through the mouth of multi-stomached ruminants (eructation, ~90% of emissions) or absorbed in the blood system. The CH<sub>4</sub> produced in the intestines and partially transmitted through the rectum is only ~10% (Hill et al. 2016).

The total number of livestock continues to grow steadily. There are currently (2020) about 1.5 billion cattle globally, almost 1.3 billion sheep, and nearly as many goats (<http://www.fao.org/faostat/en/#data/GE>). Livestock numbers are linearly related to CH<sub>4</sub> emissions in inventories using the Tier 1 IPCC approach such as FAOSTAT. In practice, some non-linearity may arise due to dependencies of emissions on the total weight of the animals and their diet, which are better captured by Tier 2 and higher approaches. Cattle, due to their large population, large individual size, and particular digestive characteristics, account for the majority of enteric fermentation CH<sub>4</sub> emissions from livestock worldwide (Tubiello, 2019; FAO, 2022), particularly in intensive agricultural systems in wealthier and emerging economies, including the United States (USEPA, 2016). CH<sub>4</sub> emissions from enteric fermentation also vary from one country to another as cattle may experience diverse living conditions that vary spatially and temporally, especially in the tropics (Chang et al., 2019).

Anaerobic conditions often characterise manure decomposition in a variety of manure management systems globally (e.g., liquid/slurry treated in lagoons, ponds, tanks, or pits), with the volatile solids in manure producing CH<sub>4</sub>. In contrast, when manure is handled as a solid (e.g., in stacks or dry-lots) or deposited on pasture, range, or paddock lands, it tends to decompose aerobically and to produce little or no CH<sub>4</sub>. However aerobic decomposition of manure tends to produce nitrous oxide (N<sub>2</sub>O), which has a larger global warming impact than CH<sub>4</sub>. Ambient temperature, moisture, energy contents of the feed, manure composition, and manure storage or residency time affect the amount of CH<sub>4</sub> produced. Despite these complexities, most global datasets used herein apply a simplified IPCC Tier 1 approach, where amounts of manure treated depend on animal numbers and simplified climatic conditions by country.

Global CH<sub>4</sub> emissions from enteric fermentation and manure management are estimated in the range of 114-124 Tg CH<sub>4</sub> yr<sup>-1</sup>, for the year 2020, in the GAINS model and CEDS, USEPA, FAO-CH<sub>4</sub> and EDGARv7 inventories (Table 3). Using the Tier 2 method adopted from the 2019 Refinement to 2006 IPCC guidelines, a recent study (Zhang et al., 2022) estimated that global CH<sub>4</sub> emissions from livestock increased from 31.8 [26.5–37.1] (mean [minimum–maximum of 95% confidence interval]) Tg CH<sub>4</sub> yr<sup>-1</sup> in 1890 to 131.7 [109.6–153.7] Tg CH<sub>4</sub> yr<sup>-1</sup> in 2019, a fourfold increase in the past 130 years. Chang et al. (2021) estimates enteric fermentation and manure management emissions based on mixed Tier 1&2 and Tier1 approaches and calculate livestock emissions being 120±13 and 136±15 Tg CH<sub>4</sub> yr<sup>-1</sup> respectively for 2018. Chang et al. (2021) and Zhang et al. (2022) estimates for 2018 or 2019 are on average a bit higher than the inventories estimates but in agreement considering the uncertainties. It is worth recalling here that the ranges provided in this study correspond to the minimum-maximum of the existing estimates and do not include the uncertainty of the individual estimate; these uncertainties could be larger than the range proposed here.

For the period 2010-2019, we estimated total emissions of 112 [107-118] Tg CH<sub>4</sub> yr<sup>-1</sup> for enteric fermentation and manure management, about one third of total global anthropogenic emissions (Table 3).

**Rice cultivation.** Most of the world's rice is grown in flooded paddy fields (Baicich, 2013). The water management systems, particularly flooding, used to cultivate rice are one of the most important factors influencing CH<sub>4</sub> emissions and one of the most promising approaches for CH<sub>4</sub> emission mitigation: periodic drainage and aeration not only cause existing soil CH<sub>4</sub> to oxidise, but also inhibit further CH<sub>4</sub> production in soils (Simpson et al., 1995; USEPA, 2016; Zhang, 2016). Upland rice fields are not typically flooded, and therefore are not a significant source of CH<sub>4</sub>. Other factors that influence CH<sub>4</sub> emissions from flooded rice fields include fertilisation practices (i.e., the use of urea and organic fertilisers), soil temperature, soil type (texture and aggregated size), rice variety and cultivation practices (e.g., tillage, seeding, and weeding practices) (Conrad et al., 2000; Kai et al., 2011; USEPA, 2011; Yan et al., 2009). For instance, CH<sub>4</sub> emissions from rice paddies increase with organic amendments (Cai et al., 1997) but can be mitigated by applying other types of fertilisers (mineral, composts, biogas residues) or using wet seeding (Wassmann et al., 2000).

The geographical distribution of rice emissions has been assessed by global (e.g., Janssens-Maenhout et al., 2019; Tubiello, 2019; USEPA, 2012) and regional (e.g., Castelán-Ortega et al., 2014; Chen et al., 2013; Chen and Prinn, 2006; Peng et al.,

2016; Yan et al., 2009; Zhang and Chen, 2014) inventories and land surface models (Li et al., 2005; Pathak et al., 2005; Ren et al., 2011; Spahni et al., 2011; Tian et al., 2010, 2011; Zhang, 2016). The emissions show a seasonal cycle, peaking in the summer months in the extra-tropics associated with monsoons and land management. Emissions from rice paddies are influenced not only by the extent of rice field area, but also by changes in the productivity of plants (Jiang et al., 2017) as these alter the CH<sub>4</sub> emission factor used in inventories. However, the inventories considered herein are largely based on IPCC Tier 1 methods, which mainly scale with cultivated areas and include regional specific emission factors but do not account for changes in plant productivity and detailed cultivation practices.

The largest emissions from rice cultivation are found in Asia accounting for 30 to 50% of global emissions (Fig. 3). The decrease of CH<sub>4</sub> emissions from rice cultivation over recent decades is confirmed in most inventories, because of the decrease in rice cultivation area, changes in agricultural practices, and a northward shift of rice cultivation since the 1970s, as in China (e.g., Chen et al., 2013).

Based on the global inventories considered in this study, global CH<sub>4</sub> emissions from rice paddies are estimated to be 32 [25-37] Tg CH<sub>4</sub> yr<sup>-1</sup> for the 2010-2019 decade (Table 3), or about 9% of total global anthropogenic emissions of CH<sub>4</sub>. These estimates are consistent with the 29 Tg CH<sub>4</sub> yr<sup>-1</sup> estimated for the year 2000 by Carlson et al. (2017).

**Waste management.** This sector includes emissions from managed and non-managed landfills (solid waste disposal on land), and wastewater handling, where all kinds of waste are deposited. CH<sub>4</sub> production from waste depends on the pH, moisture, and temperature of the material. The optimum pH for CH<sub>4</sub> emission is between 6.8 and 7.4 (Thorneloe et al., 2000). The development of carboxylic acids leads to low pH, which limits methane emissions. Food or organic waste, such as leaves and grass clippings, ferment quite easily, while wood and wood products generally ferment slowly, and cellulose and lignin even more slowly (USEPA, 2010a).

Waste management was responsible for about 11% of total global direct anthropogenic CH<sub>4</sub> emissions in 2000 (Kirschke et al., 2013). A recent assessment of CH<sub>4</sub> emissions in the USA found landfills to account for almost 26% of total USA anthropogenic CH<sub>4</sub> emissions in 2014, the largest contribution of any single CH<sub>4</sub> source in the United States of America (USEPA, 2016). In Europe, gas control has been mandatory on all landfills since 2009, and more importantly for CH<sub>4</sub> emissions, the EU Landfill Directive (1999) with subsequent amendments, has diverted most biodegradable waste away from landfills towards source separation, recycling, composting and energy recovery, and with a legally binding target not to landfill more than 10% of municipal solid waste by 2035.

Wastewater from domestic and industrial sources is treated in municipal sewage treatment facilities and private effluent treatment plants. The principal factor in determining the CH<sub>4</sub> generation potential of wastewater is the amount of degradable organic material in the wastewater. Wastewater with high organic content is treated anaerobically, which leads to increased emissions (André et al., 2014). Excessive and rapid urban development worldwide, especially in Asia and Africa, could enhance methane emissions from waste unless adequate mitigation policies are designed and implemented rapidly.

The GAINS model and CEDS and EDGAR inventories give robust emission estimates from solid waste in the range of 37-42 Tg CH<sub>4</sub> yr<sup>-1</sup> for the year 2019, and more uncertain wastewater emissions in the range 20-45 Tg CH<sub>4</sub> yr<sup>-1</sup>. In our study, the global emission of CH<sub>4</sub> from waste management is estimated in the range of 56-80 Tg CH<sub>4</sub> yr<sup>-1</sup> for the 2010-2019 period with a mean value of 69 Tg CH<sub>4</sub> yr<sup>-1</sup>, about 19% of total global anthropogenic emissions (Table 3).

**3.1.5 Biomass and biofuel burning**

This category includes CH<sub>4</sub> emissions from biomass burning in forests, savannahs, grasslands, peats, agricultural residues, as well as, from the burning of biofuels in the residential sector (stoves, boilers, fireplaces). Biomass and biofuel burning emit CH<sub>4</sub> under incomplete combustion conditions (i.e., when oxygen availability is insufficient for complete combustion), for example in charcoal manufacturing and smouldering fires. The amount of CH<sub>4</sub> emitted during the burning of biomass depends primarily on the amount of biomass, burning conditions, fuel moisture and the specific material burned. In this study, we use large-scale biomass burning (forest, savannah, grassland, and peat fires) from five biomass burning inventories (described below) and the biofuel burning contribution from anthropogenic emission inventories (EDGARv6 and v7, CEDS, GAINS and USEPA). The spatial distribution of emissions from the burning of biomass and biofuel over the 2010-2019 decade is presented in Fig. 3 based on data listed in Table 1. At the global scale, during the period of 2010-2019, biomass and biofuel burning generated CH<sub>4</sub> emissions of 28 [21-39] Tg CH<sub>4</sub> yr<sup>-1</sup> (Table 3), of which 30-50% is from biofuel burning.

**Biomass burning.** Fire is an important disturbance event in terrestrial ecosystems globally (van der Werf et al., 2010), and can be of either natural (typically ~10% of fires, ignited by lightning strikes or started accidentally) or anthropogenic origin (~90%, human initiated fires) (USEPA, 2010b, chapter 9.1). As previously noted all fires are accounted as anthropogenic in Table 3. Anthropogenic fires are concentrated in the tropics and subtropics, where forests, savannahs and grasslands may be burned to clear land for agricultural purposes or to maintain pastures and rangelands. Small fires associated with agricultural activity, such as field burning and agricultural waste burning, are often not detected by moderate resolution remote sensing methods and are instead estimated based on cultivated area or through in-situ measurements such as dedicated airborne campaigns (e.g., Barker et al., 2023). Emission rates of biomass burning vary with biomass loading (depending on the biomes) at the location of the fire, the efficiency of the fire (depending on the vegetation type), the fire type (smouldering or flaming) and emission factor (mass of the considered species / mass of biomass burned). Depending on the approach, these parameters can be derived using satellite data and/or biogeochemical model, or through simpler IPCC default approaches. In this study, we use five products to estimate biomass burning emissions. The Global Fire Emission Database (GFED) is the most widely used global biomass burning emission dataset and provides estimates from 1997 onwards. Here, we use GFEDv4.1s (van der Werf et al., 2017), based on the Carnegie-Ames-Stanford-Approach (CASA) biogeochemical model

773 (van der Werf et al., 2010) driven by satellite derived vegetation characteristics and burned area mostly from the MODerate  
 774 resolution Imaging Sensor, MODIS (Giglio et al., 2013). GFEDv4.1s (with small fires) is available at a 0.25° resolution and  
 775 on a daily basis from 1997 to 2020. One characteristic of the GFEDv4.1s burned area is that small fires are better accounted  
 776 for compared to GFEDv4.1 (Randerson et al., 2012), increasing carbon emissions by approximately 35% at the global scale.  
 777 The latest version GFEDv5 (Chen et al., 2023) suggest 61% higher burned area than GFEDv4.1s, in closer agreement with  
 778 burned area products from higher resolution satellite sensors. The next budget would benefit from GFEDv5 to revisit the  
 779 estimates of biomass burning emissions (which would likely go up) based on more specific comparison studies.  
 780 The Quick Fire Emissions Dataset (QFED) is calculated using the fire radiative power (FRP) approach, in which the thermal  
 781 energy emitted by active fires (detected by MODIS) is converted to an estimate of CH<sub>4</sub> flux using biome specific emissions  
 782 factors and a unique method of accounting for cloud cover. Further information related to this method and the derivation of  
 783 the biome specific emission factors can be found in Darnenov and da Silva (2015). Here we use the historical QFEDv2.5  
 784 product available daily on a 0.1x0.1 grid for 2000 to 2020.  
 785 The Fire INventory from the National Center for Atmospheric Research (FINNv2.5, Wiedinmyer et al., 2023) provides  
 786 daily, 1 km resolution estimates of gas and particle emissions from open burning of biomass (including wildfire, agricultural  
 787 fires and prescribed burning) over the globe for the period 2002-2020. FINNv2.5 uses MODIS and VIIRS satellite  
 788 observations for active fires, land cover and vegetation density.  
 789 We use v1.3 of the Global Fire Assimilation System (GFAS, Kaiser et al., 2012), which calculates emissions of biomass  
 790 burning by assimilating Fire Radiative Power (FRP) observations from MODIS at a daily frequency and 0.5° resolution and  
 791 is available for 2000-2020.  
 792 The FAO-CH<sub>4</sub> yearly biomass burning emissions are based on the most recent MODIS 6 burned area products (Prosperi et  
 793 al., 2020), coupled with a pixel level (500 m) implementation of the IPCC Tier 1 approach, and are available from 1990 to  
 794 2020 (Table 1).  
 795 The differences in emission estimates for biomass burning arise from specific geographical and meteorological conditions  
 796 and fuel composition, which strongly impact combustion completeness and emission factors. The latter vary greatly  
 797 according to fire type, ranging from 2.2 g CH<sub>4</sub> kg<sup>-1</sup> dry matter burned for savannah and grassland fires up to 21 g CH<sub>4</sub> kg<sup>-1</sup>  
 798 dry matter burned for peat fires (van der Werf et al., 2010). Biomass burning emissions encountered large inter annual  
 799 variability related to meteorological conditions, with generally higher emissions during El-Nino periods as in 2019 (20 [14-  
 800 28] Tg CH<sub>4</sub> yr<sup>-1</sup>), 2015 (22 [15-28] Tg CH<sub>4</sub> yr<sup>-1</sup>) and 2010 to a lesser extent (18 [15-29] Tg CH<sub>4</sub> yr<sup>-1</sup>).  
 801 In this study, based on the five aforementioned products, biomass burning emissions are estimated at 17 Tg CH<sub>4</sub> yr<sup>-1</sup> [12-  
 802 24] for 2010-2019, representing about 5% of total global anthropogenic CH<sub>4</sub> emissions (Table 3).  
 803  
 804 **Biofuel burning.** Burning of biomass to produce energy for domestic, industrial, commercial, or transportation purposes is  
 805 hereafter called biofuel burning. A largely dominant fraction of CH<sub>4</sub> emissions from biofuel burning comes from domestic



806 cooking or heating in stoves, boilers, and fireplaces, mostly in open cooking fires where wood, charcoal, agricultural  
807 residues, or animal dung are burned. It is estimated that more than two billion people, mostly in developing countries, use  
808 solid biofuels to cook and heat their homes daily (André et al., 2014), and yet CH<sub>4</sub> emissions from biofuel combustion have  
809 received relatively little attention. Biofuel burning estimates are gathered from the CEDS, USEPA, GAINS and EDGAR  
810 inventories. Due to the sectoral breakdown of the EDGAR and CEDS inventories the biofuel component of the budget has  
811 been estimated as equivalent to the “RCO - Energy for buildings” sector as defined in Worden et al. (2017) and Hoesly et  
812 al. (2018) (Table S2). This is equivalent to the sum of the IPCC 1A4a\_Commercial-institutional, 1A4b\_Residential,  
813 1A4c\_Agriculture-forestry-fishing and 1A5\_Other-unspecified reporting categories. This definition is consistent with that  
814 used in Saunio et al. (2016) and Kirschke et al. (2013). While this sector incorporates biofuel use, it also includes the use  
815 of other combustible materials (e.g., coal or gas) for small-scale heat and electricity generation within residential and  
816 commercial premises. Data provided by the GAINS inventory suggests that this approach may overestimate biofuels  
817 emissions by between 5 and 50%. Further study into this category would be needed to better disentangle biofuels from fossil  
818 combustibles.  
819 In our study, biofuel burning is estimated to contribute 11 [8-14] Tg CH<sub>4</sub> yr<sup>-1</sup> to the global CH<sub>4</sub> budget, about 3% of total  
820 global anthropogenic CH<sub>4</sub> emissions for 2010-2019 (Table3).

821 **3.1.6 Other anthropogenic sources (not explicitly included in this study)**

822 Other anthropogenic sources not included in this study are related to agriculture and land-use management. In particular,  
823 increases in agricultural areas (such as global palm oil production) have led to the clearing of natural peat forests, reducing  
824 natural peatland area and associated natural CH<sub>4</sub> emissions. Peatlands planted to forests (like in Northern Europe) also lead  
825 to reduced CH<sub>4</sub> emissions. While studies have long suggested that CH<sub>4</sub> emissions from peatland drainage ditches are likely  
826 to be significant (e.g., Minkinen and Laine, 2006, Peacock et al., 2021), CH<sub>4</sub> emissions related to palm oil plantations have  
827 yet to be properly quantified (e.g., Manning et al, 2019). Taylor et al. (2014) have quantified global palm oil wastewater  
828 treatment fluxes to be 4 ± 32 Tg CH<sub>4</sub> yr<sup>-1</sup> for 2010-2013. This currently represents a small and highly uncertain source of  
829 methane but one potentially growing in the future.

830 **3.2 Natural and indirect anthropogenic sources**

831 As introduced in section 2.4, natural and indirect anthropogenic sources refer to pre-agricultural CH<sub>4</sub> emissions even if they  
832 are perturbed by anthropogenic climate change or other global change factors (e.g., eutrophication), and indirect emissions  
833 resulting from anthropogenic perturbation of the landscape (reservoirs) and the biogeochemical characteristics of soil. They  
834 include vegetated wetland emissions and inland freshwater systems (lakes, small ponds, reservoirs, and rivers), land  
835 geological sources (gas-oil seeps, mud volcanoes, microseepage, geothermal manifestations, and volcanoes), wild animals,  
836 wildfires, termites, thawing terrestrial and marine permafrost, and coastal and oceanic sources (biogenic, geological and

hydrate). In water-saturated or flooded ecosystems, the decomposition of organic matter gradually depletes most of the oxygen in the soil or the sediment zone, resulting in anaerobic conditions and CH<sub>4</sub> production. Once produced, CH<sub>4</sub> can reach the atmosphere through a combination of three processes: (1) diffusive loss of dissolved CH<sub>4</sub> across the air-water boundary; (2) ebullition flux from sediments; and (3) flux mediated by emergent aquatic macrophytes and terrestrial plants (plant transport). On its way to the atmosphere, in the soil or water columns, CH<sub>4</sub> can be partly or completely oxidised by microorganisms, which use CH<sub>4</sub> as a source of energy and carbon (USEPA, 2010b). Concurrently, methane from the atmosphere can diffuse into the soil column and be oxidised (See Sect. 3.3.4 on soil uptake).

### 3.2.1 Wetlands

Wetlands are generally defined as ecosystems in which mineral or peat soils are water-saturated at some depth or where surface inundation (permanent or not) has a dominating influence on the soil biogeochemistry and determines the ecosystem species composition (USEPA, 2010b). To refine such an overly broad definition for CH<sub>4</sub> emissions, we define wetlands as ecosystems with inundated or saturated soils or peats where anaerobic conditions below the water table lead to CH<sub>4</sub> production (Matthews and Fung, 1987; USEPA, 2010b). Brackish water emissions are discussed separately in Sect. 3.2.6. Our definition of wetlands includes ombrotrophic and minerotrophic peatlands (i.e., bogs and fens), mineral soil wetlands (swamps and marshes), and seasonal or permanent floodplains. It excludes exposed water surfaces without emergent macrophytes, such as lakes, rivers, estuaries, ponds, and reservoirs (addressed in the next section), as well as rice agriculture (see Sect. 3.1.4, rice cultivation paragraph), and wastewater ponds. It also excludes coastal vegetated ecosystems (mangroves, seagrasses, salt marshes) with salinities usually >0.5 (See Sect. 3.2.6). Even with this definition, some wetlands could be considered as anthropogenic systems, being affected by human land-use changes such as impoundments, drainage, or restoration (Woodward et al., 2012). In the following, we retain the generic denomination “wetlands” for natural and human-influenced wetlands, as discussed in Sect. 2.2.

The three most important factors influencing CH<sub>4</sub> production in wetlands are the spatial and temporal extent of anoxia (linked to water saturation), temperature, and substrate availability (Valentine et al., 1994; Wania et al., 2010; Whalen, 2005; Delwiche et al., 2021; Knox et al., 2021).

Land surface models estimate CH<sub>4</sub> emissions through a series of processes, including CH<sub>4</sub> production, oxidation, and transport. The models are then forced with inputs accounting for changing environmental factors (Melton et al., 2013; Poulter et al., 2017; Tian et al., 2010; Wania et al., 2013; Xu et al., 2010). CH<sub>4</sub> emissions from wetlands are computed as the product of an emission flux density and a CH<sub>4</sub> producing area or surface extent (see Supplementary Material; Bohn et al., 2015; Melton et al., 2013). The areal extent of different wetland types (having large differences in areal CH<sub>4</sub> emission rates) appears to be a primary contributor to uncertainties in the absolute flux of CH<sub>4</sub> emissions from wetlands, with meteorological response being the main source of uncertainty for seasonal and interannual variability (Poulter et al., 2017; Kuhn et al., 2021; Parker et al., 2022; McNicol et al., 2023; Karlson and Bastviken 2023). However, large uncertainty

remains in both spatial and temporal emission distributions, especially over tropical wetlands where data are lacking to evaluate the models but are nevertheless a key region for climate feedbacks (Nisbet, 2023; Zhang et al., 2023). Direct measurement campaigns and remote sensing are providing key insights where to improve the land surface models (e.g., France et al., 2022; Shaw et al., 2022).

In this work, sixteen land surface models computing net CH<sub>4</sub> emissions (Table 2) were run under a common protocol with a spin-up using repeated climate data from 1901-1920 to pre-industrial conditions followed by a transient simulation through the end of 2020. Of the 16 models, 13 previously contributed to Saunio et al. (2020), and three models were new to this release (CH4MOD<sub>wetland</sub> (Li et al., 2010), ISAM (Shu et al., 2020; Xu et al., 2021), and SDGVM (Beerling and Woodward, 2001; Hopcroft et al., 2011; Hopcroft et al., 2020)) (Table 2, see also in the Supplementary Material Table S3 for a history of the contributing models). Climatic forcing uncertainties are considered in the ensemble estimate by using two climate datasets, CRU/CRU-JRA55 (Harris, 2014) and GSWP3-W5E5 (Dirmeyer et al., 2006; Kim 2017; Lange, 2019; Cucchini et al., 2020). Atmospheric CO<sub>2</sub> was also prescribed in the models. For all models, two wetland area dynamic schemes were applied: a diagnostic scheme using a remote sensing-based wetland area and dynamics dataset called WAD2M (Wetland Area Dynamics for Methane Modeling; Zhang et al., 2021a; 2021b) available at 0.25 degree of horizontal resolution, as in Saunio et al. (2020), and a prognostic scheme using internal model-specific hydrologic models.

The diagnostic wetland extent product WAD2Mv1.0 (Zhang et al., 2021a) has been updated since Saunio et al. (2020) to WAD2Mv2.0 (Zhang et al., 2021b) and extended to 2020. It uses the same Surface Water Microwave Product Series (SWAMPSv3.2) for capturing inundation dynamics (Jenson and McDonald, 2019), which was extended to 2020. To reduce potential double-counting with the freshwater budget, the surface areas of rivers/streams and lakes/ponds are excluded by using the products Global River Widths from Landsat (GRWL) database v01.01 (Allen and Pavelsky, 2018) and HydroLakes v1.0 (Messenger et al., 2016), instead of the Global Surface Water (GSW) product (Pekel et al., 2016) used in WAD2Mv1.0. The GRWL and Hydrolakes are also the datasets used separately in the upscaling of the freshwater budget allowing for a more consistent approach between the wetland and freshwater CH<sub>4</sub> budgets (Sect. 3.2.2). This update in WAD2M leads to a downward revised annual average wetland extent by 0.5 Mkm<sup>2</sup> for the mid-high latitudes (mainly due to larger lake extent in HydroLakes than in the GSW dataset) with small impacts in other regions. However, since HydroLakes includes only vectorized lakes larger than 0.1 km<sup>2</sup>, smaller lakes/ponds under 0.1 km<sup>2</sup> are implicitly still included as wetlands in WAD2Mv2.0. For the high-latitude region, the recent peatland extent product from Hugelius et al. (2020) is applied, which indicates a slightly higher peatland area by 0.2 Mkm<sup>2</sup> primarily in regions above 60°N, compared to the Northern Circumpolar Soil Carbon Database (NCSCD) product (Hugelius et al., 2013) used in WAD2Mv1.0. Rice agriculture was removed using the Monthly Irrigated and Rainfed Crop Areas (MIRCA2000, Portmann et al. (2010)) dataset from circa 2000, as a fixed distribution.

The combined remote-sensing and inventory WAD2Mv2.0 product leads to a maximum wetland area of 13.6 Mkm<sup>2</sup> during the peak season (7.9 Mkm<sup>2</sup> on annual average, with a range of 7.5 to 8.4 Mkm<sup>2</sup> from 2000-2020, about 5.2% of the global

land surface). The largest wetland areas in WAD2Mv2.0 are in Amazonia, the Congo Basin, and the Western Siberian Lowlands, which in previous studies were underestimated by inventories (Bohn et al., 2015). However, the SWAMPS v3.2 dataset which serves as a proxy of temporal variations of wetland extent, has discontinuity issues over a few tropical hotspots since 2015 and hence affects the temporal variations of WAD2M. Consequently, this affects CH<sub>4</sub> emissions estimates for a subset of land surface models that are particularly sensitive to inundation in these hotspots. Meanwhile, prognostic estimates show moderate consistency in capturing the spatial distribution of wetland area with WAD2M, with an annual average wetland area of  $8.0 \pm 2.0$  Mkm<sup>2</sup> during the peak season for 2000-2020. The ensemble mean of annual wetland area anomaly by the prognostic models show reasonable agreement with satellite-based estimates in capturing the response of wetland area to climate variations (Zhang et al., in review), with higher agreement over temperate and boreal regions than in the tropics.

For the wetland methane emissions estimate, we use the decadal mean from the prognostic runs and adjust these flux estimates for double counting from inland waters (described in next section) given the reliance of the prognostic models on satellite flooded area data like WAD2Mv2 to parameterize maximum wetland extent (Zhang et al., in review). The average emission from wetlands for 2010-2019 for the 16 models is plotted in Fig. 3. The zones with the largest emissions are the Amazon basin, equatorial Africa and Asia, Canada, western Siberia, eastern India, and Bangladesh. Regions where CH<sub>4</sub> emissions have high inter-model agreement (defined as regions where mean flux is larger than the standard deviation of the models, on a decadal mean) represent 72% of the total CH<sub>4</sub> flux due to natural wetlands. The different sensitivities of the models to temperature, vapour pressure, precipitation, and radiation can generate substantially different patterns, such as in India. Emission estimates over regions with lower emissions (in total) are also consistently inferred between models (e.g., Scandinavia, Continental Europe, Eastern Siberia, Central United States of America, and Southern Africa).

The resulting global flux range for vegetated wetland emissions from the prognostic runs is 117-195 Tg CH<sub>4</sub> yr<sup>-1</sup> for the 2000-2020 period, with an average of 157 Tg CH<sub>4</sub> yr<sup>-1</sup> and a one-sigma standard deviation of 24 Tg CH<sub>4</sub> yr<sup>-1</sup>. Using the prognostic set of simulations, the average ensemble emissions were 159 [119-203] Tg CH<sub>4</sub> yr<sup>-1</sup> for the 2010-2019 period (Table 3). The estimated average ensemble annual total from the two sets of simulations by CRU/CRU-JRA55 and GSWP3-W5E5 are 158 [126-193] and 158 [118-203] for 2010-2019, respectively. Generally, the magnitude and interannual variability agree between these two sets of simulations (Zhang et al., 2024). Wetland emissions represent about 25% of the total (natural plus anthropogenic) CH<sub>4</sub> sources estimated by bottom-up approaches. The large range in the estimates of wetland CH<sub>4</sub> emissions results from difficulties in defining wetland CH<sub>4</sub> producing areas as well as in parameterizing terrestrial anaerobic conditions that drive sources and the oxidative conditions leading to sinks (Melton et al., 2013; Poulter et al., 2017; Wania et al., 2013). The ensemble mean emission using the same simulation setup (i.e., diagnostic wetland extent and CRU/CRU-JRA55) in the models is 163 [117-195] Tg CH<sub>4</sub> yr<sup>-1</sup>, higher by ~22 Tg CH<sub>4</sub> yr<sup>-1</sup> than the one previously reported (see Table 3, for 2000-2009 with comparison to Saunio et al., 2020). This difference is mainly due to the updated

934 model structure and parameterizations in the wetland CH<sub>4</sub> models compared to the versions in the previous budget and the  
935 inclusion of three new land surface models.  
936 For the last decade 2010-2019, we report in this budget an average ensemble estimate of 159 Tg CH<sub>4</sub> yr<sup>-1</sup> with a range of  
937 119-203 (based on prognostic wetland extent runs, Table 3) .

### 938 **3.2.2 Inland freshwater ecosystems (lakes, ponds, reservoirs, streams, rivers)**

939 This category includes CH<sub>4</sub> emissions from freshwater systems (lakes, ponds, reservoirs, streams, and rivers). Numerous  
940 advances have been made in the freshwater greenhouse gases knowledge base in the last few years (Lauerwald et al., 2023a).  
941 These advances include improvements in the underlying databases used to estimate inland water surface areas and model  
942 their dynamics, a rapidly growing number of direct measurements of methane fluxes, and improvements in our process-  
943 based understanding of methane biogeochemistry. Despite this, aspects of global freshwater methane estimates remain rather  
944 crude and continue to have large uncertainties. This includes the overall temperature dependency of methane emissions, the  
945 relative role of ebullition (i.e., bubble flux, which may represent the most important, but most difficult-to-capture emission  
946 path in many standing water bodies), fluxes from the smallest standing water bodies (sometimes referred to as ponds) having  
947 large emissions per m<sup>2</sup> but uncertain area extent, and the magnitude of anthropogenic influence on emissions, all which are  
948 discussed below.

949  
950 **Streams and rivers.** The last global CH<sub>4</sub> budget used an estimate of 27 Tg CH<sub>4</sub> yr<sup>-1</sup> for global streams and rivers based  
951 largely on a data compilation by Stanley et al. (2016). This estimate was scaled from a simple data compilation without a  
952 spatial component or an estimate of ebullition. More recently, Rosentreter et al. (2021) performed a new data compilation  
953 of 652 flux estimates, including diffusive and ebullitive fluxes, coupled to an ice corrected surface area estimate of ~625,000  
954 km<sup>2</sup> that was aggregated to 5 latitudinal bands to come up with a global estimate of 6 and 31± 17 Tg CH<sub>4</sub> yr<sup>-1</sup> (respectively  
955 for the median and mean ± c.i. 95%). We believe, due to better data representation in underlying datasets, that the mean  
956 estimate of Rosentreter et al. (2021) is more representative statistically because the median does not capture hotspots and  
957 hot moments of intense ebullitive fluxes. Finally, Rocher-Ros et al. (2023) used a new Global River Methane (GRiMeDB)  
958 database (Stanley et al., 2023) with > 24,000 observations of CH<sub>4</sub> concentrations to predict ~28±17 Tg CH<sub>4</sub> yr<sup>-1</sup> (±c.i. 95%)  
959 river emissions globally. This approach used machine learning methods coupled to the latest spatially and temporally explicit  
960 mapping of monthly stream surface area (the smallest streams are still extrapolated) which incorporates drying and freezing  
961 effects (yearly average 672,000 km<sup>2</sup>, Liu et al., 2022) and includes an ebullitive flux estimated from a correlation between  
962 measured diffusive and ebullitive emissions in the GRiMeDB database (Stanley et al., 2023). Thus, for this study we use an  
963 estimate of 29±17 (±c.i. 95%) Tg CH<sub>4</sub> yr<sup>-1</sup> for streams and rivers (Figure 4), which averages the mean estimate of Rosentreter  
964 et al. (2021) and Rocher-Ros et al. (2023). Currently, ebullitive fluxes remain a major unknown quantity in streams and  
965 rivers but appear to be coarsely linearly correlated in a log-space to diffusive fluxes and of similar magnitude (Rocher-Ros

et al., 2023). Methodologically, the high-water velocity of many streams and rivers make measurement of ebullitive fluxes challenging (Robison et al., 2021). Effluxes are also linked to hydrology (Aho et al., 2021) although very few studies have sampled over a representative hydrograph. Plant-mediated effluxes of CH<sub>4</sub> in running waters also remain difficult to constrain, with a recent compilation highlighting very few measurements (Bodmer et al. 2024). Connected adjacent wetlands is a common source of CH<sub>4</sub> to streams and rivers (Borges et al., 2019) which may be important for the regulation of running water emissions but is currently difficult to assess at the global scale. Overall, the poor representation of sites and deficient mechanistic understanding make it difficult to model and predict methane evasion from streams and rivers using process-based models.

**Lakes and ponds.** The previous global CH<sub>4</sub> budget used an estimate of 71 Tg CH<sub>4</sub> yr<sup>-1</sup> for lakes and 18 Tg CH<sub>4</sub> yr<sup>-1</sup> for reservoirs. These estimates were based on an early study by Bastviken et al. (2011) coupled with a newer estimate for lakes north of 50°N (Wik et al., 2016b). There have been three new lake studies that have published their data with global estimates of 56 and 151± 73 (Rosentreter et al., 2021; respectively for the median and mean ± c.i. 95%, 22±8 (Zhuang et al., 2023; ±lake-area-weighted normalised RMSE for all parameterized lake types), process-based model), and 41±36 Tg CH<sub>4</sub> yr<sup>-1</sup> (Johnson et al., 2022, mean ±c.i. 95%). This large range in estimated emissions can be attributed to the differences in the datasets and methods used to calculate the surface area of small waterbodies, as well as the differences between how the flux data were analyzed and extrapolated between studies. For instance, total surface areas of all lakes and ponds of 3712-5688 × 10<sup>3</sup> km<sup>2</sup> (Rosentreter et al., 2021) and 2806 × 10<sup>3</sup> km<sup>2</sup> (Johnson et al., 2022) were used along with measurement data from 198 and 575 individual lake systems, respectively. In contrast, Zhuang et al. (2023) generated estimates using higher temporal resolution data from just 54 lakes to build a process-based model, which generated much lower flux estimates from tropical lakes than previously implemented statistical approaches, but in line with the most recent assessments by Borges et al. (2022). For this study, we explicitly excluded lakes <0.1 km<sup>2</sup> which are treated separately (see below). If we re-assess these three studies for only lakes greater than 0.1 km<sup>2</sup>, we obtain global effluxes of 17 and 42.9±20.8 Tg CH<sub>4</sub> yr<sup>-1</sup> (Rosentreter et al. (2021); median and mean ± c.i. 95% of global flux), 21.9±8.0. (Zhuang et al., 2023, ±lake-area-weighted normalised RMSE for all parameterized lake types), and 35.3±31.0 Tg CH<sub>4</sub> yr<sup>-1</sup> (Johnson et al. 2022, ±95% C.I.) (with areas of 2556-3468 ×10<sup>3</sup>, 2640×10<sup>3</sup>, and 2676×10<sup>3</sup> km<sup>2</sup> respectively). Thus, for lakes >0.1 km<sup>2</sup>, we propose an efflux of 33±26 Tg CH<sub>4</sub> yr<sup>-1</sup> (an average of the mean from Rosentreter et al., 2021 Zhuang et al., 2023, and Johnson et al., 2022, with the average c.i. 95% from Rosentreter et al., 2021 and Johnson et al. 2022) as represented in Figure 4.

Small waterbody emissions, hereafter small lakes and ponds<0.1 km<sup>2</sup>, remain difficult to assess. Evidence is emerging that there is a lower limit to the power scaling laws that early studies used to extrapolate the surface area of these small systems (Bastviken et al., 2023; Kyzivat et al., 2022). Thus, for small lakes and ponds < 0.1 km<sup>2</sup> (and >0.001 km<sup>2</sup>), we disregard the higher end surface area used in Rosentreter et al., 2021 which relied on these earlier estimates and scale their numbers to the evasion estimates to the lower end surface area of 1,002×10<sup>3</sup> to obtain a mean flux of 33 Tg CH<sub>4</sub> yr<sup>-1</sup> (Rosentreter et al.,

2021). Johnson et al. (2022) estimated a surface area of only 166x103 km<sup>2</sup> for this size class to obtain an efflux of 6.3 Tg CH<sub>4</sub> yr<sup>-1</sup>, which we acknowledge as a lower limit. Averaging these two values provide a conservative estimate of [6-33] Tg CH<sub>4</sub> yr<sup>-1</sup>, which is close to the number proposed by Holgerson and Raymond (2016) for diffusion effluxes only for this size class. The experts involved in this assessment have low confidence in this estimate. This estimate also does not include artificial ponds, which we discuss below. As a result, combined CH<sub>4</sub> emissions from large lakes (>0.1 km<sup>2</sup>) and small lakes and ponds (<0.1km<sup>2</sup>) are estimated at 53 [19-86] Tg CH<sub>4</sub> yr<sup>-1</sup> (Figure 4), which is lower than the 71 Tg estimated in the previous budget.

**Reservoirs.** New mean estimates of diffusive + ebullitive CH<sub>4</sub> emissions from reservoirs include 15 and 24±8 (the median and mean± c.i. 95% from Rosentreter et al., 2021), 10±4 (Johnson et al., 2021, mean±95% C.I.), 10 (Harrison et al., 2021, low and high c.i. 95% 7 and 22, respectively), and 2.1 Tg CH<sub>4</sub> yr<sup>-1</sup> (Zhuang et al., 2023). We compile the first three estimates to a direct efflux of ~14 Tg CH<sub>4</sub> yr<sup>-1</sup> (with ± c.i. 95% of 9 and 23). We note the fourth estimate as a lower bound, but exclude it from this budget given that it was generated via a model that only included data from six reservoir systems (Zhuang et al., 2023). We also add in an additional 12 Tg CH<sub>4</sub> yr<sup>-1</sup> (c.i. 95% 7 and 37) that is estimated to degas in dam turbines (Harrison et al., 2021), which was not addressed in the studies by Rosentreter et al. (2021), Zhuang et al. (2023), or Johnson et al. (2021). Rocher-Ros et al. (2023) also excluded river observations below dams when executing their statistical model, and so did not capture downstream dam emissions. Thus, we use a direct reservoir emission here of ~13 [6-28] Tg CH<sub>4</sub> yr<sup>-1</sup> and estimate an additional ~12 [7-37] Tg CH<sub>4</sub> yr<sup>-1</sup> from dam turbine degassing fluxes, giving a total of 25 [13-65] Tg CH<sub>4</sub> yr<sup>-1</sup> from reservoirs (Figure 4).

**Uncertainties and confidence levels.** The emission estimates of lakes, reservoirs and ponds described above are limited by several uncertainties. First, a major unknown for lakes remains the size cut off and the representation of small lakes and ponds (Deemer and Holgerson, 2021), which are also more variable than larger water bodies in their CH<sub>4</sub> concentrations and fluxes (Rosentreter et al. 2021, Ray et al., 2023). Interestingly, there is also a lack of methane data representation from large lakes that are a large component of global lake surface area (Deemer and Holgerson, 2021; Messenger et al., 2016). There is also a growing knowledge base on the importance of high CH<sub>4</sub> fluxes from lake littoral zones that is not yet well incorporated into global scaling efforts (e.g., Grinham et al., 2011; Natchimuthu et al., 2016), and emergent vegetation (Bastviken et al., 2023; Kyzivat et al., 2022). Ebullition is more constrained in lakes/reservoirs compared to streams/rivers but is still difficult to measure and model accurately. Finally, for all inland water systems a greater scrutiny for the limiting factors (including the impact of ice-cover and seasonality, stratification of the water column) of different CH<sub>4</sub> production, consumption and transport pathways is needed. In addition, a better understanding of the climatic, environmental and geomorphological controls on key CH<sub>4</sub> processes (e.g., sedimentary diffusive and ebullitive production, bubble dissolution, CH<sub>4</sub> oxidation) on the large-scale remains critically needed. For instance, the consistently lower global emissions determined

1032 by the process-based model of Zhuang et al. (2023) compared to observations, suggest that current datasets are too limited  
1033 to fully capture the spatio-temporal variability in CH<sub>4</sub> dynamics and their key control factors, possibly leading to biased-  
1034 high estimates.

1035 The majority of the inland water CH<sub>4</sub> estimates are from a limited number of studies, some without spatial representation or  
1036 reported statistical uncertainties. Furthermore, as mentioned above the knowledge base of the surface area of these  
1037 ecosystems is new and rapidly expanding, but not standardised between studies leading to uncertainty (but see Lauerwald  
1038 et al. 2023b), particularly for ponds. For this study, we are able to provide confidence intervals from the original studies for  
1039 all fluxes except the smallest lake/pond size class.

1040  
1041 **The Surface Area of Inland Freshwaters.** For all of these ecosystems, determining their surface area remains a central  
1042 challenge. Since the last GMB, several methodological advances have reduced the uncertainty associated with the surface  
1043 area estimates of rivers, streams, lakes, and reservoirs. Using a single geospatial dataset that includes both lakes and  
1044 reservoirs (Messenger et al., 2016) has decreased double counting of lakes and reservoirs (Johnson et al., 2022; Rosentreter  
1045 et al., 2021). For rivers and streams, high-resolution global streamflow simulations, informed by satellite observations,  
1046 enabled a much finer scale estimate of surface areas for rivers with a new temporal component (Allen and Pavelsky, 2018;  
1047 Lin et al., 2019; Liu et al., 2022), although the surface for the smaller streams are still estimated indirectly, and mapping of  
1048 human-created drainage ditches and canals is lacking. Seasonal ice cover and melt turnover corrections also have been newly  
1049 incorporated into rivers, streams, lakes, and reservoirs (Harrison et al., 2021; Johnson et al., 2022; Lauerwald et al., 2023b;  
1050 Rocher-Ros et al., 2023; Rosentreter et al., 2021; Zhuang et al., 2023). Finally, removing open water body surface areas  
1051 from wetland surface areas based on geographic location has reduced double counting between these two land cover types,  
1052 as described in the wetlands section of the GMB. Yet, the surface area of small lakes and ponds (<0.1 km<sup>2</sup>) is still highly  
1053 uncertain, and new techniques for counting these systems and determining the overlap with wetland data bases is paramount.

1054  
1055 **Anthropogenic Contributions to Inland Freshwater Emissions.** We argue that all reservoirs should be categorised as a  
1056 direct anthropogenic source of emissions. Most of the surface area of reservoirs are human-made and reservoir construction  
1057 leads to anoxic sediments and/or bottom waters with labile organic matter sourced from the watershed and to in-situ nutrient  
1058 augmented phytoplankton production (Deemer et al., 2016; Maavara et al., 2017; Prairie et al., 2018). It is also clear that the  
1059 cultural eutrophication of natural lakes driven by run-off of agricultural nitrogen fertilizer and manure is augmenting  
1060 CH<sub>4</sub> emissions (DelSontro et al., 2018; Li et al., 2021), with shallow lakes particularly likely to experience eutrophication  
1061 (Qin et al., 2020). For instance, Beaulieu et al. (2019) modelled a 15% reduction in lake CH<sub>4</sub> with a 25% reduction in lake  
1062 phosphorus concentrations. Several recent studies have estimated that anywhere between 30 and 50% of lakes are eutrophic  
1063 (Cael et al., 2022; Qin et al., 2020; Sayers et al., 2015; Wu et al., 2022). These studies estimate numerical percentages (one  
1064 by depth class: Qin et al., 2020), but none have estimated the percent of lake surface area that is eutrophic nor have any



1065 determined the extent of anthropogenic vs. natural eutrophication. Still, numerous studies have noted widespread increases  
 1066 in eutrophication indicators across lakes due to nutrient loading and warming (Griffiths et al., 2022; Ho et al., 2019; Taranu  
 1067 et al., 2015), thus we estimate that  $\frac{1}{3}$ , or 11 Tg CH<sub>4</sub> yr<sup>-1</sup> of CH<sub>4</sub> emissions from lakes >0.1 km<sup>2</sup> could be anthropogenic  
 1068 (Figure 4). Similarly, CH<sub>4</sub> emissions from small lakes and ponds are influenced by human factors, with emissions increasing  
 1069 with eutrophication (Deemer and Holgerson, 2021), erosion and runoff in agricultural landscapes (Heathcote et al., 2013),  
 1070 and warming, the latter likely to have a disproportionately greater effect in small, shallow systems (Woolway et al., 2016).  
 1071 Thus, we adopt the same  $\frac{1}{3}$  number as for lakes for the proportion of anthropogenic emissions in small lakes and ponds  
 1072 (<0.1 km<sup>2</sup>), which amounts to 6 Tg CH<sub>4</sub> yr<sup>-1</sup> (Figure 4).  
 1073 There are also human-made small lakes and ponds, notably for agriculture, aquaculture, and recreation, that generally have  
 1074 conditions favourable for high CH<sub>4</sub> emissions (Downing, 2010; Holgerson and Raymond, 2016; Malerba et al., 2022;  
 1075 Ollivier et al., 2019; Zhao et al., 2021; Dong et al., 2023). Downing (2010) estimated that farm ponds comprise a global  
 1076 surface area of ~77,000 km<sup>2</sup>; using a conservative emission rate of 265 mg CH<sub>4</sub> m<sup>-2</sup> d<sup>-1</sup> and an ice correction factor of 0.6  
 1077 leads to an emission of 4.5 Tg yr<sup>-1</sup> that is anthropogenically sourced from farm ponds. Here the value is rounded to 5 Tg yr<sup>-1</sup>  
 1078 (Figure 4). Clearly, more work is required to assess the anthropogenic component of CH<sub>4</sub> emissions from lakes and ponds.  
 1079 It remains difficult to parse out an anthropogenic component to stream and river CH<sub>4</sub> fluxes. Although some studies have  
 1080 noticed a temperature dependence with stream sediments (Comer-Warner et al., 2018; Zhu et al., 2020), Rocher-Ros et al.  
 1081 (2023) noted a small temperature dependence of CH<sub>4</sub> emissions in streams and rivers compared to other freshwater  
 1082 ecosystems, potentially due to the many other external processes affecting fluxes in these dynamic flowing ecosystems.  
 1083 Urbanisation can lead to elevated river CH<sub>4</sub> emissions, particularly in regions with elevated organic matter and nutrient  
 1084 loading due to limited wastewater treatment (Begum et al., 2021; Nirmal Rajkumar et al., 2008; Wang et al., 2021a). Some  
 1085 studies have found agricultural streams and ditches can have higher effluxes due to inputs of fine sediments (Comer-Warner  
 1086 et al., 2018; Crawford and Stanley, 2016), organic carbon, and nutrients (Borges et al., 2018) that lead to in-situ methane  
 1087 production. Furthermore, the creation of drainage ditches in organic soils tap CH<sub>4</sub> rich waters from water-logged horizons  
 1088 and heighten emissions from ex-situ sources (Peacock et al., 2021), although limitations in both the geographic scope of  
 1089 existing ditch emission estimates our ability to estimate global surface area of ditches precludes their inclusion in this budget.  
 1090 Finally, extremely high rates of CH<sub>4</sub> emission have been linked to ongoing permafrost thaw in Asia's Qinghai-Tibet Plateau  
 1091 (Zhang et al., 2020). However, the loss and disconnection of wetlands to rivers may have resulted in a decrease in the input  
 1092 of dissolved CH<sub>4</sub> from this source. A recent expert elicitation (Rosentreter, et al. 2024) reported that 35% of all inland  
 1093 freshwater sources were anthropogenic and given that some of the river flux is from upstream reservoirs, we assign a 30%  
 1094 anthropogenic contribution to the stream and river flux (9 Tg CH<sub>4</sub> yr<sup>-1</sup>, Figure 4), which approximates the expert elicitation  
 1095 via the impact of eutrophication and urban influences.  
 1096

1097 **Combination (lakes, ponds, reservoirs, streams and rivers, farm ponds).** Combining the aforementioned emissions from  
1098 lakes  $>0.1 \text{ km}^2$  (33 [13-53]  $\text{Tg CH}_4 \text{ yr}^{-1}$ ), small lakes and ponds  $< 0.1 \text{ km}^2$  (20 [6-33]  $\text{Tg CH}_4 \text{ yr}^{-1}$ ), reservoirs (25 [13-65]  
1099  $\text{Tg CH}_4 \text{ yr}^{-1}$ ), streams and rivers (29 [12-46]  $\text{Tg CH}_4 \text{ yr}^{-1}$ ) and farm ponds (5  $\text{Tg CH}_4 \text{ yr}^{-1}$ ), leads to a total of  $\sim 112 \text{ Tg CH}_4$   
1100  $\text{yr}^{-1}$  from freshwater systems, with a range of [49-202]  $\text{Tg CH}_4 \text{ yr}^{-1}$ . This estimate is about 50  $\text{Tg}$  lower than in Sauniois et  
1101 al. (2020) and is broadly consistent with the recent regionalized estimate by Lauerwald et al. (2023b) compiled for the  
1102 Regional Carbon Cycle Assessment and Processes (RECCAP2, <https://www.globalcarbonproject.org/reccap/>; 103  $\text{Tg CH}_4$   
1103  $\text{yr}^{-1}$ , IQR= 82.1–134.8). The updated budget from these ecosystems and their anthropogenic components are represented i  
1104 n Fig. 4. The gridded products for emissions from lakes and ponds by Johnson et al. (2022), from reservoirs by Johnson et  
1105 al. (2021) and from streams and rivers by Rocher-Ros et al. (2023) have been combined into a single map presented in Fig.  
1106 5.

1107  
1108 **Double-counting inland freshwater ecosystems in the bottom-up estimates.** To address the differences found between  
1109 bottom-up and top-down  $\text{CH}_4$  budgets, and to acknowledge advances in addressing the central issue of double counting  $\text{CH}_4$   
1110 emissions for inland freshwater ecosystems, we introduce here a new correction term. Historically, the bottom-up estimate  
1111 of global  $\text{CH}_4$  emissions has been higher than the top-down estimate, first recognized in Kirschke et al. (2013) and confirmed  
1112 in Sauniois et al. (2016, 2020). The larger bottom-up emissions estimate has been partly attributed to double-counting  
1113 vegetated wetland emissions with inland freshwater emissions (including lakes, ponds, rivers, streams, and reservoirs) and  
1114 also the emissions of  $\text{CH}_4$  produced in vegetated wetlands and then transported via aquatic processes and emitted from  
1115 inland freshwaters (Pangala et al., 2017; Kirk and Cohen, 2023). The Sauniois et al. (2020)  $\text{CH}_4$  budget addressed the issue  
1116 of double counting through the use of a revised vegetated wetland area dataset, WAD2M v1.0 (Zhang et al., 2021), that  
1117 removed inland waters from the SWAMPS (Jenson and McDonald, 2019) surface-inundation dataset, allowing for  
1118 independent vegetated wetlands and inland freshwater  $\text{CH}_4$  emissions to be compiled. Yet, the Sauniois et al. (2020)  $\text{CH}_4$   
1119 budget still had a  $\sim 150 \text{ Tg CH}_4 \text{ yr}^{-1}$  difference between bottom-up and top-down estimates. In this budget, we refined the  
1120 vegetated wetland area dataset with WAD2M v2.0 (see section 3.2.1, where HydroLakes is used to remove lakes and ponds  
1121  $>0.1 \text{ km}^2$ ). Additionally, we applied numbers from peer-reviewed publications and expert elicitation to account for lateral  
1122  $\text{CH}_4$  flux emissions. This most recent bottom-up budget estimates 159 [119-203]  $\text{Tg CH}_4 \text{ yr}^{-1}$  from vegetated wetlands for  
1123 2010-2019 and 112  $\text{Tg CH}_4 \text{ yr}^{-1}$  from inland freshwaters that includes 83  $\text{Tg CH}_4 \text{ yr}^{-1}$  from lakes, ponds, and reservoirs and  
1124 29  $\text{Tg CH}_4 \text{ yr}^{-1}$  from rivers and streams, leading to a combined wetland and inland freshwater flux of 271  $\text{Tg CH}_4 \text{ yr}^{-1}$ . Here,  
1125 we propose a correction of 20  $\text{Tg CH}_4 \text{ yr}^{-1}$  to account for double counting of small lakes and ponds ( $< 0.1 \text{ km}^2$ ) that are  
1126 likely included in our vegetated wetlands estimate, and removing 1-3  $\text{Tg CH}_4 \text{ yr}^{-1}$  from river emissions due to lateral  
1127 transport of  $\text{CH}_4$  originating in adjacent vegetated wetlands. The river flux correction arises from assuming that for  
1128 catchments with  $>10\%$  wetlands, rivers provide 5-10% of vegetated  $\text{CH}_4$  emissions. The total double-counting correction  
1129 term of 23  $\text{Tg CH}_4$  reduces the bottom-up budget for combined wetlands and inland waters from 271  $\text{Tg CH}_4 \text{ yr}^{-1}$  to 248  $\text{Tg}$

CH<sub>4</sub> yr<sup>-1</sup> (see Fig. 4 and Table 3). Comparing the 2000-2009 decadal emissions from wetlands and inland freshwater ecosystems across the last three previous assessments of the budget shows a significant downward revision with 305 (183+122) Tg CH<sub>4</sub> yr<sup>-1</sup>, 356 (147+209) Tg CH<sub>4</sub> yr<sup>-1</sup> and 248 (159+112-23) Tg CH<sub>4</sub> yr<sup>-1</sup> (respectively from Saunio et al. (2016; 2020) and this work). Finally, it is worth noting that inland freshwater ecosystems can overlap with geological seepage systems in some areas, i.e., they may occur in correspondence with geological structures that emit fossil (microbial, thermogenic, or abiotic) CH<sub>4</sub> generated in the Earth's crust. Examples have been documented in the Fisherman Lake in Canada (Smith et al., 2005), in the Baikal lake (Schmid et al, 2007), and in rice paddies in Japan (Etiope et al., 2011). Thus, some gas emissions in freshwater environments, particularly as bubble plumes, can be incorrectly attributed to modern biological (ecosystem) activities if appropriate isotopic and molecular analyses are not performed.

### 3.2.3 Onshore and offshore geological sources

Significant amounts of CH<sub>4</sub>, produced within the Earth's crust, naturally migrate to the atmosphere through tectonic faults and fractured rocks. Major emissions are related to hydrocarbon formation in sedimentary basins (microbial and thermogenic methane), through continuous or episodic exhalations from onshore and shallow marine hydrocarbon seeps and through diffuse soil microseepage (Etiope, 2015). Specifically, five source categories have been considered. Four are onshore sources: gas-oil seeps, mud volcanoes, diffuse microseepage, and geothermal manifestations including volcanoes. One source is offshore: submarine seepage, which may include the same types of gas manifestations occurring on land. Etiope et al. (2019) have produced the first gridded maps of geological CH<sub>4</sub> emissions and their isotopic signature for these five categories, with a global total of 37.4 Tg CH<sub>4</sub> yr<sup>-1</sup> (reproduced in Fig. 5). However, these maps are based on incomplete data on geological sites due to missing information and difficulties in defining all current geological emitting sites. Combining the best estimates for the five categories of geological sources (from grid maps or from previous statistical and process-based models), the breakdown by category reveals that onshore microseepage dominate (24 Tg CH<sub>4</sub> yr<sup>-1</sup>), the other categories having similar smaller contributions: as mean values, 4.7 Tg CH<sub>4</sub> yr<sup>-1</sup> for geothermal manifestations, about 7 Tg CH<sub>4</sub> yr<sup>-1</sup> for submarine seepage and 9.6 Tg CH<sub>4</sub> yr<sup>-1</sup> for onshore seeps and mud volcanoes. These values lead to a global bottom-up geological emission mean of 45 [27-63] Tg CH<sub>4</sub> yr<sup>-1</sup> (Etiope and Schwietzke, 2019). While all bottom-up and some top-down estimates, following different and independent techniques from different authors, consistently suggest a global geo-CH<sub>4</sub> emission in the order of 40-50 Tg yr<sup>-1</sup>, the radiocarbon (<sup>14</sup>C-CH<sub>4</sub>) data in ice cores reported by Hmiel et al. (2020) appear to give a much lower estimate, with a minimum of about 1.6 Tg CH<sub>4</sub> yr<sup>-1</sup> and a maximum value of 5.4 Tg CH<sub>4</sub> yr<sup>-1</sup> (95 percent confidence) for the pre-industrial period. Dyonisius et al. (2020) also suggest a low range of geological emissions over the last deglaciation period and for the late Holocene (0-10 Tg CH<sub>4</sub> yr<sup>-1</sup>). The discrepancy between Hmiel et al. (2020) and all other estimates has been discussed in Thornton et al. (2021), which demonstrated that the global near-zero geologic CH<sub>4</sub> emission estimate in Hmiel et al. (2020) is incompatible with the sum

of multiple independent bottom-up estimates, based on a wide variety of methodologies, from individual natural geological seepage areas: for example, from the Black Sea (up to 1 Tg CH<sub>4</sub> yr<sup>-1</sup>), the Eastern Siberian Arctic Shelf (ESAS, up to 4.6 Tg CH<sub>4</sub> yr<sup>-1</sup>, referring mostly to thermogenic gas), onshore Alaska (up to 1.4 Tg CH<sub>4</sub> yr<sup>-1</sup>) and a single seepage site in Indonesia (releasing 0.1 Tg CH<sub>4</sub> yr<sup>-1</sup> as estimated by satellite measurement) (see Thornton et al. (2021) and references therein). Jackson et al. (2020) expressed doubt about the low Hmiel et al. (2020) estimates, noting that they are difficult to reconcile with the results of many other researchers and with bottom-up approaches in general. This discrepancy highlights another main unresolved uncertainty in the methane budget and calls for further investigations to reconcile the different estimates and reduce the uncertainty on geological emissions. Waiting for further investigation to better understand discrepancies between radiocarbon approaches and other studies, we decided to keep the estimates from Etiope and Schwietzke (2019) for the mean values, and associate it to the lowest estimates reported in Etiope et al. (2019), as in Saunio et al. (2020). Thus, we report a total global geological emission of 45 [18-63] Tg CH<sub>4</sub> yr<sup>-1</sup>, with a breakdown between offshore emissions of 7 [5-10] Tg CH<sub>4</sub> yr<sup>-1</sup> and onshore emissions of 38 [13-53] Tg CH<sub>4</sub> yr<sup>-1</sup> (Table 3), similar to Saunio et al. (2020). This bottom-up estimate is slightly lower than in the Saunio et al. (2016) budget mostly due to a reduction of estimated emissions of onshore and offshore seeps (see Sect. 3.2.6 for more offshore contribution explanations).

#### 3.2.4 Termites

Termites are decomposers playing a central role in ecosystem nutrient fluxes at tropical and subtropical latitudes, in particular (Abe et al., 2000). Termites represent a natural CH<sub>4</sub> source due to methanogenesis occurring in their hindgut during the symbiotic metabolic breakdown of lignocellulose (Sanderson, 1996; Brune, 2014). The upscaling of CH<sub>4</sub> emissions from termites from site to global level is characterised by high uncertainty (Sanderson, 1996; Kirschke et al., 2013; Saunio et al., 2016) due to the combination of factors that need to be considered and the scarcity of information for each of these factors for global upscaling. Needed data include termite biomass density (Sanderson, 1996), species distribution within and among ecosystems (Sugimoto et al., 1998), variation of termite CH<sub>4</sub> emission rates per species and dietary group (Sanderson, 1996), the role played by the termite mound structure in affecting the fraction of produced CH<sub>4</sub> that is effectively released into the atmosphere (Sugimoto et al., 1998; Nauer et al., 2018). In Kirschke et al. (2013) and Saunio et al. (2016) a global upscaling of termite CH<sub>4</sub> emissions was proposed, where CH<sub>4</sub> emissions, E<sub>CH<sub>4</sub></sub> (kg CH<sub>4</sub> ha<sup>-1</sup>yr<sup>-1</sup>), were estimated as the product of three terms: termite biomass (B<sub>TERM</sub> g fresh weight m<sup>-2</sup>), a scalar correction factor (LU) expressing the effect of land use/cover change on termite biomass density, a termite CH<sub>4</sub> emission factor (EF<sub>TERM</sub>, µg CH<sub>4</sub> g<sup>-1</sup> B<sub>TERM</sub> h<sup>-1</sup>). The approach between the two re-analyses of CH<sub>4</sub> emissions varied only for the data sources of gross primary productivity (GPP) and land use which were used to attribute biomass values of termite per ecosystem surface unit, in order to cover different time spans, 1980s, 1990s and 2000s in Kirschke et al. (2013) and 2000-2007 and 2010-2016 in Saunio et al. (2016). For the present update, additional changes have been introduced compared with the previous versions. Here we summarise the key data used for the new upscaling. CH<sub>4</sub> fluxes were modelled between 45°S and 45°N and within

1194 35°S and 35°N. The termite biomass density,  $\text{Bio}_{\text{TERM}}$ , for tropical ecosystems was estimated as function (Kirschke et al.,  
 1195 2013;  $\text{Bio}_{\text{TERM}} = 1.21 \cdot e^{0.0008 \cdot \text{GPP}}$  of the gross primary production (GPP,  $\text{g C m}^{-2} \text{ yr}^{-1}$ ) using the 0.25° native resolution  
 1196 VODCA2GPP dataset covering the period 2001-2020 (Wild et al., 2022). Wetlands, barren areas, water bodies and artificial  
 1197 surfaces were excluded from this estimation and set as no data (no emissions). The scalar correction factor LU of 0.4 (60%)  
 1198 for agricultural areas (i.e., croplands) (Kirschke et al., 2013) was applied to the GPP value of the nearest natural areas to  
 1199 account for anthropic disturbance. The annual (2001-2020) land cover information was obtained from the MODIS  
 1200 Terra+Water Combined Land Cover product (MCD12C1v006; <https://lpdaac.usgs.gov/products/mcd12c1v006/>), using the  
 1201 International Geosphere-Biosphere Programme (IGBP) classification with a 0.05° spatial resolution. For desert and arid lands,  
 1202 within 35°S and 35°N, a fixed  $\text{Bio}_{\text{TERM}}$  value of  $1.56 \text{ g m}^{-2}$  was instead used (Sanderson, 1996; Heděnc et al., 2022).  
 1203 Similarly, fix values from the few available studies reported in literature were used to estimate  $\text{Bio}_{\text{TERM}}$  between 35°- 45° N  
 1204 and 35°- 45° S as follows:  $1.83 \text{ g m}^{-2}$  for temperate forests and grasslands (Wood and Sands, 1978; Petersen and Luxton,  
 1205 1982; Sanderson, 1996; Bignell and Eggleton, 2000; King et al., 2013; conversion factor from dry to fresh biomass is 0.27  
 1206 from Petersen and Luxton, 1982),  $5.3 \text{ g m}^{-2}$  for scrublands and Mediterranean areas of Australia (Sanderson, 1996),  $1.09 \text{ g}$   
 1207  $\text{m}^{-2}$  for the other Mediterranean shrubland ecosystems (Heděnc et al., 2022). Other climates and land covers were set as no  
 1208 data. Climate zoning was defined using the Climate Zones Köppen-Geiger dataset (Beck et al., 2018), this product is  
 1209 representative for the 1980-2016 time period and has a 0.0083° native resolution. The  $\text{EF}_{\text{TERM}}$  was revised compared with  
 1210 previous estimates (Kirschke et al., 2013; Saunio et al., 2016), in order to consider the different distribution of termite  
 1211 families and subfamilies in the different continents and ecosystems, characterised by different feeding habits and nest  
 1212 typologies, as reported by Sugimoto et al. (1998), which might influence the EF. The species of each family and subfamily  
 1213 of the two major groups of lower and higher termites, listed by Sugimoto et al. (1998) were associated with EF values based  
 1214 on emissions from in-vitro experiments as reported by Sanderson (1996) and Eggleton et al. (1999), to which a correction  
 1215 factor ( $\text{cf}_{\text{MOUND}}$ ) of 0.5 (Nauer et al., 2018; Chiri et al., 2020; 2021) was applied in order to take into account the mound  
 1216 effect on the  $\text{CH}_4$  produced by termites, once inside the nest. The average  $\text{EF}_{\text{TERM}}$  for tropical and temperate areas was hence  
 1217 estimated as the weighted  $\text{EF}_{\text{TERM}}$  derived from the product of the percentage weight of each family or subfamily of termites  
 1218 in the “community composition” in each geographical area and ecosystem (Sugimoto et al. (1998, Table 6), the respective  
 1219 calculated EF of each family or subfamily, a scalar or correction factor which considers the nest type (as in Table 5 from  
 1220 Sugimoto et al. 1998). For desert and arid lands and temperate areas, which were not reported in Sugimoto et al. (1998), EF  
 1221 rates were calculated directly from data reported in literature for the most representative species which were the genus  
 1222 *Amitermes* for the former (EF from data by Sanderson 1996, Eggleton et al. 1999, Jamali et al. 2011) and the genus  
 1223 *Reticulitermes* (family Rhinotermitidae) for the latter (EF from data by Odelson and Breznak, 1983; Sanderson, 1996;  
 1224 Eggleton et al., 1999; Myer et al., 2021). The following  $\text{EF}_{\text{TERMS}}$  were hence obtained to scale up emissions:  $3.26 \pm 1.79 \mu\text{g}$   
 1225  $\text{CH}_4 \text{ g}^{-1} \text{ termite h}^{-1}$  ( $28.56 \text{ mg CH}_4 \text{ g}^{-1} \text{ termite year}^{-1}$ ) for tropical ecosystems,  $1.82 \pm 1.54 \mu\text{g CH}_4 \text{ g}^{-1} \text{ termite h}^{-1}$  for temperate  
 1226 forests, grasslands, and Mediterranean areas,  $1.24 \pm 1.22 \mu\text{g CH}_4 \text{ g}^{-1} \text{ termite h}^{-1}$  for deserts and arid lands (warm climate).

1227 Annual CH<sub>4</sub> fluxes were computed for all the years from 2001 to 2020 producing 20 global maps at 0.05° resolution of  
1228 yearly total emissions. A further map of the estimated error representative of the entire time period was elaborated at the  
1229 same resolution as the emissions dataset.

1230 Termite CH<sub>4</sub> emissions over the period 2001-2020 varied between 9.7-10.8 Tg CH<sub>4</sub> yr<sup>-1</sup>, with an average of 10.2 ± 6.2 Tg  
1231 CH<sub>4</sub> yr<sup>-1</sup>. Considering a 20-year average, tropical and subtropical moist broadleaf forests contributed to 46% of the total  
1232 average flux, while tropical and subtropical grasslands, savannas, and shrublands to another 36%. In terms of regional  
1233 contribution, 37.2% of fluxes were attributed to South America, 31.5% to Africa, 18.1% to Asia, 5.5% to Australia, 7.4%  
1234 to North America and less than 1% to Europe. The present estimate value is within the range of previous up-scaling studies,  
1235 spanning from 2 to 22 Tg CH<sub>4</sub> yr<sup>-1</sup> (Ciais et al., 2013). In this study, we report a decadal value of 10 Tg CH<sub>4</sub> yr<sup>-1</sup> with a  
1236 range of [4-16] (Table 3).

1237 **3.2.5 Wild animals**

1238 Wild ruminants emit CH<sub>4</sub> through microbial fermentation that occurs in their rumen, similarly to domesticated livestock  
1239 species (USEPA, 2010b). Using a total animal population of 100-500 million, Crutzen et al. (1986) estimated the global  
1240 emissions of CH<sub>4</sub> from wild ruminants to be in the range of 2-6 Tg CH<sub>4</sub> yr<sup>-1</sup>. More recently, Pérez-Barbería (2017) lowered  
1241 this estimate to 1.1-2.7 Tg CH<sub>4</sub> yr<sup>-1</sup> using a total animal population estimate of 214 million (range of 210-219), arguing that  
1242 the maximum number of animals (500 million) used in Crutzen et al. (1986) was poorly justified. Moreover Pérez-Barbería  
1243 (2017) also stated that the value of 15 Tg CH<sub>4</sub> yr<sup>-1</sup> found in the last IPCC reports is much higher than their estimate because  
1244 this value comes from an extrapolation of Crutzen's work for the last glacial maximum when the population of wild animals  
1245 was much larger, as originally proposed by Chappellaz et al. (1993). Recently, based on the modelling of grassland extent,  
1246 Kleinen et al. (2023) also suggest that the population of wild animal during the last glacial maximum proposed by Crutzen  
1247 et al. (1986) and further used by Chappellaz et al. (1993) were overestimated. However, the estimate of 1-3 Tg CH<sub>4</sub> yr<sup>-1</sup>  
1248 seems underestimated when considering that Hempson et al. (2017) found actual CH<sub>4</sub> emissions from African wildlife alone  
1249 to be around 9 Tg CH<sub>4</sub> yr<sup>-1</sup> but without discussing the uncertainty of this value. As a result, high uncertainty remains and  
1250 recalls the need for further investigation of this natural source of CH<sub>4</sub>.  
1251 Based on these findings and waiting for further global estimates, the range adopted in this updated CH<sub>4</sub> budget is 2 [1-3] Tg  
1252 CH<sub>4</sub> yr<sup>-1</sup> (Table 3).

1253 **3.2.6 Coastal and oceanic sources**

1254 Coastal and oceanic sources comprise CH<sub>4</sub> release from estuaries, coastal vegetated habitats, as well as marine waters  
1255 including seas and oceans. Possible sources of coastal and oceanic CH<sub>4</sub> include (1) in-situ biogenic production through  
1256 various pathways in oxygenated sea-surface waters (Oremland, 1979; Karl et al., 2008; Lenhart et al., 2016; Repeta et al.,  
1257 2016), a flux that can be enhanced in the coastal ocean because of submarine groundwater discharge (USEPA, 2010b); (2)

production from shallow and marine (bare and vegetated) sediments including free gas or destabilised hydrates and thawing subsea permafrost containing modern ( $^{14}\text{C}$ -bearing) microbial gas; (3) geological marine seepage (see also Sect. 3.2.3), including hydrates, containing fossil ( $^{14}\text{C}$ -free) microbial or thermogenic  $\text{CH}_4$ .  $\text{CH}_4$  produced in marine sediments and seabed  $\text{CH}_4$  seepage can be transported across the water column to the sea-surface by upwelling waters (once at the surface methane can cross the sea-air interface via diffusion) and gas bubble plumes (for instance from geological marine seeps; e.g., Judd, 2004; Etiope et al., 2019). Gas bubble plumes generally reach the atmosphere in relatively shallow waters (<400 m) of continental shelves depending on the intensity of the events (e.g., Westbrook et al., 2009); however massive deep-water seepage events could contribute a significant amount of  $\text{CH}_4$  to the atmosphere, even from depths > 1000 m (e.g., Schmale et al., 2005.; Greinert et al., 2006; Solomon et al., 2009). In coastal vegetated habitats,  $\text{CH}_4$  can also be transported to the atmosphere through the aerenchyma of emergent aquatic plants (Purvaja et al., 2004).

We distinguish between coastal and oceanic “geological” and “modern biogenic”  $\text{CH}_4$  sources. Coastal and oceanic “geological” emissions refer to  $\text{CH}_4$  seepage from the Earth’s crust (mostly in hydrocarbon-rich sedimentary basins), which is typically evaluated by combining geochemical analyses (isotopic and molecular, including radiocarbon,  $^{14}\text{C}$ , analyses) and geological observations (degassing along faults, seeps, mud volcanoes). Geological emissions do not contain modern biogenic gas that is fossil ( $^{14}\text{C}$ -free). Coastal and oceanic “biogenic”  $\text{CH}_4$  refers to  $\text{CH}_4$  formed *in situ* in coastal and marine sediments and in the water column by recent or modern microbial activity (therefore with measurable amounts of radiocarbon ( $^{14}\text{C}$ )). To avoid double-counting, we assume that all diffusive  $\text{CH}_4$  emissions outside of geological seepage regions (identified in global grid maps; Etiope et al., 2019) are fuelled by biogenic  $\text{CH}_4$ . Finally, we briefly discuss the case of  $\text{CH}_4$  hydrates, which can be considered either a “geological” source when they host fossil  $\text{CH}_4$  or a “biogenic” source when they host modern  $\text{CH}_4$ .

**Coastal and oceanic modern biogenic methane emissions.** Area-integrated diffusive modern biogenic  $\text{CH}_4$  emissions from coastal ecosystems are 1-2 magnitudes lower than from inland freshwaters but significantly higher than biogenic emissions from the open ocean (Rosentreter et al., 2021; Rosentreter et al., 2023; Weber et al., 2019). Particularly the shallow vegetated coastline fringed by mangroves, salt marshes, and seagrasses is a  $\text{CH}_4$  hotspot in the coastal ocean, characterised by significantly higher flux densities than other coastal settings such as estuaries or the continental shelves (Rosentreter et al., 2021; Rosentreter et al., 2023). Coastal ecosystems are thus being increasingly recognized as weak global sources to the atmosphere (Weber et al., 2019; Saunio et al., 2020; Rosentreter et al., 2021). Hydrogenotrophic and acetoclastic methanogenesis are largely outcompeted by sulphate reduction in coastal/marine sediments, which is often shown by a decreasing trend of  $\text{CH}_4$  concentrations with increasing salinity from upper tidal (low salinity) to marine (high salinity) regions. Much of the  $\text{CH}_4$  produced below the sulfate-reduction zone is indeed re-oxidized by sedimentary anaerobic methane oxidation or re-oxidized in the water column, leading to small emissions despite much larger production (Knittel and Boetius 2009; Regnier et al., 2011). Methylated compounds such as methylamines and methyl sulphides are non-competitive substrates that are exclusively used by methanogens, therefore methylated methanogenesis can occur in coastal

regions with high sulphate concentrations, for example, in organic-rich (Maltby et al., 2018), vegetated (Schorn et al., 2022), and hypersaline coastal sediments (Xiao et al., 2018). Coastal CH<sub>4</sub> can be driven by the exchange of pore water or groundwater (high in CH<sub>4</sub>) with coastal surface waters in tidal systems, referred to as tidal pumping (Ovalle et al., 1990; Call et al., 2015). Anthropogenic impacts such as wastewater pollution and land-use change can increase CH<sub>4</sub> fluxes in estuaries (Wells et al., 2020). A large increase of CH<sub>4</sub> emissions follows the conversion of natural coastal habitats to aquaculture farms (Yuan et al., 2019; Yang et al., 2022).

Currently available global modern biogenic CH<sub>4</sub> flux data show high spatiotemporal variability within and between coastal systems, but also because of the overall global paucity of data. Therefore, global estimates have high uncertainties and show large ranges in both empirical (Rosentreter et al., 2021) and machine-learning based approaches (Weber et al., 2019). According to a recent data-driven meta-data analysis, global estuaries, including tidal systems and deltas, lagoons, and fjords, are estimated to emit median (Q1-Q3) 0.25 (0.07-0.46) Tg CH<sub>4</sub> yr<sup>-1</sup> (Rosentreter et al., 2023). Coastal vegetation, including mangrove forests, salt marshes, and seagrasses are estimated to emit 0.77 (0.47-1.41) Tg CH<sub>4</sub> yr<sup>-1</sup>, which is 3 times more than global estuaries (Rosentreter et al., 2023). The combined median (Q1-Q3) emission of 1.01 (0.54-1.87) Tg CH<sub>4</sub> yr<sup>-1</sup> for coastal vegetation and estuaries by Rosentreter et al. (2023) is lower than the recent observation-based global synthesis including tidal flats and aquaculture ponds (median 1.49 (0.22-6.48) Tg CH<sub>4</sub> yr<sup>-1</sup>) by Rosentreter et al. (2021). Total shallow coastal modern biogenic CH<sub>4</sub> emissions based on existing data including emissions from estuaries, coastal vegetation (Rosentreter et al., 2023), tidal flats, and man-made coastal aquaculture ponds (Rosentreter et al., 2021) amount to median (Q1-Q3) 1.8 (0.59-5.57) Tg CH<sub>4</sub> yr<sup>-1</sup>. This range is about 3-4 times lower than the earlier global assessment by Borges and Abril (2011) and also lower than the value of 4-5 Tg CH<sub>4</sub> yr<sup>-1</sup> reported in the previous CH<sub>4</sub> budget for inner and outer estuaries including marshes and mangroves (Saunois et al., 2020), which was based on a significantly smaller dataset (n=80) and larger estuarine surface areas (Laruelle et al., 2013) than used here (Laruelle et al., 2025).

The near-shore (0-50 m), inner shelf diffusive modern biogenic CH<sub>4</sub> flux of median (Q1-Q3) 1.33 (0.93-2.10) Tg CH<sub>4</sub> yr<sup>-1</sup> by Weber et al. (2019) based on machine-learning is similar to the combined shallow coastal (estuaries and coastal vegetation) median by Rosentreter et al. (2021, 2023). Adding the diffusive modern biogenic CH<sub>4</sub> flux for the outer shelf (50-200 m) (median (Q1-Q3) of 0.54 (0.40-0.73) Tg CH<sub>4</sub> yr<sup>-1</sup>) and for the slope (200-2000m) (median (Q1-Q3) of 0.28 (0.22-0.37) Tg CH<sub>4</sub> yr<sup>-1</sup>) (Weber et al., 2019), and excluding geological seepage regions (Etioppe et al., 2019; see below), gives a total median (Q1-Q3) of 3.95 (2.14-8.77) Tg CH<sub>4</sub> yr<sup>-1</sup> for combined coastal shallow, near-shore, outer shelf and slope diffusive modern biogenic CH<sub>4</sub> emissions. The previous budget by Saunois (2020) also included poorly constrained emissions (upper bound value: 1-2 Tg CH<sub>4</sub> yr<sup>-1</sup>) from large river plumes protruding onto the shelves. However, here we assume that emissions from large river plumes are accounted for in the near-shore and outer shelf estimates by Weber et al. (2019). Area-integrated diffusive CH<sub>4</sub> emissions from the open ocean and deep seas (>2000 m) are much lower than from other coastal systems but amount to median (Q1-Q3) 0.91 (0.75-1.12) Tg CH<sub>4</sub> yr<sup>-1</sup> because of the large surface area of the open ocean (>300 x 10<sup>6</sup> km<sup>2</sup>) (Weber et al., 2019). Overall, these marine biogenic emissions are sustained by a mixture of



1324 sedimentary production and in-situ production in the sea-surface layers (including the methylphosphonate pathway) (e.g.,  
1325 Karl et al., 2008; Repeta et al., 2016; Resplandy et al., 2024). The total coastal and ocean diffusive modern biogenic  
1326 emissions retained here amount to 5 (3-10) Tg CH<sub>4</sub> yr<sup>-1</sup> (Table 3).

1327

1328 **Coastal and oceanic geological methane emissions** Submarine geological CH<sub>4</sub> emission is the offshore component of the  
1329 general geological emissions of natural gas from the Earth's crust (Judd, 2004; Etiope, 2009; Etiope et al., 2019). The  
1330 onshore components include terrestrial seeps, mud volcanoes, microseepage, and geothermal manifestations, addressed in  
1331 Sect. 3.2.3. Natural gas seeping at the seabed as bubble plumes can reach the surface in relatively shallow waters (<400 m),  
1332 but CH<sub>4</sub>-rich bubble plumes reaching the atmosphere from depths >500 m have been observed in some cases (e.g., Solomon  
1333 et al., 2009), and upwelling of bottom marine waters can, in theory, transport geological CH<sub>4</sub> (dissolved) to the surface from  
1334 any depth. This represents, however, a small and poorly known fraction of geological CH<sub>4</sub> emission. Geological CH<sub>4</sub> can be  
1335 either microbial or thermogenic, produced throughout diverse geological periods in hydrocarbon source rocks in  
1336 sedimentary basins (therefore it is always fossil, <sup>14</sup>C-free). The seepage at the seafloor is typically related to tectonic faults,  
1337 sometimes forming mud diapirs and mud volcanoes (Mazzini and Etiope, 2017). Published estimates of geological CH<sub>4</sub>  
1338 submarine emissions range from 3 to 20 Tg yr<sup>-1</sup>, with a best guess of 7 Tg yr<sup>-1</sup> (Etiope and Schwietzke, 2019; Etiope et al.,  
1339 2019 and references therein).

1340 Here, the diffusive geological CH<sub>4</sub> emissions are estimated at 0.16 (0.11-0.24) Tg CH<sub>4</sub> yr<sup>-1</sup> for near-shore (0-50 m), 0.03  
1341 (0.02-0.05) Tg CH<sub>4</sub> yr<sup>-1</sup> for outer shelf (50-200 m), and 0.02 (0.01-0.03) Tg CH<sub>4</sub> yr<sup>-1</sup> for slope (200-2000 m) by calculating  
1342 the fraction of the Weber et al. (2019) diffusive fluxes that occur within the identified geological seepage regions from  
1343 Etiope et al. (2019). No geological seepage regions were identified in the open ocean and deep seas (> 2000 m).

1344 In this study, we consider the ebullitive flux as geologically sourced CH<sub>4</sub>. While modern biogenic CH<sub>4</sub> gas production  
1345 appears ubiquitous in shallow sediments (Fleischer et al., 2001; Best et al., 2006), no global dataset is currently available to  
1346 estimate the biogenic ebullitive CH<sub>4</sub> flux to the atmosphere. Omission of this flux thus constitutes a significant knowledge  
1347 gap in the coastal and oceanic CH<sub>4</sub> budget. Global geological CH<sub>4</sub> ebullition from continental shelf and slope, referring only  
1348 to depths <200 m, were estimated at 5.06 (1.99-8.16) Tg CH<sub>4</sub> yr<sup>-1</sup> (Weber et al., 2019). This estimate is based on prior  
1349 estimates of the geological flux from the seafloor (Hovland et al., 1993) and bubble transfer efficiency to the ocean surface  
1350 (McGinnis et al., 2006). Etiope et al. (2019) estimated a partial fraction of geological emissions in the form of gas bubbles  
1351 of 3.9 (1.8-6) Tg CH<sub>4</sub> yr<sup>-1</sup>, only referring to the sum of published estimates from 15 geological seepage regions, which are  
1352 also deeper than 200 m. Global extrapolation including other 16 identified seepage zones (where flux data are not available)  
1353 was suggested to be at least 7 (3-10) Tg CH<sub>4</sub> yr<sup>-1</sup> (Etiope et al., 2019), and this value coincides with the mean emission value  
1354 (best guess) derived by combining literature data, see Etiope and Schwietzke (2019) for further details. It is worth noting  
1355 that the Weber et al. (2019) estimate of 5.06 (1.99-8.16) Tg CH<sub>4</sub> yr<sup>-1</sup>, which considers only the continental shelf at depths  
1356 <200 m, is compatible with the overall submarine emission of 7 (3-10) Tg CH<sub>4</sub> yr<sup>-1</sup> (including seeps > 200 m deep) indicated

1357 in Etiope and Schwietzke (2019) and Etiope et al. (2019). Although 300-400 m is considered a general depth limit for  
1358 efficient transport (with limited oxidation and dissolution) of CH<sub>4</sub> bubbles to the atmosphere (e.g., Judd, 2004; Schmale et  
1359 al., 2005; Etiope et al., 2019), in some cases oil coatings on bubbles inhibit gas dissolution so that CH<sub>4</sub>-rich bubbles can  
1360 reach the atmosphere from depths >500 m (e.g., Solomon et al., 2009). As mentioned above, a fraction of geological CH<sub>4</sub>  
1361 released in deep seas (such as in the areas with gas-charged sediments inventoried in Fleischer et al., 2001) can also be  
1362 transported to the surface by upwelling bottom waters. Further research is needed to better evaluate the atmospheric impact  
1363 of such deep seeps.

1364 Geological submarine emissions, thus, would amount to 0.21 (0.14-0.32) Tg CH<sub>4</sub> yr<sup>-1</sup> in the form of a diffusive flux while  
1365 the ebullitive flux would be 5.06 (3.01-7.88) Tg CH<sub>4</sub> yr<sup>-1</sup>, considering only < 200 m deep seepage, and 7 (3-10) Tg CH<sub>4</sub> yr<sup>-1</sup>  
1366 considering all data available (Etiope and Schwietzke, 2019). Here, we select the Etiope and Schwietzke (2019) assessment  
1367 in order to account for all potential seepage areas, including those located at water depths > 200m. While we use the estimate  
1368 by Etiope and Schwietzke (2019) estimate, we acknowledge that high uncertainty remains and other studies suggest a lower  
1369 ranges of emissions based on radiocarbon (<sup>14</sup>C-CH<sub>4</sub>) data in ice cores (e.g., Hmiel et al., 2020). The suggested estimate may  
1370 overestimate this source and be part of the top-down bottom-up discrepancy as discussed in Section 5.1.2.

1371 As a result, here we report a (rounded) median of 12 Tg CH<sub>4</sub> yr<sup>-1</sup> with a range of 6-20 Tg CH<sub>4</sub> yr<sup>-1</sup> for all coastal and oceanic  
1372 sources (Table 3).

1373  
1374 **Methane emissions from gas hydrates.** Among the different origins of coastal and oceanic CH<sub>4</sub>, hydrates have attracted a  
1375 lot of attention. CH<sub>4</sub> hydrates (or clathrates) are ice-like crystals formed under specific temperature and pressure conditions  
1376 (Milkov, 2005). Hydrates may host either modern microbial CH<sub>4</sub>, containing <sup>14</sup>C and formed *in situ* in shallow sediments  
1377 (this type of hydrates is also called “autochthonous”) or fossil, microbial or thermogenic CH<sub>4</sub>, migrated from deeper  
1378 sediments, generally from reservoirs in hydrocarbon-rich sedimentary basins (this type of hydrates is also called  
1379 “allochthonous”; Milkov, 2005; Foschi et al., 2023). The total stock of marine CH<sub>4</sub> hydrates is large but uncertain, with  
1380 global estimates ranging from hundreds to thousands of Pg CH<sub>4</sub> (Klauda and Sandler, 2005; Wallmann et al., 2012). Note  
1381 that the highly climate-sensitive subsea permafrost reservoir beneath Arctic Ocean shelves also contributes to the hydrate  
1382 inventory (Ruppel and Kassler, 2017).

1383 Concerning more specifically atmospheric emissions from marine hydrates, Etiope (2015) points out that current estimates  
1384 of CH<sub>4</sub> air-sea flux from hydrates (2–10 Tg CH<sub>4</sub> yr<sup>-1</sup> in Ciais et al., 2013, or Kirschke et al., 2013) originate from the  
1385 hypothetical values of Cicerone and Oremland (1988). No experimental data or estimation procedures have been explicitly  
1386 described along the chain of references since then (Denman et al., 2007; IPCC, 2001; Kirschke et al., 2013; Lelieveld et al.,  
1387 1998). It was estimated that ~473 Tg CH<sub>4</sub> has been released into the water column over 100 years (Kretschmer et al., 2015).  
1388 Those few teragrams per year become negligible once consumption within the water column has been accounted for. While

1389 events such as submarine slumps may trigger local releases of considerable amounts of CH<sub>4</sub> from hydrates that may reach  
1390 the atmosphere (Etiopé, 2015; Paull et al., 2002), on a global scale, present-day atmospheric CH<sub>4</sub> emissions from hydrates  
1391 do not appear to be a significant source to the atmosphere, and at least formally, we should consider 0 (< 0.1) Tg CH<sub>4</sub> yr<sup>-1</sup>  
1392 emissions.

1393 **3.2.7 Terrestrial permafrost**

1394 Permafrost is defined as frozen soil, sediment, or rock having temperatures at or below 0°C for at least two consecutive  
1395 years (Harris et al., 1988). The total extent of permafrost in the Northern Hemisphere is about 14 million km<sup>2</sup> or 15% of the  
1396 exposed land surface (Obu et al., 2019). As the climate warms, a rise in soil temperatures has been observed across the  
1397 permafrost region, and permafrost thaw occurs when temperatures pass 0°C, often associated with melting of ice in the  
1398 ground (Biskaborn et al., 2019). Permafrost thaw is most pronounced in southern and spatially isolated permafrost zones,  
1399 but also occurs in northern continuous permafrost (Obu et al., 2019). Thaw occurs either as a gradual, often widespread,  
1400 deepening of the active layer (surface soils that thaw every summer) or as more rapid localised thaw associated with loss of  
1401 massive ground ice (thermokarst) (Turetsky et al., 2020). A total of 1000 ± 200 Pg of carbon can be found in the upper 3  
1402 meters of permafrost region soils, or 1400-2000 Pg C for all permafrost (Hugelius et al., 2014; Strauss et al., 2021).

1403 The thawing permafrost can generate direct and indirect CH<sub>4</sub> emissions. Direct CH<sub>4</sub> emissions are from the release of  
1404 CH<sub>4</sub> contained within the thawing permafrost. This flux to the atmosphere is small and estimated to be a maximum of 1 Tg  
1405 CH<sub>4</sub> yr<sup>-1</sup> at present (USEPA, 2010b). Increased release of CH<sub>4</sub> from deep geogenic sources that occurs as seepage along  
1406 permafrost boundaries and lake beds may also be considered a direct, and this is estimated to be 2±0.4 Tg CH<sub>4</sub> yr<sup>-1</sup> (Walter  
1407 Anthony et al., 2012). Indirect CH<sub>4</sub> emissions are probably more important. They are caused by 1) methanogenesis induced  
1408 when the organic matter contained in thawing permafrost becomes available for microbial decomposition; 2) thaw induced  
1409 soil wetting and changes in land surface hydrology possibly enhancing CH<sub>4</sub> production (McCalley et al., 2014; Schuur et  
1410 al., 2022); and 3) the landscape topography changes driven by abrupt thaw processes and loss of ground ice, including the  
1411 formation of thermokarst lakes, hill-slope thermokarst, and wetland thermokarst (Turetsky et al., 2020). Such  
1412 CH<sub>4</sub> production is probably already significant today and is likely to become more important in the future associated with  
1413 climate change and strong positive feedback from thawing permafrost (Schuur et al., 2022). However, indirect  
1414 CH<sub>4</sub> emissions from permafrost thawing are difficult to estimate at present, with very few data to refer to, and in any case  
1415 largely overlap with wetland and freshwater emissions occurring above or around thawing areas. In a recent synthesis of  
1416 full permafrost region CH<sub>4</sub> budgets for the period 2000-2017, Hugelius et al. (2023) compared CH<sub>4</sub> budgets from bottom-  
1417 up and top-down (atmospheric inversion models) approaches. They estimate an integrated bottom-up budget of 50 (23, 53;  
1418 mean upper and lower 95% CI) Tg CH<sub>4</sub> yr<sup>-1</sup> while the top-down estimate is 19 (15, 24) Tg CH<sub>4</sub> yr<sup>-1</sup>. The bottom-up estimate  
1419 is based on a combination of data-driven upscaling reported by Ramage et al. (2023) and process-based model estimates for  
1420 wetland CH<sub>4</sub> flux calculated from model ensembles used in Saunio et al. (2020). The top-down estimate is calculated from

ensembles of atmospheric inversion models used in Saunio et al. (2020). Although it is difficult with direct process-attribution, fluxes of ca. 20-30 Tg CH<sub>4</sub> yr<sup>-1</sup> in the bottom-up budget are caused by land cover types affected by previous permafrost thaw (thermokarst lakes, wetlands, hillslope). Because pre-thaw land cover types often have near neutral CH<sub>4</sub> balances (Ramage et al. 2023), these fluxes can largely be seen as driven by permafrost thaw, however the thaw may have occurred decades, or even centuries, before today. Here, we choose to report only the direct emission range of 0-1 Tg CH<sub>4</sub> yr<sup>-1</sup> (Table 3), keeping in mind that current wetland, thermokarst lakes and other freshwater methane emissions already likely include a significant indirect contribution originating from thawing permafrost.

### 3.2.8 Vegetation

Three distinct pathways for the production and emission of CH<sub>4</sub> by living vegetation are considered here (see Covey and Megonigal (2019) and Bastviken et al. (2023) for extensive reviews). Firstly, plants produce CH<sub>4</sub> through an abiotic photochemical process induced by stress (Keppler et al., 2006). This pathway was initially questioned (e.g., Dueck et al., 2007; Nisbet et al., 2009), and although numerous studies have since confirmed aerobic emissions from plants and better resolved its physical drivers (Fraser et al., 2015), global estimates still vary by two orders of magnitude (Liu et al., 2015). This plant source has not been confirmed in-field however, and although the potential implication for the global CH<sub>4</sub> budget remains unclear, emissions from this source are certainly much smaller than originally estimated in Keppler et al. (2006) (Bloom et al., 2010; Fraser et al., 2015). Second, and of clearer significance, plant stems act as “straws”, drawing up and releasing microbially produced CH<sub>4</sub> from anoxic soils (Cicerone and Shetter, 1981; Rice et al., 2010; Nisbet et al., 2009). For instance, in the forested wetlands of Amazonia, tree stems are the dominant ecosystem flux pathway for soil-produced CH<sub>4</sub>, therefore, including stem emissions in ecosystem budgets can reconcile regional bottom-up and top-down estimates (Pangala et al., 2017; Gauci et al., 2022). Third, the stems of both living trees (Covey et al., 2012) and dead wood (Covey et al., 2016) provide an environment suitable for microbial methanogenesis. Static chambers demonstrate locally significant through-bark flux from both soil- (Pangala et al., 2013, 2015), and tree stem-based methanogens (Pitz and Megonigal, 2017; Wang et al., 2016). A synthesis indicates stem CH<sub>4</sub> emissions significantly increase the source strength of forested wetlands, and modestly decrease the sink strength of upland forests (Covey and Megonigal, 2019). Recently, field-work suggested that trees may also act as a CH<sub>4</sub> sink (Machacova et al., 2021; Gorgolewski et al., 2023; Gauci et al., 2024). The scientific activity covering CH<sub>4</sub> emissions in forested ecosystems reveals a far more complex story than previously thought, with an interplay of productive/consumptive, aerobic/anaerobic, and biotic/abiotic processes occurring between upland/wetland soils, trees, and atmosphere. Understanding the complex processes that regulate CH<sub>4</sub> source–sink dynamics in forests and estimating their contribution to the global CH<sub>4</sub> budget requires cross-disciplinary research, more observations, and new models that can overcome the classical binary classifications of wetland versus upland forest and of emitting versus uptaking soils (Barba et al., 2019; Covey and Megonigal, 2019). Although we recognize these emissions are potentially large

1453 (particularly tree transport from inundated soil), global estimates for each of these pathways remain highly uncertain and/or  
1454 are currently included here within other flux category sources (e/g. inland waters, wetlands, upland soils).

### 1455 **3.3 Methane sinks and lifetime**

1456 CH<sub>4</sub> is the most abundant reactive trace gas in the troposphere and its reactivity is important to both tropospheric and  
1457 stratospheric chemistry. The main atmospheric sink of CH<sub>4</sub> (~90% of the total sink mechanism) is oxidation by the hydroxyl  
1458 radical (OH), mostly in the troposphere (Ehhalt, 1974). Other losses are by photochemistry in the stratosphere (reactions  
1459 with chlorine atoms (Cl) and excited atomic oxygen (O(<sup>1</sup>D)), oxidation in soils (Curry, 2007; Dutaur and Verchot, 2007),  
1460 and by photochemistry in the marine boundary layer (reaction with Cl; Allan et al. (2007), Thornton et al. (2010)).  
1461 Uncertainties in the total sink of CH<sub>4</sub> as estimated by atmospheric chemistry models are in the order of 20-40% (Saunois et  
1462 al., 2016). It is much less (10-20%) when using atmospheric proxy methods (e.g., methyl chloroform, see below) as in  
1463 atmospheric inversions (Saunois et al., 2016). In the present release of the global CH<sub>4</sub> budget, we estimate bottom-up  
1464 CH<sub>4</sub> chemical sinks and lifetime mainly based on global model results from the Chemistry Climate Model Initiative (CCMI)  
1465 2022 activity (Plummer et al., 2021) and CMIP6 simulations (Collins et al., 2017).

#### 1466 **3.3.1 Tropospheric OH oxidation**

1467 OH radicals are produced following the photolysis of ozone (O<sub>3</sub>) in the presence of water vapour. OH is destroyed by  
1468 reactions with carbon monoxide (CO), CH<sub>4</sub>, and non-methane volatile organic compounds.  
1469 Following the Atmospheric Chemistry and Climate Model Intercomparison Project (ACCMIP), which studied the long-term  
1470 changes in atmospheric composition between 1850 and 2100 (Lamarque et al., 2013), a new series of experiments was  
1471 conducted by several chemistry-climate models and chemistry-transport models participating in the Chemistry-Climate  
1472 Model Initiative (CCMI) (Plummer et al., 2021). Mass-weighted OH tropospheric concentrations do not directly represent  
1473 CH<sub>4</sub> loss, as the spatial and vertical distributions of OH affect this loss through, in particular, the temperature dependency  
1474 and the distribution of CH<sub>4</sub> (e.g., Zhao et al., 2019). However, estimating OH concentrations and, spatial and vertical  
1475 distributions is a key step in estimating methane loss through OH. Over the period 2000-2010, the global mass-weighted  
1476 OH tropospheric concentration is estimated at 13.3 [11.7-18.2] x 10<sup>5</sup> molecules cm<sup>-3</sup> by 8 CCMI-2022 models and at 11.8  
1477 [9.4-13.5] x 10<sup>5</sup> molecules cm<sup>-3</sup> by 9 models contributing CMIP6 historical run (Collins et al., 2021) (see supplementary  
1478 Table S4). The ranges calculated here are similar to the ones proposed previously in Saunois et al. (2020), where the multi-  
1479 model mean (11 models) global mass-weighted OH tropospheric concentration was 11.7±1.0 x 10<sup>5</sup> molecules cm<sup>-3</sup> (range  
1480 9.9-14.4 x 10<sup>5</sup> molecules cm<sup>-3</sup>, Zhao et al. (2019)) consistent with the previous estimates from ACCMIP (11.7±1.0 x  
1481 10<sup>5</sup> molecules cm<sup>-3</sup>, with a range of 10.3-13.4 x 10<sup>5</sup> molecules cm<sup>-3</sup>, Voulgarakis et al. (2013) for year 2000) and the  
1482 estimates of Prather et al. (2012) of 11.2±1.3 x 10<sup>5</sup> molecules cm<sup>-3</sup>. Nicely et al. (2017) attribute the differences in OH  
1483 simulated by different chemistry transport models to, in decreasing order of importance, different chemical mechanisms,

1484 various treatments of the photolysis rate of  $O_3$ , and modelled  $O_3$  and CO. Besides the uncertainty on global OH  
 1485 concentrations, there is an uncertainty in the spatial and temporal distribution of OH. Models often simulate higher OH in  
 1486 the northern hemisphere (NH) than in the southern hemisphere (SH), leading to a NH/SH OH ratio greater than 1 (e.g., Zhao  
 1487 et al., 2019). However, there is evidence for parity in inter-hemispheric OH concentrations (Patra et al., 2014), which needs  
 1488 to be confirmed by other observational and model-derived estimates. The analysis of the latest CCMI (Plummer et al., 2021)  
 1489 and CMIP6 (Collins et al., 2021) model outputs show that structural uncertainties in the atmospheric chemistry models  
 1490 remain large, probably due to inherent biases in OH precursors. Such biases have been highlighted in the OH 3D fields  
 1491 simulated by two atmospheric chemistry models (Zhao et al., 2023), and were corrected using OH precursors observations.  
 1492 Such corrections resulted in tropospheric OH mean concentrations lowered by  $2 \cdot 10^5$  molecules  $cm^{-3}$ , leading to around  $10$   
 1493  $\times 10^5$  molecules  $cm^{-3}$ , and a NH/SH OH ratio closer to 1, in better agreement with methyl chloroform (MCF)-based  
 1494 approaches. This study highlights the need for further improvement of the atmospheric chemistry model.  
 1495 OH concentrations and their changes can be sensitive to climate variability (e.g., Nicely et al., 2018; Anderson et al., 2021),  
 1496 biomass burning (e.g., Anderson et al., 2024), and anthropogenic emissions of precursors (Peng et al., 2022; Stevenson et  
 1497 al., 2020). OH distributions calculated by chemistry climate models show large regional differences and various vertical  
 1498 profiles (Zhao et al., 2019). OH changes present also regional differences over the long term (Stevenson et al., 2020).  
 1499 Despite large regional changes, the global mean OH concentration was suggested to have changed only slightly from  
 1500 1850 to 1980, but followed by strong (9 %) increases up to the present day (Stevenson et al., 2020). This increase simulated  
 1501 by models over 2000-2015 are however not in agreement with observation-based approaches (Thompson et al., 2024; Patra  
 1502 et al., 2020; Nicely et al., 2018; Rigby et al., 2017; Turner et al., 2017) where OH decreases or remain constant over the  
 1503 period. CCMI and CMIP6 models show OH interannual variability ranging from 0.9% to 1.8% over 2000-2010 (Table S4),  
 1504 in agreement with the values of IAV derived from some observationally constrained studies (e.g., Thompson et al., 2024;  
 1505 Montzka et al., 2011) but lower than value deduced from methyl chloroform measurements (Patra et al., 2021; Naus et al.,  
 1506 2021). However, chemistry climate simulations consider meteorology variability but not fully emission interannual  
 1507 variability (e.g., from biomass burning) and thus are expected to simulate lower OH inter annual variability than in reality.  
 1508 Using an empirical model constrained by global observations of  $O_3$ , water vapour,  $CH_4$ , and temperature as well as the  
 1509 simulated effects of changing  $NO_x$  emissions and tropical expansion, Nicely et al. (2017) found an interannual variability  
 1510 in OH of about 1.3-1.6% between 1980 and 2015, in agreement with methyl chloroform based estimates (Montzka et al.,  
 1511 2011).  
 1512 Over 2000-2009, the tropospheric loss (tropopause height at 200 hPa) of  $CH_4$  by OH oxidation derived from the ten and  
 1513 CCMI modelling activities (see supplementary Table S5) is estimated at of 546 [446-663] Tg  $CH_4$   $yr^{-1}$  (Table 3), which is  
 1514 similar to the one reported previously in Saunio et al. (2020) from CCMI model (553 [476-677] Tg  $CH_4$   $yr^{-1}$ ) and still  
 1515 slightly higher than the one from the ACCMIP models (528 [454-617] Tg  $CH_4$   $yr^{-1}$  reported in Kirschke et al. (2013) and  
 1516 Saunio et al. (2016).

For the recent 2010-2019 decade, we report a climatological value based on only five models that contributed to CMIP6 runs (historical run followed by SSP3-7.0 projections starting in 2015, Collins et al. (2021)) to acknowledge the impact of the rise in atmospheric methane on the methane chemical sink. Hence, for 2010-2019, we report the climatological value of 563 [462-663] Tg CH<sub>4</sub> yr<sup>-1</sup> (Table 3).

### 3.3.2 Stratospheric loss

In the stratosphere, CH<sub>4</sub> is lost through reactions with excited atomic oxygen O(<sup>1</sup>D), atomic chlorine (Cl), atomic fluorine (F), and OH (Brasseur and Solomon, 2005; le Texier et al., 1988). Uncertainties in the chemical loss of stratospheric CH<sub>4</sub> are large, due to uncertain interannual variability in stratospheric transport (Zhang et al., 2023) as well as its chemical interactions and feedbacks with stratospheric O<sub>3</sub> (Morgenstern et al., 2018). Particularly, the fraction of stratospheric loss due to the different oxidants is still uncertain, with possibly 20-35% due to halons, about 25% due to O(<sup>1</sup>D) mostly in the high stratosphere and the rest due to stratospheric OH (McCarthy et al., 2003).

In this study, six chemistry climate models that contributed to CMIP6 modelling activities (Table S5) provided estimates of CH<sub>4</sub> chemical loss, including reactions with OH, O(<sup>1</sup>D), and Cl; CH<sub>4</sub> photolysis is also included but occurs only above the stratosphere. Considering a 200 hPa tropopause height, these six CMIP6 simulations suggest an estimate of 34 [10-51] Tg CH<sub>4</sub> yr<sup>-1</sup> for the CH<sub>4</sub> stratospheric sink for the 2000-2009 decade (Table S5), similar to the value derived from the previous CCMI activity reported in Saunio et al. (2020) (31 [12-41] Tg CH<sub>4</sub> yr<sup>-1</sup>). The lowest estimate provided by a model (10 Tg CH<sub>4</sub> yr<sup>-1</sup>) is quite unrealistic and would yield a methane stratospheric lifetime of several hundreds of years. As a result, this outlier is excluded and we prefer to report a mean of 39 Tg CH<sub>4</sub> yr<sup>-1</sup> associated with a range of [27-51] for 2000-2009.

For 2010-2019, we report here a climatological range of 28-43 Tg CH<sub>4</sub> yr<sup>-1</sup> associated with a mean value of 37 Tg CH<sub>4</sub> yr<sup>-1</sup> (Table 3) based on five models that contributed to CMIP6 runs (historic followed by SSP3-7.0 projections starting in 2015; Table S5).

### 3.3.3 Tropospheric reaction with Cl

Halogen atoms can also contribute to the oxidation of CH<sub>4</sub> in the troposphere. Allan et al. (2005) measured mixing ratios of methane and δ<sup>13</sup>C-CH<sub>4</sub> at two stations in the southern hemisphere from 1991 to 2003, and found that the apparent kinetic isotope effect (KIE) of the atmospheric CH<sub>4</sub> sink was significantly larger than that explained by OH alone. A seasonally varying sink due to Cl in the marine boundary layer of between 13 and 37 Tg CH<sub>4</sub> yr<sup>-1</sup> was proposed as the explanatory mechanism (Allan et al., 2007; Platt et al., 2004). This sink was estimated to occur mainly over coastal and marine regions, where sodium chloride (NaCl) from evaporated droplets of seawater react with NO<sub>2</sub> to eventually form Cl<sub>2</sub>, which then UV-dissociates to Cl. However significant production of nitryl chloride (ClNO<sub>2</sub>) at continental sites has been recently reported (Riedel et al., 2014) and suggests the broader presence of Cl, which in turn would expand the significance of the Cl sink in the troposphere. Recently, Hossaini et al. (2016), Sherwen et al. (2016), and Wang et al. (2019b, 2021b) have made

significant improvements in tropospheric chemistry modelling and they conclude to an oxidation contribution of 2.6%, 2%, 1% and 0.8%, respectively. These values correspond to a tropospheric CH<sub>4</sub> loss of around 12-13 Tg CH<sub>4</sub> yr<sup>-1</sup>, 9 Tg CH<sub>4</sub> yr<sup>-1</sup>, 5 Tg yr<sup>-1</sup>, and 3 Tg CH<sub>4</sub> yr<sup>-1</sup> respectively, much lower than the first estimates by Allan et al. (2007). The recent work of Wang et al. (2021b) is the most comprehensive modelling study and based upon Sherwen et al. (2016) and Wang et al. (2019b). Both the KIE approach and chemistry transport model simulations carry uncertainties (extrapolations based on only a few sites and use of indirect measurements, for the former and missing sources, coarse resolution, underestimation of some anthropogenic sources for the latter). However, Gromov et al. (2018) found that Cl can contribute only 0.23% the tropospheric sink of CH<sub>4</sub> (about 1 Tg CH<sub>4</sub> yr<sup>-1</sup>) in order to balance the global <sup>13</sup>C(CO) budget (see their Table S1). While tropospheric Cl has a marginal impact on the total CH<sub>4</sub> sink (few percents), it influences more significantly the atmospheric isotopic δ<sup>13</sup>C-CH<sub>4</sub> signal and improved estimates of the tropospheric Cl amount should be used for isotopic CH<sub>4</sub> modelling studies (Strode et al., 2020; Thanwerdas et al., 2022b). Each recent Cl estimate suggests a reduced contribution to the methane loss than previously reported by Allan et al. (2007). As a result, we suggest here to use the mean, minimum and maximum of the last five estimates published since 2016, leading to a climatological value of 6 [1-13] Tg CH<sub>4</sub> yr<sup>-1</sup> (Table 3), thus reducing both the magnitude and the uncertainty range compared to Saunio et al. (2020).

#### 3.3.4 Soil uptake

Unsaturated oxic soils are sinks of atmospheric CH<sub>4</sub> due to the presence of methanotrophic bacteria, which consume CH<sub>4</sub> as a source of energy. Dutaur and Verchot (2007) conducted a comprehensive meta-analysis of field measurements of CH<sub>4</sub> uptake spanning a variety of ecosystems. Extrapolating to the global scale, they reported a range of 36 ± 23 Tg CH<sub>4</sub> yr<sup>-1</sup>, but also showed that stratifying the results by climatic zone, ecosystem, and soil type led to a narrower range (and lower mean estimate) of 22 ± 12 Tg CH<sub>4</sub> yr<sup>-1</sup>. Modelling studies, employing meteorological data as external forcing, have also produced a considerable range of estimates. Using a soil depth-averaged formulation based on Fick's law with parameterizations for diffusion and biological oxidation of CH<sub>4</sub>, Ridgwell et al. (1999) estimated the global sink strength at 38 Tg CH<sub>4</sub> yr<sup>-1</sup>, with a range 20-51 Tg CH<sub>4</sub> yr<sup>-1</sup> reflecting the model structural uncertainty in the base oxidation parameter. Curry (2007) improved on the latter by employing an exact solution of the one-dimensional diffusion-reaction equation in the near-surface soil layer (i.e., exponential decrease in CH<sub>4</sub> concentration below the surface), a land surface hydrology model, and calibration of the oxidation rate to field measurements. This resulted in a global estimate of 28 Tg CH<sub>4</sub> yr<sup>-1</sup> (9-47 Tg CH<sub>4</sub> yr<sup>-1</sup>), the result reported by Zhuang et al. (2013), Kirschke et al. (2013) and Saunio et al. (2016). Ito and Inatomi (2012) used an ensemble methodology to explore the variation in estimates produced by these parameterizations and others, which spanned the range 25-35 Tg CH<sub>4</sub> yr<sup>-1</sup>. For the period 2000-2020, as part of the wetland emissions modelling activity, JSBACH (Kleinen et al., 2020) and VISIT (Ito and Inatomi, 2012) models compute a global CH<sub>4</sub> soil uptake to 18 and 35 Tg CH<sub>4</sub> yr<sup>-1</sup>, respectively.



1580 Murguía-Flores et al. (2018) further refined the Curry (2007) model's structural and parametric representations of key  
 1581 drivers of soil methanotrophy, demonstrating good agreement with the observed latitudinal distribution of soil uptake  
 1582 (Dutaur and Verchot, 2007). Their model (MeMo) simulates a CH<sub>4</sub> soil sink of 37.5 Tg CH<sub>4</sub> yr<sup>-1</sup> for the period 2010-2019  
 1583 (Fig. S4), compared to 39.5 and 31.3 Tg CH<sub>4</sub> yr<sup>-1</sup> using the Ridgwell et al. (1999) and Curry (2007) parameterizations,  
 1584 respectively, under the same meteorological forcing, run specifically for this study. For the 2000s period, the simulations  
 1585 estimate the soil uptake at 30.4, 36.7 and 38.3 Tg CH<sub>4</sub> yr<sup>-1</sup> based on the parameterization of Curry, MeMo, and Ridgwell,  
 1586 respectively. As part of a more comprehensive model accounting for a range of CH<sub>4</sub> sources and sinks, Tian et al. (2010,  
 1587 2015, 2016) computed vertically-averaged CH<sub>4</sub> soil uptake including the additional mechanisms of aqueous diffusion and  
 1588 plant-mediated (*aerenchyma*) transport, arriving at the estimate 30±19 Tg CH<sub>4</sub> yr<sup>-1</sup> (Tian et al., 2016) for the 2000s. The  
 1589 still more comprehensive biogeochemical model of Riley et al. (2011) included vertically resolved representations of the  
 1590 same processes considered by Tian et al. (2016), in addition to grid cell fractional inundation and, importantly, the joint  
 1591 limitation of uptake by both CH<sub>4</sub> and O<sub>2</sub> availability in the soil column. Riley et al. (2011) estimated a global CH<sub>4</sub> soil sink  
 1592 of 31 Tg CH<sub>4</sub> yr<sup>-1</sup> with a structural uncertainty of 15-38 Tg CH<sub>4</sub> yr<sup>-1</sup> (a higher upper limit resulted from an elevated gas  
 1593 diffusivity to mimic convective transport; as this is not usually considered, we adopt the lower upper bound associated with  
 1594 no limitation of uptake at low soil moisture). A model of this degree of complexity is required to explicitly simulate situations  
 1595 where the soil water content increases enough to inhibit the diffusion of oxygen, and the soil becomes a methane source  
 1596 (Lohila et al., 2016). This transition can be rapid, thus creating areas (for example, seasonal wetlands) that can be either a  
 1597 source or a sink of methane depending on the season.  
 1598 The previous Curry (2007) estimate can be revised upward slightly based on subsequent work and the increase in CH<sub>4</sub>  
 1599 concentration since that time. Indeed, Murguía-Flores et al. (2021) estimated that the global soil-uptake doubled between  
 1600 1900 and 2015 and could further increase due to enhanced diffusion of CH<sub>4</sub> into soil as a result of increases in atmospheric  
 1601 CH<sub>4</sub> mole fraction. Further investigation of the soil uptake is required to better constrain this process at the global scale  
 1602 while it is highly dependent on local scale microbial activity and environmental conditions (e.g., D'Imperio et al., 2023;  
 1603 Fest et al., 2017).  
 1604 Considering the latest estimates (based on VISIT, JSBACH, and Memo models, Table S6 in the supplementary) we report  
 1605 here a mean estimate of 31 [17-39] Tg CH<sub>4</sub> yr<sup>-1</sup> for 2000-2009 and 32 [18-40] for 2010-2019 Tg CH<sub>4</sub> yr<sup>-1</sup> (Table 3).

### 1606 **3.3.5 CH<sub>4</sub> lifetime**

1607 The atmospheric lifetime of a given gas in steady state may be defined as the global atmospheric burden (Tg) divided by the  
 1608 total sink (Tg yr<sup>-1</sup>) (IPCC, 2001). This value is different from what is called perturbation lifetime. Perturbation lifetime is  
 1609 used to determine how a one-time pulse emission may decay as a function of time as needed for the calculation of Global  
 1610 Warming Potentials (GWPs), and as a result is related to a theoretical concept. For CH<sub>4</sub>, the corresponding perturbation  
 1611 lifetime that should be used in the GWP calculation is 11.8 ± 1.8 years (Forster et al., 2021). In this section, we discuss the

1612 global atmospheric lifetime (also called ‘burden lifetime’ or ‘turnover lifetime’) that characterises the time required to turn  
1613 over the global atmospheric burden and defined as the burden divided by the removal flux.

1614 Global models provide an estimate of the loss of the gas due to individual sinks, which can then be used to derive lifetime  
1615 due to a specific sink. For example, the tropospheric lifetime of CH<sub>4</sub> is determined as the global atmospheric CH<sub>4</sub> burden  
1616 divided by the loss from OH oxidation in the troposphere, sometimes called “chemical lifetime”. The total lifetime of  
1617 CH<sub>4</sub> corresponds to the global burden divided by the total loss including tropospheric loss from OH oxidation, stratospheric  
1618 chemistry and soil uptake. The CCMI (Plummer et al., 2021) and CMIP6 (Collins et al., 2021) runs estimate the tropospheric  
1619 methane lifetime at about 9.2 years (average over years 2000-2009), with a range of 7.5-11 years (see Table S5). This range  
1620 agrees with previous values found in ACCMIP and CCMI (9.3 [7.1-10.6] years, Voulgarakis et al. (2013), 9 [7.2-10.1] years,  
1621 Saunio et al. (2020)). Adding 31 Tg to account for the soil uptake to the total chemical loss of the CMIP6 and CCMI  
1622 models, we derive a total CH<sub>4</sub> lifetime of 8.2 years (average over 2000-2009 with a range of 6.8-9.7 years). The lifetime  
1623 calculated over 2010-2019 based on CMIP6 simulations is similar (Table S5). These updated model estimates of total  
1624 CH<sub>4</sub> lifetime agree with the previous estimates from ACCMIP (8.2 [6.4-9.2] years for year 2000, Voulgarakis et al. (2013))  
1625 and Saunio et al. (2020) based CCMI models. Reducing the large spread in CH<sub>4</sub> lifetime (between models, and between  
1626 models and observation-based estimates) would 1) bring an improved constraint on global total methane emissions, and 2)  
1627 ensure an accurate forecast of future climate.

## 1628 **4 Atmospheric observations and top-down inversions**

### 1629 **4.1 Atmospheric observations**

1630 Systematic atmospheric CH<sub>4</sub> observations began in 1978 (Blake et al., 1982) with infrequent measurements from discrete  
1631 air samples collected in the Pacific at a range of latitudes from 67°N to 53°S. Because most of these air samples were from  
1632 well-mixed oceanic air masses and the measurement technique was precise and accurate, they were sufficient to establish  
1633 an increasing trend and the first indication of the latitudinal gradient of methane. Spatial and temporal coverage was greatly  
1634 improved soon after (Blake and Rowland, 1986) with the addition of the Earth System Research Laboratory from US  
1635 National Oceanic and Atmospheric Administration (NOAA/GML) flask network (Steele et al. (1987); Lan et al. (2024), Fig.  
1636 1), and the Advanced Global Atmospheric Gases Experiment (AGAGE) (Cunnold et al., 2002; Prinn et al., 2018), the  
1637 Commonwealth Scientific and Industrial Research Organisation (CSIRO, Francey et al. (1999)), the University of California  
1638 Irvine (UCI, Simpson et al., 2012) and in situ and flask measurements from regional networks, such as ICOS (Integrated  
1639 Carbon Observation System) in Europe (<https://www.icos-ri.eu/>). The combined datasets provide the longest time series of  
1640 globally averaged CH<sub>4</sub> abundances. Since the early-2000s, CH<sub>4</sub> column-averaged mole fractions have been retrieved through  
1641 passive remote sensing from space (Buchwitz et al., 2005a, 2005b; Butz et al., 2011; Crevoisier et al., 2009; Frankenberg et  
1642 al., 2005; Hu et al., 2018). Ground-based Fourier transform infrared (FTIR) measurements at fixed locations also provide

1643 time-resolved CH<sub>4</sub> column observations during daylight hours, and a validation dataset against which to evaluate the satellite  
1644 measurements such as the Total Carbon Column Observing Network (TCCON) network (e.g., Pollard et al., 2017; Wunch  
1645 et al., 2011), or Network for Detection of Atmospheric Composition Change (NDACC) (e.g., Bader et al., 2017).  
1646 In this budget, in-situ observations from the different networks were used in the top-down atmospheric inversions to estimate  
1647 CH<sub>4</sub> sources and sinks over the period 2000-2020. Satellite observations from the TANSO/FTS instrument on board the  
1648 satellite GOSAT were used to estimate CH<sub>4</sub> sources and sinks over the period 2010-2020. Other atmospheric data (FTIR,  
1649 airborne measurements, AirCore, isotopic measurements, etc.) have been used for validation by some groups, but not  
1650 specifically in this study. However, further information is provided in Tables S7, S8, S9, S10, and S11 and a more  
1651 comprehensive validation of the inversions is planned to use some of these data.

#### 1652 **4.1.1 In situ CH<sub>4</sub> observations and atmospheric growth rate at the surface**

1653 We use globally averaged CH<sub>4</sub> mole fractions at the Earth's surface from the four observational networks (NOAA/GML,  
1654 AGAGE, CSIRO and UCI). The data are archived at the World Data Centre for Greenhouse Gases (WDCGG) of the WMO  
1655 Global Atmospheric Watch (WMO-GAW) program (<https://gaw.kishou.go.jp/>), including measurements from other sites  
1656 that are not operated as part of the four networks. The CH<sub>4</sub> in-situ monitoring network has grown significantly over the last  
1657 decade due to the emergence of laser diode spectrometers which are robust and accurate enough to allow deployments with  
1658 low maintenance enabling the development of denser networks in developed countries (Stanley et al., 2018; Yver Kwok et  
1659 al., 2015), and new stations in remote environments (Bian et al., 2015; Nisbet et al., 2019).  
1660 The networks differ in their sampling strategies, including the frequency of observations, spatial distribution, and methods  
1661 of calculating globally averaged CH<sub>4</sub> mole fractions. Details are given in the supplementary material of Kirschke et al.  
1662 (2013). The global average values of CH<sub>4</sub> abundances at Earth's surface presented in Fig. 1 are computed using long-term  
1663 measurements from background conditions with minimal influence from immediate emissions. All measurements are  
1664 calibrated against gas standards either on the current WMO reference scale or on independent scales with well-estimate  
1665 differences from the WMO scale. The current WMO reference scale, maintained by NOAA/ESRL, WMO-X2004A  
1666 (Dlugokencky et al., 2005) was updated in July 2015. NOAA and CSIRO global means are on this scale. AGAGE uses an  
1667 independent standard scale (based on work by Tohoku University (Aoki et al., 1992) and maintained at Scripps Institution  
1668 of Oceanography (SIO)), but direct comparisons of standards and indirect comparisons of atmospheric measurements show  
1669 that differences are well below 5 ppb (Tans and Zwellberg, 2014; Vardag et al., 2014) and the TU-1987 scale used for  
1670 AGAGE measurements is only 0.5 ppb difference from WMO-X2004A at 1900 ppb level. UCI uses another independent  
1671 scale that was established in 1978 and is traceable to NIST (Flores et al., 2015; Simpson et al., 2012), but has not been  
1672 included in standard exchanges with other networks so differences with the other networks cannot be quantitatively defined.  
1673 Additional experimental details are presented in the supplementary material from Kirschke et al. (2013) and references  
1674 therein.

In Fig. 1 (a) globally averaged CH<sub>4</sub> and (b) its growth rate (derivative of the deseasonalized trend curve) through to 2022 are plotted for the four measurement programs using a procedure of signal decomposition described in Thoning et al. (1989). We define the annual  $G_{ATM}$  as the increase in the atmospheric concentrations from Jan. 1 in one year to Jan. 1 in the next year. Agreement among the four networks is good for the global growth rate, especially since ~1990. The large differences observed mainly before 1990 probably reflect the different spatial coverage of each network. The long-term behaviour of globally averaged atmospheric CH<sub>4</sub> shows a positive growth rate (defined as the derivative of the deseasonalized mixing ratio) that is slowing down from the early-1980s through 1998, a near-stabilisation of CH<sub>4</sub> concentrations from 1999 to 2006, and a renewed period with positive persistent overall accelerating growth rates since 2007, slightly larger after 2014. From 1999 to 2006, the annual increase of atmospheric CH<sub>4</sub> was remarkably small at  $0.6 \pm 0.1$  ppb yr<sup>-1</sup>. After 2006, the atmospheric growth rate has increased to a level similar to that of the mid-1990s ( $\sim 5$  ppb yr<sup>-1</sup>), and for 2014 and 2015 even to that of the 1980s ( $> 10$  ppb yr<sup>-1</sup>). In the two recent years 2020 and 2021, the highest growth rates of 15 ppb yr<sup>-1</sup> and 18 ppb yr<sup>-1</sup> (see Sect. 6) were unprecedented since the 1980s. On decadal timescales, the annual increase is on average  $2.2 \pm 0.3$  ppb yr<sup>-1</sup> for 2000-2009,  $7.6 \pm 0.3$  ppb yr<sup>-1</sup> for 2010-2019 and  $15.2 \pm 0.4$  ppb yr<sup>-1</sup> for the year 2020 (Table 3). Both climate variability and anthropogenic emission changes are responsible for variations in atmospheric CH<sub>4</sub> growth rates. Indeed, climate variation such as El Nino Southern Oscillation induce changes in emissions such as biomass burning or wetland emission but also impact OH oxidation (e.g., Rowlinson et al., 2019; Zhao et al., 2020b; Peng et al., 2022).

#### 4.1.2 Satellite data of column average CH<sub>4</sub>

In this budget, we use satellite data from the JAXA satellite Greenhouse Gases Observing SATellite (GOSAT) launched in January 2009 (Butz et al., 2011; Morino et al., 2011) containing the TANSO-FTS instrument, which observes in the shortwave infrared (SWIR). Different retrievals of CH<sub>4</sub> based on TANSO-FTS/GOSAT products are made available to the community: from NIES (Yoshida et al., 2013), from SRON (Schepers et al., 2012) and from University of Leicester (Parker et al., 2020; Parker and Boesch, 2020). The three retrievals are used by the top-down systems (Table 4 and S6). Although GOSAT retrievals still show significant unexplained biases and limited sampling in cloud covered regions and in the high latitude winter, it represents an important improvement compared to the first satellite measuring CH<sub>4</sub> from space, SCIAMACHY (Scanning Imaging Absorption spectrometer for Atmospheric Cartography) both for random and systematic observation errors (see Table S2 of Buchwitz et al. (2016)).

Here, as in Saunio et al. (2020), only inversions using GOSAT retrievals are used.

#### 4.2 Top-down inversions used in the budget

An atmospheric inversion is the optimal combination of atmospheric observations, of a model of atmospheric transport and chemistry, of a prior estimate of CH<sub>4</sub> sources and sinks, and of their uncertainties, to provide improved estimates of the

1705 sources and sinks, and their uncertainty. The theoretical principle of CH<sub>4</sub> inversions is detailed in the Supplementary  
 1706 Material and an overview of the different methods applied to CH<sub>4</sub> is presented in Houweling et al. (2017).  
 1707 We consider an ensemble of inversions gathering various chemistry transport models, differing in vertical and horizontal  
 1708 resolutions, meteorological forcing, advection and convection schemes, and boundary layer mixing. Including these  
 1709 different systems is a conservative approach that allows us to cover different potential uncertainties of the inversion, among  
 1710 them: model transport, set-up issues, and prior dependency. General characteristics of the inversion systems are provided in  
 1711 Table 4. Further details can be found in the referenced papers and in the Supplementary Material. Each group was asked to  
 1712 provide gridded flux estimates for the period 2000-2020, using either surface or satellite data, but no additional constraints  
 1713 were imposed so that each group could use their preferred inversion setup. Two sets of prior emission distributions were  
 1714 built from the most recent inventories or model-based estimates (see Supplementary Material), but its use was not mandatory  
 1715 (see Table S8 to S11 for the inversion characteristics). This approach corresponds to a flux assessment, but not to a model  
 1716 inter-comparison as the protocol was not too stringent. Estimating posterior uncertainty is time and computer resource  
 1717 consuming, especially for the 4D-var approaches and Monte Carlo methods. Posterior uncertainties have not been requested  
 1718 for this study, but they were found to be lower than the ensemble spread in Sauniois et al. (2020). Indeed, chemistry transport  
 1719 models differ in inter-hemispheric transport, stratospheric CH<sub>4</sub> profiles, and OH distribution, limitations which are not fully  
 1720 considered in the individual posterior uncertainty. As a result, we report the minimum-maximum range among the different  
 1721 top-down approaches.  
 1722 Seven atmospheric inversion systems using global Eulerian transport models were used in this study; they contributed to the  
 1723 previous budgets that included eight atmospheric inversion systems in Sauniois et al. (2016) and nine in Sauniois et al. (2020).  
 1724 Each inversion system provided one or several simulations, including sensitivity tests varying the assimilated observations  
 1725 (surface or satellite), the OH interannual variability, or the prior fluxes ensemble. This represents a total of 24 inversion runs  
 1726 with different time coverage: generally, 2000-2020 for surface-based observations, and 2010-2020 for GOSAT-based  
 1727 inversions (Table 4 and Table S7). In poorly observed regions, top-down surface inversions may rely on the prior estimates  
 1728 and bring little or no additional information to constrain (often) spatially overlapping emissions (e.g., in India, China). Also,  
 1729 we recall that many top-down systems solve for the total fluxes at the surface only or for some categories that may differ  
 1730 from the GCP categories. When multiple sensitivity tests were performed the mean of this ensemble was used not to  
 1731 overweight one particular inverse system. It should also be noticed that some satellite-based inversions are in fact combined  
 1732 satellite and surface inversions as they use surface-based inversions to correct the latitudinal bias of the satellite retrievals  
 1733 against the optimised atmosphere measurements to correct for errors in the transport model especially in the stratosphere  
 1734 (e.g., Segers et al., 2022; Maasakkers et al., 2019). Nevertheless, these inversions are still referred to as satellite-based  
 1735 inversions. Most of the top-down models use the OH distribution from the TRANSCOM experiment (Patra et al., 2011)  
 1736 either as fixed over the period or with the interannual variability derived by Patra et al. (2021).

Each group provided gridded monthly maps of emissions for both their prior and posterior total and for sources per category (see the categories Sect. 2.3). Results are reported in Sect. 5. Atmospheric sinks from the top-down approaches have been provided for this budget, and are compared with the values reported in Sauniois et al. (2020). Not all inverse systems report their chemical sink; as a result, the global mass imbalance for the top-down budget is derived as the difference between total sources and total sinks for each model when both fluxes were reported.

**5 Methane budget: top-down and bottom-up comparison**

**5.1 Global methane budget**

**5.1.1 Global total methane emissions**

**Top-down estimates.** At the global scale, the total annual emissions inferred by the ensemble of 24 inversions is 575 [553-586] Tg CH<sub>4</sub> yr<sup>-1</sup> for the 2010-2019 decade (Table 3), with the highest ensemble mean emission of 608 [581-627] Tg CH<sub>4</sub> yr<sup>-1</sup> for 2020. Global emissions for 2000-2009 (543 Tg CH<sub>4</sub> yr<sup>-1</sup>) are consistent with Sauniois et al. (2016, 2020) and the range for global emissions, 526-558 Tg CH<sub>4</sub> yr<sup>-1</sup> falls within the range in Sauniois et al. (2016) (535-569) and Sauniois et al. (2020) (524-560), although the ensemble of inverse systems contributing to this budget is different from Sauniois et al. (2016, 2020). Changes in ensemble members contributing to the different budgets are a feature of each new GMB release and, therefore, introduce a source of variation (Table S7). The range reported gives the minimum and maximum values among studies and does not reflect the individual full uncertainties. In addition, most of the top-down models use the same OH distribution from the TRANSCOM experiment (Patra et al., 2011), which introduces less variability to the global budget than is likely justified, and so contributes to the rather low range (10%) compared to bottom-up estimates (see below). We recall here that Zhao et al. (2020a) found an uncertainty of about 17% in global methane emissions (518 to 611 Tg CH<sub>4</sub> yr<sup>-1</sup> for the early 2000s) due to changes in OH burden and distribution (OH ranging from 10.3 to 12.6 10<sup>5</sup> molec cm<sup>-3</sup>)

**Bottom-up estimates.** The bottom-up estimates considered here differ substantially from the top-down results, with annual global emissions being about 15% larger at 669 [512-849] Tg CH<sub>4</sub> yr<sup>-1</sup> for 2010-2019 (Table 3). Yet, thanks to the double counting corrections in this budget, bottom-up and top-down budgets are in better agreement compared to previous GMB releases. For the period 2000-2009, the discrepancy between bottom-up and top-down was about 30% of the top-down estimates in Sauniois et al. (2016, 2020) (167 and 156 Tg CH<sub>4</sub> yr<sup>-1</sup>, respectively), a value that has been reduced significantly in this budget (now 95 Tg CH<sub>4</sub> yr<sup>-1</sup> (<17%) for the same 2000-2009 period). This reduction is due to improvements from an important decrease in the estimate of emissions from natural and indirect anthropogenic emissions from bottom-up approaches, and more specifically inland freshwater emissions. From the previous budget, the estimate for inland freshwater emissions (lakes, ponds, reservoirs, rivers, and streams) has decreased from 159 Tg CH<sub>4</sub> yr<sup>-1</sup> to 112 Tg CH<sub>4</sub> yr<sup>-1</sup> (47 Tg decrease). Then, 23 Tg have been removed in the total freshwater ecosystem emissions due to double counting between vegetated wetlands and mostly small ponds and lakes (Sect. 3.2.2). As a result, the combined wetland and inland freshwater

emissions are estimated to be 242 Tg CH<sub>4</sub> yr<sup>-1</sup> for 2000-2009 (Table 3), compared with 306 Tg CH<sub>4</sub> yr<sup>-1</sup> in Sauniois et al. (2020).

This budget is the first that reconciles bottom-up and top-down total emissions within the uncertainty ranges. However, the uncertainty in the global budget remains high because of the large range reported for emissions from freshwater systems. Still, the upper bound of global emissions from bottom-up approaches is not consistent with top-down estimates that rely on OH burden constrained by methyl chloroform atmospheric observations and is still likely overestimated.

#### 5.1.2 Global methane emissions per source category

The global CH<sub>4</sub> emissions from natural and anthropogenic sources (see Sect. 2.3) for 2010-2019 are presented in Fig. 6, Fig. 7, and Table 3. Top-down estimates attribute about 65% of total emissions to anthropogenic activities (range of 55-70%), and 35% to natural emissions. Bottom-up estimates attribute 57% of emissions to direct anthropogenic and the rest to natural plus indirect anthropogenic emissions. A current predominant role of direct anthropogenic sources of CH<sub>4</sub> emissions is consistent with and strongly supported by available ice core and atmospheric CH<sub>4</sub> records. These data indicate that atmospheric CH<sub>4</sub> varied around 700 ppb during the last millennium before increasing by a factor of 2.6 to ~1800 ppb since pre-industrial times. Accounting for the decrease in mean-lifetime over the industrial period, Prather et al. (2012) estimated from these data a total source of 554±56 Tg CH<sub>4</sub> in 2010 of which about 64% (352±45 Tg CH<sub>4</sub>) was of direct anthropogenic origin, consistent with the range in our top-down estimates.

**Natural and indirect anthropogenic emissions.** Although smaller than in previous Global Methane Budget releases, the main remaining discrepancy between top-down and bottom-up budgets is found for the natural and indirect anthropogenic emission total (105 Tg), with 311 [183-462] Tg CH<sub>4</sub> yr<sup>-1</sup> for bottom-up and only 206 [188-225] Tg CH<sub>4</sub> yr<sup>-1</sup> for top-down over the 2010-2019 decade (Table 3). In the bottom-up estimates, this discrepancy comes first from the estimates in both inland freshwater sources (64 Tg) and second from other natural sources (20 Tg from geological sources, termites, oceans, and permafrost). The top-down approaches may be biased due to missing fluxes (mainly inland freshwaters) in their prior estimates.

For 2010-2019, the top-down and bottom-up derived estimates for wetlands emissions of 165 [145-214] Tg CH<sub>4</sub> yr<sup>-1</sup> and 159 [119-203] Tg CH<sub>4</sub> yr<sup>-1</sup> (Table 3), respectively, are comparable within their range. Based on diagnostic wetland area values (see notes in Table 3), bottom-up mean wetland emissions for the 2000-2009 period are smaller in this study than those of Sauniois et al. (2016) but larger than in Sauniois et al. (2020). The changes in wetland emissions from bottom-up models may be related to updates on the wetland extent data set (WAD2M), the use of two different meteorological forcings for this study and a different set of models (see Sect. 3.2.1). Conversely, the current 2000-2009 mean top-down wetland estimates are lower than those of Sauniois et al. (2016) and Sauniois et al. (2020) (Table 3). In the bottom-up estimates, the amplitude of the range of emissions of 116-189 is roughly similar to Sauniois et al. (2016) (151-222) and Sauniois et al.

(2020) (102-179) for 2000-2009. Here, the larger range in bottom-up estimates of wetland emissions is due to the use of GSWP3-W5E5 and greater sensibilities of some models to the climate parameters, as discussed in Sect. 3.2.1. Bottom-up and top-down estimates for wetland emissions agree better in this study ( $\sim 5 \text{ Tg yr}^{-1}$  for 2000-2009) than in Sauniois et al. (2016, 2020) ( $\sim 17 \text{ Tg yr}^{-1}$  and  $\sim 30 \text{ Tg yr}^{-1}$ , respectively). Natural emissions from inland freshwater systems were not included in the prior fluxes used in the top-down approaches, due to unavailable or uncertain gridded products at the start of the modelling activity. However, emissions from these inland freshwater systems may be implicitly included in the posterior estimates of the top-down models, as these two sources are close and probably overlap at the rather coarse resolution of the top-down models. This is the reason why the ‘wetland emissions’ in the top-down budget in fact better correspond to the sum of combined wetland and inland freshwaters emissions in the bottom-up budget. The double-counting of  $23 \text{ Tg CH}_4$  reduces the bottom-up budget for combined wetland and inland freshwaters from  $271 \text{ Tg CH}_4 \text{ yr}^{-1}$  to  $248 \text{ Tg CH}_4 \text{ yr}^{-1}$  (Sect. 3.2.2). Comparing the 2000-2009 decadal emissions from wetlands and inland freshwater ecosystems estimated by the bottom-up approaches across the last three Global Methane Budgets shows an upward and then a downward revision with  $305 (183+122) \text{ Tg CH}_4 \text{ yr}^{-1}$ ,  $356 (147+209) \text{ Tg CH}_4 \text{ yr}^{-1}$  and  $248 (159+112-23) \text{ Tg CH}_4 \text{ yr}^{-1}$  (respectively from Sauniois et al. (2016, 2020) and this work; the sum in bracket corresponds to the sum of vegetated wetland emissions and inland water emissions estimated through the different budgets). The combined wetland and inland freshwater emissions discrepancy between bottom-up and top-down approaches amount to  $105 \text{ Tg CH}_4 \text{ yr}^{-1}$  for the 2010-2019 decade. From a top-down point of view, the sum of all the natural sources is more robust than the partitioning between wetlands, inland waters, and other natural sources. Including all known spatio-temporal distributions of natural emissions in top-down prior fluxes would be a step forward to consistently compare natural versus anthropogenic total emissions between top-down and bottom-up approaches.

In the top-down budget, wetlands represent 28% on average of the total methane emissions but only 24% in the bottom-up budget (because of higher total emissions inferred) (see Table 3). Given the large uncertainties, neither bottom-up nor top-down approaches included in this study point to significant changes in wetland emissions between the two decades 2000-2009 and 2010-2019 at the global scale.

For the 2010-2019 decade, top-down inversions infer “Other natural emissions” (Table 3) at  $43 [40-46] \text{ Tg CH}_4 \text{ yr}^{-1}$ , whereas the sum of the individual bottom-up emissions is  $63 [24-93] \text{ Tg CH}_4 \text{ yr}^{-1}$ , contributing to a  $20 \text{ Tg}$  discrepancy between bottom-up and top-down approaches. Atmospheric inversions infer the same amount over the decade 2000-2009 as over 2010-2019, which is almost half of the value reported in Sauniois et al. (2016) ( $68 [21-130] \text{ Tg CH}_4 \text{ yr}^{-1}$ ). This reduction in magnitude and uncertainty is due to 1) a more consistent way of considering other natural emissions in the various inverse systems (same prior estimate as in this budget) and 2) a difference in the ensemble of top-down inversions reported here compared to previous releases. It is worth noting that, most of the top-down models include about the same ocean and onshore geological emissions and termite emissions in their prior scenarios. However,, none include freshwater or permafrost emissions in their prior fluxes, and thus in their posterior estimates.



Geological emissions are associated with relatively large uncertainties, and marine seepage emissions are still widely debated (Thornton et al., 2020). However, summing up all bottom-up fossil-CH<sub>4</sub> related sources (including anthropogenic emissions) leads to a total of 165 [135-190] Tg CH<sub>4</sub> yr<sup>-1</sup> in 2010-2019, which is about 29% of the top-down global CH<sub>4</sub> emissions, and 25% of the bottom-up total global estimate. These results agree with the value inferred from <sup>14</sup>C atmospheric isotopic analyses of 30% contribution of fossil-CH<sub>4</sub> to global emissions (Etiope et al., 2008; Lassey et al., 2007b). This total fossil fuel emissions from bottom-up approaches agrees well with the <sup>13</sup>C-based estimate of Schwietzke et al. (2016) of 192 ± 32 Tg CH<sub>4</sub> yr<sup>-1</sup>. In the bottom-up budget, the larger total emissions (due to uncertainties in bottom-up estimates of natural emissions) leads to a lower fossil fuel contribution compared to Lassey et al. (2007b).

**Anthropogenic direct emissions.** Total anthropogenic direct emissions for the period 2010-2019 were assessed to be statistically consistent between top-down (369 Tg CH<sub>4</sub> yr<sup>-1</sup>, range 350-391) and bottom-up approaches (358 Tg CH<sub>4</sub> yr<sup>-1</sup>, range 329-387), albeit top-down approaches infer direct anthropogenic emissions larger by 11 Tg CH<sub>4</sub> yr<sup>-1</sup> on average compared to bottom-up approaches (Table 3). The partitioning of anthropogenic direct emissions between agriculture and waste, fossil fuels extraction and use, and biomass and biofuel burning, also shows good consistency between top-down and bottom-up approaches, though top-down approaches still suggest less fossil fuel and more agriculture and waste emissions than bottom-up estimates (Table 3 and Fig. 6 and 7). For 2010-2019, agriculture and waste contributed an estimated 228 [213-242]Tg CH<sub>4</sub> yr<sup>-1</sup> in the top-down budget and 211 [195-231]Tg CH<sub>4</sub> yr<sup>-1</sup> in the bottom-up budget. Fossil fuel emissions contributed 115 [100-124] Tg CH<sub>4</sub> yr<sup>-1</sup> in the top-down budget and 120 [117-125] Tg CH<sub>4</sub> yr<sup>-1</sup> in the bottom-up budget. Biomass and biofuel burning contributed 27 [26-27] Tg CH<sub>4</sub> yr<sup>-1</sup> in the top-down budget and 28 [21-39]Tg CH<sub>4</sub> yr<sup>-1</sup> in the bottom-up budget. Biofuel CH<sub>4</sub> emissions rely on very few estimates currently (Wuebbles and Hayhoe, 2002). Although biofuel is a small source globally (~12 Tg CH<sub>4</sub> yr<sup>-1</sup>), more estimates are needed to allow a proper uncertainty assessment. Overall for top-down inversions the global fraction of total emissions for the different source categories is 40% for agriculture and waste, 20% for fossil fuels, and 5% for biomass and biofuel burning. With the exception of biofuel emissions, the uncertainty associated with global anthropogenic emissions appears to be smaller than that of natural sources but with an asymmetric uncertainty distribution (mean significantly different than median). The relative agreement between top-down and bottom-up approaches may indicate a limited capability of the inversion to separate emissions and a dependency to their prior fluxes; this agreement should therefore be treated with caution. Indeed, in poorly observed regions, top-down inversions rely on the prior estimates and bring little or no additional information to constrain (often) spatially overlapping emissions (e.g., in India, China). Also, as many top-down systems solve for the total fluxes at the surface or for some categories that may differ from the GCP categories, their posterior partitioning relies on the prior ratio between categories that are prescribed using bottom-up inventories.

### 1863 5.1.3 Global budget of total methane sinks

1864 **Top-down estimates.** The annual CH<sub>4</sub> chemical removal from the atmosphere is estimated to be 521 Tg CH<sub>4</sub> yr<sup>-1</sup> averaged  
1865 over the period 2010-2019, with an uncertainty of about ±2% (range 485-532 Tg CH<sub>4</sub> yr<sup>-1</sup>) (Table 3). All the inverse models  
1866 account for CH<sub>4</sub> oxidation by OH and O(<sup>1</sup>D), and some include stratospheric Cl oxidation (Table S8 to S11). Most of the  
1867 top-down models use the OH distribution from the TRANSCOM experiment (Patra et al., 2011) either as fixed over the  
1868 period or including interannual variability from Patra et al. (2021). This study shows no trend in OH and IAV below ±4%,  
1869 in agreement with Thompson et al. (2024) (no significant OH trend and IAV < 2%). As a result, the range of the top-down  
1870 sink estimates is rather low compared to bottom-up estimates (see below). Differences between transport models affect the  
1871 chemical removal of CH<sub>4</sub>, leading to different chemical loss rates, even with the same OH distribution. However,  
1872 uncertainties in the OH distribution and magnitude (around ±10% at the global scale, Zhao et al., 2019) are not considered  
1873 in our study, while they could contribute to a significant change in the chemical sink, and then in the derived posterior  
1874 emissions through the inverse process ((Zhao et al., 2020), around ±17% at the global scale, much larger than the model  
1875 spread derived here. The chemical sink represents more than 90% of the total sink, the rest being attributable to soil uptake  
1876 (35 [35-36] Tg CH<sub>4</sub> yr<sup>-1</sup>). The rather narrow range is due to the use of the same climatological soil sink provided within the  
1877 modelling protocol which is based on Murgia-Flores et al. (2018). This sink estimate used as prior in the inversions is a bit  
1878 higher than the mean estimate of the soil sink calculated by bottom-up models (30 Tg CH<sub>4</sub> yr<sup>-1</sup>, Sec. 3.3.4).

1879 **Bottom-up estimates.** The total chemical loss for the 2010s reported here is 602 Tg CH<sub>4</sub> yr<sup>-1</sup> with an uncertainty of 21%  
1880 (~125 Tg CH<sub>4</sub> yr<sup>-1</sup>). Differences in chemistry schemes in the models (especially in the stratosphere) and in the volatile  
1881 organic compound treatment probably explain most of the discrepancies among models (Zhao et al., 2019).

### 1882 5.2 Latitudinal and regional methane budgets

1883 The latitudinal and regional breakdown of the bottom-up budget is based on crude assumptions that we acknowledge here.  
1884 Natural and indirect anthropogenic emissions are based on wetland gridded products from land surface models and the  
1885 combination of the maps from lakes and ponds from Johnson et al. (2022), reservoirs from Johnson et al. (2022) and streams  
1886 and rivers from Rocher-Ros et al. (2023), the sum of those three scaled to 89 Tg CH<sub>4</sub> yr<sup>-1</sup> (shown in Fig. 5) to artificially  
1887 include the double counting (estimated only at the global scale) and match the global estimate. However, we acknowledge  
1888 that this procedure distributes the double counting relatively to the final emission distribution and not according to the  
1889 freshwater ecosystems where the double counting probably occurs. Wild animal and permafrost maps do not exist and are  
1890 missing from the calculation, leading to at least 3 Tg CH<sub>4</sub> yr<sup>-1</sup> of discrepancy. However, as aforementioned (Sections 3.2.5  
1891 and 3.2.7) this 3 Tg CH<sub>4</sub> yr<sup>-1</sup> estimate is probably underestimated in the bottom-up budget. Geological and ocean sources  
1892 are based on Etiope et al. (2019) and Weber et al. (2019) gridded products scaled to 50 Tg CH<sub>4</sub> yr<sup>-1</sup> to be consistent to the  
1893 reported global values. Finally, we use the termite emission map produced for this budget and used in the global budget.

1894 The latitudinal budget does not include the estimates from FAO and USEPA for the direct anthropogenic emissions as they  
1895 are only provided at country scale.

1896 **5.2.1 Latitudinal budget of total methane emissions**

1897 The latitudinal breakdown of emissions inferred from atmospheric inversions reveals a dominance of emissions in the  
1898 latitudinal band 90°S-30°N of 364 [337-390] Tg CH<sub>4</sub> yr<sup>-1</sup>, representing 64% of the global total (Table 5 and 6). As emissions  
1899 in the Tropics (30°S-30°N) dominate this latitudinal contribution, we may refer to 90°S-30°N as the Tropics in the following  
1900 32% of the emissions are from the mid-latitudes (187 [160-204] Tg CH<sub>4</sub> yr<sup>-1</sup>) and 4% from high latitudes (above 60°N). The  
1901 amounts of emissions depend on the land surface area of the region, however the 90°S-30°N latitudinal band represents 53%  
1902 of global land surfaces and the boreal region 60°N-90°N around 13%. Hence, the relative contribution of the emissions from  
1903 the 90°S-30°N region is much larger (11 points of percent more) than the percentage of its land surface areas, on the contrary  
1904 the boreal regions (60°N-90°N) emissions contribute significantly less than the surface area percentage of this region (9  
1905 points of percent less). The ranges around the mean latitudinal emissions are larger than for the global CH<sub>4</sub> sources. While  
1906 the top-down uncertainty is less than ±5% at the global scale, it increases to ±7% for the tropics, to ±12% the northern mid-  
1907 latitudes and to more than ±20% in the northern high-latitudes (for 2010-2019, Table 5). Both top-down and bottom-up  
1908 approaches consistently show that CH<sub>4</sub> decadal emissions have increased by +21-27 Tg CH<sub>4</sub> yr<sup>-1</sup> in the tropics, and by +5-  
1909 16 Tg CH<sub>4</sub> yr<sup>-1</sup> in the northern mid-latitudes between 2000-2009 and 2010-2019 using the mean ensemble estimate.  
1910 Over 2010-2019, at the global scale, satellite-based inversions infer almost identical emissions to ground-based inversions  
1911 (difference of +1 [-3-9] Tg CH<sub>4</sub> yr<sup>-1</sup>, with GOSAT based inversion a bit higher than surface measurements-based inversions),  
1912 when comparing consistently surface versus satellite-based inversions for each system, similar to Saunio et al. (2020). This  
1913 difference is much lower than the range derived between the different systems (range of 20 Tg CH<sub>4</sub> yr<sup>-1</sup> using surface- or  
1914 satellite-based inversions). This result reflects that differences in atmospheric transport among the systems probably have  
1915 more impact on the estimated global emissions than the types of observations assimilated.  
1916 As expected, considering the different coverage of observation datasets, regional distributions of inferred emissions differ  
1917 depending on the nature of the observations used (satellite or surface). The largest differences (satellite-based minus surface-  
1918 based inversions) are observed over the tropical region, between -10 and +43 Tg CH<sub>4</sub> yr<sup>-1</sup> (90°S to 30°N), and the northern  
1919 mid-latitudes (between -36 and -2 Tg CH<sub>4</sub> yr<sup>-1</sup>). Satellite data provide stronger constraints on fluxes in tropical regions than  
1920 surface data, due to a much larger spatial coverage. It is therefore not surprising that differences between these two types of  
1921 observations are found in the tropical band, and consequently in the northern mid-latitudes to balance total emissions, thus  
1922 affecting the north-south gradient of emissions. However, the regional patterns of these differences are not consistent  
1923 through the different inverse systems. Indeed, some systems found higher emissions in the tropics when using GOSAT  
1924 instead of surface observations, while others found the opposite. This difference between inversion systems may depend on

Supprimé: While t

Supprimé: s,

Supprimé: 12

Supprimé: relative importance

Supprimé: the

Supprimé: for the 90°S-30°N region

Supprimé: relative importance of their

Supprimé: s

1933 whether or not a bias correction is applied to the satellite data based on surface observations, and also on the modelled  
1934 horizontal and vertical transports, in the troposphere and in the stratosphere.

1935 **5.2.2 Latitudinal methane emissions per source category**

1936 The analysis of the latitudinal CH<sub>4</sub> budget per source category (Fig. 8 and Table 6) can be performed both for bottom-up  
1937 and top-down approaches but with limitations. Bottom-up estimates of natural and indirect anthropogenic emissions are  
1938 based on assumptions as specified at the beginning of this section 5.2. For top-down estimates, as already noted, the  
1939 partitioning of emissions per source category has to be considered with caution. Indeed, using only atmospheric  
1940 CH<sub>4</sub> observations to constrain CH<sub>4</sub> emissions makes this partitioning largely dependent on prior emissions. However,  
1941 differences in spatial patterns and seasonality of emissions can be utilised to constrain emissions from different categories  
1942 by atmospheric methane observations (for those inversions solving for different sources categories, see Sect. 2.3).

1943 Agriculture and waste are the largest sources of CH<sub>4</sub> emissions in the tropics and southern hemisphere (140 [121-150] Tg  
1944 CH<sub>4</sub> yr<sup>-1</sup> in the bottom-up budget and 150 [135-168] Tg CH<sub>4</sub> yr<sup>-1</sup> in the top-down budget, about 40% of total CH<sub>4</sub> emissions  
1945 in this region) (Table 6). However, combined wetland and inland freshwater emissions are nearly as large with 151 [85-234]  
1946 Tg CH<sub>4</sub> yr<sup>-1</sup> in the bottom-up budget and 128 [112-155] Tg CH<sub>4</sub> yr<sup>-1</sup> in the top-down budget (Table 6). Anthropogenic  
1947 emissions dominate in the northern mid-latitudes, with the highest contribution from agriculture and waste emissions (40%  
1948 of total emissions in the top-down budget), closely followed by fossil fuel emissions (32% of total emissions, top-down  
1949 budget). Boreal regions are largely dominated by inland freshwater emissions (41% and 54% of total emissions, top-down  
1950 and bottom-up budget, respectively) (Table 6).

1951 The largest discrepancies between the top-down and the bottom-up budgets are found in the mid-latitudes and boreal regions  
1952 from the natural and indirect sources with bottom-up estimates twice as large as the top-down ones, especially in the inland  
1953 freshwater category.

1954 The uncertainty for wetlands and inland freshwater emissions is larger in the bottom-up models than in the top-down models  
1955 (mostly wetlands), while uncertainty in anthropogenic emissions is larger in the top-down models than in the bottom-up  
1956 inventories. The large uncertainty in tropical inland freshwater emissions (mostly wetlands) of ±44% results from large  
1957 regional differences between the bottom-up land-surface models. Although they are using the same forcings, their responses  
1958 in terms of flux density show different sensitivities to temperature, water vapour pressure, precipitation, and radiation.

1959 **5.2.3 Regional budget for total emissions**

1960 The regional breakdown of emissions is provided for 18 continental regions (see map in Fig. S3 and Table S1 with the  
1961 country aggregation in the supplementary materials).

1962 At the regional scale and, for the 2010-2019 decade (Table 7), total methane emissions are dominated by South East Asia  
1963 with 63 [52-71] Tg CH<sub>4</sub> yr<sup>-1</sup>, China with 57 [37-72] Tg CH<sub>4</sub> yr<sup>-1</sup>, and South Asia with 52 [43-60] Tg CH<sub>4</sub> yr<sup>-1</sup> (top-down

1964 budget). These top three emitters contribute 30% of total global CH<sub>4</sub> emissions. The following high emitting regions are  
1965 Brazil 47 [41-58] Tg CH<sub>4</sub> yr<sup>-1</sup>, Equatorial Africa 47 [39-59] Tg CH<sub>4</sub> yr<sup>-1</sup>, USA 38 [32-46] Tg CH<sub>4</sub> yr<sup>-1</sup>, Southwest South  
1966 America 38 [30-48] Tg CH<sub>4</sub> yr<sup>-1</sup>, Russia 36 [27-45] Tg CH<sub>4</sub> yr<sup>-1</sup>, Europe 31 [24-36] Tg CH<sub>4</sub> yr<sup>-1</sup>, Middle East 31 [24-39] Tg  
1967 CH<sub>4</sub> yr<sup>-1</sup>, Northern Africa 25 [23-29] Tg CH<sub>4</sub> yr<sup>-1</sup>, and Canada 20 [17-24 ] Tg CH<sub>4</sub> yr<sup>-1</sup>. Other regions contribute less than  
1968 20 Tg CH<sub>4</sub> yr<sup>-1</sup>.

1969 **5.2.4 Regional budget per source category**

1970 **Natural and indirect anthropogenic emissions versus direct anthropogenic emissions.** In agreement with Stavert et al.  
1971 (2021), natural and indirect anthropogenic emissions are dominated by Brazil, Canada, Russia, Equatorial Africa and  
1972 Southeast Asia, contributing 126 Tg CH<sub>4</sub> yr<sup>-1</sup> in the bottom-up and 105 Tg CH<sub>4</sub> yr<sup>-1</sup> in the top-down budget (Table 7), i.e.,  
1973 47% and 50% of the global natural and indirect anthropogenic emissions in these budgets, respectively. At regional scale  
1974 also, the range of uncertainty in natural and indirect anthropogenic emissions are much larger in the bottom-up budget than  
1975 in the top-down budget (Fig. S5). Except for 4 regions (Canada, Brazil, Northern South America, Southwest South America),  
1976 direct anthropogenic emissions contribute more than half of the total regional emissions. Due to the large uncertainty and  
1977 discrepancies in natural and indirect emissions estimates, the regional direct anthropogenic fractions may differ between the  
1978 bottom-up and top-down budgets. However, in absolute values, the highest direct anthropogenic emitters are the same in  
1979 the two budgets with China and South Asia being the top two by far, contributing 56 [51-66] Tg CH<sub>4</sub> yr<sup>-1</sup> and 45 [44-47] Tg  
1980 CH<sub>4</sub> yr<sup>-1</sup>, respectively (bottom-up values, Fig. 9 and Table 7). These two regions contribute 28% (26%) of the global direct  
1981 anthropogenic emissions in the bottom-up (top-down) budget. The ranks of direct anthropogenic emitters are similar to those  
1982 presented in the last budget (Stavert et al., 2021). Southeast Asia, United States of America, Middle East, Europe, Equatorial  
1983 Africa, and Russia emit between 32 Tg CH<sub>4</sub> yr<sup>-1</sup> and 23 Tg CH<sub>4</sub> yr<sup>-1</sup> as direct anthropogenic emissions (bottom-up values,  
1984 Fig 8). Brazil, Northern Africa, and Southwest South America emit between 10 CH<sub>4</sub> yr<sup>-1</sup> and 20 CH<sub>4</sub> yr<sup>-1</sup>, while the rest of  
1985 the regions emit less than 10 CH<sub>4</sub> yr<sup>-1</sup> direct anthropogenic emissions (Table 7 and Fig. S5).

1986  
1987 **Sectoral emissions.** The sectoral partitioning at the regional scale has been derived from both bottom-up and top-down  
1988 approaches. However, the top-down budget has more limitations, as the sectoral partitioning is usually based on the prior  
1989 fluxes fractions at the pixel scale, and assimilating only total methane observations does not allow to disentangle the different  
1990 source sectors overlapping in a pixel grid. However, differences in spatial patterns and seasonality of emissions can still be  
1991 constrained by atmospheric CH<sub>4</sub> observations for those inversions solving for different sources categories (see Sect. 2.3).  
1992 Bottom-up approaches allow deeper sectorial splitting, especially in terms of direct anthropogenic emissions (Fig. 9). Table  
1993 7, Fig. 9 and Fig. 10 present the estimations of CH<sub>4</sub> emissions on average over 2010-2019. Fig. 10 presents the budgets for  
1994 three main categories (Combined wetland and inland freshwaters, Fossil fuels and Agriculture & Waste), a more detailed  
1995 figure and table including the five categories is available in the supplementary material (Fig. S6 and Table S13 to S18).

1996 Values for each individual data-set for the decades 2000-2009, 2010-2019, and the last year 2020 are made available in a  
 1997 spreadsheet (see Data Availability).  
 1998 For most regions, “Combined wetland and inland freshwater emissions” are the most uncertain in the bottom-up budget,  
 1999 and generally their range is larger than in the top-down budget. In the top-down budget for 2010-2019 (Table 7), this category  
 2000 contributes the most to the regional emissions in Brazil 24 [20-33] Tg CH<sub>4</sub> yr<sup>-1</sup>, Southeast Asia 24 [14-29] Tg CH<sub>4</sub> yr<sup>-1</sup>  
 2001 (though similar to their Agriculture and Waste emissions 24 [21-31] Tg CH<sub>4</sub> yr<sup>-1</sup>), Equatorial Africa 22 [19-28] Tg CH<sub>4</sub> yr-  
 2002 <sup>1</sup>, Southwest South America 22 [14-33] Tg CH<sub>4</sub> yr<sup>-1</sup>, Canada 12 [9-18] Tg CH<sub>4</sub> yr<sup>-1</sup>, Northern South America 8 [6-10] Tg  
 2003 CH<sub>4</sub> yr<sup>-1</sup>, Southern Africa 7 [4-9] Tg CH<sub>4</sub> yr<sup>-1</sup>. Agriculture and Waste emissions dominates in South Asia 39 [33-43] Tg CH<sub>4</sub>  
 2004 yr<sup>-1</sup>, China 30 [13-37] Tg CH<sub>4</sub> yr<sup>-1</sup>, Europe 19 [16-23] Tg CH<sub>4</sub> yr<sup>-1</sup>, United States of America 13 [9-16] Tg CH<sub>4</sub> yr<sup>-1</sup>, Northern  
 2005 Africa 13 [12-14] Tg CH<sub>4</sub> yr<sup>-1</sup>, Central America 9 [8-10] Tg CH<sub>4</sub> yr<sup>-1</sup>, and Korea and Japan 3 [3-4] Tg CH<sub>4</sub> yr<sup>-1</sup>. Fossil fuel  
 2006 emissions dominate in the Middle East 18 [11-24] Tg CH<sub>4</sub> yr<sup>-1</sup> and Russia 14 [8-23] Tg CH<sub>4</sub> yr<sup>-1</sup> (close to their combined  
 2007 wetland and inland freshwater emissions of 11 [8-13] Tg CH<sub>4</sub> yr<sup>-1</sup>).  
 2008 The four largest contributors to the Fossil Fuel sector remain China, the Middle East, Russia, and the United States of  
 2009 America. Altogether they contribute 67 (64) Tg CH<sub>4</sub> yr<sup>-1</sup> in the bottom-up (top-down) budget, around 55% of the global  
 2010 fossil fuel emissions. The bottom-up and top-down approaches generally agree in terms of ensemble mean, except for China  
 2011 for which the top-down estimates suggest lower emissions than the inventories. While Chinese fossil fuel emissions occur  
 2012 mainly through coal mining activity (88%), the Middle East, Russia and the USA extract mainly oil and gas (100%, 80%,  
 2013 72%).  
 2014 The three largest contributors to the Agriculture and Waste sector remain South Asia, China, and Southeast Asia. Together  
 2015 they contribute 88 (92) Tg CH<sub>4</sub> yr<sup>-1</sup> in the bottom-up (top-down) budget, around 40% of the global agriculture and Waste  
 2016 sector (Table 7). While the ensemble means tend to agree between bottom-up and top-down budgets, the uncertainty derived  
 2017 from the top-down approaches is larger, especially for these three regions. CH<sub>4</sub> emissions due to rice cultivation originate  
 2018 mostly from these same three regions (South East Asia, China and South Asia). Livestock management emissions occurs  
 2019 mainly in South Asia 20 [18-22] Tg CH<sub>4</sub> yr<sup>-1</sup>, Brazil 12 [11-13] Tg CH<sub>4</sub> yr<sup>-1</sup>, China 11 [8-16] Tg CH<sub>4</sub> yr<sup>-1</sup>, and Europe 11  
 2020 [10-12] Tg CH<sub>4</sub> yr<sup>-1</sup> (bottom-up estimates, Table 7). The United States of America, Equatorial Africa, Northern Africa and  
 2021 Southwest South America emit between 7 Tg CH<sub>4</sub> yr<sup>-1</sup> and 10 Tg CH<sub>4</sub> yr<sup>-1</sup> in this sub-sector. Other regions emit less than 4  
 2022 Tg CH<sub>4</sub> yr<sup>-1</sup> in the livestock management sector. The Waste sector emissions are dominated by three regions: China 11 [6-  
 2023 14] Tg CH<sub>4</sub> yr<sup>-1</sup>, South Asia 9 [4-11] Tg CH<sub>4</sub> yr<sup>-1</sup>, and Europe 8 [6-12] Tg CH<sub>4</sub> yr<sup>-1</sup> (bottom-up estimates, Table 7). These  
 2024 three regions contribute around 40% of the global emissions of the Waste sector. It is worth noting that the uncertainty in  
 2025 the inventory estimates at the regional scale is around 40% (from the min-max range of the estimate, not including the  
 2026 uncertainty from each inventory).

2027 **6 Insights on the methane cycle from 2020-2022 during which there has been unprecedented high growth rates of**  
2028 **methane emissions**

2029 The mean emissions estimate for the last year of the budget (2020) was 608 [581-627] Tg CH<sub>4</sub> yr<sup>-1</sup> (Top-down), with 65%  
2030 of the emissions from direct anthropogenic sources. This is 65 Tg CH<sub>4</sub> yr<sup>-1</sup> higher (11%) than the mean emissions of the  
2031 2000-2009 decade and 6% higher than 2010-2019. In Jackson et al. (2024), we estimated that total methane emissions  
2032 increased by around 20% between the early 2000s (2000-2002) and the late 2010s (2018-2020). 2020 was a second highest  
2033 year in terms of atmospheric CH<sub>4</sub> growth rate (+15.2 ppb/yr) since systematic measurements began in the late 1980s, coming  
2034 in just behind the highest in 2021 at 17.97 ppb/yr. A few studies analysed the large growth rate increase between 2019 (+9.7  
2035 ppb/yr) and 2020 (+15.2 ppb/yr) of +5.4 ppb/yr (corresponding to +14.4 ± 2.0 Tg CH<sub>4</sub> yr<sup>-1</sup>) (Peng et al., 2022; Stevenson  
2036 et al., 2022). Peng et al. (2022) estimated that the 2019-2020 growth rate change was almost equally due to an increase in  
2037 wetland emissions (6.9 ± 2.1 Tg CH<sub>4</sub> yr<sup>-1</sup>) and a decrease of the OH chemical loss (7.5 ± 0.8 Tg CH<sub>4</sub> yr<sup>-1</sup>) due to reduced  
2038 OH precursor emissions during the COVID lockdown (Laughner et al., 2021). The COVID19 lockdown resulted in  
2039 decreased NO<sub>x</sub> emissions and reduced fossil fuel related CH<sub>4</sub> emissions (Thorpe et al., 2023), leading to less OH production.  
2040 At the global scale, Feng et al. (2023) calculated an emission increase of 27 Tg CH<sub>4</sub> yr<sup>-1</sup> between 2019 and 2020 considering  
2041 constant OH, and a smaller increase of 21 Tg CH<sub>4</sub> yr<sup>-1</sup> when including a 1.4% decrease of OH. Increased emissions were  
2042 mainly found in the northern tropics. Qu et al. (2022) also inferred a 31 Tg CH<sub>4</sub> yr<sup>-1</sup> increase of emissions, mostly in the  
2043 tropics, half of it in Africa. Furthermore, Niwa et al. (2024) suggested emission increases by 10–18 Tg CH<sub>4</sub> yr<sup>-1</sup> in 15°S–  
2044 10°N and by 20 Tg CH<sub>4</sub> yr<sup>-1</sup> in 10–35°N from 2016–2019 to 2020–2022. Such a result is compatible with wetland driven  
2045 abnormal emissions during a consecutive 3-year La Nina event spanning from 2020 to 2022 (Zhang et al., 2023; Nisbet et  
2046 al., 2023). The difference in terms of methodology and approaches between these three studies make it difficult to compare  
2047 them quantitatively but provide a robust understanding on the possible causes. Importantly, all the studies indicate, in various  
2048 proportions, increasing CH<sub>4</sub> emissions in the tropics and in the boreal region, potentially driven by microbial emission from  
2049 wetlands due to wetter and warmer climate, and a significant contribution of reduced OH concentrations due to COVID  
2050 lockdown.

2051 Based on our ensemble of data, we find that top-down approaches infer a much larger change in CH<sub>4</sub> emissions (median  
2052 [Q1-Q3] at +23 [10-31] Tg CH<sub>4</sub> yr<sup>-1</sup>) than bottom-up approaches (-1 [-5-3] Tg CH<sub>4</sub> yr<sup>-1</sup>) between 2019 and 2020 (Fig. S7).  
2053 Bottom-up approaches suggest a very small increase in wetland emissions (around +1 [0-3] Tg CH<sub>4</sub> yr<sup>-1</sup>), while top-down  
2054 approaches suggest on average a larger increase for wetlands of +8 [5-11] Tg CH<sub>4</sub> yr<sup>-1</sup>, mainly in the tropics and mid-  
2055 latitudes. It is worth noting that large uncertainties exist for a given year and that the inter-annual variability is much lower  
2056 than the ensemble spread. While bottom-up approaches suggest almost constant fossil fuel emissions and slight increase in  
2057 agriculture and waste (+3 Tg CH<sub>4</sub> yr<sup>-1</sup>), top-down approaches tend to derive higher emissions changes (+6 Tg CH<sub>4</sub> yr<sup>-1</sup>  
2058 from the fossil fuel sector and +11 Tg CH<sub>4</sub> yr<sup>-1</sup> from agriculture and waste as the median over the ensemble). Biomass

burning emissions decreased using both approaches by about 5 Tg CH<sub>4</sub> yr<sup>-1</sup> in agreement with Peng et al. (2022). Some inversions were run with IAV of OH from Patra et al. (2021) and others with constant OH. However, the inferred OH IAV in 2019 and 2020 are rather low (0.3% and 0.15% on yearly average) in Patra et al. (2021), leading to a small impact in terms of emissions changes between 2019-2020, with +22 [9-31] (median [Q1-Q3]) based on the inversions with constant OH and 19 [7-28] based on the inversions with varying OH (Fig S8).

This first analysis based on our ensemble shows how challenging it is to attribute CH<sub>4</sub> emissions changes to a specific sector or region between two years, because related uncertainties remain much larger than the targeted signal to explain. This calls again for further improvement of both approaches.

NOAA estimates of 2021 and 2022 methane atmospheric growth rates 17.8.0±0.5 ppb/yr and 14.0±0.8 ppb/yr, respectively (Lan et al., 2024). They show a continuation of very high growth rates, challenging again our understanding of the methane budget. The very high values of CH<sub>4</sub> growth rate over 2020-2022 have also been accompanied by a sharp decline in the stable isotopic signal, δ<sup>13</sup>C<sub>CH<sub>4</sub></sub>, which suggest that this recent increase of methane growth rate is at least partly explained by increased emissions from microbial sources such as those found in wetlands, inland waters, agriculture and waste systems (Nisbet et al., 2023; Michel et al., 2024). However, it is worth noting that almost all published top-down studies aforementioned include constraints only on CH<sub>4</sub>, and do not discuss the consistency with the atmospheric isotopic signal.

As of the time of submission of this manuscript, bottom-up estimates for anthropogenic emissions for 2021 and 2022 are only available from the EDGARv8 data set ([https://edgar.jrc.ec.europa.eu/dataset\\_ghg80](https://edgar.jrc.ec.europa.eu/dataset_ghg80); EDGAR, 2023). This research inventory suggests that anthropogenic emissions continued to increase from 2020 (374 Tg CH<sub>4</sub> yr<sup>-1</sup>) to 2021 (379 Tg CH<sub>4</sub> yr<sup>-1</sup>) and 2022 (386 Tg CH<sub>4</sub> yr<sup>-1</sup>) with around 62% of the increase due to the fossil fuel sources, 23 % from the Waste sector, and 14% from the agriculture sector (Table S19). The bottom-up estimate of wetland emissions for 2021-2023, derived from a single wetland model, indicates positive anomalies of 26 Tg CH<sub>4</sub> yr<sup>-1</sup> in 2020, 23 Tg CH<sub>4</sub> yr<sup>-1</sup> in 2021, and 21 Tg CH<sub>4</sub> yr<sup>-1</sup> 2022 relative to the 2000-2006 baseline (<https://earth.gov/ghgcenter/data-catalog/lpjwsl-wetlandch4-grid-v1>; Zhang et al., 2023).

## 2082 **7 Future developments, missing elements, and remaining uncertainties**

2083 In this budget, robust features and uncertainties on sources and sinks estimated by bottom-up or top-down approaches have  
 2084 been highlighted as well as discrepancies between the two budgets. Limitations of the different approaches have also been  
 2085 highlighted. Four shortcomings of the CH<sub>4</sub> budget were already identified in Kirschke et al. (2013) and Saunio et al. (2016,  
 2086 2020) and are revisited below pointing to key research areas. Although much progress has been made, they are still relevant,  
 2087 and actions are needed. However, these actions fall into different timescales and actors. Here, we revisit the four  
 2088 shortcomings of the contemporary methane budget and discuss how each weakness has been addressed since Saunio et al.  
 2089 (2020). Each section ends by discussing remaining research needs with a list of suggestions, from higher to lower priority.



2090

2091 1. Shortcoming 1: *Towards a decrease of the high uncertainty in the amount of methane emitted by wetland and inland*

2092 *water systems, and a weakened double counting issue.*

2093 This first shortcoming has probably received the largest interest in the last few years with significant improvements. First a

2094 community effort has been made based on more studies, documenting, or modelling more inland freshwater systems and

2095 synthesising emissions from the complex and heterogeneous ensemble of emitting areas: wetlands, ponds, lakes, reservoirs,

2096 streams, rivers, estuaries, and marine systems. The range of wetland and inland water emissions has been narrowed down

2097 with improved wetland extent and refined estimates for inland freshwater systems. Double counting between inland

2098 freshwater systems has been estimated for the first time and accounted for in this budget. All these improvements decreased

2099 the discrepancy between top-down and bottom-up estimate of combined wetland and inland freshwater emissions from 156

2100 Tg CH<sub>4</sub> yr<sup>-1</sup> in Sauniois et al. (2020) down to 85 Tg CH<sub>4</sub> yr<sup>-1</sup> in this update for the 2000-2009 decade. Gridded maps for

2101 lakes, ponds, reservoirs, and streams and rivers freshwater emissions have been produced over the past years (Johnson et

2102 al., 2021, 2022; Rocher-Ros et al., 2023) making the spatial distribution of CH<sub>4</sub> sources almost complete for the first time

2103 and allowing better description of prior emissions in future top-down inversions.

2104 Next steps include on the short term from highest to lowest priority include:

2105 (i) integration of spatial distribution of inland waters in atmospheric inversion models to reach a full description of prior

2106 methane sources and sinks.

2107 (ii) refinement of double counting estimation and its possible reduction with more precise spatial and temporal distributions

2108 of the different systems contributing to inland freshwater emissions by using very high-resolution satellite data (down to

2109 metre resolutions) to properly separate them. The development of a dynamical global high-resolution (typically few metres)

2110 classification of saturated soils and inundated surfaces based on satellite data (visible and microwave), surface inventories,

2111 and expert knowledge.

2112 (iii) continuation of ongoing efforts to calibrate and evaluate land surface models for wetland emissions against in-situ

2113 observations such as FLUXNET-CH<sub>4</sub> (Knox et al., 2019; Delwiche et al., 2021) or BAWLD-CH<sub>4</sub> (Kuhn et al., 2021) for

2114 boreal regions and avoid dependence on top-down estimates. It is still critical to increase the limited number of tropical

2115 observations and to assimilate them in the inverse systems to help address the issue (e.g., Kallingal et al., 2024).

2116 (iv) continuation of ongoing efforts to develop a diversity of modelling approaches (among them process-based model or

2117 machine learning approaches) to estimate wetland and inland freshwater CH<sub>4</sub> emissions, including lateral fluxes, and

2118 reducing upscaling issues, as done by e.g. Zhuang et al. (2023) for lakes.

2119 (v) continuous integration of collected flux measurements such as in the FLUXNET-CH<sub>4</sub> activity (Knox et al., 2019;

2120 Delwiche et al., 2021) or in BAWLD-CH<sub>4</sub> data set (Kuhn et al., 2021) to provide global flux maps based on machine

2121 learning approaches or other approaches (Peltola et al., 2019, McNicol et al., 2023).

Supprimé: 2023

2123 Over the long run, developing measurement systems will help to improve estimates of the diversity of wetland and inland  
 2124 freshwater sources, and further reduce uncertainties:

- 2125 - More systematic measurements of CH<sub>4</sub> fluxes and their isotopic signatures from sites reflecting the diversity of  
 2126 environment of wetlands and inland waters, complemented with environmental meta-data (e.g., soil temperature  
 2127 and moisture, vegetation types, water temperature, acidity, nutrient concentrations, NPP, soil carbon density for  
 2128 wetlands, lake morphologies) will allow us to better understand and estimate the processes of production and  
 2129 transport to the atmosphere (diffusive, ebullitive, plants mediated.. ) and to better constrain methane fluxes and  
 2130 their isotopic signatures in the different modelling approaches (Glagolev et al., 2011; Turetsky et al., 2014).  
 2131

2132 2. Shortcoming 2: *Towards a better assessment of uncertainties for global methane sinks in top-down and bottom-up*  
 2133 *budgets.*

2134 The inverse systems used here have similar caveats than those described in Saunio et al. (2016, 2020) (same OH field, same  
 2135 kind of proxy method to optimise it) leading to quite constrained atmospheric sink and therefore total global CH<sub>4</sub> sources.  
 2136 Although we have used the latest release of CCMI-2022 (Plummer et al., 2021) and CMIP6 simulations (Collins et al.,  
 2137 2017), the uncertainty of derived CH<sub>4</sub> chemical loss from the chemistry climate models remains at the same (large) level  
 2138 compared to the previous intercomparison project ACCMIP (Lamarque et al., 2013). The causes of uncertainties on the  
 2139 CH<sub>4</sub> loss and the differences between the different OH fields derived from Chemistry Transport Models (CTM) and Climate  
 2140 Chemistry Models (CCM) have been widely discussed (e.g., Nicely et al., 2017; Zhao et al., 2019, 2020a). These results  
 2141 emphasise the need to first assess, and then improve, atmospheric transport and chemistry models, especially vertically, and  
 2142 to integrate robust representation of OH fields in atmospheric models. Recently, numerous efforts based on satellite data  
 2143 have been made to constrain OH distribution, variability and trends ( e.g. Anderson, 2023,2024; Pimlott et al. 2022; Zhao  
 2144 et al., 2023; Zhu et al., 2022). Finally, soil uptake estimates rely on very few studies, and interannual variations remain  
 2145 underconstrained.

2146 Next steps, in the short term, could include developments by the modelling community in:

- 2147 - Estimating the soil uptake with different land surface models (creating an ensemble) and discussing its variations  
 2148 over the past decade.
- 2149 - Assessing the impact of using updated and varying soil uptake estimates, especially considering a warmer climate  
 2150 in the top-down approach. Indeed, for top-down models resolving for the net flux of CH<sub>4</sub> at the surface integrating  
 2151 a larger estimate of soil uptake would allow larger emissions, and then reduce the uncertainty with the bottom-up  
 2152 estimates of total CH<sub>4</sub> sources.
- 2153 - Further studying the reactivity of the air parcels in the chemistry climate models and defining new diagnostics to  
 2154 assess modelled CH<sub>4</sub> lifetimes such as in Prather et al. (2023).

2155 - Developing benchmarking of CTM and CCM regarding simulated OH distribution and variability (as in Zhao et  
 2156 al. (2019) for example) to increase efforts to assess biases and improve atmospheric chemical schemes in CTM and  
 2157 CCM.

2158 - Developing methods to better constrain OH. Numerous have been proposed: satellite CH<sub>4</sub> observations (Zhang et  
 2159 al., 2018; Anderson et al., 2023; 2024) could afford this but strategy is needed (see Duncan et al., 2024 and  
 2160 references therein); using halogenated compounds beyond methyl chloroform (MCF), such as done in box models  
 2161 (Thompson et al., 2024) to derive a 3D dynamical OH. Such methods should be able to reach very low uncertainty  
 2162 for OH burden and trends (<2%) in order to really better constrain the CH<sub>4</sub> budget. Duncan et al. (2024) discuss  
 2163 the existing satellite-based methods and propose a strategy to constrain OH from space-based approaches.

2164 - Integrating the aforementioned different potential OH chemical fields, including also inter annual variability, to  
 2165 assess the impact on the methane budget following Zhao et al. (2020).

2166 Over the long run, other parameters should be (better) integrated into top-down approaches, among them:

2167 - The magnitude of the CH<sub>4</sub> loss through oxidation by tropospheric Cl, a process debated in the recent literature.  
 2168 More modelling (e.g., Thanwerdas et al., 2022b) and instrumental studies should be devoted to reducing the  
 2169 uncertainty of this potential additional sink before integrating it in top-down models. This would be especially  
 2170 critical if inversions using <sup>13</sup>C-CH<sub>4</sub> observations are included in GMB in the future.

2171

2172 3. *Shortcoming 3: Towards a better partitioning of methane sources and sinks by region and process using top-down*  
 2173 *models*

2174 In this work, we report inversions assimilating satellite data from GOSAT, which bring more constraints than provided by  
 2175 surface stations alone, especially over tropical continents. However, we still found that satellite- and surface-based  
 2176 inversions, and the different inversion systems do not consistently infer the same regional flux distribution.

2177 The estimates contributing to the Global Methane budget are further used in more specific studies focusing on the  
 2178 comparison of the estimates from bottom-up and top-down approaches at national (Deng et al., 2022) and regional scales,  
 2179 including efforts from the GCP-Regional Carbon Cycle Assessment and Processes (RECCAP2) (Petrescu et al., 2021; 2023;  
 2180 Tibrewal et al., 2024; Lauerwald et al., 2023b; and other RECCAP-2 publications to come, see  
 2181 <https://www.globalcarbonproject.org/reccap/publications.htm>).

2182 Next steps, in the short term, could integrate developments to be made by the top-down community:

2183 - Including GOSAT 2 retrievals (Noël et al., 2022; Imasu et al., 2023) for the GOSAT-based inversions and  
 2184 considering TROPOMI-based inversions (as done in Tsuruta et al. (2023), Shen et al. (2023), Chen et al. (2022),  
 2185 Qu et al. (2021) or Y u et al. (2023)) in the next releases once at least 8 years of data are available to provide  
 2186 a decadal estimate and biases are reduced for global scale use (Lorente et al., 2023; Balasu et al., 2023). Indeed,

2187 recent satellite developments have provided higher temporal and spatial resolutions of CH<sub>4</sub> observations in regions  
 2188 with poor in-situ measurements (Figure S9, such as TROPOMI observations in North Africa).

- 2189 - Integrating the newly available updated gridded products for the different natural sources of CH<sub>4</sub> in their prior  
 2190 fluxes (e.g. inland freshwaters) to reach a full spatial description of sources and sinks, and to be able to better  
 2191 compare the top-down budget with the bottom-up budget.
- 2192 - Integration of the newly developed 4D variational inversion systems using isotopic species in the top-down budget  
 2193 (Basu et al., 2022; Thanwerdas et al., 2024; Drinkwater et al. 2023; Mannisenaho et al., 2023).
- 2194 - Improving the availability of in-situ data at high temporal resolution for the scientific community, especially ones  
 2195 covering poorly documented regions such as China (Liu et al., 2021b; Guo et al., 2020), India (Nomura et al., 2021;  
 2196 Lin et al., 2015; Tiwari and Kumar, 2012) and Siberia (Sasakawa et al., 2010, 2017; Fujita et al., 2020; Winderlich  
 2197 et al., 2010), which are not delivered so far to international databases, or only at poor temporal resolution.
- 2198 - Integrating the information from imagery satellites (e.g., TROPOMI, Carbon Mapper, Methane Sat, GHG Sat.) of  
 2199 high to super-emitters to improve prior fluxes of anthropogenic emissions in terms of quantity and locations for  
 2200 each covered sector.

2201 Over the long run, integrating more measurements and regional studies will help to improve the top-down systems, and  
 2202 further reduce the uncertainties:

- 2203 - Extending the CH<sub>4</sub> surface networks to poorly observed regions (e.g., Tropics, China, India, high latitudes) and to  
 2204 the vertical dimension: aircraft regular measurements (e.g., Filges et al., 2015; Brenninkmeijer et al., 2007; Paris  
 2205 et al., 2010; Sweeney et al., 2015); Aircore campaigns (e.g., Andersen et al., 2018; Membrive et al., 2017) ; TCCON  
 2206 observations (e.g., Wunch et al., 2011, 2019) remains critical to complement satellite data that do not observe well  
 2207 in cloudy regions and at high latitudes, and also to evaluate and eventually correct satellite biases (Buchwitz et al.,  
 2208 2016).
- 2209 - Extending and developing continuous isotopic measurements of CH<sub>4</sub> to help partitioning methane sources and to  
 2210 be integrated in 4D variational isotopic inversions (e.g., Yacovitch et al., 2021).
- 2211 - Integrating global data from future satellite instruments with intrinsic low-bias, such as active LIDAR techniques  
 2212 with MERLIN (Ehret et al., 2017), that are promising to overcome issues of systematic errors (Bousquet et al.,  
 2213 2018) and should provide measurements over the Arctic, contrary to the existing and planned passive missions.
- 2214 - Other co-emitted species such as radiocarbon for fossil/non-fossil emissions (Lassey et al., 2007a, 2007b; Petrenko  
 2215 et al., 2017), CO (e.g., Zheng et al., 2019) for biomass burning emissions, and ethane for fugitive emissions (e.g.,  
 2216 Ramsden et al., 2022) could bring additional information for partitioning emissions.

2217

2218 4. Shortcoming 4: *Towards reducing uncertainties in the modelling of atmospheric transport in the models used in the*  
 2219 *top-down budget*

2220 The TRANSCOM experiment synthesised in Patra et al. (2011) showed a large sensitivity of the representation of  
 2221 atmospheric transport on CH<sub>4</sub> abundances in the atmosphere. In particular, the modelled CH<sub>4</sub> budget appeared to depend  
 2222 strongly on the troposphere-stratosphere exchange rate and thus on the model vertical grid structure and circulation in the  
 2223 lower stratosphere. Also, regional changes in the CH<sub>4</sub> budget depend on the characteristics of the atmospheric transport  
 2224 models used in the inversion (Bruhwiler et al., 2017; Locatelli et al., 2015). This axis of research is demanding important  
 2225 development from the atmospheric modelling community. Waiting for future improvements (finer horizontal and vertical  
 2226 resolutions, more accurate physical parameterization, increase in computing resources...), assessing atmospheric transport  
 2227 error and the impact on the top-down budget remain crucial and mostly rely on the use of an ensemble of models.  
 2228 Methodology changes that could be integrated into the next methane budget releases include:

- 2229 - Evaluating more deeply the inversions provided against independent measurements such as aircraft regular  
 2230 campaigns available through for example the CH<sub>4</sub> GLOBALVIEWplus v6.0 ObsPack (Schuldt et al., 2023), the  
 2231 IAGOS data portal (<https://iagos.aeris-data.fr/download/>), the NIES portal  
 2232 (<https://db.cger.nies.go.jp/ged/en/datasetlist/index.html>) for CONTRAIL (e.g., Machida et al., 2008) and Siberian  
 2233 measurements (e.g., Sasakawa et al., 2017), the WDCGG data portal (<https://gaw.kishou.go.jp/>) for additional  
 2234 flights over three other Japanese airports and Orléans, France ; Aircore campaigns data set can be downloaded  
 2235 through the NOAA Global Monitoring Laboratory website (<https://gml.noaa.gov/ccgg/arc/?id=144>, Baier et al.,  
 2236 2021) and the French AirCore Program for atmospheric sampling (<https://aircore.aeris-data.fr>, Membrive et al.,  
 2237 2017); TCCON observations (<https://tccondata.org>; e.g., Wunch et al., 2011, 2019), and use this evaluation to  
 2238 weight the different models used in the CH<sub>4</sub> budget.

2239 Next steps, in the short term, could include some development to be addressed by the top-down community to reduce  
 2240 atmospheric transport errors:

- 2241 - Developing further methodologies to extract stratospheric partial column abundances from observations such as  
 2242 TCCON data (Saad et al., 2014; Wang et al., 2014), Aircore (e.g. Andersen et al., 2018; Membrive et al., 2017) or,  
 2243 ACE-FTS (De Mazière et al., 2018) or MIPAS (Glatthor et al., 2023) satellite data.
- 2244 - Combining SWIR and TIR measurements from space to better constrain the tropospheric column, from TROPOMI  
 2245 and IASI for example in the MethanePlus ESA project (<https://methaneplus.eu/#docs>, Buchwitz et al., 2023) or  
 2246 GOSAT (Kuze et al., 2020).
- 2247 - Porting transport models codes to run on Graphics processing Units (GPU) to achieve sub-degrees resolution global  
 2248 inversions (Chevallier et al., 2023).

2249 In the long run, developments within the dynamical core of the atmospheric transport models through the implementation  
 2250 of hexagonal-icosaedric grid with finer resolution (Dubos et al., 2015; Niwa et al., 2017, 2022; Lloret et al., 2023), and  
 2251 improvements in the simulated boundary layer dynamics or troposphere-stratosphere exchanges are promising to reduce  
 2252 atmospheric transport errors.

## 2253        **8 Conclusions**

2254        We have built an updated global methane budget by using and synthesising a large ensemble of published methods and new  
2255        results using a consistent, transparent, and traceable approach, including atmospheric observations and inversions (top-down  
2256        models), process-based models for land surface emissions and atmospheric chemistry, and inventories of anthropogenic  
2257        emissions (bottom-up models and inventories). For the 2010-2019 decade, global CH<sub>4</sub> emissions are 575 Tg CH<sub>4</sub> yr<sup>-1</sup> (range  
2258        of 553-586 Tg CH<sub>4</sub> yr<sup>-1</sup>), as estimated by top-down inversions. About 65% of global emissions are anthropogenic (range of  
2259        63-68%). Bottom-up models and inventories suggest larger global emissions (669 Tg CH<sub>4</sub> yr<sup>-1</sup> [512-849]) mostly because  
2260        of larger and more uncertain natural emissions from inland freshwater systems, natural wetlands, and geological seepage  
2261        , and likely some unresolved double counting of these sources. It is also likely that some of the individual bottom-up  
2262        emission estimates are too high, leading to larger global emissions from the bottom-up approach than the atmospheric  
2263        constraints suggest. However, the important progress in this update is that for the first time, the bottom-up and top-down  
2264        budgets agree within their uncertainty ranges. This is substantial progress toward defining more accurate global methane  
2265        emissions.

2266        The latitudinal breakdown inferred from the top-down approach reveals a dominant role of tropical emissions (~64%)  
2267        compared to mid (~32%) and high (~4%) northern latitudes (above 60°N) emissions.

2268        Our results, including an extended set of atmospheric inversions, are compared with the previous budget syntheses of  
2269        Kirschke et al. (2013) and Saunio et al. (2016; 2020). They show overall good consistency when comparing the same  
2270        decade (2000-2009) at the global and latitudinal scales. The magnitude and uncertainty of most natural or indirect  
2271        anthropogenic sources have been revised and updated. In particular, this new budget benefits from large efforts and  
2272        collaborations from the research community to provide improved estimates of the magnitude and uncertainty of the different  
2273        freshwater sources and helps reduce the potential double counting at the global scale. Of note, newly available gridded  
2274        datasets for lakes, ponds, reservoirs, streams, and rivers allow building latitudinal and regional estimates for all these sources  
2275        for the first time in these estimates. In the next review, we hope to be able to reduce uncertainties in emissions from inland  
2276        freshwater systems by better quantifying the emission factors of each contributing sub-systems (streams, rivers, lakes,  
2277        ponds) and estimating double counting at regional scale or avoiding double counting by better defining the surface areas of  
2278        each ecosystem. Another important priority for improvements is the uncertainty on the chemical loss of CH<sub>4</sub> which still  
2279        needs to be better assessed in both the top-down and the bottom-up budgets. Building on the improvement of the points  
2280        detailed in Sect. 7, our aim is to update this budget synthesis as a living review paper regularly (~every three or four years).  
2281        Each update will produce a more recent decadal CH<sub>4</sub> budget, highlight changes in emissions and trends, and incorporate  
2282        newly available data and model improvements.

2283  
2284        It is still under debate why exactly there is a sustained increase of atmospheric CH<sub>4</sub> (more than +5 ppb yr<sup>-1</sup>) since 2007  
2285        (Nisbet et al., 2019; Nisbet et al., 2023; Turner et al., 2019). Some likely explanations, already introduced by Saunio et al.

(2017) and further investigated by Jackson et al. (2020; 2024) and other studies, include, by decreasing order of certainty: 1) a positive contribution from microbial and fossil sources (e.g., Nisbet et al., 2019; Nisbet et al., 2023; Schwietzke et al., 2016; Jackson et al., 2020), a negative contribution from biomass burning emissions before 2014 (Giglio et al., 2013; Worden et al., 2017); 2) a negligible role of Arctic emission changes (e.g., Nisbet et al., 2019; Saunio et al., 2017); and 3) a tropical dominance of the increasing emissions (e.g., Saunio et al., 2017; Jackson et al., 2020; Wilson et al., 2021; Drinkwater et al., 2023). Although the accelerated atmospheric methane growth rate in 2020 (15.2 ppb/yr) has found some explanation with the impact of the world Pandemia in 2020, the sustained observed growth rates in 2021 (17.8 ppb/yr) and 2022 (14 ppb/yr) still challenge our understanding of the global methane cycle. While in Jackson et al. (2020; 2024), the increase in CH<sub>4</sub> emissions over the last two decades is almost attributed entirely to direct anthropogenic emissions, the uncertainty range from the GMB ensemble is large, and the contribution from natural emissions (wetlands) is still largely uncertain. Besides the decadal change in CH<sub>4</sub> emissions, large interannual variability can occur from these natural emissions. The recent high record of CH<sub>4</sub> growth rate highlights the potential of large variations from natural emissions from one year to another, in particular wetland emissions (e.g., Peng et al., 2022; Feng et al., 2023). These remain the challenges to be overcome in better quantifying global methane emissions.

Further investigation is needed in follow-up studies to (1) compare these results to the official UNFCCC declarations and to important assessment (as those of IEA) as done previously for example in Deng et al. (2022; 2024) or more specifically for fossil fuel emissions in Tibrewal et al. (2024) and (2) further discuss the trend and interannual variability of CH<sub>4</sub> sources and sinks at sectoral and regional scales as in Jackson et al. (2020, 2024), Stavert et al. (2021) or RECCAP-2 related publications (e.g., Petrescu et al., 2021; 2023; Lauerwald et al., 2023b), and discuss the compatibility of the budget against the atmospheric isotopic signal such as in Saunio et al. (2017). The next budgets will be critical to assess whether the Global Methane Pledge is successful and assess methane mitigation efforts.

The GCP will continue to support and coordinate the development of improved flux estimates for all budget components and new underlying science to support improved modelling, acquisition of observations, and data integration. At regular intervals (3–4 years), we will continue to bring all flux components together to produce an improved and updated global CH<sub>4</sub> budget, and provide a global benchmark for other CH<sub>4</sub> products and assessments.

## 2311 **9 Data availability**

2312 The data presented here are made available in the belief that their dissemination will lead to greater understanding and new  
 2313 scientific insights on the methane budget and changes to it, and help to reduce its uncertainties. For research projects, if the  
 2314 data used are essential to the work to be published, or if the conclusion or results largely depend on the data, co-authorship  
 2315 should be considered. Full contact details and information on how to cite the data are given in the accompanying database.

2316 The accompanying database includes a netcdf file defining the regions used, an archive with the maps of prior fluxes used  
2317 in the top-down activity, an archive with data corresponding to Fig. 3 and 5, and one Excel file organised in the following  
2318 spreadsheets.

2319 The file Global\_Methane\_Budget\_2000-2020\_v1.0.xlsx includes (1) a summary, (2) the methane observed mixing ratio and  
2320 growth rate from the four global networks (NOAA, AGAGE, CSIRO and UCI), (3) the evolution of global anthropogenic  
2321 methane emissions (including biomass burning emissions) used to produce Fig. 2, (4) the global and latitudinal budgets over  
2322 2000–2009 based on bottom-up approaches, (5) the global and latitudinal budgets over 2000–2009 based on top-down  
2323 approaches, (6) the global and latitudinal budgets over 2010–2019 based on bottom-up approaches, (7) the global and  
2324 latitudinal budgets over 2010–2019 based on top-down approaches, (8) the global and latitudinal budgets for year 2020  
2325 based on bottom-up approaches, (9) the global and latitudinal budgets for year 2020 based on top-down approaches, and  
2326 (10) the list of contributors to contact for further information on specific data.

2327 This database is available from ICOS Carbon Portal (<https://doi.org/10.18160/GKQ9-2RHT>, Martinez et al., 2024).

#### 2329 **Author contributions.**

2330 MS, AM, and JT gathered the bottom-up and top-down data sets and performed the post processing and analysis.

2331 MS, BP, PB, PeC, and RJ coordinated the global budget. MS, BP, PB, PeC, RJ, PP and PCi contributed to the update of the  
2332 full text and all coauthors appended comments. AM, ED, and XL produced the figures. DJB, NG, PH, AI, AJ, TK, TL, XL,  
2333 KMcD, JMe, JMu, SP, CP, WR, HT, YY, WZ, ZZ, Qing Z, Qian Z and Qianlai Z performed surface land model simulations  
2334 to compute wetland emissions. GA, DB, SC, BRD, GE, MAH, GH, MSJ, RL, SN, GRR, JAR, EHS, PRa, PRe, and TSW  
2335 provided data sets useful for natural emission estimates and/or contributed to text on bottom-up natural emissions. LHI, SJS,  
2336 TNF, GRvW, and MC provided anthropogenic data sets and contributed to the text for this section. AM, JT, PP, DBE, RJ,  
2337 YN, AS, AT, and BZ performed atmospheric inversions to compute top-down methane emission estimates for sources and  
2338 sinks. EJD, XL, DRB, PBK, JM, RJP, MR, MS, DWo, and YYo are PI of atmospheric observations used in top-down  
2339 inversions and/or contributed the text describing atmospheric methane observations. FD, MS, and JT contributed to the  
2340 bottom-up chemical sink section by providing data sets, processing data and/or contributing to the text. FMF provided data  
2341 for the soil sink.

2343 **Competing interests.** At least one of the (co-)authors is a member of the editorial board of Earth System Science Data.

#### 2345 **Acknowledgements**

2346 This paper is the result of a collaborative international effort under the umbrella of the Global Carbon Project, a project of  
2347 Future Earth and a research partner of the World Climate Research Programme (WCRP). We acknowledge all the people  
2348 and institutions who provided the data used in the global methane budget as well as the institutions funding parts of this



2349 effort (see Table A3). We are very grateful for the help provided by Alex Vermeulen in publishing the Global Methane  
2350 Budget dataset on the Integrated Carbon Observation System (ICOS) website. We acknowledge the modelling groups for  
2351 making their simulations available for this analysis, the joint WCRP Stratosphere-troposphere Processes And their Role in  
2352 Climate/International Global Atmospheric Chemistry (SPARC/IGAC) Chemistry-Climate Model Initiative (CCMI) for  
2353 organising and coordinating the model data analysis activity, and the British Atmospheric Data Centre (BADC) for  
2354 collecting and archiving the CCMI model output. We acknowledge the long-term support provided by the Commonwealth  
2355 Scientific and Industrial Research Organisation (CSIRO) and the National Environmental Science Program - Climate  
2356 Systems Hub to coordinate and support activities of the Global Carbon Project. We are grateful to the Emissions Database  
2357 for Global Atmospheric Research (EDGAR) team (M. Crippa, D. Guizzardi, F. Pagani, M. Banja, E. Schaaf, M. Muntean,  
2358 W. Becker, F. Monforti-Ferrario) for the work needed to publish the EDGAR greenhouse gas emission datasets used in this  
2359 work (<https://edgar.jrc.ec.europa.eu/>). We are particularly indebted to the dedicated station/instrumental operators/scientists  
2360 that have gathered the data and ensured their high quality.

2361 We acknowledge more specifically Katherine Jensen for her contribution to the Surface Water Microwave Product Series  
2362 SWAMPS, Fortunat Joos for his contribution to simulations with the Land surface Processes and eXchanges model (LPX  
2363 Bern), Ray Langenfeld for his contribution to CSIRO network, Paul Miller for his contribution to simulations with the  
2364 Lund-Potsdam-Jena General Ecosystem Simulator (LPJ-GUESS), Peng Shushi for his contribution to simulations with the  
2365 Organising Carbon and Hydrology In Dynamic Ecosystems (ORCHIDEE) model, Shamil Maksyutov for his contribution  
2366 for simulations with the inverse model at the National Institute for Environmental Studies (NIES), Isobel Simpson for her  
2367 contribution to the University of California Irvine (UCI) network, Paul Steele for his former contribution to CSIRO  
2368 network, Ray Weiss for his contribution to the Advanced Global Atmospheric Gases Experiment (AGAGE) network,  
2369 Christine Widenmeyer for her contribution with the Fire INventory from the National Center for Atmospheric Research  
2370 (FINN) database, Xiaoming Xu for his contribution to simulations with the The Integrated Science Assessment Model  
2371 (ISAM), Yuanzhi Yao for his contribution to simulations with the Dynamic Land Ecosystem Model (DLEM), Diego  
2372 Guizzardi for his contribution to EDGAR, Maria Tenkanen for her contribution with the Carbon Tracker – Europe (CTE)  
2373 outputs, Giulia Conchedda for her contribution to the Food and Agriculture Organization (FAO) database. FAOSTAT data  
2374 collection, analysis, and dissemination is funded through FAO regular budget funds. The contribution of relevant experts in  
2375 member countries is gratefully acknowledged. We acknowledge Juha Hatakka from the Finnish Meteorological Institute  
2376 (FMI) for making methane measurements at the Pallas station and sharing the data with the community. We thank Ariana  
2377 Sutton-Grier and Lisamarie Windham-Myers for reviewing an earlier version of this manuscript. Any use of trade, firm, or  
2378 product names is for descriptive purposes only and does not imply endorsement by the US Government. We warmly thank  
2379 the three anonymous reviewers for their time and their feedbacks that helped improving greatly the manuscript.

2380

2381

Supprimé: s

2383 **References**

2384 Abe, Y., Bignell, D. E. and Higashi, T., Eds.: Termites: Evolution, Sociality, Symbioses, Ecology, Springer Netherlands,

2385 Dordrecht., 2000.

2386 Aho, K.S., J.H. Fair, J.D. Hosen, E.D. Kyzivat, L.A. Logozzo, G. Rocher-Ros, L.C. Weber, B. Yoon, and P.A. Raymond:

2387 Distinct concentration-discharge dynamics in temperate streams and rivers: CO<sub>2</sub> exhibits chemostasis while CH<sub>4</sub>

2388 exhibits source limitation due to temperature control, *Limnology and Oceanography*, 66(10): p. 3656-3668., 2021

2389 Allan, W., Lowe, D. C., Gomez, A. J., Struthers, H. and Brailsford, G. W.: Interannual variation of <sup>13</sup>C in tropospheric

2390 methane: Implications for a possible atomic chlorine sink in the marine boundary layer, *J. Geophys. Res.-Atmospheres*,

2391 110(D11), doi:10.1029/2004JD005650, 2005.

2392 Allan, W., Struthers, H. and Lowe, D. C.: Methane carbon isotope effects caused by atomic chlorine in the marine

2393 boundary layer: Global model results compared with Southern Hemisphere measurements, *J. Geophys. Res.-*

2394 *Atmospheres*, 112(D4), D04306, doi:10.1029/2006jd007369, 2007.

2395 Allen, G. H., & Pavelsky, T. M.: Global extent of rivers and streams. *Science*, 361(6402), 585–588.

2396 <https://doi.org/10.1126/science.aat0636>, 2018

2397 Andersen, T., Scheeren, B., Peters, W. and Chen, H.: A UAV-based active AirCore system for measurements of

2398 greenhouse gases, *Atmospheric Meas. Tech.*, 11(5), 2683–2699, doi:10.5194/amt-11-2683-2018, 2018.

2399 Anderson, D. C., Duncan, B. N., Fiore, A. M., Baublitz, C. B., Follette-Cook, M. B., Nicely, J. M., and Wolfe, G. M.:

2400 Spatial and temporal variability in the hydroxyl (OH) radical: understanding the role of large-scale climate features

2401 and their influence on OH through its dynamical and photochemical drivers, *Atmos. Chem. Phys.*, 21, 6481–6508,

2402 <https://doi.org/10.5194/acp-21-6481-2021>, 2021.

2403 Anderson, D. C., Duncan, B. N., Nicely, J. M., Liu, J., Strode, S. A., and Follette-Cook, M. B.: Technical note:

2404 Constraining the hydroxyl (OH) radical in the tropics with satellite observations of its drivers – first steps toward

2405 assessing the feasibility of a global observation strategy, *Atmos. Chem. Phys.*, 23, 6319–6338,

2406 <https://doi.org/10.5194/acp-23-6319-2023>, 2023.

2407 Anderson, D. C., Duncan, B. N., Liu, J., Nicely, J. M., Strode, S. A., Follette-Cook, M. B., Souri, A. H., Ziemke, J. R.,

2408 Gonzales-Abad, G. and Ayazpour, Z.: Trends and interannual variability of the hydroxyl radical in the remote tropics

2409 during boreal autumn inferred from satellite proxy data. *Geophysical Research Letters*, 51, e2024GL108531,

2410 <https://doi.org/10.1029/2024GL108531>, 2024

2411 André, J.-C., Boucher, O., Bousquet, P., Chanin, M.-L., Chappellaz, J. and Tardieu, B.: Le méthane : d'où vient-il et quel

2412 est son impact sur le climat ?, EDP Sciences, Académie des Sciences et Technologies, Paris., 2014.

2413 Aoki, S., Nakazawa, T., Murayama, S. and Kawaguchi, S.: Measurements of atmospheric methane at the Japanese

2414 Antarctic Station. Syowa., *Tellus*, 44B(4), 273–281, doi:10.1034/j.1600-0889.1992.t01-3-00005.x., 1992.

2415 Arora, V. K., Melton, J. R. and Plummer, D.: An assessment of natural methane fluxes simulated by the CLASS-CTEM

model, Biogeosciences, 15(15), 4683–4709, doi:10.5194/bg-15-4683-2018, 2018.

Bader, W., Bovy, B., Conway, S., Strong, K., Smale, D., Turner, A. J., Blumenstock, T., Boone, C., Collaud Coen, M., Coulon, A., Garcia, O., Griffith, D. W. T., Hase, F., Hausmann, P., Jones, N., Krummel, P., Murata, I., Morino, I., Nakajima, H., O'Doherty, S., Paton-Walsh, C., Robinson, J., Sandrin, R., Schneider, M., Servais, C., Sussmann, R. and Mahieu, E.: The recent increase of atmospheric methane from 10 years of ground-based NDACC FTIR observations since 2005, Atmospheric Chem. Phys., 17(3), 2255–2277, doi:10.5194/acp-17-2255-2017, 2017.

Baichich, P.: The Birds and Rice Connection, Bird Watch. Dig. [online] Available from: [http://www.greatbirdingprojects.com/images/BWD\\_J-A\\_13\\_BIRDS\\_N\\_RICE.pdf](http://www.greatbirdingprojects.com/images/BWD_J-A_13_BIRDS_N_RICE.pdf), 2013.

Baier, B., Sweeney, C., Newberger, T., Higgs, J., Wolter, S., & NOAA Global Monitoring Laboratory : NOAA AirCore atmospheric sampling system profiles (Version 20230831) [Data set]. NOAA GML. <https://doi.org/10.15138/6AV0-MY81>, 2021

Balasu, N., Jacob, D. J., Lorente, A., Maasakkers, J. D., Parker, R. J., Boesch, H., Chen, Z., Kelp, M. M., Nesser, H., and Varon, D. J.: A blended TROPOMI+GOSAT satellite data product for atmospheric methane using machine learning to correct retrieval biases, Atmos. Meas. Tech., 16, 3787–3807, <https://doi.org/10.5194/amt-16-3787-2023>, 2023.

Bansal, S., Van Der Berg, M.P., Fern, R.R., Jones, J.W., Lo, R., McKenna, O.P., Tangen, B.A., Zhang, Z., and Gleason, R.A.: Large increases in methane emissions expected from North America's largest wetland complex, Sci. Adv., 9, eade1112, doi:10.1126/sciadv.ade1112, 2023.

Barba, J., Bradford, M. A., Brewer, P. E., Bruhn, D., Covey, K., van Haren, J., Megonigal, J. P., Mikkelsen, T. N., Pangala, S. R., Pihlatie, M., Poulter, B., Rivas-Ubach, A., Schadt, C. W., Terazawa, K., Warner, D. L., Zhang, Z. and Vargas, R.: Methane emissions from tree stems: a new frontier in the global carbon cycle, New Phytol., 222(1), 18–28, doi:10.1111/nph.15582, 2019.

Barker, P. A., Allen, G., Gallagher, M., Pitt, J. R., Fisher, R. E., Bannan, T., Nisbet, E. G., Bauguitte, S. J.-B., Pasternak, D., Cliff, S., Schimpf, M. B., Mehra, A., Bower, K. N., Lee, J. D., Coe, H., and Percival, C. J.: Airborne measurements of fire emission factors for African biomass burning sampled during the MOYA campaign, Atmos. Chem. Phys., 20, 15443–15459, <https://doi.org/10.5194/acp-20-15443-2020>, 2020.

Bastviken, D., Tranvik, L. J., Downing, J. A., Crill, P. M. and Enrich-Prast, A.: Freshwater Methane Emissions Offset the Continental Carbon Sink, Science, 331(6013), 50–50, doi:10.1126/science.1196808, 2011.

Bastviken, D., C.C. Treat, S.R. Pangala, V. Gauci, A. Enrich-Prast, M. Karlson, M. Gålfalk, M.B. Romano, and H.O. Sawakuchi, The importance of plants for methane emission at the ecosystem scale. Aquatic Botany, 184: p. 103596, 2023.

Basu, S., Lan, X., Dlugokencky, E., Michel, S., Schwietzke, S., Miller, J. B., Bruhwiler, L., Oh, Y., Tans, P. P., Apadula, F., Gatti, L. V., Jordan, A., Necki, J., Sasakawa, M., Morimoto, S., Di Iorio, T., Lee, H., Arduini, J., and Manca, G.: Estimating emissions of methane consistent with atmospheric measurements of methane and  $\delta^{13}\text{C}$  of methane, Atmos.

Chem. Phys., 22, 15351–15377, <https://doi.org/10.5194/acp-22-15351-2022>, 2022.

Beaulieu, J.J., DelSontro, T. & Downing, J.A.: Eutrophication will increase methane emissions from lakes and impoundments during the 21st century. *Nat Commun* 10, 1375, <https://doi.org/10.1038/s41467-019-09100-5>, 2019

Beck, H., Zimmermann, N., McVicar, T. *et al.* Present and future Köppen-Geiger climate classification maps at 1-km resolution. *Sci Data* 5, 180214, [doi.org/10.1038/sdata.2018.214](https://doi.org/10.1038/sdata.2018.214), 2018

Beerling, D.J., Woodward, F.I., Vegetation and the Terrestrial Carbon Cycle: Modelling the First 400 Million Years. Cambridge University Press, Cambridge, 2001

Begum, M.S., M.J. Bogard, D.E. Butman, E. Chea, S. Kumar, X. Lu, O.K. Nayna, L. Ran, J.E. Richey, S.M. Tareq, D.T. Xuan, R. Yu, and J.-H. Park, Localized Pollution Impacts on Greenhouse Gas Dynamics in Three Anthropogenically Modified Asian River Systems. *Journal of Geophysical Research: Biogeosciences*, 126(5): p. e2020JG006124, 2021

Bergamaschi, P., Houweling, S., Segers, A., Krol, M., Frankenberg, C., Scheepmaker, R. A., Dlugokencky, E., Wofsy, S. C., Kort, E. A., Sweeney, C., Schuck, T., Brenninkmeijer, C., Chen, H., Beck, V. and Gerbig, C.: Atmospheric CH<sub>4</sub> in the first decade of the 21st century: Inverse modeling analysis using SCIAMACHY satellite retrievals and NOAA surface measurements, *J. Geophys. Res. Atmospheres*, 118(13), 7350–7369, [doi:10.1002/jgrd.50480](https://doi.org/10.1002/jgrd.50480), 2013.

Bergamaschi, P., DANILA, A. M., Weiss, R., Thompson, R. L., Brunner, D., Levin, I., meijer, Y., Chevallier, F., Janssens-Maenhout, G., Bovensmann, H., Crisp, D., Basu, S., Dlugokencky, E. J., Engelen, R., Gerbig, C., Günther, D., Hammer, S., Henne, S., Houweling, S., Karstens, U., Kort, E. A., Maione, M., Manning, A. J., Miller, J., Montzka, S., Pandey, S., Peters, W., Peylin, P., Pinty, B., Ramonet, M., Reimann, S., Röckmann, T., Schmidt, M., Strogies, M., Sussams, J., Tarasova, O., Van Aardenne, J., Vermeulen, A. and Vogel, F.: Atmospheric monitoring and inverse modelling for verification of greenhouse gas inventories, EUR - Scientific and Technical Research Reports, Publications Office of the European Union. [online] Available from: <https://ec.europa.eu/jrc/en/publication/euro-scientific-and-technical-research-reports/atmospheric-monitoring-and-inverse-modelling-verification-greenhouse-gas-inventories> (Accessed 17 March 2020a), 2018.

Best, A. I., Richardson, M. D., Boudreau, B. P., Judd, A. G., Leifer, I., Lyons, A. P., et al.: Shallow Seabed Methane Gas Could Pose Coastal hazard. *Eos Trans. AGU* 87 (22), 213–217. [doi:10.1029/2006EO220001](https://doi.org/10.1029/2006EO220001), 2006

Bian, L., Gao, Z., Sun, Y., Ding, M., Tang, J. and Schnell, R. C.: CH<sub>4</sub> Monitoring and Background Concentration at Zhongshan Station, Antarctica, *Atmospheric Clim. Sci.*, 6(1), 135–144, [doi:10.4236/acs.2016.61012](https://doi.org/10.4236/acs.2016.61012), 2015.

Bignell, D.E., Eggleton, P. Termites in ecosystems. In: Abe, T., Higashi, M. and Bignell, D.E. (Eds), *Termites: Evolution, Sociality, Symbioses, Ecology*. Kluwer, Dordrecht, Netherlands, 363–387, 2000.

Biskaborn, B.K., Smith, S.L., Noetzli, J. *et al.* Permafrost is warming at a global scale. *Nat Commun* 10, 264, [https://doi-org.insu.bib.cnrs.fr/10.1038/s41467-018-08240-4](https://doi.org/insu.bib.cnrs.fr/10.1038/s41467-018-08240-4), 2019

Blake, D. R. and Rowland, F. S.: World-wide increase in tropospheric methane, 1978–1983, *J. Atmospheric Chem.*, 4, 43–62, 1986.

2482 Blake, D. R., Mayer, E. W., Tyler, S. C., Makide, Y., Montague, D. C. and Rowland, F. S.: Global Increase in Atmospheric  
 2483 Methane Concentrations between 1978 and 1980, *Geophys. Res. Lett.*, 9(4), 477–480, 1982.

2484 Bloom, A. A., Lee-Taylor, J., Madronich, S., Messenger, D. J., Palmer, P. I., Reay, D. S. and McLeod, A. R.: Global  
 2485 methane emission estimates from ultraviolet irradiation of terrestrial plant foliage, *New Phytol.*, doi:10.1111/j.1469-  
 2486 8137.2010.03259.x, 2010.

2487 Bohn, T. J., Melton, J. R., Ito, A., Kleinen, T., Spahni, R., Stocker, B. D., Zhang, B., Zhu, X., Schroeder, R., Glagolev, M.  
 2488 V., Maksyutov, S., Brovkin, V., Chen, G., Denisov, S. N., Eliseev, A. V., Gallego-Sala, A., McDonald, K. C., Rawlins,  
 2489 M. A., Riley, W. J., Subin, Z. M., Tian, H., Zhuang, Q. and Kaplan, J. O.: WETCHIMP-WSL: Intercomparison of  
 2490 wetland methane emissions models over West Siberia, *Biogeosciences*, 12(11), 3321–3349, doi:10.5194/bg-12-3321-  
 2491 2015, 2015.

2492 Bodmer, P., Vroom, R. J. E., Stepina, T., del Giorgio, P. A., Kosten, S.: Methane dynamics in vegetated habitats in inland  
 2493 waters: quantification, regulation, and global significance, *Frontiers in Water*, 5, DOI=10.3389/frwa.2023.1332968,  
 2494 2024

2495 Borges, A. V. and Abril, G.: Carbon Dioxide and Methane Dynamics in Estuaries, in *Treatise on Estuarine and Coastal*  
 2496 *Science*, vol. 5, pp. 119–161, Academic Press, Waltham. [online] Available from: doi:10.1016/B978-0-12-374711-  
 2497 2.00504-0, 2011.

2498 Borges, A., G. Abril, and S. Bouillon: Carbon dynamics and CO<sub>2</sub> and CH<sub>4</sub> outgassing in the Mekong delta,  
 2499 *Biogeosciences*, 15: p. 1093-1114., 2018

2500 Borges, A.V., F. Darchambeau, T. Lambert, C. Morana, G.H. Allen, E. Tambwe, A. Toengaho Sembaito, T. Mambo, J.  
 2501 Nlandu Wabakhangazi, J.P. Descy, C.R. Teodoru, and S. Bouillon: Variations in dissolved greenhouse gases (CO<sub>2</sub>,  
 2502 CH<sub>4</sub>, N<sub>2</sub>O) in the Congo River network overwhelmingly driven by fluvial-wetland connectivity, *Biogeosciences*,  
 2503 16(19): p. 3801-3834, 2019

2504 Borges, A. V., Deirmendjian, L., Bouillon, S., Okello, W., Lambert, T., Roland, F.A. E., Razanamahandry, V. F. ,  
 2505 Voarintsoa, N.R. G., Darchambeau, F., Kimirei, I. A. , Descy, J-P., Allen, G. H. and Morana, C.: Greenhouse gas  
 2506 emissions from African lakes are no longer a blind spot. *Sci. Adv.* 8, eabi8716, DOI:10.1126/sciadv.abi8716, 2022

2507 Bousquet, P., Ciais, P., Miller, J. B., Dlugokencky, E. J., Hauglustaine, D. A., Prigent, C., Van der Werf, G. R., Peylin, P.,  
 2508 Brunke, E. G., Carouge, C., Langenfelds, R. L., Lathiere, J., Papa, F., Ramonet, M., Schmidt, M., Steele, L. P., Tyler,  
 2509 S. C. and White, J.: Contribution of anthropogenic and natural sources to atmospheric methane variability, *Nature*,  
 2510 443(7110), 439–443, 2006.

2511 Bousquet, P., Pierangelo, C., Bacour, C., Marshall, J., Peylin, P., Ayar, P. V., Ehret, G., Bréon, F.-M., Chevallier, F.,  
 2512 Crevoisier, C., Gibert, F., Rairoux, P., Kiemle, C., Armante, R., Bès, C., Cassé, V., Chinaud, J., Chomette, O.,  
 2513 Delahaye, T., Edouard, D., Estève, F., Fix, A., Friker, A., Klonecki, A., Wirth, M., Alpers, M. and Millet, B.: Error  
 2514 Budget of the Methane Remote Lidar mission and Its Impact on the Uncertainties of the Global Methane Budget, J.

2515 Geophys. Res. Atmospheres, 123(20), 11,766–11,785, doi:10.1029/2018JD028907, 2018.

2516 Brandt, A. R., Heath, G. A., Kort, E. A., O’Sullivan, F., Pétron, G., Jordaán, S. M., Tans, P., Wilcox, J., Gopstein, A. M.,  
 2517 Arent, D., Wofsy, S., Brown, N. J., Bradley, R., Stucky, G. D., Eardley, D. and Harriss, R.: Methane Leaks from North  
 2518 American Natural Gas Systems, *Science*, 343(6172), 733–735, doi:10.1126/science.1247045, 2014.

2519 Brasseur, G. P. and Solomon, S.: *Aeronomy of the Middle Atmosphere: Chemistry and Physics of the Stratosphere and*  
 2520 *Mesosphere*, 3rd ed., Springer Netherlands., 2005.

2521 Brenninkmeijer C. A. M., Crutzen, P., Boumard, F., Dauer, T., Dix, B., Ebinghaus, R., Filippi, D., Fischer, H., Franke, H.,  
 2522 Fries, U., Heintzenberg, J., Helleis, F., Hermann, M., Kock, H. H., Koeppel, C., Lelieveld, J., Leuenberger, M.,  
 2523 Martinsson, B. G., Miemczyk, S., Moret, H. P., Nguyen, H. N., Nyfeler, P., Oram, D., O’Sullivan, D., Penkett, S., Platt,  
 2524 U., Pupek, M., Ramonet, M., Randa, B., Reichelt, M., Rhee, T. S., Rohwer, J., Rosenfeld, K., Scharffe, D., Schlager,  
 2525 H., Schumann, U., Slemr, F., Sprung, D., Stock, P., Thaler, R., Valentino, F., van Velthoven, P., Waibel, A., Wandel,  
 2526 A., Waschitschek, K., Wiedensohler, A., Xueref-Remy, I., Zahn, A., Zech, U., and Ziereis, H.: Civil Aircraft for the  
 2527 regular investigation of the atmosphere based on an instrumented container: The new CARIBIC system, *Atmos. Chem.*  
 2528 *Phys.*, 7, 4953–4976, doi:10.5194/acp-7-4953-2007, 2007.

2529 Bruhwiler, L. M., Basu, S., Bergamaschi, P., Bousquet, P., Dlugokencky, E., Houweling, S., Ishizawa, M., Kim, H.-S.,  
 2530 Locatelli, R., Maksyutov, S., Montzka, S., Pandey, S., Patra, P. K., Petron, G., Saunio, M., Sweeney, C., Schwietzke,  
 2531 S., Tans, P. and Weatherhead, E. C.: U.S. CH<sub>4</sub> emissions from oil and gas production: Have recent large increases  
 2532 been detected?, *J. Geophys. Res. Atmospheres*, 122(7), 4070–4083, doi:10.1002/2016JD026157, 2017.

2533 Brune, A.: Symbiotic digestion of lignocellulose in termite guts, *Nat Rev Microbiol* 12, 168–180,  
 2534 [doi.org/10.1038/nrmicro3182](https://doi.org/10.1038/nrmicro3182), 2014

2535 Buchwitz, M., de Beek, R., Burrows, J. P., Bovensmann, H., Warneke, T., Notholt, J., Meirink, J. F., Goede, A. P. H.,  
 2536 Bergamaschi, P., Korner, S., Heimann, M. and Schulz, A.: Atmospheric methane and carbon dioxide from  
 2537 SCIAMACHY satellite data: initial comparison with chemistry and transport models, *Atmospheric Chem. Phys.*, 5,  
 2538 941–962, 2005a.

2539 Buchwitz, M., de Beek, R., Noel, S., Burrows, J. P., Bovensmann, H., Bremer, H., Bergamaschi, P., Korner, S. and  
 2540 Heimann, M.: Carbon monoxide, methane and carbon dioxide columns retrieved from SCIAMACHY by WFM-  
 2541 DOAS: year 2003 initial data set, *Atmospheric Chem. Phys.*, 5, 3313–3329, 2005b.

2542 Buchwitz, M., Dils, B., Boesch, H., Crevoisier, C., Detmers, R., Frankenberg, C., Hasekamp, O., Hewson, W., Laeng, A.,  
 2543 Noel, S., Notholt, J., Parker, R., Reuter, M. and Schneising, O.: Product Validation and Intercomparison Report  
 2544 (PVIR) for the Essential Climate Variable (ECV) Greenhouse Gases (GHG), ESA Climate Change Initiative (CCI),  
 2545 report version 4, Feb 2016, [http://www.esa-ghg-cci.org/?q=webfm\\_send/300](http://www.esa-ghg-cci.org/?q=webfm_send/300), 2016.

2546 Buchwitz, M., Schneising, O., Vanselow, S., Houweling, S., van Peet, J., Siddans, R., Kerridge, B., Ventress, L., Knappett,  
 2547 D., Crevoisier, C., Meilhac, N., Borsdorf, T., Lorente, A. and Aben, I.: Final Report of the Methane Plus ESA project,

2548 TN-D15/16-CH4PLUS, <https://methaneplus.eu/#docs>, Accessed on February 13 2024, 202

2549 Butz, A., Guerlet, S., Hasekamp, O., Schepers, D., Galli, A., Aben, I., Frankenberg, C., Hartmann, J. M., Tran, H., Kuze,

2550 A., Keppel-Aleks, G., Toon, G., Wunch, D., Wennberg, P., Deutscher, N., Griffith, D., Macatangay, R.,

2551 Messerschmidt, J., Notholt, J. and Warneke, T.: Toward accurate CO<sub>2</sub> and CH<sub>4</sub> observations from GOSAT, *Geophys.*

2552 *Res. Lett.*, 38(14), L14812, doi:10.1029/2011gl047888, 2011.

2553 Cai, Z. C., Xing, G., Yan, X., Xu, H., Tsuruta, H., Yagi, K. and Minami, K.: Methane and nitrous oxide emissions from

2554 rice paddy fields as affected by nitrous fertilizers and water management, *Plant Soil*, 196, 7–14, 1997.

2555 Cael, B.B., J. Biggs, and D.A. Seekell, The size-distribution of earth’s lakes and ponds: Limits to power-law behavior.

2556 *Frontiers in Environmental Science*, 10-, 2022

2557 Call, M., D. T. Maher, I. R. Santos, and others.: Spatial and temporal variability of carbon dioxide and methane fluxes

2558 over semi-diurnal and spring–neap–spring timescales in a mangrove creek. *Geochim. Cosmochim. Acta* **150**: 211–225.

2559 doi:10.1016/j.gca.2014.11.023, 2015

2560 Canadell, J.G., P.M.S. Monteiro, M.H. Costa, L. Cotrim da Cunha, P.M. Cox, A.V. Eliseev, S. Henson, M. Ishii, S. Jaccard,

2561 C. Koven, A. Lohila, P.K. Patra, S. Piao, J. Rogelj, S. Syampungani, S. Zaehle, and K. Zickfeld: Global Carbon and

2562 other Biogeochemical Cycles and Feedbacks. In *Climate Change 2021: The Physical Science Basis. Contribution of*

2563 *Working Group I to the Sixth Assessment Report of the Intergovernmental Panel on Climate Change* [Masson-

2564 Delmotte, V., P. Zhai, A. Pirani, S.L. Connors, C. Péan, S. Berger, N. Caud, Y. Chen, L. Goldfarb, M.I. Gomis, M.

2565 Huang, K. Leitzell, E. Lonnoy, J.B.R. Matthews, T.K. Maycock, T. Waterfield, O. Yelekçi, R. Yu, and B. Zhou (eds.)].

2566 Cambridge University Press, Cambridge, United Kingdom and New York, NY, USA, pp. 673–816, doi:

2567 10.1017/9781009157896.007, 2021

2568 Carlson, K. M., Gerber, J. S., Mueller, N. D., Herrero, M., MacDonald, G. K., Brauman, K. A., Havlik, P., O’Connell, C.

2569 S., Johnson, J. A., Saatchi, S. and West, P. C.: Greenhouse gas emissions intensity of global croplands, *Nat. Clim.*

2570 *Change*, 7(1), 63–68, doi:10.1038/nclimate3158, 2017.

2571 Castelán-Ortega, O. A., Carlos Ku-Vera, J. and Estrada-Flores, J. G.: Modeling methane emissions and methane

2572 inventories for cattle production systems in Mexico, *Atmósfera*, 27(2), 185–191, doi:10.1016/S0187-6236(14)71109-

2573 9, 2014.

2574 Cathles, L., Brown, L., Taam, M. and Hunter, A.: A commentary on “The greenhouse-gas footprint of natural gas in shale

2575 formations” by R.W. Howarth, R. Santoro, and Anthony Ingraffea, *Clim. Change*, 113(2), 525–535,

2576 doi:10.1007/s10584-011-0333-0, 2012.

2577 Chandra, N., P. K. Patra, J. S. H. Bisht, A. Ito, T. Umezawa, S. Morimoto, S. Aoki, G. Janssens-Maenhout, R. Fujita,

2578 M. Takigawa, S. Watanabe, N. Saitoh, J.G. Canadell, Emissions from the oil and gas sectors, coal mining and ruminant

2579 farming drive methane growth over the past three decades, *J. Meteorol. Soc. Jpn.*, 99(2), doi:10.2151/jmsj.2021-015,

2580 2021.

2581 Chandra, N., Patra, P.K., Fujita, R., Höglund-Isaksson, L., Umezawa, T., Goto, D., Morimoto, S., Vaughn, B. H., and  
 2582 Röckmann, T.: Methane emissions decreased in fossil fuel exploitation and sustainably increased in microbial source  
 2583 sectors during 1990–2020, *Comm. Earth Environ.*, 5, <https://doi.org/10.1038/s43247-024-01286-x>, 2024  
 2584 Chang, J., Peng, S., Ciais, P., Saunois, M., Dangal, S. R. S., Herrero, M., Havlik, P., Tian, H. and Bousquet, P.: Revisiting  
 2585 enteric methane emissions from domestic ruminants and their  $\delta^{13}\text{C}$  CH<sub>4</sub> source signature, *Nat. Commun.*, 10(1), 1–  
 2586 14, doi:10.1038/s41467-019-11066-3, 2019.  
 2587 Chang, J., Peng, S., Yin, Y., Ciais, P., Havlik, P., & Herrero, M.: The key role of production efficiency changes in  
 2588 livestock methane emission mitigation. *AGU Advances*, 2, e2021AV000391, <https://doi.org/10.1029/2021AV000391>,  
 2589 2021  
 2590 Chappellaz, J., Blunier, T., Raynaud, D., Barnola, J. M., Schwander, J. and Stauffert, B.: Synchronous changes in  
 2591 atmospheric CH<sub>4</sub> and Greenland climate between 40 and 8 kyr BP, *Nature*, 366(6454), 443–445,  
 2592 doi:10.1038/366443a0, 1993.  
 2593 Chen, H., Zhu, Q., Peng, C., Wu, N., Wang, Y., Fang, X., Jiang, H., Xiang, W., Chang, J., Deng, X. and Yu, G.: Methane  
 2594 emissions from rice paddies natural wetlands, lakes in China: Synthesis new estimate, *Glob. Change Biol.*, 19(1), 19–  
 2595 32, doi:10.1111/gcb.12034, 2013.  
 2596 Chen, Y. H. and Prinn, R. G.: Estimation of atmospheric methane emissions between 1996 and 2001 using a three-  
 2597 dimensional global chemical transport model, *J. Geophys. Res.-Atmospheres*, 111(D10307),  
 2598 doi:10.1029/2005JD006058, 2006.  
 2599 Chen, Z., Jacob, D. J., Nesser, H., Sulprizio, M. P., Lorente, A., Varon, D. J., Lu, X., Shen, L., Qu, Z., Penn, E., and Yu,  
 2600 X.: Methane emissions from China: a high-resolution inversion of TROPOMI satellite observations, *Atmos. Chem.*  
 2601 *Phys.*, 22, 10809–10826, <https://doi.org/10.5194/acp-22-10809-2022>, 2022.  
 2602 Chen, Y., Hall, J., van Wees, D., Andela, N., Hantson, S., Giglio, L., van der Werf, G. R., Morton, D. C., and Randerson,  
 2603 J. T.: Multi-decadal trends and variability in burned area from the fifth version of the Global Fire Emissions Database  
 2604 (GFED5), *Earth Syst. Sci. Data*, 15, 5227–5259, <https://doi.org/10.5194/essd-15-5227-2023>, 2023.  
 2605 Chevallier, F., Lloret, Z., Cozic, A., Takache, S., and Remaud, M.: Toward high-resolution global atmospheric inverse  
 2606 modeling using graphics accelerators. *Geophysical Research Letters*, 50(5), 1–9.  
 2607 <https://doi.org/10.1029/2022GL102135>, 2023  
 2608 Chiri, E., Greening, C., Lappan, R., Waite D. W., Jirapanjawat, T., Dong, X., Arndt, S. K., and Nauer, P. A.: Termite  
 2609 mounds contain soil-derived methanotroph communities kinetically adapted to elevated methane concentrations. *ISME*  
 2610 *J* 14, 2715–273, <https://doi.org/10.1038/s41396-020-0722-3>, 2020  
 2611 Chiri, E., Nauer, P. A., Lappan, R., Jirapanjawat, T., Waite, D. W., Handley, K. M., Hugenholtz, P., Cook, P. L. M., Arndt,  
 2612 S. K., and Greening, C.: Termite gas emissions select for hydrogenotrophic microbial communities in termite mounds.  
 2613 *Proceedings of the National Academy of Sciences of the United States of America*, 118(30), e2102625118.



<https://doi.org/10.1073/pnas.2102625118>, 2021  
 Ciais, P., Sabine, C., Bala, G., Bopp, L., Brovkin, V., Canadell, J., Chhabra, A., DeFries, R., Galloway, J., Heimann, M., Jones, C., Le Quéré, C., Myneni, R. B., Piao, S. and Thornton, P.: Carbon and Other Biogeochemical Cycles, in In Climate Change 2013: The Physical Science Basis. Contribution of Working Group I to the Fifth Assessment Report of IPCC, edited by T. F. Stocker, D. Qin, G.-K. Plattner, M. Tignor, S. K. Allen, J. Boschung, A. Nauels, Y. Xia, V. Bex, and P. M. Midgley, Cambridge University Press, Cambridge., 2013.  
 Cicerone, R. J. and Oremland, R. S.: Biogeochemical aspects of atmospheric methane, *Glob. Biogeochem. Cycles*, 2, 299–327, 1988.  
 Cicerone, R. J. and Shetter, J. D.: Sources of atmospheric methane: Measurements in rice paddies and a discussion, *J. Geophys. Res.*, 86, 7203–7209, 1981.  
 Collins, W. J., Lamarque, J. F., Schulz, M., Boucher, O., Eyring, V., Hegglin, M. I., Maycock, A., Myhre, G., Prather, M., Shindell, D. and Smith, S.J.: AerChemMIP: quantifying the effects of chemistry and aerosols in CMIP6. *Geoscientific Model Development* 10, 585–607. doi:10.5194/gmd-10-585-2017, 2017.  
 Comer-Warner, S.A., P. Romeijn, D.C. Gooddy, S. Ullah, N. Kettridge, B. Marchant, D.M. Hannah, and S. Krause: Thermal sensitivity of CO<sub>2</sub> and CH<sub>4</sub> emissions varies with streambed sediment properties. *Nature Communications*, 9(1): p. 2803, 2018  
 Conley, S., Franco, G., Faloona, I., Blake, D. R., Peischl, J. and Ryerson, T. B.: Methane emissions from the 2015 Aliso Canyon blowout in Los Angeles, CA, *Science*, 351(6279), 1317–1320, doi:10.1126/science.aaf2348, 2016.  
 Conrad, R., Klose, M. and Claus, P.: Phosphate Inhibits Acetotrophic Methanogenesis on Rice Roots, *Appl. Environ. Microbiol.*, 66(2), 828–831, 2000.  
 Covey, K. R. and Magonigal, J. P.: Methane production and emissions in trees and forests, *New Phytol.*, 222(1), 35–51, doi:10.1111/nph.15624, 2019.  
 Covey, K. R., Wood, S. A., Warren, R. J., Lee, X. and Bradford, M. A.: Elevated methane concentrations in trees of an upland forest, *Geophys. Res. Lett.*, 39(15), doi:10.1029/2012gl052361, 2012.  
 Covey, K. R., de Mesquita, C. P. B., Oberle, B., Maynard, D. S., Bettigole, C., Crowther, T. W., Duguid, M. C., Steven, B., Zanne, A. E., Lapin, M., Ashton, M. S., Oliver, C. D., Lee, X. and Bradford, M. A.: Greenhouse trace gases in deadwood, *Biogeochemistry*, 130(3), 215–226, doi:10.1007/s10533-016-0253-1, 2016.  
 Crawford, J.T. and E.H. Stanley: Controls on methane concentrations and fluxes in streams draining human-dominated landscapes. *Ecological Applications*, 26(5): p. 1581-1591, 2016  
 Crevoisier, C., Nobileau, D., Fiore, A. M., Armante, R., Chedin, A. and Scott, N. A.: Tropospheric methane in the tropics - first year from IASI hyperspectral infrared observations, *Atmospheric Chem. Phys.*, 9(17), 6337–6350, 2009.  
 Crippa, M., Guizzardi, D., Solazzo, E., Muntean, M., Schaaf, E., Monforti-Ferrario, F., Banja, M., Olivier, J.G.J., Grassi, G., Rossi, S., Vignati, E., GHG emissions of all world countries - 2021 Report, EUR 30831 EN, Publications Office of

the European Union, Luxembourg, 2021, ISBN 978-92-76-41547-3, doi:10.2760/173513, JRC126363, 2021

Crippa, M., Guizzardi, D., Pagani, F., Banja, M., Muntean, M., Schaaf E., Becker, W., Monforti-Ferrario, F., Quadrelli, R., Risquez Martin, A., Taghavi-Moharamli, P., Köykkä, J., Grassi, G., Rossi, S., Brandao De Melo, J., Oom, D., Branco, A., San-Miguel, J., Vignati, E., GHG emissions of all world countries, Publications Office of the European Union, Luxembourg, 2023, doi:10.2760/953322, JRC134504, 2023

Crutzen, P. J., Aselmann, I. and Seiler, W.: Methane production by domestic animals, wild ruminants, other herbivorous fauna, and humans, *Tellus B*, 38B(3–4), 271–284, doi:10.1111/j.1600-0889.1986.tb00193.x, 1986.

Cucchi, M., Weedon, G. P., Amici, A., Bellouin, N., Lange, S., Müller Schmied, H., Hersbach, H. and Buontempo, C.: WFDE5: bias-adjusted ERA5 reanalysis data for impact studies. *Earth System Science Data*, 12, 2097–2120, 2020

Cunnold, D. M., Steele, L. P., Fraser, P. J., Simmonds, P. G., Prinn, R. G., Weiss, R. F., Porter, L. W., O'Doherty, S., Langenfelds, R. L., Krummel, P. B., Wang, H. J., Emmons, L., Tie, X. X. and Dlugokencky, E. J.: In situ measurements of atmospheric methane at GAGE/AGAGE sites during 1985-2000 and resulting source inferences, *J. Geophys. Res. - Atmospheres*, 107(D14), doi:10.1029/2001jd001226, 2002.

Curry, C. L.: Modeling the soil consumption of atmospheric methane at the global scale, *Glob. Biogeochem. Cycles*, 21(4), GB4012, doi:10.1029/2006gb002818, 2007.

Dalsøren, S. B., Isaksen, I. S. A., Li, L. and Richter, A.: Effect of emission changes in Southeast Asia on global hydroxyl and methane lifetime, *Tellus B*, 61(4), 588–601, doi:10.1111/j.1600-0889.2009.00429.x, 2009.

Darmenov, A. and da Silva, A.: The quick fire emissions dataset (QFED) - Documentation of versions 2.1, 2.2 and 2.4, Technical Report Series on Global Modeling and Data Assimilation, NASA Global Modeling and Assimilation Office., [online] Available from: <https://gmao.gsfc.nasa.gov/pubs/docs/Darmenov796.pdf> (Accessed 11 March 2020), 2015.

De Mazière, M., Vigouroux, C., Bernath, P. F., Baron, P., Blumenstock, T., Boone, C., Brogniez, C., Catoire, V., Coffey, M., Duchatelet, P., Griffith, D., Hannigan, J., Kasai, Y., Kramer, I., Jones, N., Mahieu, E., Manney, G. L., Piccolo, C., Randall, C., Robert, C., Senten, C., Strong, K., Taylor, J., Tétard, C., Walker, K. A., and Wood, S.: Validation of ACE-FTS v2.2 methane profiles from the upper troposphere to the lower mesosphere, *Atmos. Chem. Phys.*, 8, 2421–2435, <https://doi.org/10.5194/acp-8-2421-2008>, 2008.

Deemer, B. R., Harrison, J. A., Li, S., Beaulieu, J. J., DelSontro, T., Barros, N., Bezerra-Neto, J. F., Powers, S. M., dos Santos, M. A. and Vonk, J. A.: Greenhouse Gas Emissions from Reservoir Water Surfaces: A New Global Synthesis, *BioScience*, 66(11), 949–964, doi:10.1093/biosci/biw117, 2016.

Deemer, B.R. and M.A. Holgerson, Drivers of Methane Flux Differ Between Lakes and Reservoirs, Complicating Global Upscaling Efforts. *Journal of Geophysical Research: Biogeosciences* 126(4): p. e2019JG005600., 2021.

Defratyka, S. M., Paris, J.-D., Yver-Kwok, C., Fernandez, J. M., Korben, P., and Bousquet, P.: Mapping Urban Methane Sources in Paris, France, *Environmental Science & Technology*, 55, 8583–8591, 10.1021/acs.est.1c00859, 2021.

2680 DelSontro, T., Beaulieu, J. J. and Downing, J. A.: Greenhouse gas emissions from lakes and impoundments: Upscaling in  
 2681 the face of global change, *Limnol. Oceanogr. Lett.*, 3(3), 64–75, doi:10.1002/lol2.10073, 2018.

2682 Delwiche, K. B., Knox, S. H., Malhotra, A., Fluet-Chouinard, E., McNicol, G., Feron, S., Ouyang, Z., Papale, D., Trotta,  
 2683 C., Canfora, E., Cheah, Y.-W., Christianson, D., Alberto, Ma. C. R., Alekseychik, P., Aurela, M., Baldocchi, D.,  
 2684 Bansal, S., Billesbach, D. P., Bohrer, G., Bracho, R., Buchmann, N., Campbell, D. I., Celis, G., Chen, J., Chen, W.,  
 2685 Chu, H., Dalmagro, H. J., Dengel, S., Desai, A. R., Detto, M., Dolman, H., Eichelmann, E., Euskirchen, E., Famulari,  
 2686 D., Fuchs, K., Goeckede, M., Gogo, S., Gondwe, M. J., Goodrich, J. P., Gottschalk, P., Graham, S. L., Heimann, M.,  
 2687 Helbig, M., Helfter, C., Hemes, K. S., Hirano, T., Hollinger, D., Hörtnagl, L., Iwata, H., Jacotot, A., Jurasinski, G.,  
 2688 Kang, M., Kasak, K., King, J., Klatt, J., Koebsch, F., Krauss, K. W., Lai, D. Y. F., Lohila, A., Mammarella, I., Belelli  
 2689 Marchesini, L., Manca, G., Matthes, J. H., Maximov, T., Merbold, L., Mitra, B., Morin, T. H., Nemitz, E., Nilsson, M.  
 2690 B., Niu, S., Oechel, W. C., Oikawa, P. Y., Ono, K., Peichl, M., Peltola, O., Reba, M. L., Richardson, A. D., Riley, W.,  
 2691 Runkle, B. R. K., Ryu, Y., Sachs, T., Sakabe, A., Sanchez, C. R., Schuur, E. A., Schäfer, K. V. R., Sonnentag, O.,  
 2692 Sparks, J. P., Stuart-Haëntjens, E., Sturtevant, C., Sullivan, R. C., Szutu, D. J., Thom, J. E., Torn, M. S., Tuittila, E.-  
 2693 S., Turner, J., Ueyama, M., Valach, A. C., Vargas, R., Varlagin, A., Vazquez-Lule, A., Verfaillie, J. G., Vesala, T.,  
 2694 Vourlitis, G. L., Ward, E. J., Wille, C., Wohlfahrt, G., Wong, G. X., Zhang, Z., Zona, D., Windham-Myers, L., Poulter,  
 2695 B., and Jackson, R. B.: FLUXNET-CH4: a global, multi-ecosystem dataset and analysis of methane seasonality from  
 2696 freshwater wetlands , *Earth Syst. Sci. Data*, 13, 3607–3689, <https://doi.org/10.5194/essd-13-3607-2021>, 2021.

2697 Deng, Z., Ciais, P., Tzompa-Sosa, Z. A., Saunio, M., Qiu, C., Tan, C., Sun, T., Ke, P., Cui, Y., Tanaka, K., Lin, X.,  
 2698 Thompson, R. L., Tian, H., Yao, Y., Huang, Y., Lauerwald, R., Jain, A. K., Xu, X., Bastos, A., Sitch, S., Palmer, P. I.,  
 2699 Lauvaux, T., d'Aspremont, A., Giron, C., Benoit, A., Poulter, B., Chang, J., Petrescu, A. M. R., Davis, S. J., Liu, Z.,  
 2700 Grassi, G., Albergel, C., Tubiello, F. N., Perugini, L., Peters, W., and Chevallier, F.: Comparing national greenhouse  
 2701 gas budgets reported in UNFCCC inventories against atmospheric inversions, *Earth Syst. Sci. Data*, 14, 1639–1675,  
 2702 <https://doi.org/10.5194/essd-14-1639-2022>, 2022.

2703 Deng, Z., Ciais, P., Hu, L., Martinez, A., Saunio, M., Thompson, R. L., Tibrewal, K., Peters, W., Byrne, B., Grassi, G.,  
 2704 Palmer, P. I., Luijkx, I. T., Liu, Z., Liu, J., Fang, X., Wang, T., Tian, H., Tanaka, K., Bastos, A., Sitch, S., Poulter, B.,  
 2705 Albergel, C., Tsuruta, A., Maksyutov, S., Janardanan, R., Niwa, Y., Zheng, B., Thanwerdas, J., Belikov, D., Segers,  
 2706 A., and Chevallier, F.: Global Greenhouse Gas Reconciliation 2022, *Earth Syst. Sci. Data Discuss.* [preprint],  
 2707 <https://doi.org/10.5194/essd-2024-103>, in review, 2024.

2708 Denman, K. L., G. Brasseur, A. Chidthaisong, P. Ciais, P. M. Cox, R. E. Dickinson, D. Hauglustaine, C. Heinze, E.  
 2709 Holland, D. Jacob, U. Lohmann, S. Ramachandran, P. L. da Silva Dias, S. C. Wofsy and X. Zhang: *Couplings Between*  
 2710 *Changes in the Climate System and Biogeochemistry*, Cambridge University Press, Cambridge, United Kingdom and  
 2711 New York, NY, USA., 2007.

2712 D'Imperio, L., B.-B. Li, J. M. Tiedje, Oh, Y., Christiansen, J.R., Kepfer-Rojas, S., Westergaard-Nielsen, A., Brandt, K.

2713 K., Holm P.E., Wang, P., Ambus, P., and Elberling, B.: Spatial Controls of Methane Uptake in Upland Soils Across  
 2714 Climatic and Geological Regions in Greenland, *Communications Earth & Environment*, 4-46,  
 2715 <https://doi.org/10.1038/s43247-023-01143-3>, 2023.

2716 Dirmeyer, P. A., Gao, X., Zhao, M., Guo, Z., Oki, T., and Hanasaki, N. GSWP-2: Multimodel analysis and impli-  
 2717 cations for our perception of the land surface. *Bulletin of the American Meteorological Society*, 87(10):1381–1398, 2006.

2718 Dlugokencky, E. J., Dutton, E. G., Novelli, P. C., Tans, P. P., Masarie, K. A., Lantz, K. O. and Madronich, S.: Changes in  
 2719 CH<sub>4</sub> and CO growth rates after the eruption of Mt Pinatubo and their link with changes in tropical tropospheric UV  
 2720 flux, *Geophys. Res. Lett.*, 23(20), 2761–2764, 1996.

2721 Dlugokencky, E. J., Myers, R. C., Lang, P. M., Masarie, K. A., Crotwell, A. M., Thoning, K. W., Hall, B. D., Elkins, J.  
 2722 W. and Steele, L. P.: Conversion of NOAA atmospheric dry air CH<sub>4</sub> mole fractions to a gravimetrically prepared  
 2723 standard scale, *J Geophys Res*, 110(D18306), doi:10.1029/2005JD006035., 2005.

2724 Dlugokencky, E. J., Bruhwiler, L., White, J. W. C., Emmons, L. K., Novelli, P. C., Montzka, S. A., Masarie, K. A., Lang,  
 2725 P. M., Crotwell, A. M., Miller, J. B. and Gatti, L. V.: Observational constraints on recent increases in the atmospheric  
 2726 CH<sub>4</sub> burden, *Geophys. Res. Lett.*, 36, 5 PP., doi:200910.1029/2009GL039780, 2009.

2727 Dlugokencky, E. J., Nisbet, E. G., Fisher, R. and Lowry, D.: Global atmospheric methane: budget, changes and dangers,  
 2728 *Philos. Trans. R. Soc. - Math. Phys. Eng. Sci.*, 369(1943), 2058–2072, 2011.

2729 Dong, B., Xi, Y., Cui, Y., and Peng, S.: Quantifying Methane Emissions from Aquaculture Ponds in China, *Environ. Sci.*  
 2730 *Technol.*, 57, 1576–1583, <https://doi.org/10.1021/acs.est.2c05218>, 2023.

2731 Downing, J.: Emerging global role of small lakes and ponds: Little things mean a lot. *Limnetica*, 29: p. 9-24, 2010

2732 Drinkwater, A., Palmer, P. I., Feng, L., Arnold, T., Lan, X., Michel, S. E., Parker, R., and Boesch, H.: Atmospheric data  
 2733 support a multi-decadal shift in the global methane budget towards natural tropical emissions, *Atmos. Chem. Phys.*,  
 2734 23, 8429–8452, <https://doi.org/10.5194/acp-23-8429-2023>, 2023.

2735 Dubos, T., Dubey, S., Tort, M., Mittal, R., Meurdesoif, Y. and Hourdin, F.: DYNAMICO-1.0, an icosahedral hydrostatic  
 2736 dynamical core designed for consistency and versatility, *Geosci. Model Dev.*, 8(10), 3131–3150, doi:10.5194/gmd-8-  
 2737 3131-2015, 2015.

2738 Dueck, T. A., de Visser, R., Poorter, H., Persijn, S., A. Gorissen, A., W. de Visser, W., Schapendonk, A., Verhagen, J.,  
 2739 Snel, J., Harren, F. J. M., Ngai, A. K. Y., Verstappen, F., Bouwmeester, H., Voesenek, L. A. C. J. and van der Werf,  
 2740 A.: No evidence for substantial aerobic methane emission by terrestrial plants: a <sup>13</sup>C-labelling approach, *New Phytol.*,  
 2741 doi:10.1111/j.1469-8137.2007.02103.x, 2007.

2742 Duncan, B., Anderson, D., Fiore, A., Joiner, J., Krotkov, N., Li, C., Millet, D., Nicely, J., Oman, L., St. Clair, J., Shutter, J.,  
 2743 Souri, A., Strode, S., Weir, B., Wolfe, G., Worden, H., and Zhu, Q.: Opinion: Beyond Global Means: Novel Space-Based  
 2744 Approaches to Indirectly Constrain the Concentrations, Trends, and Variations of Tropospheric Hydroxyl Radical (OH),  
 2745 EGU sphere [preprint], <https://doi.org/10.5194/egusphere-2024-2331>, 2024.

2746 Dutaur, L. and Verchot, L. V.: A global inventory of the soil CH<sub>4</sub> sink, *Glob. Biogeochem Cycles*, 21, GB4012,  
 2747 doi:10.1029/2006GB002734, 2007.

2748 Dyonisius, M. N., Petrenko, V. V., Smith, A. M., Hua, Q., Yang, B., Schmitt, J., Beck, J., Seth, B., Bock, M., Hmiel, B.,  
 2749 Vimont, I., Menking, J. A., Shackleton, S. A., Baggenstos, D., Bauska, T. K., Rhodes, R. H., Sperlich, P., Beaudette,  
 2750 R., Harth, C., Kalk, M., Brook, E.J., Fisher, H., Severinghaus, J.P., and Weiss, R. F.: Old carbon reservoirs were not  
 2751 important in the deglacial methane budget, *Science*, 367(6480), 907–910. <https://doi.org/10.1126/science.aax0504>,  
 2752 2020

2753 EDGAR (Emissions Database for Global Atmospheric Research) Community GHG Database (a collaboration between  
 2754 the European Commission, Joint Research Centre (JRC), the International Energy Agency (IEA), and comprising IEA-  
 2755 EDGAR CO<sub>2</sub>, EDGAR CH<sub>4</sub>, EDGAR N<sub>2</sub>O, EDGAR F-GASES version 7.0, European Commission, JRC (Datasets),  
 2756 available at [https://edgar.jrc.ec.europa.eu/dataset\\_ghg70#sources](https://edgar.jrc.ec.europa.eu/dataset_ghg70#sources), 2022

2757 EDGAR (Emissions Database for Global Atmospheric Research) Community GHG Database, a collaboration between the  
 2758 European Commission, Joint Research Centre (JRC), the International Energy Agency (IEA), and comprising IEA-  
 2759 EDGAR CO<sub>2</sub>, EDGAR CH<sub>4</sub>, EDGAR N<sub>2</sub>O, EDGAR F-GASES version 8.0, European Commission, JRC (Datasets),  
 2760 available at [https://edgar.jrc.ec.europa.eu/dataset\\_ghg80](https://edgar.jrc.ec.europa.eu/dataset_ghg80), 2023

2761 Eggleton, P., Homathevi, R., Jones, D., MacDonald, J., Jeeva, D., Bignell, D., Davies, R., and Maryati, M.: Termite  
 2762 assemblages, forest disturbance and greenhouse gas fluxes in Sabah, East Malaysia, *Philos. T. Roy. Soc. B*, 354, 1791–  
 2763 1802, doi: 10.1098/rstb.1999.0521, 1999

2764 Ehhalt, D., Prather, M., Dentener, F., Derwent, R., Dlugokencky, E., Holland, E., Isaksen, I., Katima, J., Kirchhoff, V.,  
 2765 Matson, P., Midgley, P. and Wang, M.: Atmospheric chemistry and greenhouse gases. In: *Climate Change 2001: The*  
 2766 *Scientific Basis. Contribution of Working Group I to the Third Assessment Report of the Intergovernmental Panel on*  
 2767 *Climate Change*. [Houghton, J.T., et al. (eds.)]. Cambridge University Press, Cambridge, United Kingdom and New  
 2768 York, NY, USA, pp. 239-287, 2001.

2769 Ehhalt, D. H.: The atmospheric cycle of methane, *Tellus*, 26(1–2), 58–70, doi:10.1111/j.2153-3490.1974.tb01952.x, 1974.

2770 Ehret, G., Bousquet, P., Pierangelo, C., Alpers, M., Millet, B., Abshire, J. B., Bovensmann, H., Burrows, J. P., Chevallier,  
 2771 F., Ciais, P., Crevoisier, C., Fix, A., Flamant, P., Frankenberg, C., Gibert, F., Heim, B., Heimann, M., Houweling, S.,  
 2772 Hubberten, H. W., Jockel, P., Law, K., Low, A., Marshall, J., Agusti-Panareda, A., Payan, S., Prigent, C., Rairoux, P.,  
 2773 Sachs, T., Scholze, M. and Wirth, M.: MERLIN: A French-German Space Lidar Mission Dedicated to Atmospheric  
 2774 Methane, *Remote Sens.*, 9(10), 2017.

2775 Etiope, G.: *Natural Gas Seepage. The Earth's Hydrocarbon Degassing*, Springer International Publishing, 2015.

2776 Etiope G.: Natural emissions of methane from geological seepage in Europe. *Atmosph. Environment*, 43, 1430-1443,  
 2777 doi:10.1016/j.atmosenv.2008.03.014., 2009

2778 Etiope, G. and Schwietzke, S.: Global geological methane emissions: an update of top-down and bottom-up estimates,

2779 Elem Sci Anth, 7(1), 47, doi:10.1525/elementa.383, 2019.

2780 Etiopie, G., Lassey, K. R., Klusman, R. W. and Boschi, E.: Reappraisal of the fossil methane budget and related emission  
2781 from geologic sources, *Geophys. Res. Lett.*, 35(9), L09307, doi:10.1029/2008gl033623, 2008.

2782 Etiopie, G., Nakada, R., Tanaka, K. and Yoshida, N.: Gas seepage from Tokamachi mud volcanoes, onshore Niigata  
2783 Basin (Japan): origin, post-genetic alterations and CH<sub>4</sub>-CO<sub>2</sub> fluxes. *App. Geochem.*, 26, 348-359, 2011.

2784 Etiopie, G., Ciotoli, G., Schwietzke, S. and Schoell, M.: Gridded maps of geological methane emissions and their isotopic  
2785 signature, *Earth Syst Sci Data*, 11(1), 1–22, doi:10.5194/essd-11-1-2019, 2019.

2786 EU-Landfill-Directive: <https://eur-lex.europa.eu/legal-content/EN/TXT/?uri=CELEX:31999L0031>, 1999.

2787 FAO: FAOSTAT Emissions Land Use database. Food and Agriculture Organization of the United Nations. Statistical  
2788 Division., [online] Available from: <http://www.fao.org/faostat/en/#data/GL> (Accessed December 2022), 2022.

2789 Federici, S., Tubiello, F. N., Salvatore, M., Jacobs, H. and Schmidhuber, J.: New estimates of CO<sub>2</sub> forest emissions and  
2790 removals: 1990–2015, *For. Ecol. Manag.*, 352, 89–98, doi:10.1016/j.foreco.2015.04.022, 2015.

2791 Feng, L., Braun, C., Arnold, S. R. and Gidden, M.: iiasa/emissions\_downscaling: Supplemental Data,  
2792 doi:10.5281/zenodo.2538194, 2019.

2793 Feng, L., Palmer, P. I., Parker, R. J., Lunt, M. F., and Bösch, H.: Methane emissions are predominantly responsible for  
2794 record-breaking atmospheric methane growth rates in 2020 and 2021, *Atmos. Chem. Phys.*, 23, 4863–4880,  
2795 <https://doi.org/10.5194/acp-23-4863-2023>, 2023.

2796 Fest, B. J., Hinko-Najera, N., Wardlaw, T., Griffith, D. W. T., Livesley, S. J., and Arndt, S. K.: Soil methane oxidation in  
2797 both dry and wet temperate eucalypt forests shows a near-identical relationship with soil air-filled porosity,  
2798 *Biogeosciences*, 14, 467–479, <https://doi.org/10.5194/bg-14-467-2017>, 2017.

2799 Filges, A., Gerbig, C., Chen, H., Franke, H., Klaus, C., and Jordan, A.: The IAGOS-core greenhouse gas package: a  
2800 measurement system for continuous airborne observations of CO<sub>2</sub>, CH<sub>4</sub>, H<sub>2</sub>O and CO, *Tellus B*, 68, 27989,  
2801 <https://doi.org/10.3402/tellusb.v67.27989>, 2015.

2802 Fleischer, P., Orsi, T. H., Richardson, M. D., and Anderson, A. L. (2001). Distribution of free gas in marine sediments: a  
2803 global overview. *Geo-Marine Lett.*, 21, 103–122, 2001.

2804 Flores, E., Rhoderick, G. C., Viallon, J., Moussay, P., Choteau, T., Gameson, L., Guenther, F. R. and Wielgosz, R. I.:  
2805 Methane standards made in whole and synthetic air compared by cavity ring down spectroscopy and gas  
2806 chromatography with flame ionization detection for atmospheric monitoring applications, *Anal. Chem.*, 87(6), 3272–  
2807 3279, doi:10.1021/ac5043076, 2015.

2808 Fluet-Chouinard, E., Stocker, BD, Zhang, Z., Malhotra, A., Melton, JR, Poulter, B, Kaplan, JO, Goldewijk, KK, Siebert, S,  
2809 Minayeva, T, Hugelius, G, Joosten, H, Barthelmes, A, Prigent, C, Aires, F, Hoyt, AM, Davidson, N, Finlayson, CM,  
2810 Lehner, B, Jackson, RB, McIntyre, PB: Extensive global wetland loss over the past three centuries, *Nature*, 614(7947)  
2811 281–286, doi:10.1038/s41586-022-05572-6, 2023

Forster, P., T. Storelvmo, K. Armour, W. Collins, J.-L. Dufresne, D. Frame, D.J. Lunt, T. Mauritsen, M.D. Palmer, M. Watanabe, M. Wild, and H. Zhang: The Earth's Energy Budget, Climate Feedbacks, and Climate Sensitivity. In Climate Change 2021: The Physical Science Basis. Contribution of Working Group I to the Sixth Assessment Report of the Intergovernmental Panel on Climate Change [Masson-Delmotte, V., P. Zhai, A. Pirani, S.L. Connors, C. Péan, S. Berger, N. Caud, Y. Chen, L. Goldfarb, M.I. Gomis, M. Huang, K. Leitzell, E. Lonnoy, J.B.R. Matthews, T.K. Maycock, T. Waterfield, O. Yelekçi, R. Yu, and B. Zhou (eds.)]. Cambridge University Press, Cambridge, United Kingdom and New York, NY, USA, pp. 923–1054, doi: [10.1017/9781009157896.009](https://doi.org/10.1017/9781009157896.009), 2021

Foschi M., Etiope G., Cartwright J.A.: Seismic evidence of extensive microbial gas migration and trapping in submarine marine hydrates (Rakhine Basin, Bay of Bengal). *Mar. Petrol. Geol.*, 149, 106100, <https://doi.org/10.1016/j.marpetgeo.2023.106100>, 2023

France, J. L., Lunt, M. F., Andrade, M., Moreno, I., Ganesan, A. L., Lachlan-Cope, T., Fisher, R. E., Lowry, D., Parker, R. J., Nisbet, E. G., and Jones, A. E.: Very large fluxes of methane measured above Bolivian seasonal wetlands, *P. Natl. Acad. Sci. USA*, 119, e2206345119, <https://doi.org/10.1073/pnas.2206345119>, 2022.

Francey, R. J., Steele, L. P., Langenfelds, R. L. and Pak, B. C.: High precision long-term monitoring of radiatively active and related trace gases at surface sites and from aircraft in the southern hemisphere atmosphere, *J. Atmospheric Sci.*, 56(2), 279–285, 1999.

Frankenberg, C., Meirink, J. F., van Weele, M., Platt, U. and Wagner, T.: Assessing methane emissions from global space-borne observations, *Science*, 308(5724), 1010–1014, 2005.

Fraser, P. J., Rasmussen, R. A., Creffield, J. W., French, J. R. and Khalil, M. A. K.: Termites and global methane – Another assessment, *J. Atmospheric Chem.*, 4, 295–310, 1986.

Fraser, W. T., Blei, E., Fry, S. C., Newman, M. F., Reay, D. S., Smith, K. A. and McLeod, A. R.: Emission of methane, carbon monoxide, carbon dioxide and short-chain hydrocarbons from vegetation foliage under ultraviolet irradiation, *Plant Cell Environ.*, 38(5), 980–989, doi:10.1111/pce.12489, 2015.

Fujita, R., Morimoto, S., Maksyutov, S., Kim, H.-S., Arshinov, M., Brailsford, G., Aoki, S. and Nakazawa, T.: Global and Regional CH<sub>4</sub> Emissions for 1995–2013 Derived From Atmospheric CH<sub>4</sub>, δ<sup>13</sup>C-CH<sub>4</sub>, and δD-CH<sub>4</sub> Observations and a 715 Chemical Transport Model. *J. Geophys. Res. Atmos.*, 125: e2020JD032903. <https://doi.org/10.1029/2020JD032903>, 2020

Gauci, V., Figueiredo, V., Gedney, N., Pangala, S. R., Stauffer, T., Weedon, G., P. and Enrich-Prast A. Non-flooded riparian Amazon trees are a regionally significant methane source , *Phil. Trans. R. Soc. A*, 3802020044620200446 <http://doi.org/10.1098/rsta.2020.0446>, 2022.

Gauci, V., Pangala, S.R., Shenkin, A., Barba, J., Bastviken, D., Figueiredo, V., Gomez, C., Enrich-Prast A., Sayer, E., Staufer, T., Welch, B., Elias, D., McNamara, N., Allen, M. and Malhi Y.: Global atmospheric methane uptake by upland tree woody surfaces, *Nature*, 631, 796–800 , <https://doi.org/10.1038/s41586-024-07592-w>, 2024

2845 Gedney, N., Huntinford, C., Comyn Platt, E. and Wiltshire, A. Significant feedbacks of wetland methane release on climate  
2846 change and the causes of their uncertainty. *Env. Res. Letts.* 14, 084027 doi:10.1088/1748-9326/ab2726, 2019.

2847 Gidden, M. J., Riahi, K., Smith, S. J., Fujimori, S., Luderer, G., Kriegler, E., Vuuren, D. P. van, Berg, M. van den, Feng,  
2848 L., Klein, D., Calvin, K., Doelman, J. C., Frank, S., Fricko, O., Harmsen, M., Hasegawa, T., Havlik, P., Hilaire, J.,  
2849 Hoesly, R., Horing, J., Popp, A., Stehfest, E. and Takahashi, K.: Global emissions pathways under different  
2850 socioeconomic scenarios for use in CMIP6: a dataset of harmonized emissions trajectories through the end of the  
2851 century, *Geosci. Model Dev.*, 12(4), 1443–1475, doi:10.5194/gmd-12-1443-2019, 2019.

2852 Giglio, L., Randerson, J. T. and van der Werf, G. R.: Analysis of daily, monthly, and annual burned area using the fourth-  
2853 generation global fire emissions database (GFED4), *J. Geophys. Res. - Biogeosciences*, 118(1), 317–328,  
2854 doi:10.1002/jgrg.20042, 2013.

2855 Glagolev, M., Kleptsova, I., Filippov, I., Maksyutov, S. and Machida, T.: Regional methane emission from West Siberia  
2856 mire landscapes, *Environ. Res. Lett.*, 6(4), 045214, doi:doi:10.1088/1748-9326/6/4/045214, 2011.

2857 Glatthor, N., von Clarmann, T., Funke, B., Garcia-Comas, M., Grabowski, U., Höpfner, M., Kellmann, S., Kiefer, M.,  
2858 Laeng, A., Linden, A., Lopez-Puertas, M., and Stiller, G. P.: IMK/IAA MIPAS retrievals version 8: CH<sub>4</sub> and N<sub>2</sub>O,  
2859 *EGUsphere* [preprint], <https://doi.org/10.5194/egusphere-2023-919>, 2023.

2860 Global Methane Pledge, Global Methane Pledge website: Pledges, 1 September. [https://www.](https://www.globalmethanepledge.org/#pledges)  
2861 [globalmethanepledge.org/#pledges](https://www.globalmethanepledge.org/#pledges). Accessed 28 September 2023, 2023.

2862 Gorgolewski, A. S., Caspersen, J. P., Vantellingen, J., and Thomas, S. C.: Tree foliage is a methane sink in upland  
2863 temperate forests, *Ecosystems*, 26, 174–186, 2023.

2864 Greinert, J., Artemov, Y., Egorov, V., De Batist, M., McGinnis, D.: 1300-m-high rising bubbles from mud volcanoes at  
2865 2080 m in the Black Sea: Hydroacoustic characteristics and temporal variability, *Earth and Planetary Science Letters*,  
2866 244, 1-2, <https://doi.org/10.1016/j.epsl.2006.02.011>, 2006

2867 Griffiths, K., A. Jeziorski, D. Antoniadis, M. Beaulieu, J.P. Smol, and I. Gregory-Eaves, Pervasive changes in algal  
2868 indicators since pre-industrial times: A paleolimnological study of changes in primary production and diatom  
2869 assemblages from ~200 Canadian lakes. *Science of The Total Environment*, 838: p. 155938., 2022.

2870 Grinham, A., M. Dunbabin, D. Gale, and J. Udy, Quantification of ebullitive and diffusive methane release to atmosphere  
2871 from a water storage. *Atmospheric Environment*, 45(39): p. 7166-7173., 2011.

2872 Gromov, S., Brenninkmeijer, C. A. M. and Jöckel, P.: A very limited role of tropospheric chlorine as a sink of the  
2873 greenhouse gas methane, *Atmospheric Chem. Phys.*, 18(13), 9831–9843, doi:10.5194/acp-18-9831-2018, 2018.

2874 Guo, M., Fang, S., Liu, S., Liang, M., Wu, H., Yang, L., Li, Z., Liu, P., Zhang, F: Comparison of atmospheric CO<sub>2</sub>, CH<sub>4</sub>,  
2875 and CO at two stations in the Tibetan Plateau of China, *Earth Space Sci.*, 7, e2019EA001051, 2020

2876 Gurney, K. R., Law, R. M., Denning, A. S., Rayner, P. J., Pak, B. C., Baker, D., Bousquet, P., Bruhwiler, L., Chen, Y. H.,  
2877 Ciais, P., Fung, I. Y., Heimann, M., John, J., Maki, T., Maksyutov, S., Peylin, P., Prather, M. and Taguchi, S.: Transcom



3 inversion intercomparison: Model mean results for the estimation of seasonal carbon sources and sinks, *Glob. Biogeochem. Cycles*, 18(1), GB2010, doi:10.1029/2003gb002111, 2004.

Harris, S. A., French, H. M., Heginbottom, J. A., Johnston, G. H., Ladanyi, B., Sego, D. C. and van Everdingen, R. O.: Glossary of permafrost and related ground-ice terms, National Research Council of Canada. Associate Committee on Geotechnical Research. Permafrost Subcommittee., 1988.

Harris, I., Jones, P.D., Osborn, T.J. and Lister, D.H.: Updated high-resolution grids of monthly climatic observations – the CRU TS3.10 Dataset, *Int. J. Climatol.*, 34: 623-642. <https://doi.org/10.1002/joc.3711>, 2014

Harrison, J.A., Y.T. Prairie, S. Mercier-Blais, and C. Soued: Year-2020 Global Distribution and Pathways of Reservoir Methane and Carbon Dioxide Emissions According to the Greenhouse Gas From Reservoirs (G-res) Model. *Global Biogeochemical Cycles* 35(6): p. e2020GB006888, 2021.

Heathcote, A. J., C. T. Filstrup, and J. A. Downing (2013): Watershed sediment losses to lakes accelerating despite agricultural soil conservation efforts, *PLoS One*, 8(1), e53554, doi:10.1371/journal.pone.0053554, 2013

Heděnc, P., Jiménez, J.J., Moradi, J. *et al.*: Global distribution of soil fauna functional groups and their estimated litter consumption across biomes. *Sci Rep* 12, 17362, <https://doi.org/10.1038/s41598-022-21563-z>, 2022

Hempson, G.P., Archibald, S. and Bond, W.J.: The consequences of replacing wildlife with livestock in Africa, *Sci Rep*, 7, 17196, <https://doi.org/10.1038/s41598-017-17348-4>, 2017

Hill, J., McSweeney, C., Wright, A.-D. G., Bishop-Hurley, G., and Kalantar-zadeh, K.: Measuring Methane Production from Ruminants, *Trends in Biotechnology*, Volume 34, Issue 1, doi:10.1016/j.tibtech.2015.10.004, 2016

Hmiel, B., Petrenko, V. V., Dyonisius, M. N., Buizert, C., Smith, A. M., Place, P. F., Harth, C., Beaudette, R., Hua, Q., Yang, B., Vimont, I., Michel, S. E., Severinghaus, J. P., Etheridge, D., Bromley, T., Schmitt, J., Faïn, X., Weiss, R. F. and Dlugokencky, E.: Preindustrial 14 CH<sub>4</sub> indicates greater anthropogenic fossil CH<sub>4</sub> emissions, *Nature*, 578(7795), 409–412, doi:10.1038/s41586-020-1991-8, 2020.

Ho, J.C., A.M. Michalak, and N. Pahlevan: Widespread global increase in intense lake phytoplankton blooms since the 1980s. *Nature*, 574(7780): p. 667-670, 2019

Hoesly, R. M., Smith, S. J., Feng, L., Klimont, Z., Janssens-Maenhout, G., Pitkanen, T., Seibert, J. J., Vu, L., Andres, R. J., Bolt, R. M., Bond, T. C., Dawidowski, L., Kholod, N., Kurokawa, J. I., Li, M., Liu, L., Lu, Z., Moura, M. C. P., O'Rourke, P. R. and Zhang, Q.: Historical (1750–2014) anthropogenic emissions of reactive gases and aerosols from the Community Emissions Data System (CEDS), *Geosci Model Dev*, 11(1), 369–408, doi:10.5194/gmd-11-369-2018, 2018.

Höglund-Isaksson, L.: Bottom-up simulations of methane and ethane emissions from global oil and gas systems 1980 to 2012, *Environ. Res. Lett.*, 12(2), 024007, doi:10.1088/1748-9326/aa583e, 2017.

Höglund-Isaksson, L., Thomson, A., Kupiainen, K., Rao, S. and Janssens-Maenhout, G.: Anthropogenic methane sources, emissions and future projections, Chapter 5 in *AMAP Assessment 2015: Methane as an Arctic Climate Forcer*, p. 39-

59, available at <http://www.amap.no/documents/doc/AMAP-Assessment-2015-Methane-as-an-Arctic-climate-forcer/1285>, 2015.

Höglund-Isaksson, L., Gómez-Sanabria, A., Klimont, Z., Rafaj, P., Schöpp, W.,: Technical potentials and costs for reducing global anthropogenic methane emissions in the 2050 timeframe -results from the GAINS model, *Environ. Res. Comm.* 2(2), <https://iopscience.iop.org/article/10.1088/2515-7620/ab7457> , 2020

Holgerson, M. A. and Raymond, P. A.: Large contribution to inland water CO<sub>2</sub> and CH<sub>4</sub> emissions from very small ponds, *Nat. Geosci.*, 9(3), 222–226, doi:10.1038/ngeo2654, 2016.

Holmes, C. D., Prather, M. J., Søvde, O. A. and Myhre, G.: Future methane, hydroxyl, and their uncertainties: key climate and emission parameters for future predictions, *Atmospheric Chem. Phys.*, 13(1), 285–302, doi:10.5194/acp-13-285-2013, 2013.

Hopcroft, P.O. , P.J. Valdes & D.J. Beerling, (2011). Simulating idealised Dansgaard-Oeschger events and their potential influence on the global methane cycle, *Quaternary Science Reviews*, 30, 3258-3268, doi: 10.1016/j.quascirev.2011.08.01., 2011

Hossaini, R., Chipperfield, M. P., Saiz-Lopez, A., Fernandez, R., Monks, S., Feng, W., Brauer, P. and Glasow, R. von: A global model of tropospheric chlorine chemistry: Organic versus inorganic sources and impact on methane oxidation, *J. Geophys. Res. Atmospheres*, 121(23), 14,271-14,297, doi:10.1002/2016JD025756, 2016.

Houweling, S., Bergamaschi, P., Chevallier, F., Heimann, M., Kaminski, T., Krol, M., Michalak, A. M. and Patra, P.: Global inverse modeling of CH<sub>4</sub> sources and sinks: an overview of methods, *Atmospheric Chem. Phys.*, 17(1), 235–256, doi:10.5194/acp-17-235-2017, 2017.

M. Hovland, A.G. Judd, R.A. Burke: The global flux of methane from shallow submarine sediments, *Chemosphere*, Volume 26, Issues 1–4, Pages 559-578, doi:10.1016/0045-6535(93)90442-8., 1993

Howarth, R. W.: Ideas and perspectives: is shale gas a major driver of recent increase in global atmospheric methane?, *Biogeosciences*, 16(15), 3033–3046, doi:10.5194/bg-16-3033-2019, 2019.

Hu, H., Landgraf, J., Detmers, R., Borsdorff, T., Brugh, J. A. de, Aben, I., Butz, A. and Hasekamp, O.: Toward Global Mapping of Methane With TROPOMI: First Results and Intersatellite Comparison to GOSAT, *Geophys. Res. Lett.*, 45(8), 3682–3689, doi:10.1002/2018GL077259, 2018.

Hugelius, G., Tarnocai, C., Broll, G., Canadell, J. G., Kuhry, P., & Swanson, D. K.: The Northern Circumpolar Soil Carbon Database: spatially distributed datasets of soil coverage and soil carbon storage in the northern permafrost regions. *Earth System Science Data*, 5(1), 3–13. <https://doi.org/10.5194/essd-5-3-2013>, 2013

Hugelius, G., Strauss, J., Zubrzycki, S., Harden, J. W., Schuur, E. A. G., Ping, C. L., Schirmermeister, L., Grosse, G., Michaelson, G. J., Koven, C. D., O'Donnell, J. A., Elberling, B., Mishra, U., Camill, P., Yu, Z., Palmtag, J. and Kuhry, P.: Estimated stocks of circumpolar permafrost carbon with quantified uncertainty ranges and identified data gaps, *Biogeosciences*, 11(23), 6573–6593, doi:10.5194/bg-11-6573-2014, 2014.

2944 Hugelius, Gustaf, Loisel, J., Chadburn, S., Jackson, R. B., Jones, M., MacDonald, G., et al. : Large stocks of peatland  
 2945 carbon and nitrogen are vulnerable to permafrost thaw. *Proceedings of the National Academy of Sciences*, 117(34),  
 2946 20438–20446. <https://doi.org/10.1073/pnas.1916387117>, 2020

2947 Hugelius, G., Ramage, J.L., Burke, E.J., Chatterjee, A., Smallman, T.L., Aalto, T., Bastos, A., Biasi, C., Canadell, J.G.,  
 2948 Chandra, N. and Chevallier, F., et al. Two decades of permafrost region CO<sub>2</sub>, CH<sub>4</sub>, and N<sub>2</sub>O budgets suggest a small  
 2949 net greenhouse gas source to the atmosphere. Preprint in ESS Open Archive. September 11, 2023. DOI:  
 2950 10.22541/essoar.169444320.01914726/v1, 2023

2951 IEA, *Coal Information: Overview*, IEA, Paris <https://www.iea.org/reports/coal-information-overview>, License: CC BY  
 2952 4.0, Accessed 17 January 2024, 2021

2953 IEA (2023), Energy Statistics Data Browser, IEA, Paris [https://www.iea.org/data-and-statistics/data-tools/energy-](https://www.iea.org/data-and-statistics/data-tools/energy-statistics-data-browser)  
 2954 [statistics-data-browser](https://www.iea.org/data-and-statistics/data-tools/energy-statistics-data-browser), Accessed 17 January 2024, 2023a

2955 IEA, US natural gas production by source, 2013-2023, IEA, Paris [https://www.iea.org/data-and-statistics/charts/us-](https://www.iea.org/data-and-statistics/charts/us-natural-gas-production-by-source-2013-2023)  
 2956 [natural-gas-production-by-source-2013-2023](https://www.iea.org/data-and-statistics/charts/us-natural-gas-production-by-source-2013-2023), IEA. Licence: CC BY 4.0, Accessed 17 January 2024, 2023b

2957 Imasu, R.; Matsunaga, T.; Nakajima, M.; Yoshida, Y.; Shiomi, K.; Morino, I.; Saitoh, N.; Niwa, Y.; Someya, Y.; Oishi,  
 2958 Y.; et al. Greenhouse Gases Observing SATellite 2 (GOSAT-2): Mission Overview. *Prog. Earth Planet. Sci.*, 10, 33.,  
 2959 2023,

2960 Inoue, M., Morino, I., Uchino, O., Nakatsuru, T., Yoshida, Y., Yokota, T., Wunch, D., Wennberg, P. O., Roehl, C. M.,  
 2961 Griffith, D. W. T., Velazco, V. A., Deutscher, N. M., Warneke, T., Notholt, J., Robinson, J., Sherlock, V., Hase, F.,  
 2962 Blumenstock, T., Rettinger, M., Sussmann, R., Kyrö, E., Kivi, R., Shiomi, K., Kawakami, S., Mazière, M. D., Arnold,  
 2963 S. G., Feist, D. G., Barrow, E. A., Barney, J., Dubey, M., Schneider, M., Iraci, L. T., Podolske, J. R., Hillyard, P. W.,  
 2964 Machida, T., Sawa, Y., Tsuboi, K., Matsueda, H., Sweeney, C., Tans, P. P., Andrews, A. E., Biraud, S. C., Fukuyama,  
 2965 Y., Pittman, J. V., Kort, E. A. and Tanaka, T.: Bias corrections of GOSAT SWIR XCO<sub>2</sub> and XCH<sub>4</sub> with TCCON data  
 2966 and their evaluation using aircraft measurement data, *Atmospheric Meas. Tech.*, 9(8), 3491–3512, doi:10.5194/amt-9-  
 2967 3491-2016, 2016.

2968 IPCC: Good Practice Guidance and Uncertainty Management in National Greenhouse Gas Inventories. Intergovernmental  
 2969 Panel on Climate Change, National Greenhouse Gas Inventories Programme. Montreal, IPCC-  
 2970 XVI/Doc.10(1.IV.2000), May 2000., 2000.

2971 IPCC: Climate change 2001: The scientific basis. Contribution of working group I to the third assessment report of the  
 2972 Intergovernmental Panel on Climate Change, Cambridge University Press, Cambridge, United Kingdom and New  
 2973 York, NY, USA., 2001.

2974 IPCC: IPCC Guidelines for National Greenhouse Gas Inventories. The National Greenhouse Gas Inventories Programme,  
 2975 Eggleston H.S., Buendia L., Miwa K., Ngara T. and Tanabe K. (eds). The Intergovernmental Panel on Climate Change,  
 2976 IPCC TSU NGGIP, IGES. Institute for Global Environmental Strategy, Hayama, Kanagawa, Japan. Available online

at: [http://www.ipcc-nggip.iges.or.jp/support/Primer\\_2006GLs.pdf](http://www.ipcc-nggip.iges.or.jp/support/Primer_2006GLs.pdf), 2006.

IPCC: 2019 Refinement to the 2006 IPCC Guidelines for National Greenhouse Gas Inventories — IPCC. [online] Available from: <https://www.ipcc.ch/report/2019-refinement-to-the-2006-ipcc-guidelines-for-national-greenhouse-gas-inventories/> (Accessed 17 March 2020), 2019.

Ito, A. and Inatomi, M.: Use of a process-based model for assessing the methane budgets of global terrestrial ecosystems and evaluation of uncertainty, *Biogeosciences*, 9(2), 759–773, doi:10.5194/bg-9-759-2012, 2012.

Jacob, D. J., Varon, D. J., Cusworth, D. H., Dennison, P. E., Frankenberg, C., Gautam, R., Guanter, L., Kelley, J., McKeever, J., Ott, L. E., Poulter, B., Qu, Z., Thorpe, A. K., Worden, J. R., and Duren, R. M.: Quantifying methane emissions from the global scale down to point sources using satellite observations of atmospheric methane, *Atmos. Chem. Phys.*, 22, 9617–9646, <https://doi.org/10.5194/acp-22-9617-2022>, 2022.

Jackson, R. B., Down, A., Phillips, N. G., Ackley, R. C., Cook, C. W., Plata, D. L. and Zhao, K.: Natural gas pipeline leaks across Washington, D.C, *Environ. Sci. Technol.*, 48(3), 2051–2058, doi:10.1021/es404474x, 2014a.

Jackson, R. B., Sauniois, M., Bousquet, P., Canadell, J. G., Poulter, B., Stavert, A. R., Poulter, B., Bergamaschi, P., Niwa, Y., Segers, A., Tsuruta, A.: Increasing anthropogenic methane emissions arise equally from agricultural and fossil fuel sources, *Environmental Research Letters*, 15, 7, <https://doi.org/10.1088/1748-9326/ab9ed2>, 2020

Jackson, R. B., Sauniois, M., Martinez, A., Canadell, J. G., Yu, X., Li, M., Poulter, B., Raymind, P., Regnier, P., Davis, S.J., and Patra, P.: Human activities now fuel two-thirds of global methane emissions, *Environmental Research Letters*, 19, 101002, DOI:10.1088/1748-9326/ad6463, 2024

Jamali, H., Livesley, S.J., Dawes, T.Z. *et al.* Termite mound emissions of CH<sub>4</sub> and CO<sub>2</sub> are primarily determined by seasonal changes in termite biomass and behaviour. *Oecologia* 167, 525–534, [doi.org/10.1007/s00442-011-1991-3](https://doi.org/10.1007/s00442-011-1991-3), 2011

Janssens-Maenhout, G., Crippa, M., Guizzardi, D., Muntean, M., Schaaf, E., Dentener, F., Bergamaschi, P., Pagliari, V., Olivier, J., Peters, J., van Aardenne, J., Monni, S., Doering, U., Petrescu, R., Solazzo, E. and Oreggioni, G.: EDGAR v4.3.2 Global Atlas of the three major Greenhouse Gas Emissions for the period 1970-2012, *Earth Syst Sci Data Discuss*, 2019, 1–52, doi:10.5194/essd-2018-164, 2019.

JAXA: GOSAT-2: Greenhouse gases Observing SATellite-2@ibuki2\_JAXA"IBUKI-2", [online] Available from: <https://global.jaxa.jp/projects/sat/gosat2/index.html> (Accessed 25 March 2020), 2019.

Jensen, K. and Mcdonald, K.: Surface Water Microwave Product Series Version 3: A Near-Real Time and 25-Year Historical Global Inundated Area Fraction Time Series From Active and Passive Microwave Remote Sensing, *IEEE Geosci. Remote Sens. Lett.*, 16(9), 1402–1406, doi:10.1109/LGRS.2019.2898779, 2019.

Jiang, Y., Groenigen, K. J. van, Huang, S., Hungate, B. A., Kessel, C. van, Hu, S., Zhang, J., Wu, L., Yan, X., Wang, L., Chen, J., Hang, X., Zhang, Y., Horwath, W. R., Ye, R., Linquist, B. A., Song, Z., Zheng, C., Deng, A. and Zhang, W.: Higher yields and lower methane emissions with new rice cultivars, *Glob. Change Biol.*, 23(11), 4728–4738,

doi:10.1111/gcb.13737, 2017.

Johnson, D. E., Phetteplace, H. W. and Seidl, A. F.: Methane, nitrous oxide and carbon dioxide emissions from ruminant livestock production systems, edited by J. Takahashi and B. A. Young, pp. 77–85, Elsevier, Amsterdam, The Netherlands., 2002.

Johnson, M.S., E. Matthews, J. Du, V. Genovese, and D. Bastviken, Methane Emission From Global Lakes: New Spatiotemporal Data and Observation-Driven Modeling of Methane Dynamics Indicates Lower Emissions, *Journal of Geophysical Research: Biogeosciences*, 127(7): p. e2022JG006793, 2022

Johnson, M. S., E. Matthews, D. Bastviken, B. Deemer, J. Du, and V. Genovese, Spatiotemporal methane emission from global reservoirs, *Journal of Geophysical Research: Biogeosciences*, 126, e2021JG006305, <https://doi.org/10.1029/2021JG006305>, 2021

Judd, A.G. (2004). Natural seabed seeps as sources of atmospheric methane, *Environ. Geol.*, 46, 988–996, 2004.

Jung, M., Reichstein, M., Margolis, H. A., Cescatti, A., Richardson, A. D., Arain, M. A., Arneth, A., Bernhofer, C., Bonal, D., Chen, J., Gianelle, D., Gobron, N., Kiely, G., Kutsch, W., Lasslop, G., Law, B. E., Lindroth, A., Merbold, L., Montagnani, L., Moors, E. J., Papale, D., Sottocornola, M., Vaccari, F., and Williams, C.: Global patterns of land-atmosphere fluxes of carbon dioxide, latent heat, and sensible heat derived from eddy covariance, satellite, and meteorological observations, *J. Geophys. Res.*, 116, G00J07, <https://doi.org/10.1029/2010jg001566>, 2011.

Kai, F. M., Tyler, S. C., Randerson, J. T. and Blake, D. R.: Reduced methane growth rate explained by decreased Northern Hemisphere microbial sources, *Nature*, 476(7359), 194–197, 2011.

Kaiser, J. W., Heil, A., Andreae, M. O., Benedetti, A., Chubarova, N., Jones, L., Morcrette, J. J., Razinger, M., Schultz, M. G., Suttie, M. and van der Werf, G. R.: Biomass burning emissions estimated with a global fire assimilation system based on observed fire radiative power, *Biogeosciences*, 9(1), 527–554, doi:10.5194/bg-9-527-2012, 2012.

Kallingal, J. T., Lindström, J., Miller, P. A., Rinne, J., Raivonen, M., and Scholze, M.: Optimising CH<sub>4</sub> simulations from the LPJ-GUESS model v4.1 using an adaptive Markov chain Monte Carlo algorithm, *Geosci. Model Dev.*, 17, 2299–2324, <https://doi.org/10.5194/gmd-17-2299-2024>, 2024.

Karl, D., Beversdorf, L., Björkman, K. *et al.* Aerobic production of methane in the sea. *Nature Geosci* **1**, 473–478, <https://doi.org/10.1038/ngeo234>, 2008

Karlson, M., and Bastviken, D.: Multi-Source Mapping of Peatland Types Using Sentinel-1, Sentinel-2, and Terrain Derivatives—A Comparison Between Five High-Latitude Landscapes. *Journal of Geophysical Research: Biogeosciences* 128, e2022JG007195. <https://doi.org/10.1029/2022JG007195>, 2023

Keppler, F., Hamilton, J. T. G., Brass, M. and Rockmann, T.: Methane emissions from terrestrial plants under aerobic conditions, *Nature*, 439, 187–191, doi:10.1038/nature04420, 2006.

Kholod, N., Evans, M., Pilcher, R. C., Roshchanka, V., Ruiz, F., Coté, M. and Collings, R.: Global methane emissions from coal mining to continue growing even with declining coal production, *J. Clean. Prod.*, 256, 120489,

Mis en forme : Anglais (E.U.)

**Supprimé:** Kallingal, J. T., Lindström, J., Miller, P. A., Rinne, J., Raivonen, M., and Scholze, M.: Optimising CH<sub>4</sub> simulations from the LPJ-GUESS model v4.1 using an adaptive MCMC algorithm, *Geosci. Model Dev. Discuss.* [preprint], <https://doi.org/10.5194/gmd-2022-302>, in review, 2023.

doi:10.1016/j.jelepro.2020.120489, 2020.

Kim H., Global Soil Wetness Project Phase 3 Atmospheric Boundary Conditions (Experiment 1) [Data set]. Data Integration and Analysis System (DIAS)., <https://doi.org/10.20783/DIAS.501>, 2017

King, J.R., Warren, R.J., Bradford, M.A. Correction: Social Insects Dominate Eastern US Temperate Hardwood Forest Macroinvertebrate Communities in Warmer Regions. PLOS ONE 8(10): 10.1371/annotation/87285c86-f1df-4f8b-bc08-d64643d351f4, 2013.

Kirk, L. and MJ Cohen: River Corridor Sources Dominate CO<sub>2</sub> Emissions From a Lowland River Network. Journal of Geophysical Research, Biogeosciences, 128(1), e2022JG006954, 2023.

Kirschke, S., Bousquet, P., Ciais, P., Saunio, M., Canadell, J. G., Dlugokencky, E. J., Bergamaschi, P., Bergmann, D., Blake, D. R., Bruhwiler, L., Cameron-Smith, P., Castaldi, S., Chevallier, F., Feng, L., Fraser, A., Heimann, M., Hodson, E. L., Houweling, S., Josse, B., Fraser, P. J., Krummel, P. B., Lamarque, J. F., Langenfelds, R. L., Le Quere, C., Naik, V., O'Doherty, S., Palmer, P. I., Pison, I., Plummer, D., Poulter, B., Prinn, R. G., Rigby, M., Ringeval, B., Santini, M., Schmidt, M., Shindell, D. T., Simpson, I. J., Spahni, R., Steele, L. P., Strode, S. A., Sudo, K., Szopa, S., van der Werf, G. R., Voulgarakis, A., van Weele, M., Weiss, R. F., Williams, J. E. and Zeng, G.: Three decades of global methane sources and sinks, Nat. Geosci., 6(10), 813–823, doi:10.1038/ngeo1955, 2013.

Klauda, J. B. and Sandler, S. I.: Global distribution of methane hydrate in ocean sediment, Energy Fuels, 19(2), 459–470, 2005.

Kleinen, T., Brovkin, V. and Schuldt, R. J.: A dynamic model of wetland extent and peat accumulation: results for the Holocene, Biogeosciences, 9(1), 235–248, doi:10.5194/bg-9-235-2012, 2012.

Kleinen, T., Mikolajewicz, U., and Brovkin, V.: Terrestrial methane emissions from the Last Glacial Maximum to the preindustrial period, Clim. Past, 16, 575–595, doi:10.5194/cp-16-575-2020, 2020.

Kleinen, T., Gromov, S., Steil, B., and Brovkin, V.: Atmospheric methane underestimated in future climate projections, Environ. Res. Lett., 16, 094006, doi:10.1088/1748-9326/ac1814, 2021.

Kleinen, T., Gromov, S., Steil, B., and Brovkin, V.: Atmospheric methane since the last glacial maximum was driven by wetland sources, Clim. Past, 19, 1081–1099, doi:10.5194/cp-19-1081-2023, 2023

Knittel K and Boetius A : Anaerobic oxidation of methane: progress with an unknown process methane. Annu Rev Microbiol 63:311–334, 2009

Knox, S. H., Jackson, R. B., Poulter, B., McNicol, G., Fluet-Chouinard, E., Zhang, Z., Hugelius, G., Bousquet, P., Canadell, J. G., Saunio, M., Papale, D., Chu, H., Keenan, T. F., Baldocchi, D., Torn, M. S., Mammarella, I., Trotta, C., Aurela, M., Bohrer, G., Campbell, D. I., Cescatti, A., Chamberlain, S., Chen, J., Chen, W., Dengel, S., Desai, A. R., Euskirchen, E., Friborg, T., Gasbarra, D., Goded, I., Goeckede, M., Heimann, M., Helbig, M., Hirano, T., Hollinger, D. Y., Iwata, H., Kang, M., Klatt, J., Krauss, K. W., Kutzbach, L., Lohila, A., Mitra, B., Morin, T. H., Nilsson, M. B., Niu, S., Noormets, A., Oechel, W. C., Peichl, M., Peltola, O., Reba, M. L., Richardson, A. D., Runkle, B. R. K., Ryu,

3081 Y., Sachs, T., Schäfer, K. V. R., Schmid, H. P., Shurpali, N., Sonnentag, O., Tang, A. C. I., Ueyama, M., Vargas, R.,  
 3082 Vesala, T., Ward, E. J., Windham-Myers, L., Wohlfahrt, G. and Zona, D.: FLUXNET-CH4 Synthesis Activity:  
 3083 Objectives, Observations, and Future Directions, *Bull. Am. Meteorol. Soc.*, 100(12), 2607–2632, doi:10.1175/BAMS-  
 3084 D-18-0268.1, 2019.  
 3085 Knox, S. H., Bansal, S., McNicol, G., Schafer, K., Sturtevant, C., Ueyama, M., et al.: Identifying dominant environmental  
 3086 predictors of freshwater wetland methane fluxes across diurnal to seasonal time scales. *Global Change Biology*,  
 3087 27(15), 3582–3604. <https://doi.org/10.1111/gcb.15661>, 2021  
 3088 Kretschmer, K., Biastoch, A., Rüpke, L. and Burwicz, E.: Modeling the fate of methane hydrates under global warming,  
 3089 *Glob. Biogeochem Cycles*, 29(5), 610–625, doi:1002/2014GB005011, 2015.  
 3090 Kuhn, M.A., Varner, R.K., Bastviken, D., Crill, P., MacIntyre, S., Turetsky, M., Walter Anthony, K., McGuire, A.D., and  
 3091 Olefeldt, D. (2021). BAWLD-CH4: a comprehensive dataset of methane fluxes from boreal and arctic ecosystems.  
 3092 *Earth Syst. Sci. Data* 13, 5151-5189. 10.5194/essd-13-5151-2021.  
 3093 Kuze A, Kikuchi N, Kataoka F, Suto H, Shiomi K, Kondo Y. Detection of Methane Emission from a Local Source Using  
 3094 GOSAT Target Observations. *Remote Sensing*, 12(2):267. <https://doi.org/10.3390/rs12020267>, 2020  
 3095 Kyzivat, E.D., L.C. Smith, F. Garcia-Tigueros, C. Huang, C. Wang, T. Langhorst, J.V. Fayne, M.E. Harlan, Y. Ishitsuka,  
 3096 D. Feng, W. Dolan, L.H. Pitcher, K.P. Wickland, M.M. Domblaser, R.G. Striegl, T.M. Pavelsky, D.E. Butman, and  
 3097 C.J. Gleason, The Importance of Lake Emergent Aquatic Vegetation for Estimating Arctic-Boreal Methane Emissions.  
 3098 *Journal of Geophysical Research: Biogeosciences* 127(6): p. e2021JG006635, 2022.  
 3099 Lamarque, J. F., Shindell, D. T., Josse, B., Young, P. J., Cionni, I., Eyring, V., Bergmann, D., Cameron-Smith, P., Collins,  
 3100 W. J., Doherty, R., Dalsoren, S., Faluvegi, G., Folberth, G., Ghan, S. J., Horowitz, L. W., Lee, Y. H., MacKenzie, I.  
 3101 A., Nagashima, T., Naik, V., Plummer, D., Righi, M., Rumbold, S. T., Schulz, M., Skeie, R. B., Stevenson, D. S.,  
 3102 Strode, S., Sudo, K., Szopa, S., Voulgarakis, A. and Zeng, G.: The Atmospheric Chemistry and Climate Model  
 3103 Intercomparison Project (ACCMIP): overview and description of models, simulations and climate diagnostics, *Geosci.*  
 3104 *Model Dev.*, 6(1), 179–206, doi:10.5194/gmd-6-179-2013, 2013.  
 3105 Lamb, B. K., Edburg, S. L., Ferrara, T. W., Howard, T., Harrison, M. R., Kolb, C. E., Townsend-Small, A., Dyck, W.,  
 3106 Possolo, A. and Whetstone, J. R.: Direct Measurements Show Decreasing Methane Emissions from Natural Gas Local  
 3107 Distribution Systems in the United States, *Environ. Sci. Technol.*, 49(8), 5161–5169, doi:10.1021/es505116p, 2015.  
 3108 Lan, X., K.W. Thoning, and E.J. Dlugokencky: Trends in globally-averaged CH4, N2O, and SF6 determined from NOAA  
 3109 Global Monitoring Laboratory measurements. Version 2024-02, <https://doi.org/10.15138/P8XG-AA10>, 2024  
 3110 Lange S., WFDE5 over land merged with ERA5 over the ocean (WSE5). V. 1.0. 2019. doi:10.5880/pik.2019.023, 2019  
 3111 Laruelle, G. G., Dürr, H. H., Lauerwald, R., Hartmann, J., Slomp, C. P., Goossens, N. and Regnier, P. A. G.: Global multi-  
 3112 scale segmentation of continental and coastal waters from the watersheds to the continental margins, *Hydrol. Earth*  
 3113 *Syst. Sci.*, 17(5), 2029–2051, doi:10.5194/hess-17-2029-2013, 2013.

3114 Laruelle, G.G., Rosentreter, J.A. and Regnier, P.: Extrapolation-Based Regionalized Re-evaluation of the Global Estuarine  
 3115 Surface Area. *Estuaries and Coasts*, 48, 34, <https://doi.org/10.1007/s12237-024-01463-3>, 2025  
 3116 Lassey, K. R., Etheridge, D. M., Lowe, D. C., Smith, A. M. and Ferretti, D. F.: Centennial evolution of the atmospheric  
 3117 methane budget: what do the carbon isotopes tell us?, *Atmospheric Chem. Phys.*, 7(8), 2119–2139, 2007a.  
 3118 Lassey, K. R., Lowe, D. C. and Smith, A. M.: The atmospheric cycling of radiomethane and the “fossil fraction” of the  
 3119 methane source, *Atmospheric Chem. Phys.*, 7(8), 2141–2149, 2007b.  
 3120 Lauerwald, R., Allen, G.H., Deemer, B.R., Liu, S., Maavara, T., Raymond, P., Alcott, L., Bastviken, D., Hastie, A.,  
 3121 Holgerson, M.A., Johnson, M.S., Lehner, B., Lin, P., Marzadri, A., Ran, L., Tian, H., Yang, X., Yao, Y. and Regnier,  
 3122 P. Inland water greenhouse gas budgets for RECCAP2: 1. State-of- the-art of global scale assessments. *Global*  
 3123 *Biogeochemical Cycles*, 37, e2022GB007657. <https://doi.org/10.1029/2022GB007657>, 2023a.  
 3124 Lauerwald, R., Allen, G.H., Deemer, B.R., Liu, S., Maavara, T., Raymond, P., Alcott, L., Bastviken, D., Hastie, A.,  
 3125 Holgerson, M.A., Johnson, M.S., Lehner, B., Lin, P., Marzadri, A., Ran, L., Tian, H., Yang, X., Yao, Y. and Regnier,  
 3126 P. Inland water greenhouse gas budgets for RECCAP2: 2 Regionalization and homogenization of estimates following  
 3127 the RECCAP2 framework, *Global Biogeochemical Cycles*, 37, e2022GB007658. [https://doi.](https://doi.org/10.1029/2022GB007658)  
 3128 [org/10.1029/2022GB007658](https://doi.org/10.1029/2022GB007658), 2023b.  
 3129 Laughner, J. L., Neu, J. L., Schimel, D., Wennberg, P. O., Barsanti, K., Bowman, K. W., Chatterjee, A., Croes, B. E.,  
 3130 Fitzmaurice, H. L., Henze, D. K., Kim, J., Kort, E. A., Liu, Z., Miyazaki, K., Turner, A. J., Anenberg, S., Avise, J.,  
 3131 Cao, H., Crisp, D., de Gouw, J., Eldering, A., Fyfe, J. C., Goldberg, D. L., Gurney, K. R., Hasheminassab, S., Hopkins,  
 3132 F., Ivey, C. E., Jones, D. B. A., Liu, J., Lovenduski, N. S., Martin, R. V., McKinley, G. A., Ott, L., Poulter, B., Ru, M.,  
 3133 Sander, S. P., Swart, N., Yung, Y. L., and Zeng, Z.-C.: Societal shifts due to COVID-19 reveal large-scale complexities  
 3134 and feedbacks between atmospheric chemistry and climate change, *P. Natl. Acad. Sci. USA*, 118, e2109481118,  
 3135 <https://doi.org/10.1073/pnas.2109481118>, 2021.  
 3136 Lauvaux, T., Giron, C., Mazzolini, M., d’Aspremont, A., Duren, R., Cusworth, D., Shindell, D., and Ciais, P.: Global  
 3137 assessment of oil and gas methane ultra-emitters, *Science*, 375, 557–561, <https://doi.org/10.1126/science.abj4351>,  
 3138 2022.  
 3139 Lelieveld, J., Crutzen, P. J. and Dentener, F. J.: Changing concentration, lifetime and climate forcing of atmospheric  
 3140 methane, *Tellus Ser. B-Chem. Phys. Meteorol.*, 50(2), 128–150, doi:10.1034/j.1600-0889.1998.t01-1-00002.x, 1998.  
 3141 Lelieveld, J., Lechtenbohrer, S., Assonov, S. S., Brenninkmeijer, C. A. M., Dienst, C., Fischedick, M. and Hanke, T.:  
 3142 Greenhouse gases: Low methane leakage from gas pipelines, *Nature*, 434(7035), 841–842, doi:10.1038/434841a, 2005.  
 3143 Lenhart, K., Klintzsch, T., Langer, G., Nehrke, G., Bunge, M., Schnell, S. and Keppler, F.: Evidence for methane  
 3144 production by the marine algae *Emiliania huxleyi*, *Biogeosciences*, 13(10), 3163–3174, doi:10.5194/bg-13-3163-2016,  
 3145 2016.  
 3146 Lewan, M. D.: Comment on Ideas and perspectives: is shale gas a major driver of recent increase in global atmospheric



methane? by Robert W. Howarth (2019), Biogeosciences Discuss., 1–10, doi:10.5194/bg-2019-419, 2020.

Li, C., Frolking, S., Xiao, X., Moore, B., Boles, S., Qiu, J., Huang, Y., Salas, W. and Sass, R.: Modeling impacts of farming management alternatives on CO<sub>2</sub>, CH<sub>4</sub>, and N<sub>2</sub>O emissions: A case study for water management of rice agriculture of China, *Glob. Biogeochem. Cycles*, 19(3), doi:10.1029/2004gb002341, 2005.

Li T, Huang Y, Zhang W, Song C: CH4MODwetland: A biogeophysical model for simulating methane emissions from natural wetlands. *Ecological Modelling* 221: 666–680, 2010.

Li, Y., J. Shang, C. Zhang, W. Zhang, L. Niu, L. Wang, and H. Zhang, The role of freshwater eutrophication in greenhouse gas emissions: A review. *Science of The Total Environment*, 768: p. 144582., 2021

Li, H. Z., Seymour, S. P. , MacKay, K., Wang, J. S., Warren, J., Guanter, L., Zavala-Araiza, D., Smith, M.L., and Xie, D.: Direct measurements of methane emissions from key facilities in Alberta's oil and gas supply chain, *Science of The Total Environment*, Volume 912, 169645, ISSN 0048-9697, doi:10.1016/j.scitotenv.2023.169645, 2024.

Lin, X., Indira, N. K., Ramonet, M., Delmotte, M., Ciais, P., Bhatt, B. C., Reddy, M. V., Angchuk, D., Balakrishnan, S., Jorphaill, S., Dorjai, T., Mahey, T. T., Patnaik, S., Begum, M., Brenninkmeijer, C., Durairaj, S., Kirubakaran, R., Schmidt, M., Swathi, P. S., Vinithkumar, N. V., Yver Kwok, C. and Gaur, V. K.: Long-lived atmospheric trace gases measurements in flask samples from three stations in India, *Atmospheric Chem. Phys.*, 15(17), 9819–9849, doi:10.5194/acp-15-9819-2015, 2015.

Lin, P., Pan, M., Beck, H. E., Yang, Y., Yamazaki, D., Frasson, R., et al.: Global reconstruction of naturalized river flows at 2.94 million reaches. *Water Resources Research*, 55, 6499–6516. <https://doi.org/10.1029/2019WR025287>, 2019

Liu, Z., Guan, D., Wei, W., Davis, S. J., Ciais, P., Bai, J., Peng, S., Zhang, Q., Hubacek, K., Marland, G., Andres, R. J., Crawford-Brown, D., Lin, J., Zhao, H., Hong, C., Boden, T. A., Feng, K., Peters, G. P., Xi, F., Liu, J., Li, Y., Zhao, Y., Zeng, N. and He, K.: Reduced carbon emission estimates from fossil fuel combustion and cement production in China, *Nature*, 524(7565), 335–338, doi:10.1038/nature14677, 2015.

Liu, G., Peng, S., Lin, X., Ciais, P., Li, X., Xi, Y., Lu, Z., Chang, J., Saunio, M., Wu, Y., Patra, P., Chandra, N., Zeng, H., and Piao, S.: Recent Slowdown of Anthropogenic Methane Emissions in China Driven by Stabilized Coal Production, *Environ. Sci. Technol. Lett.*, 8, 739–746, <https://doi.org/10.1021/acs.estlett.1c00463>, 2021a.

Liu, S., Fang, S., Liu, P., Liang, M., Guo, M., and Feng, Z.: Measurement report: Changing characteristics of atmospheric CH<sub>4</sub> in the Tibetan Plateau: records from 1994 to 2019 at the Mount Waliguan station, *Atmos. Chem. Phys.*, 21, 393–413, <https://doi.org/10.5194/acp-21-393-2021>, 2021b

Liu, S., C. Kuhn, G. Amatulli, K. Aho, D.E. Butman, G.H. Allen, P. Lin, M. Pan, D. Yamazaki, C. Brinkerhoff, C. Gleason, X. Xia, and P.A. Raymond: The importance of hydrology in routing terrestrial carbon to the atmosphere via global streams and rivers. *Proceedings of the National Academy of Sciences*, 119(11): p. e2106322119, 2022.

3179 Lloret, Z., Chevallier, F., Cozic, A., Remaud, M., and Meurdesoif, Y.: Simulating the variations of carbon dioxide in the  
 3180 global atmosphere on the hexagonal grid of DYNAMICO coupled with the LMDZ6 model, *Geosci. Model Dev.*  
 3181 *Discuss.* [preprint], <https://doi.org/10.5194/gmd-2023-140>, in review, 2023.

3182 Locatelli, R., Bousquet, P., Saunois, M., Chevallier, F. and Cressot, C.: Sensitivity of the recent methane budget to LMDz  
 3183 sub-grid-scale physical parameterizations, *Atmospheric Chem. Phys.*, 15(17), 9765–9780, doi:10.5194/acp-15-9765-  
 3184 2015, 2015.

3185 Lohila, A., Aalto, T., Aurela, M., Hatakka, J., Tuovinen, J.-P., Kilkki, J., Penttilä, T., Vuorenmaa, J., Hänninen, P., Sutinen,  
 3186 R., Viisanen, Y. and Laurila, T.: Large contribution of boreal upland forest soils to a catchment-scale CH<sub>4</sub> balance in  
 3187 a wet year, *Geophys. Res. Lett.*, 43(6), 2946–2953, doi:10.1002/2016gl067718, 2016.

3188 Lorente, A., Borsdorff, T., Martinez-Velarte, M. C., and Landgraf, J.: Accounting for surface reflectance spectral features  
 3189 in TROPOMI methane retrievals, *Atmos. Meas. Tech.*, 16, 1597–1608, <https://doi.org/10.5194/amt-16-1597-2023>,  
 3190 2023.

3191 Lu, X., Jacob, D. J., Zhang, Y., Maasakkers, J. D., Sulprizio, M. P., Shen, L., Qu, Z., Scarpelli, T. R., Nesser, H., Yantosca,  
 3192 R. M., Sheng, J., Andrews, A., Parker, R. J., Boesch, H., Bloom, A. A., and Ma, S.: Global methane budget and trend,  
 3193 2010–2017: complementarity of inverse analyses using in situ (GLOBALVIEWplus CH<sub>4</sub> ObsPack) and satellite  
 3194 (GOSAT) observations, *Atmos. Chem. Phys.*, 21, 4637–4657, <https://doi.org/10.5194/acp-21-4637-2021>, 2021

3195 Lu, X., Jacob, D. J., Zhang, Y., Maasakkers, J. D., Zhang, Y., Qu, Z., Chen, Z., Sulprizio, M. P., Varon, D., Hmiel, H.,  
 3196 Park, R. J., Boesch, H., and Fan, S.: Observation-derived 2010–2019 trends in methane emissions and intensities from  
 3197 US oil and gas fields tied to activity metrics, *P. Natl. Acad. Sci. USA*, 120, e2217900120,  
 3198 <https://doi.org/10.1073/pnas.2217900120>, 2023.

3199 Maasakkers, J. D., Jacob, D. J., Sulprizio, M. P., Scarpelli, T. R., Nesser, H., Sheng, J.-X., Zhang, Y., Hersher, M., Bloom,  
 3200 A. A., Bowman, K. W., Worden, J. R., Janssens-Maenhout, G., and Parker, R. J.: Global distribution of methane  
 3201 emissions, emission trends, and OH concentrations and trends inferred from an inversion of GOSAT satellite data for  
 3202 2010–2015, *Atmos. Chem. Phys.*, 19, 7859–7881, <https://doi.org/10.5194/acp-19-7859-2019>, 2019.

3203 Maasakkers, J. D., Jacob, D. J., Sulprizio, M. P., Scarpelli, T. R., Nesser, H., Sheng, J., Zhang, Y., Lu, X., Bloom, A. A.,  
 3204 Bowman, K. W., Worden, J. R., and Parker, R. J.: 2010–2015 North American methane emissions, sectoral  
 3205 contributions, and trends: a high-resolution inversion of GOSAT observations of atmospheric methane, *Atmos. Chem.*  
 3206 *Phys.*, 21, 4339–4356, <https://doi.org/10.5194/acp-21-4339-2021>, 2021.

3207 Maavara, T., Lauerwald, R., Regnier, P. and Van Capellen P.: Global perturbation of organic carbon cycling by river  
 3208 damming, *Nat Commun* 8, 153, <https://doi.org/10.1038/ncomms15347>, 2017.

3209 Machacova, K., Borak, L., Agyei, T., Schindler, T., Soosaar, K., Mander, Ü., and Ah-Peng, C: Trees as net sinks for  
 3210 methane (CH<sub>4</sub>) and nitrous oxide (N<sub>2</sub>O) in the lowland tropical rain forest on volcanic Réunion Island, *The New*  
 3211 *phytologist*, 229(4), 1983–1994, <https://doi.org/10.1111/nph.17002>, 2021

3212 Machida, T., H. Matsueda, Y. Sawa, Y. Nakagawa, K. Hirotani, N. Kondo, K. Goto, N. Nakazawa, K. Ishikawa and T.  
 3213 Ogawa: Worldwide measurements of atmospheric CO<sub>2</sub> and other trace gas species using commercial airlines, *J. Atmos.*  
 3214 *Oceanic Technol.*, 25(10), 1744-1754, doi:10.1175/2008JTECHA1082.1, 2008  
 3215 Maksyutov, S., Oda, T., Saito, M., Janardanan, R., Belikov, D., Kaiser, J. W., Zhuravlev, R., Ganshin, A., Valsala, V. K.,  
 3216 Andrews, A., Chmura, L., Dlugokencky, E., Haszpra, L., Langenfelds, R. L., Machida, T., Nakazawa, T., Ramonet,  
 3217 M., Sweeney, C. and Worthy, D.: Technical note: A high-resolution inverse modelling technique for estimating surface  
 3218 CO<sub>2</sub> fluxes based on the NIES-TM & FLEXPART coupled transport model and its adjoint, *Atmospheric Chem.*  
 3219 *Phys. Discuss.*, 1–33, doi:10.5194/acp-2020-251, 2020.  
 3220 Malerba, M.E., T. de Kluyver, N. Wright, L. Schuster, and P.I. Macreadie: Methane emissions from agricultural ponds are  
 3221 underestimated in national greenhouse gas inventories. *Communications Earth & Environment*, 3(1): p. 306, 2022  
 3222 Maltby, J., L. Steinle, C. R. Löschner, H. W. Bange, M. A. Fischer, M. Schmidt, and T. Treude: Microbial methanogenesis  
 3223 in the sulfate-reducing zone of sediments in the Eckernförde Bay, SW Baltic Sea. *Biogeosciences* **15**: 137–157.  
 3224 doi:10.5194/bg-15-137-2018, 2018  
 3225 Manning, F. C. , Kho, L. K., Hill, T. C., Cornulier, T., and Teh, Y A: Carbon Emissions From Oil Palm Plantations on  
 3226 Peat Soil, *Front. For. Glob. Change, Sec. Tropical Forests, Volume 2* , <https://doi.org/10.3389/ffgc.2019.0003>, 2019  
 3227 Mannisenaho V, Tsuruta A, Backman L, Houweling S, Segers A, Krol M, Saunio M, Poulter B, Zhang Z, Lan X, et al.  
 3228 Global Atmospheric  $\delta^{13}\text{CH}_4$  and  $\text{CH}_4$  Trends for 2000–2020 from the Atmospheric Transport Model TM5 Using  $\text{CH}_4$   
 3229 from Carbon Tracker Europe– $\text{CH}_4$  Inversions. *Atmosphere*, 14(7):1121. <https://doi.org/10.3390/atmos14071121>, 2023  
 3230 van Marle, M. J. E., Kloster, S., Magi, B. I., Marlon, J. R., Daniau, A.-L., Field, R. D., Arneth, A., Forrest, M., Hantson,  
 3231 S., Kehrwald, N. M., Knorr, W., Lasslop, G., Li, F., Mangeon, S., Yue, C., Kaiser, J. W. and Werf, G. R. van der:  
 3232 Historic global biomass burning emissions for CMIP6 (BB4CMIP) based on merging satellite observations with  
 3233 proxies and fire models (1750–2015), *Geosci. Model Dev.*, 10(9), 3329–3357, doi:10.5194/gmd-10-3329-2017, 2017.  
 3234 Martinez, A., Saunio, M., Poulter B., Zhen, Z., Raymond, P., Regnier, P. Canadell, J. G., Jackson, R. B., Patra, P. K.,  
 3235 Bousquet, P., Ciais, P., Dlugokencky, E.J., Lan, X., Allen, G., Bastviken, D., Beerling, D. J., Belikov, D., Blake, D.,  
 3236 Castaldi, S., Crippa, M., Deemer, B.R., Dennison, F., Etiope, G., Gedney, N., Höglund-Isaksson, L., Holgersson, M.A.,  
 3237 Hopcroft, P. O. , Hugelius, G., Ito, A., Jain, A. K., Janardanan, R., Johnson, M. S., Kleinen, T., Krummel, P. B.,  
 3238 Lauerwald, R., Li, T., Liu, X., McDonald, K. C., Melton, J. R., Mühle, J., Müller, J., Murguía-Flores, F., Niwa, Y.,  
 3239 Noce, S., Pan, S., Parker, R. J., Peng, C., Ramonet, M., Riley, W. J., Rocher-Ros, G., Rosentreter, J. A., Sasakawa,  
 3240 M., Segers A. , Smith, S. J., Stanley, E. H., Thanwerdas, J., Tian, H., Tsuruta, A., Tubiello, F. N., Weber, T. S., van  
 3241 der Werf, G. R., Worthy, D. E. J., Xi, Y., Yoshida Y. , Zhang, W. , Zheng, B. , Zhu, Qing , Zhu, Qian, and Zhuang,  
 3242 Q.: *Supplemental data of the Global Carbon Project Methane Budget 2024 v1*. [Data set],  
 3243 <https://doi.org/10.18160/GKQ9-2RHT>, 2024  
 3244 Matthews, E. and Fung, I.: Methane emission from natural wetlands: Global distribution, area, and environmental

characteristics of sources, *Glob. Biogeochem. Cycles*, 1(1), 61–86, doi:10.1029/GB001i001p00061, 1987.

Mazzini A., Etiope G. (2017). Mud volcanism: an updated review. *Earth Sci. Rev.*, 168, 81-112. <http://dx.doi.org/10.1016/j.earscirev.2017.03.001>, 2017

McCalley, C. K., Woodcroft, B. J., Hodgkins, S. B., Wehr, R. A., Kim, E.-H., Mondav, R., Crill, P. M., Chanton, J. P., Rich, V. I., Tyson, G. W. and Saleska, S. R.: Methane dynamics regulated by microbial community response to permafrost thaw, *Nature*, 514(7523), 478–481, doi:10.1038/nature13798, 2014.

McCarthy, M. C., Boering, K. A., Rice, A. L., Tyler, S. C., Connell, P. and Atlas, E.: Carbon and hydrogen isotopic compositions of stratospheric methane: 2. Two-dimensional model results and implications for kinetic isotope effects, *J. Geophys. Res. Atmospheres*, 108(D15), doi:10.1029/2002JD003183, 2003.

McGinnis, D. F., J. Greinert, Y. Artemov, S. E. Beaubien, and A. Wüest: Fate of rising methane bubbles in stratified waters: How much methane reaches the atmosphere?, *J. Geophys. Res.*, 111, C09007, doi:10.1029/2005JC003183, 2006

McGuire, A. D., Christensen, T. R., Heroult, A., Miller, P. A., Hayes, D., Euskirchen, E., Kimball, J. S., Yi, Y., Koven, C., Lafleur, P., Oechel, W., Peylin, P. and Williams, M.: An assessment of the carbon balance of Arctic tundra, *Comp. Obs. Process Models Atmospheric Inversions*, 9(Article), 3185–3204, doi:10.5194/bg-9-3185-2012, 2012.

McKain, K., Down, A., Raciti, S. M., Budney, J., Hutyrá, L. R., Floerchinger, C., Herndon, S. C., Nehr Korn, T., Zahniser, M. S., Jackson, R. B., Phillips, N. and Wofsy, S. C.: Methane emissions from natural gas infrastructure and use in the urban region of Boston, Massachusetts, *Proc. Natl. Acad. Sci.*, 112(7), 1941–1946, doi:10.1073/pnas.1416261112, 2015.

McNicol, G., Fluet-Chouinard, E., Ouyang, Z., Knox, S., Zhang, Z., Aalto, T., et al.: Upscaling wetland methane emissions from the FLUXNET-CH<sub>4</sub> eddy covariance network (UpCH<sub>4</sub> v1.0): Model development, network assessment, and budget comparison. *AGU Advances*, 4, e2023AV000956. <https://doi.org/10.1029/2023AV000956>, 2023

Meinshausen, M., Smith, S., Calvin, K., Daniel, J., Kainuma, M., Lamarque, J. F., Matsumoto, K., Montzka, S., Raper, S., Riahi, K., Thomson, A., Velders, G. and van Vuuren, D. P.: The RCP greenhouse gas concentrations and their extensions from 1765 to 2300, *Clim. Change*, 109(1), 213–241, doi:10.1007/s10584-011-0156-z, 2011.

Meinshausen, M., Vogel, E., Nauels, A., Lorbacher, K., Meinshausen, N., Etheridge, D. M., Fraser, P. J., Montzka, S. A., Rayner, P. J., Trudinger, C. M., Krummel, P. B., Beyerle, U., Canadell, J. G., Daniel, J. S., Enting, I. G., Law, R. M., Lunder, C. R., O'Doherty, S., Prinn, R. G., Reimann, S., Rubino, M., Velders, G. J. M., Vollmer, M. K., Wang, R. H. J., and Weiss, R.: Historical greenhouse gas concentrations for climate modelling (CMIP6), *Geosci. Model Dev.*, 10, 2057–2116, <https://doi.org/10.5194/gmd-10-2057-2017>, 2017.

Meinshausen, M., Nicholls, Z. R. J., Lewis, J., Gidden, M. J., Vogel, E., Freund, M., Beyerle, U., Gessner, C., Nauels, A., Bauer, N., Canadell, J. G., Daniel, J. S., John, A., Krummel, P. B., Luderer, G., Meinshausen, N., Montzka, S. A.,

Rayner, P. J., Reimann, S., Smith, S. J., van den Berg, M., Velders, G. J. M., Vollmer, M. K., and Wang, R. H. J.: The shared socio-economic pathway (SSP) greenhouse gas concentrations and their extensions to 2500, *Geosci. Model Dev.*, 13, 3571–3605, <https://doi.org/10.5194/gmd-13-3571-2020>, 2020.

Melton, J. R. and Arora, V. K.: Competition between plant functional types in the Canadian Terrestrial Ecosystem Model (CTEM) v. 2.0, *Geosci. Model Dev.*, 9(1), 323–361, doi:10.5194/gmd-9-323-2016, 2016.

Melton, J. R., Wania, R., Hodson, E. L., Poulter, B., Ringeval, B., Spahni, R., Bohn, T., Avis, C. A., Beerling, D. J., Chen, G., Eliseev, A. V., Denisov, S. N., Hopcroft, P. O., Lettenmaier, D. P., Riley, W. J., Singarayer, J. S., Subin, Z. M., Tian, H., Zürcher, S., Brovkin, V., van Bodegom, P. M., Kleinen, T., Yu, Z. C. and Kaplan, J. O.: Present state of global wetland extent and wetland methane modelling: conclusions from a model intercomparison project (WETCHIMP), *Biogeosciences*, 10(2), 753–788, doi:10.5194/bg-10-753-2013, 2013.

Membrive, O., Crevoisier, C., Sweeney, C., Danis, F., Hertzog, A., Engel, A., Bönsch, H. and Picon, L.: AirCore-HR: a high-resolution column sampling to enhance the vertical description of CH<sub>4</sub> and CO<sub>2</sub>, *Atmospheric Meas. Tech.*, 10(6), 2163–2181, doi:10.5194/amt-10-2163-2017, 2017.

Messenger, M. L., Lehner, B., Grill, G., Nedeva, I. and Schmitt, O.: Estimating the volume and age of water stored in global lakes using a geo-statistical approach, *Nat. Commun.*, 7(1), 1–11, doi:10.1038/ncomms13603, 2016.

Michel, SE, Lan, X, Miller, J, Tans, P, Clark, JR, Schaefer, H, Sperlich, P, Brailsford, G, Morimoto, S, Moossen, H, Li, J.: Rapid shift in methane carbon isotopes suggests microbial emissions drove record high atmospheric methane growth in 2020–2022, *Proc Natl Acad Sci U S A*, 121(44):e2411212121, doi: 10.1073/pnas.2411212121, 2024.

Mijling, B., van der A, R. J. and Zhang, Q.: Regional nitrogen oxides emission trends in East Asia observed from space, *Atmospheric Chem. Phys.*, 13(23), 12003–12012, doi:10.5194/acp-13-12003-2013, 2013.

Milkov, A. V.: Molecular and stable isotope compositions of natural gas hydrates: A revised global dataset and basic interpretations in the context of geological settings, *Org. Geochem.*, 36(5), 681–702, 2005.

Minkinen, K. and Laine, J.: Vegetation heterogeneity and ditches create spatial variability in methane fluxes from peatlands drained for forestry, *Plant Soil*, 285(1), 289–304, doi:10.1007/s11104-006-9016-4, 2006.

Monforti Ferrario, Fabio; Crippa, Monica; Guizzardi, Diego; Muntean, Marilena; Schaaf, Edwin; Lo Vullo, Eleonora; Solazzo, Efisio; Olivier, Jos; Vignati, Elisabetta: EDGAR v6.0 Greenhouse Gas Emissions. European Commission, Joint Research Centre (JRC) [Dataset] PID: <http://data.europa.eu/89h/97a67d67-c62e-4826-b873-9d972c4f670b>, 2021

Montzka, S. A., Krol, M., Dlugokencky, E., Hall, B., Jockel, P. and Lelieveld, J.: Small Interannual Variability of Global Atmospheric Hydroxyl, *Science*, 331(6013), 67–69, 2011.

Morgenstern, O., Hegglin, M. I., Rozanov, E., O'Connor, F. M., Abraham, N. L., Akiyoshi, H., Archibald, A. T., Bekki, S., Butchart, N., Chipperfield, M. P., Deushi, M., Dhomse, S. S., Garcia, R. R., Hardiman, S. C., Horowitz, L. W., Jöckel, P., Josse, B., Kinnison, D., Lin, M., Mancini, E., Manyin, M. E., Marchand, M., Marécal, V., Michou, M., Oman, L. D., Pitari, G., Plummer, D. A., Revell, L. E., Saint-Martin, D., Schofield, R., Stenke, A., Stone, K., Sudo,

3311 K., Tanaka, T. Y., Tilmes, S., Yamashita, Y., Yoshida, K., and Zeng, G.: Review of the global models used within  
 3312 phase 1 of the Chemistry–Climate Model Initiative (CCMI), *Geosci. Model Dev.*, 10, 639–671,  
 3313 <https://doi.org/10.5194/gmd-10-639-2017>, 2017.

3314 Morgenstern, O., Stone, K. A., Schofield, R., Akiyoshi, H., Yamashita, Y., Kinnison, D. E., Garcia, R. R., Sudo, K.,  
 3315 Plummer, D. A., Scinocca, J., Oman, L. D., Manyin, M. E., Zeng, G., Rozanov, E., Stenke, A., Revell, L. E., Pitari,  
 3316 G., Mancini, E., Di Genova, G., Visioni, D., Dhomse, S. S., and Chipperfield, M. P.: Ozone sensitivity to varying  
 3317 greenhouse gases and ozone-depleting substances in CCMI-1 simulations, *Atmos. Chem. Phys.*, 18, 1091–1114,  
 3318 <https://doi.org/10.5194/acp-18-1091-2018>, 2018.

3319 Morino, I., Uchino, O., Inoue, M., Yoshida, Y., Yokota, T., Wennberg, P. O., Toon, G. C., Wunch, D., Roehl, C. M.,  
 3320 Notholt, J., Warneke, T., Messerschmidt, J., Griffith, D. W. T., Deutscher, N. M., Sherlock, V., Connor, B., Robinson,  
 3321 J., Sussmann, R. and Rettinger, M.: Preliminary validation of column-averaged volume mixing ratios of carbon dioxide  
 3322 and methane retrieved from GOSAT short-wavelength infrared spectra, *Atmospheric Meas. Tech.*, 4(6), 1061–1076,  
 3323 2011.

3324 Murguía-Flores, F., Arndt, S., Ganesan, A. L., Murray-Tortarolo, G. and Hornibrook, E. R. C.: Soil Methanotrophy Model  
 3325 (MeMo v1.0): a process-based model to quantify global uptake of atmospheric methane by soil, *Geosci. Model Dev.*,  
 3326 11(6), 2009–2032, doi:10.5194/gmd-11-2009-2018, 2018.

3327 Murguía-Flores, F., Ganesan, A. L., Arndt, S., and Hornibrook, E. R. C.: Global uptake of atmospheric methane by soil  
 3328 from 1900 to 2100, *Global Biogeochemical Cycles*, 35, e2020GB006774, <https://doi.org/10.1029/2020GB006774>,  
 3329 2021.

3330 Myer, A., Myer, M.H., Trettin, C.C. and Forschler, B.T.: The fate of carbon utilized by the subterranean termite  
 3331 *Reticulitermes flavipes*. *Ecosphere* 12 (12):e03872, doi:10.1002/ecs2.3872, 2021

3332 Myhre, G., Shindell, D., Bréon, F.-M., Collins, W., Fuglestedt, J., Huang, J., Koch, D., Lamarque, J.-F., Lee, D.,  
 3333 Mendoza, B., Nakajima, T., Robock, A., Stephens, G., Takemura, T. and Zhang, H.: Anthropogenic and Natural  
 3334 Radiative Forcing., in *Climate Change 2013: The Physical Science Basis. Contribution of Working Group I to the*  
 3335 *Fifth Assessment Report of the Intergovernmental Panel on Climate Change.*, edited by T. F. Stocker, D. D. Qin, G.-  
 3336 K. Plattner, M. Tignor, S. K. Allen, J. Boschung, A. Nauels, Y. Xia, V. Bex, and P. M. Midgley, Cambridge University  
 3337 Press, Cambridge, United Kingdom and New York, NY, USA., 2013.

3338 Naik, V., Voulgarakis, A., Fiore, A. M., Horowitz, L. W., Lamarque, J. F., Lin, M., Prather, M. J., Young, P. J., Bergmann,  
 3339 D., Cameron-Smith, P. J., Cionni, I., Collins, W. J., Dalsoren, S. B., Doherty, R., Eyring, V., Faluvegi, G., Folberth,  
 3340 G. A., Josse, B., Lee, Y. H., MacKenzie, I. A., Nagashima, T., van Noije, T. P. C., Plummer, D. A., Righi, M., Rumbold,  
 3341 S. T., Skeie, R., Shindell, D. T., Stevenson, D. S., Strode, S., Sudo, K., Szopa, S. and Zeng, G.: Preindustrial to present  
 3342 day changes in tropospheric hydroxyl radical and methane lifetime from the Atmospheric Chemistry and Climate  
 3343 Model Intercomparison Project (ACCMIP), *Atmospheric Chem. Phys.*, 13(10), 5277–5298, doi:10.5194/acp-13-5277-

2013, 2013.

Nakazawa, T., Machida, T., Tanaka, M., Fujii, Y., Aoki, S. and Watanabe, O.: Differences of the atmospheric CH<sub>4</sub> concentration between the Arctic and Antarctic regions in pre-industrial/pre-agricultural era, *Geophys. Res. Lett.*, 20(10), 943–946, doi:10.1029/93GL00776, 1993.

Natchimuthu, S., I. Sundgren, M. Gålfalk, L. Klemedtsson, P. Crill, Å. Danielsson, and D. Bastviken, Spatio-temporal variability of lake CH<sub>4</sub> fluxes and its influence on annual whole lake emission estimates. *Limnology and Oceanography*, 61(S1): p. S13-S26, 2016.

Nauer, P. A., Hutley, L. B., and Arndt, S. K.: Termite mounds mitigate half of termite methane emissions, *P. Natl. Acad. Sci. USA*, 115, 13306–13311, 2018.

Naus, S., Montzka, S. A., Patra, P. K., and Krol, M. C.: A three-dimensional-model inversion of methyl chloroform to constrain the atmospheric oxidative capacity, *Atmos. Chem. Phys.*, 21, 4809–4824, <https://doi.org/10.5194/acp-21-4809-2021>, 2021.

Nicely, J. M., Salawitch, R. J., Canty, T., Anderson, D. C., Arnold, S. R., Chipperfield, M. P., Emmons, L. K., Flemming, J., Huijnen, V., Kinnison, D. E., Lamarque, J.-F., Mao, J., Monks, S. A., Steenrod, S. D., Tilmes, S. and Turquety, S.: Quantifying the causes of differences in tropospheric OH within global models, *J. Geophys. Res. Atmospheres*, 122(3), 1983–2007, doi:10.1002/2016JD026239, 2017.

Nicely, J. M., Canty, T. P., Manyin, M., Oman, L. D., Salawitch, R. J., Steenrod, S. D., Strahan, S. E., and Strode, S. A.: Changes in Global Tropospheric OH Expected as a Result of Climate Change Over the Last Several Decades, *J. Geophys. Res.-Atmos.*, 123, 10774–10795, <https://doi.org/10.1029/2018JD028388>, 2018.

Nirmal Rajkumar, A., J. Barnes, R. Ramesh, R. Purvaja, and R.C. Upstill-Goddard, Methane and nitrous oxide fluxes in the polluted Adyar River and estuary, SE India. *Marine Pollution Bulletin*, 56(12): p. 2043-2051, 2008

Nisbet, R. E. R., Fisher, R., Nimmo, R. H., Bendall, D. S., Crill, P. M., Gallego-Sala, A. V., Hornibrook, E. R. C., Lopez-Juez, E., Lowry, D., Nisbet, P. B. R., Shuckburgh, E. F., Sriskantharajah, S., Howe, C. J. and Nisbet, E. G.: Emission of methane from plants, *Proc. R. Soc. B-Biol. Sci.*, 276(1660), 1347–1354, 2009.

Nisbet, E. G., Manning, M. R., Dlugokencky, E. J., Fisher, R. E., Lowry, D., Michel, S. E., Myhre, C. L., Platt, S. M., Allen, G., Bousquet, P., Brownlow, R., Cain, M., France, J. L., Hermansen, O., Hossaini, R., Jones, A. E., Levin, I., Manning, A. C., Myhre, G., Pyle, J. A., Vaughn, B., Warwick, N. J. and White, J. W. C.: Very strong atmospheric methane growth in the four years 2014-2017: Implications for the Paris Agreement, *Glob. Biogeochem. Cycles*, 0(ja), doi:10.1029/2018GB006009, 2019.

Nisbet, E. G., Fisher, R. E., Lowry, D., France, J. L., Allen, G., Bakaloglu, S., Broderick, T.J., Cain, M., Coleman, M., Fernandez, J., Forster, G., Griffiths, P.T., Iverach, C.P., Keely, B.F.J., Manning, M.R., Nisbet-Jones, B.R., Pyle, J.A., Townsend-Samll, A., al-Shallan, A., Warwick, N. and Zazzeri, G.: Methane mitigation: methods to reduce emissions, on the path to the Paris agreement. *Reviews of Geophysics*, 58, e2019RG000675.

3377 <https://doi.org/10.1029/2019RG000675>, 2020

3378 Nisbet, E. G., Manning, M. R., Dlugokencky, E. J., Michel, S. E., Lan, X., Röckmann, T., van der Denier Gon, H. A.,  
 3379 Schmitt, J., Palmer, P. I., Dyonisius, M. N., Oh, Y., Fisher, R. E., Lowry, D., France, J. L., White, J. W. C., Brailsford,  
 3380 G., and Bromley, T.: Atmospheric methane: Comparison between methane's record in 2006–2022 and during glacial  
 3381 terminations, *Global Biogeochem. Cy.*, 37, e2023GB007875, <https://doi.org/10.1029/2023GB007875>, 2023.

3382 Nisbet, E.G.: Climate feedback on methane from wetlands, *Nat. Clim. Chang.*, 13, 421–422.  
 3383 <https://doi.org/10.1038/s41558-023-01634-3>, 2023.

3384 Niwa, Y., Fujii, Y., Sawa, Y., Iida, Y., Ito, A., Satoh, M., Imasu, R., Tsuboi, K., Matsueda, H. and Saigusa, N.: A 4D-  
 3385 Var inversion system based on the icosahedral grid model (NICAM-TM 4D-Var v1.0) – Part 2: Optimization scheme  
 3386 and identical twin experiment of atmospheric CO<sub>2</sub> inversion, *Geosci. Model Dev.*, 10(6), 2201–2219,  
 3387 doi:10.5194/gmd-10-2201-2017, 2017.

3388 Niwa, Y., Ishijima, K., Ito, A. and Iida, Y.: Toward a long-term atmospheric CO<sub>2</sub> inversion for elucidating natural carbon  
 3389 fluxes: technical notes of NISMON-CO<sub>2</sub> v2021.1. *Prog. Earth Planet Sci.* 9, 42, doi:10.1186/s40645-022-00502-6,  
 3390 2022

3391 Niwa, Y., Tohjima, Y., Terao, Y., Saeki, T., Ito, A., Umezawa, T., Yamada, K., Sasakawa, M., Machida, T., Nakaoka, S.-  
 3392 I., Nara, H., Tanimoto, H., Mukai, H., Yoshida, Y., Morimoto, S., Takatsuji, S., Tsuboi, K., Sawa, Y., Matsueda, H.,  
 3393 Ishijima, K., Fujita, R., Goto, D., Lan, X., Schuldt, K., Heliasz, M., Biermann, T., Chmura, L., Necki, J., and Xueref-  
 3394 Remy, I.: Multi-observational estimation of regional and sectoral emission contributions to the persistent high growth  
 3395 rate of atmospheric CH<sub>4</sub> for 2020–2022, *EGUsphere* [preprint], <https://doi.org/10.5194/egusphere-2024-2457>, 2024.

3396 Noël, S., Reuter, M., Buchwitz, M., Borchardt, J., Hilker, M., Schneising, O., Bovensmann, H., Burrows, J. P., Di Noia,  
 3397 A., Parker, R. J., Suto, H., Yoshida, Y., Buschmann, M., Deutscher, N. M., Feist, D. G., Griffith, D. W. T., Hase, F.,  
 3398 Kivi, R., Liu, C., Morino, I., Notholt, J., Oh, Y.-S., Ohyama, H., Petri, C., Pollard, D. F., Rettinger, M., Roehl, C.,  
 3399 Rousogonous, C., Sha, M. K., Shiomi, K., Strong, K., Sussmann, R., Tê, Y., Velazco, V. A., Vrekoussis, M., and  
 3400 Warneke, T.: Retrieval of greenhouse gases from GOSAT and GOSAT-2 using the FOCAL algorithm, *Atmos. Meas.*  
 3401 *Tech.*, 15, 3401–3437, <https://doi.org/10.5194/amt-15-3401-2022>, 2022.

3402 Nomura, S., Naja, M., Ahmed, M. K., Mukai, H., Terao, Y., Machida, T., Sasakawa, M., and Patra, P. K.: Measurement  
 3403 report: Regional characteristics of seasonal and long-term variations in greenhouse gases at Nainital, India, and  
 3404 Comilla, Bangladesh, *Atmos. Chem. Phys.*, 21, 16427–16452, <https://doi.org/10.5194/acp-21-16427-2021>, 2021

3405 Obu, J., Westermann, S., Bartsch, A., Berdnikov, N., Christiansen, H. H., Dashtseren, A., Delaloye, R., Elberling, B.,  
 3406 Etzelmüller, B., Kholodov, A., Khomutov, A., Kääb, A., Leibman, M. O., Lewkowicz, A. G., Panda, S. K.,  
 3407 Romanovsky, V., Way, R. G., Westergaard-Nielsen, A., Wu, T., Yamkhin, J. and Zou, D.: Northern Hemisphere  
 3408 permafrost map based on TTOP modelling for 2000–2016 at 1 km<sup>2</sup> scale, *Earth-Sci. Rev.*, 193, 299–316,  
 3409 doi:10.1016/j.earscirev.2019.04.023, 2019.

Mis en forme : Anglais (E.U.)

Mis en forme : Anglais (E.U.)

Mis en forme : Anglais (E.U.)

Mis en forme : Anglais (E.U.)



3410 Ocko, I. B, Sun, T., Shindell, D., Oppenheimer, M., Hristov, A. N, Pacala, S. W, Mauzerall, D. L, Xu, Y. and Hamburg,  
 3411 S. P.: Acting rapidly to deploy readily available methane mitigation measures by sector can immediately slow global  
 3412 warming, *Environ. Res. Lett.*, 16, 054042, doi :10.1088/1748-9326/abf9c8, 2021  
 3413 Odelson, D.A. and Breznak, J. A. Volatile fatty acid production by the hindgut microbiota of xilophagus termites. *Applied*  
 3414 *and Environmental Microbiology*, 45, 1602-1613, 1983. doi: 10.1128/aem.45.5.1602-1613.1983.  
 3415 Ollivier, Q. R., Maher, D. T., Pitfield, C. and Macreadie, P. I.: Punching above their weight: Large release of greenhouse  
 3416 gases from small agricultural dams, *Glob. Change Biol.*, 25(2), 721–732, doi:10.1111/gcb.14477, 2019.  
 3417 Omara, M, Zavala-Araiza,D, Lyon, DR, Hmiel, B, Roberts, KA, Hamburg, SP :Methane emissions from US low  
 3418 production oil and natural gas well sites, *Nat Commun*, 13(1):2085, doi: 10.1038/s41467-022-29709-3, 2022  
 3419 O'Neill, B. C., Tebaldi, C., Vuuren, D. P. van, Eyring, V., Friedlingstein, P., Hurtt, G., Knutti, R., Kriegler, E., Lamarque,  
 3420 J.-F., Lowe, J., Meehl, G. A., Moss, R., Riahi, K. and Sanderson, B. M.: The Scenario Model Intercomparison Project  
 3421 (ScenarioMIP) for CMIP6, *Geosci. Model Dev.*, 9(9), 3461–3482, doi: 10.5194/gmd-9-3461-2016, 2016.  
 3422 Oreggioni, G. D., F. Monforti Ferrario, M. Crippa, M. Muntean, E. Schaaf, D. Guizzardi, E. Solazzo, M. Duerr, M. Perry  
 3423 and E. Vignati: Climate change in a changing world: Socio-economic and technological transitions, regulatory  
 3424 frameworks and trends on global greenhouse gas emissions from EDGAR v.5.0, *Global Environmental Change*,  
 3425 doi:10.1016/j.gloenvcha.2021.10235, 2021  
 3426 Oremland, R. S. Methanogenic activity in plankton samples and fish intestines: a mechanism for *in situ* methanogenesis  
 3427 in oceanic surface waters. *Limnol. Oceanogr.* **24**, 1136–1141, 1979.  
 3428 O'Rourke, P. R, Smith, S. J., Mott, A., Ahsan, H., McDuffie, E. E., Crippa, M., Klimont, S., McDonald, B., Z., Wang,  
 3429 Nicholson, M. B, Feng, L., and Hoesly, R. M., CEDS v-2021-02-05 Emission Data 1975-2019 (Version Feb-05-2021).  
 3430 Zenodo. <http://doi.org/10.5281/zenodo.4509372>, 2021  
 3431 Ovale, A. R. C., C. E. Rezende, L. D. Lacerda, and C. A. R. Silva: Factors affecting the hydrochemistry of a mangrove  
 3432 tidal creek, Sepetiba Bay, Brazil. *Estuar. Coast. Shelf Sci.* 31: 639–650. doi:10.1016/0272-7714(90)90017-L, 1990  
 3433 Pacala, S. W.: Verifying greenhouse gas emissions: Methods to support international climate agreements, National  
 3434 Academies Press., 2010  
 3435 Pandey, S., Gautam, R., Houweling, S., Gon, H. D. van der, Sadavarte, P., Borsdorff, T., Hasekamp, O., Landgraf, J., Tol,  
 3436 P., Kempen, T. van, Hoogeveen, R., Hees, R. van, Hamburg, S. P., Maasakkers, J. D. and Aben, I.: Satellite  
 3437 observations reveal extreme methane leakage from a natural gas well blowout, *Proc. Natl. Acad. Sci.*, 116(52), 26376–  
 3438 26381, doi:10.1073/pnas.1908712116, 2019.  
 3439 Pangala, S. R., Moore, S., Hornibrook, E. R. C. and Gauci, V.: Trees are major conduits for methane egress from tropical  
 3440 forested wetlands, *New Phytol.*, 197(2), 524–531, doi:10.1111/nph.12031, 2013.  
 3441 Pangala, S. R., Hornibrook, E. R. C., Gowing, D. J. and Gauci, V.: The contribution of trees to ecosystem methane  
 3442 emissions in a temperate forested wetland, *Glob. Change Biol.*, 21(7), 2642–2654, doi:10.1111/gcb.12891, 2015.

3443 Pangala, S. R., Enrich-Prast, A., Basso, L. S., Peixoto, R. B., Bastviken, D., Hornibrook, E. R. C., Gatti, L. V., Marotta,  
 3444 H., Calazans, L. S. B., Sakuragai, C. M., Bastos, W. R., Malm, O., Gloor, E., Miller, J. B. and Gauci, V.: Large  
 3445 emissions from floodplain trees close the Amazon methane budget, *Nature*, 552(7684), 230–234,  
 3446 doi:10.1038/nature24639, 2017.  
 3447 Paris, J.-D., Ciais, P., Nedelec, P., Stohl, A., Belan, B. D., Arshinov, M. Y., Carouge, C., Golitsyn, G. S. and Granberg, I.  
 3448 G.: New insights on the chemical composition of the Siberian air shed from the YAK AEROSIB aircraft campaigns,  
 3449 *Bull. Am. Meteorol. Soc.*, 91(5), 625–641, doi:10.1175/2009BAMS2663.1., 2010.  
 3450 Parker, R. J., Webb, A., Boesch, H., Somkuti, P., Barrio Guillo, R., Di Noia, A., Kalaitzi, N., Anand, J. S., Bergamaschi,  
 3451 P., Chevallier, F., Palmer, P. I., Feng, L., Deutscher, N. M., Feist, D. G., Griffith, D. W. T., Hase, F., Kivi, R., Morino,  
 3452 I., Notholt, J., Oh, Y.-S., Ohyama, H., Petri, C., Pollard, D. F., Roehl, C., Sha, M. K., Shiomi, K., Strong, K., Sussmann,  
 3453 R., Té, Y., Velasco, V. A., Warneke, T., Wennberg, P. O., and Wunch, D.: A decade of GOSAT Proxy satellite CH4  
 3454 observations, *Earth Syst. Sci. Data*, 12, 3383–3412, <https://doi.org/10.5194/essd-12-3383-2020>, 2020.  
 3455 Parker, R. and Boesch, H. (2020): University of Leicester GOSAT Proxy XCH4 v9.0. Centre for Environmental Data  
 3456 Analysis, 07 May 2020. <https://dx.doi.org/10.5285/18ef8247f52a4cb6a14013f8235cc1eb>, 2020  
 3457 Parker, R. J., Wilson, C., Comyn-Platt, E., Hayman, G., Marthews, T. R., Bloom, A. A., Lunt, M. F., Gedney, N., Dadson,  
 3458 S. J., McNorton, J., Humpage, N., Boesch, H., Chipperfield, M. P., Palmer, P. I., and Yamazaki, D.: Evaluation of  
 3459 wetland CH4 in the Joint UK Land Environment Simulator (JULES) land surface model using satellite observations,  
 3460 *Biogeosciences*, 19, 5779–5805, <https://doi.org/10.5194/bg-19-5779-2022>, 2022.  
 3461 Pathak, H., Li, C. and Wassmann, R.: Greenhouse gas emissions from Indian rice fields: calibration and upscaling using  
 3462 the DNDC model, *Biogeosciences*, 1(1), 1–11, 2005.  
 3463 Patra, P. K., Houweling, S., Krol, M., Bousquet, P., Belikov, D., Bergmann, D., Bian, H., Cameron-Smith, P., Chipperfield,  
 3464 M. P., Corbin, K., Fortems-Cheiney, A., Fraser, A., Gloor, E., Hess, P., Ito, A., Kawa, S. R., Law, R. M., Loh, Z.,  
 3465 Maksyutov, S., Meng, L., Palmer, P. I., Prinn, R. G., Rigby, M., Saito, R. and Wilson, C.: TransCom model simulations  
 3466 of CH4 and related species: linking transport, surface flux and chemical loss with CH4 variability in the troposphere  
 3467 and lower stratosphere, *Atmospheric Chem. Phys.*, 11(24), 12,813–12,837, doi:10.5194/acp-11-12813-2011, 2011.  
 3468 Patra, P. K., Krol, M. C., Montzka, S. A., Arnold, T., Atlas, E. L., Lintner, B. R., Stephens, B. B., Xiang, B., Elkins, J. W.,  
 3469 Fraser, P. J., Ghosh, A., Hintsa, E. J., Hurst, D. F., Ishijima, K., Krummel, P. B., Miller, B. R., Miyazaki, K., Moore,  
 3470 F. L., Mühle, J., O'Doherty, S., Prinn, R. G., Steele, L. P., Takigawa, M., Wang, H. J., Weiss, R. F., Wofsy, S. C. and  
 3471 Young, D.: Observational evidence for interhemispheric hydroxyl-radical parity, *Nature*, 513(7517), 219–223,  
 3472 doi:10.1038/nature13721, 2014.  
 3473 Patra, P. K., Takigawa, M., Watanabe, S., Chandra, N., Ishijima, K. and Yamashita, Y.: Improved Chemical Tracer  
 3474 Simulation by MIROC4.0-based Atmospheric Chemistry-Transport Model (MIROC4-ACTM), *SOLA*, 14(0), 91–96,  
 3475 doi:10.2151/sola.2018-016, 2018.

3476 Patra, P. K., Krol, M. C., Prinn, R. G., Takigawa, M., Mühle, J., Montzka, S. A., Lal, S., Yamashita, Y., Naus, S., Chandra,  
3477 N., Weiss, R. F., Krummel, P. B., Fraser, P. J., O'Doherty, S., and Elkins, J. W.: Methyl Chloroform Continues to  
3478 Constrain the Hydroxyl (OH) Variability in the Troposphere, *J. Geophys. Res.-Atmos.*, 126, e2020JD033862,  
3479 <https://doi.org/10.1029/2020JD033862>, 2021.

3480 Paull, C. K., Brewer, P. G., Ussler, W., Peltzer, E. T., Rehder, G. and Clague, D.: An experiment demonstrating that marine  
3481 slumping is a mechanism to transfer methane from seafloor gas-hydrate deposits into the upper ocean and atmosphere,  
3482 *Geo-Mar. Lett.*, 22(4), 198–203, doi:10.1007/s00367-002-0113-y, 2002.

3483 Peacock, M., J. Audet, D. Bastviken, M.N. Futter, V. Gauci, A. Grinham, J.A. Harrison, M.S. Kent, S. Kosten, C.E.  
3484 Lovelock, A.J. Veraart, and C.D. Evans, Global importance of methane emissions from drainage ditches and canals.  
3485 *Environmental Research Letters*, 16(4): p. 044010., 2021

3486 Pekel, J.-F., Cottam, A., Gorelick, N. and Belward, A. S.: High-resolution mapping of global surface water and its  
3487 long-term changes, *Nature*, 540(7633), 418–422, doi:10.1038/nature20584, 2016.

3488 Peltola, O., Vesala, T., Gao, Y., Rätty, O., Alekseychik, P., Aurela, M., Chojnicki, B., Desai, A. R., Dolman, A. J.,  
3489 Euskirchen, E. S., Friborg, T., Göckede, M., Helbig, M., Humphreys, E., Jackson, R. B., Jocher, G., Joos, F., Klatt, J.,  
3490 Knox, S. H., Kowalska, N., Kutzbach, L., Lienert, S., Lohila, A., Mammarella, I., Nadeau, D. F., Nilsson, M. B.,  
3491 Oechel, W. C., Peichl, M., Pypker, T., Quinton, W., Rinne, J., Sachs, T., Samson, M., Schmid, H. P., Sonnentag, O.,  
3492 Wille, C., Zona, D. and Aalto, T.: Monthly gridded data product of northern wetland methane emissions based on  
3493 upscaling eddy covariance observations, *Earth Syst. Sci. Data*, 11(3), 1263–1289, doi:10.5194/essd-11-1263-2019,  
3494 2019.

3495 Peng, S. S., Piao, S. L., Bousquet, P., Ciais, P., Li, B. G., Lin, X., Tao, S., Wang, Z. P., Zhang, Y. and Zhou, F.: Inventory  
3496 of anthropogenic methane emissions in Mainland China from 1980 to 2010, *Atmospheric Chem. Phys. Discuss.*, 2016,  
3497 1–29, doi:10.5194/acp-2016-139, 2016.

3498 Peng, S., Lin, X., Thompson, R. L., Xi, Y., Liu, G., Hauglustaine, D., Lan, X., Poulter, B., Ramonet, M., Saunio, M.,  
3499 Yin, Y., Zhang, Z., Zheng, B., and Ciais, P.: Wetland emission and atmospheric sink changes explain methane growth  
3500 in 2020, *Nature*, 612, 477–482, <https://doi.org/10.1038/s41586-022-05447-w>, 2022.

3501 Pérez-Barbería, F. J.: Scaling methane emissions in ruminants and global estimates in wild populations, *Sci. Total*  
3502 *Environ.*, 579, 1572–1580, doi:10.1016/j.scitotenv.2016.11.175, 2017.

3503 Petersen, H. and Luxton, M. A comparative analysis of soil fauna populations and their role in decomposition processes.  
3504 *Oikos* 39: 287–388, [doi.org/10.2307/3544689](https://doi.org/10.2307/3544689), 1982

3505 Petrenko, V. V., Smith, A. M., Schaefer, H., Riedel, K., Brook, E., Baggenstos, D., Harth, C., Hua, Q., Buizert, C., Schilt,  
3506 A., Fain, X., Mitchell, L., Bauska, T., Orsi, A., Weiss, R. F. and Severinghaus, J. P.: Minimal geological methane  
3507 emissions during the Younger Dryas–Preboreal abrupt warming event, *Nature*, 548, 443, doi:10.1038/nature23316  
3508 <https://www.nature.com/articles/nature23316#supplementary-information>, 2017.

3509 Petrescu, A. M. R., Qiu, C., Ciais, P., Thompson, R. L., Peylin, P., McGrath, M. M., Solazzo, E., Janssens-Maenhout, G.,  
 3510 Tubiello, F. N., Bergamaschi, P., Brunner, D., Peters, G. P., Höglund-Isaksson, L., Regnier, P., Lauerwald, R.,  
 3511 Bastviken, D., Tsuruta, A., Winiwarter, W., Patra, P. P., Kuhnert, M., Oreggioni, G. D., Crippa, M., Saunio, M.,  
 3512 Perugini, L., Markkanen, T., Aalto, T., Groot Zwaftink, C. C., Yao, Y., Wilson, C. C., Conchedda, G., Günther, D.,  
 3513 Leip, A., Smith, P., Haussaire, J. M., Leppänen, A., Manning, A. J., McNorton, J., Brockmann, P., & Dolman, A. J. H.  
 3514 A. The consolidated European synthesis of CH<sub>4</sub> and N<sub>2</sub>O emissions for the European Union and United Kingdom:  
 3515 1990-2017. *Earth System Science Data*, 13(5), 2307-2362. doi:10.5194/essd-13-2307-2021, 2021.

3516 Petrescu, A. M. R., Qiu, C., McGrath, M. J., Peylin, P., Peters, G. P., Ciais, P., Thompson, R. L., Tsuruta, A., Brunner,  
 3517 D., Kuhnert, M., Matthews, B., Palmer, P. I., Tarasova, O., Regnier, P., Lauerwald, R., Bastviken, D., Höglund-  
 3518 Isaksson, L., Winiwarter, W., Etiopie, G., Aalto, T., Balsamo, G., Bastrikov, V., Berchet, A., Brockmann, P., Ciotoli,  
 3519 G., Conchedda, G., Crippa, M., Dentener, F., Groot Zwaftink, C. D., Guizzardi, D., Günther, D., Haussaire, J.-M.,  
 3520 Houweling, S., Janssens-Maenhout, G., Kouyate, M., Leip, A., Leppänen, A., Lugato, E., Maisonnier, M., Manning,  
 3521 A. J., Markkanen, T., McNorton, J., Muntean, M., Oreggioni, G. D., Patra, P. K., Perugini, L., Pison, I., Raivonen, M.  
 3522 T., Saunio, M., Segers, A. J., Smith, P., Solazzo, E., Tian, H., Tubiello, F. N., Vesala, T., van der Werf, G. R., Wilson,  
 3523 C., and Zaehle, S.: The consolidated European synthesis of CH<sub>4</sub> and N<sub>2</sub>O emissions for the European Union and United  
 3524 Kingdom: 1990–2019, *Earth Syst. Sci. Data*, 15, 1197–1268, <https://doi.org/10.5194/essd-15-1197-2023>, 2023.

3525 Phillips, N. G., Ackley, R., Crosson, E. R., Down, A., Hutrya, L. R., Brondfield, M., Karr, J. D., Zhao, K. and Jackson,  
 3526 R. B.: Mapping urban pipeline leaks: Methane leaks across Boston, *Environ. Pollut.*, 173, 1–4,  
 3527 doi:10.1016/j.envpol.2012.11.003, 2013.

3528 Pimlott, M.A., Pope, R.J., Kerridge, B.J., Latter, B.G., Knappett, D.S., Heard, D.E., Ventress, L.J., Siddans, R., Feng, W.,  
 3529 and Chipperfield, M.P.: Investigating the global OH radical distribution using steady-state approximations and satellite  
 3530 data. *Atmos. Chem. Phys.*, 22, 10467–10488, doi:10.5194/acp-22-10467-2022, 2022

3531 Pison, I., Ringeval, B., Bousquet, P., Prigent, C. and Papa, F.: Stable atmospheric methane in the 2000s: key-role of  
 3532 emissions from natural wetlands, *Atmospheric Chem. Phys. Discuss.*, 13(4), 9017–9049, doi:10.5194/acpd-13-9017-  
 3533 2013, 2013.

3534 Pitz, S. and Megonigal, J. P.: Temperate forest methane sink diminished by tree emissions, *New Phytol.*, 214(4), 1432–  
 3535 1439, doi:10.1111/nph.14559, 2017.

3536 Platt, U., Allan, W. and Lowe, D.: Hemispheric average Cl atom concentration from <sup>13</sup>C/<sup>12</sup>C ratios in atmospheric methane,  
 3537 *Atmos Chem Phys*, 4, 2393–2399, 2004.

3538 Plummer, D., Nagashima, T., Tilmes, S., Archibald, A., Chiodo, G., Fadnavis, S., Garny, H., Josse, B., Kim, J., Lamarque,  
 3539 J.-F., Morgenstern, O., Murray, L., Orbe, C., Tai, A., Chipperfield, M., Funke, B., Juckes, M., Kinnison, D., Kunze,  
 3540 M., Luo, B., Matthes, K., Newman, P. A., Pascoe, C. and Peter, T.: CCMI- 2022: a new set of Chemistry–Climate  
 3541 Model Initiative (CCMI) community simulations to update the assessment of models and support upcoming ozone

assessment activities. SPARC Newsletter 57, 22–30, 2021.

Pollard, D. F., Sherlock, V., Robinson, J., Deutscher, N. M., Connor, B. and Shiona, H.: The Total Carbon Column Observing Network site description for Lauder, New Zealand, *Earth Syst. Sci. Data*, 9(2), 977–992, doi:10.5194/essd-9-977-2017, 2017.

Portmann, F. T., Siebert, S. & Döll, P. : MIRCA2000 – Global monthly irrigated and rainfed crop areas around the year 2000: A new high-resolution data set for agricultural and hydrological modeling, *Global Biogeochemical Cycles*, 24, GB 1011, doi:10.1029/2008GB003435, 2010

Portmann, R. W., Daniel, J. S. and Ravishankara, A. R.: Stratospheric ozone depletion due to nitrous oxide: influences of other gases, *Philos. Trans. R. Soc. Lond. B Biol. Sci.*, 367(1593), 1256–1264, doi:10.1098/rstb.2011.0377, 2012.

Poulter, B., Bousquet, P., Canadell, J. G., Ciais, P., Peregon, A., Saunio, M., Arora, V. K., Beerling, D. J., Brovkin, V., Jones, C. D., Joos, F., Gedney, N., Ito, A., Kleinen, T., Koven, C. D., McDonald, K., Melton, J. R., Peng, C. H., Peng, S. S., Prigent, C., Schroeder, R., Riley, W. J., Saito, M., Spahni, R., Tian, H. Q., Taylor, L., Viovy, N., Wilton, D., Wiltshire, A., Xu, X. Y., Zhang, B. W., Zhang, Z. and Zhu, Q. A.: Global wetland contribution to 2000–2012 atmospheric methane growth rate dynamics, *Environ. Res. Lett.*, 12(9), doi:10.1088/1748-9326/aa8391, 2017.

Prairie, Y.T., J. Alm, J. Beaulieu, N. Barros, T. Battin, J. Cole, P. del Giorgio, T. DelSontro, F. Guérin, A. Harby, J. Harrison, S. Mercier-Blais, D. Serça, S. Sobek, and D. Vachon, Greenhouse Gas Emissions from Freshwater Reservoirs: What Does the Atmosphere See? *Ecosystems*, 21(5): p. 1058–1071, 2018

Prather, M. J., Holmes, C. D. and Hsu, J.: Reactive greenhouse gas scenarios: Systematic exploration of uncertainties and the role of atmospheric chemistry, *Geophys. Res. Lett.*, 39(9), L09803, doi:10.1029/2012gl051440, 2012.

Prather, M. J., Guo, H., and Zhu, X.: Deconstruction of tropospheric chemical reactivity using aircraft measurements: the Atmospheric Tomography Mission (ATom) data, *Earth Syst. Sci. Data*, 15, 3299–3349, <https://doi.org/10.5194/essd-15-3299-2023>, 2023.

Prinn, R. G., Weiss, R. F., Arduini, J., Arnold, T., DeWitt, H. L., Fraser, P. J., Ganesan, A. L., Gasore, J., Harth, C. M., Hermansen, O., Kim, J., Krummel, P. B., Li, S., Loh, Z. M., Lunder, C. R., Maione, M., Manning, A. J., Miller, B. R., Mitrevski, B., Mühle, J., O'Doherty, S., Park, S., Reimann, S., Rigby, M., Saito, T., Salameh, P. K., Schmidt, R., Simmonds, P. G., Steele, L. P., Vollmer, M. K., Wang, R. H., Yao, B., Yokouchi, Y., Young, D., and Zhou, L.: History of chemically and radiatively important atmospheric gases from the Advanced Global Atmospheric Gases Experiment (AGAGE), *Earth Syst. Sci. Data*, 10, 985–1018, <https://doi.org/10.5194/essd-10-985-2018>, 2018.

Prosperi, P., Bloise, M., Tubiello, F.N. *et al.* New estimates of greenhouse gas emissions from biomass burning and peat fires using MODIS Collection 6 burned areas. *Climatic Change* **161**, 415–432, <https://doi.org/10.1007/s10584-020-02654-0>, 2020

Purvaja, R., Ramesh, R., & Frenzel, P.: Plant-mediated methane emission from an Indian mangrove, *Global Change Biology*, 10, 1825–1834, 2004

Code de champ modifié

3575 Qin, B., Zhou, J., Elser, J.J., Gardner, W.S., Deng, J., and J.D. Brookes: Water depth underpins the relative roles and fates  
 3576 of nitrogen and phosphorus in lakes, *Environmental Science & Technology* 2020 54 (6), 3191-3198, DOI:  
 3577 10.1021/acs.est.9b05858, 2020.  
 3578 Qu, Z., Jacob, D. J., Shen, L., Lu, X., Zhang, Y., Scarpelli, T. R., Nesser, H., Sulprizio, M. P., Maasakkers, J. D., Bloom,  
 3579 A. A., Worden, J. R., Parker, R. J., and Delgado, A. L.: Global distribution of methane emissions: a comparative inverse  
 3580 analysis of observations from the TROPOMI and GOSAT satellite instruments, *Atmos. Chem. Phys.*, 21, 14159–  
 3581 14175, <https://doi.org/10.5194/acp-21-14159-2021>, 2021.  
 3582 Qu, Z., Jacob, D. J., Zhang, Y., Shen, L., Varon, D. J., Lu, X., Scarpelli, T., Bloom, A., Worden, J., and Parker, R. J.:  
 3583 Attribution of the 2020 surge in atmospheric methane by inverse analysis of GOSAT observations, *Environ. Res. Lett.*,  
 3584 17, 094003, <https://doi.org/10.1088/1748-9326/ac8754>, 2022.  
 3585 Randerson, J. T., Chen, Y., van der Werf, G. R., Rogers, B. M. and Morton, D. C.: Global burned area and biomass burning  
 3586 emissions from small fires, *J. Geophys. Res. Biogeosciences*, 117, G4, doi:10.1029/2012jg002128, 2012.  
 3587 Ramage, J.L., Kuhn, M., Virkkala, A.M., Voigt, C., Marushchak, M.E., Bastos, A., Biasi, C., Canadell, J.G., Ciais, P.,  
 3588 López-Blanco, E. Natali, S.M., et al.: The net GHG balance and budget of the permafrost region (2000-2020) from  
 3589 ecosystem flux upscaling. Preprint in ESS Open Archive. September 11, 2023. DOI:  
 3590 10.22541/essoar.169447408.86275712/v1, 2023  
 3591 Ramsden, A. E., Ganesan, A. L., Western, L. M., Rigby, M., Manning, A. J., Foulds, A., France, J. L., Barker, P., Levy,  
 3592 P., Say, D., Wisher, A., Arnold, T., Rennick, C., Stanley, K. M., Young, D., and O'Doherty, S.: Quantifying fossil fuel  
 3593 methane emissions using observations of atmospheric ethane and an uncertain emission ratio, *Atmos. Chem. Phys.*,  
 3594 22, 3911–3929, <https://doi.org/10.5194/acp-22-3911-2022>, 2022.  
 3595 Ray, N.E., Holgerson, M.A., Andersen, M.R., Bikše, J., Bortolotti, L.E., Futter, M., Kokorite, I., Law, A., McDonald, C.,  
 3596 Mesman, J.P., Peacock, M., Richardson, D.C., Arsenault, J., Bansal, S., Cawley, K., Kuhn, M., Shahabnia, A.R. and  
 3597 Smufer, F.: Spatial and temporal variability in summertime dissolved carbon dioxide and methane in temperate ponds  
 3598 and shallow lakes. *Limnol Oceanogr*, 68: 1530-1545. <https://doi.org/10.1002/lno.12362>, 2023  
 3599 Regnier P., Arndt, S., Dale, A.W., LaRowe, D.E., Mogollon, J. and Van Cappellen, P. Advances in the biogeochemical  
 3600 modeling of anaerobic oxidation of methane (AOM). *Earth Science Reviews*. 106, 105-130, 2011;  
 3601 Ren, W. E. I., Tian, H., Xu, X., Liu, M., Lu, C., Chen, G., Melillo, J., Reilly, J. and Liu, J.: Spatial and temporal patterns  
 3602 of CO<sub>2</sub> and CH<sub>4</sub> fluxes in China's croplands in response to multifactor environmental changes, *Tellus B*, 63(2), 222–  
 3603 240, doi:10.1111/j.1600-0889.2010.00522.x, 2011.  
 3604 Repeta, D. J., Ferrón, S., Sosa, O. A., Johnson, C. G., Repeta, L. D., Acker, M., DeLong, E. F. and Karl, D. M.: Marine  
 3605 methane paradox explained by bacterial degradation of dissolved organic matter, *Nat. Geosci.*, 9(12), 884–887,  
 3606 doi:10.1038/ngeo2837, 2016.

3607 Resplandy, L., Hogikyan, A., Müller, J.D., Najjar, R.G., Bange, H., W., Bianchi, D., Weber, T., Cai, W.-J., Doney, S.  
 3608 C., Fennel, K., Gehlen, M., Hauck, J., Lacroix, F., Landschützer, P., Le Quéré, C., Roobaert, A., Schwinger, J., Berthet,  
 3609 S., Bopp, L., Chau, T.T.T., Dai, M., Gruber, N., Ilyina, T., Kock, A., Manizza, M., Lachkar, Z., Laruelle, G. G., Liao,  
 3610 E., Lima, I. D., Nissen, C., Rödenbeck, C., Séférian, R., Toyama, K., Tsujino, H., and Regnier, P.: A synthesis of  
 3611 global coastal ocean greenhouse gas fluxes, *Global Biogeochemical Cycles*, 38, e2023GB007803.  
 3612 <https://doi.org/10.1029/2023GB007803>, 2024  
 3613 Riahi, K., van Vuuren, D. P., Kriegler, E., Edmonds, J., O'Neill, B. C., Fujimori, S., Bauer, N., Calvin, K., Dellink, R.,  
 3614 Fricko, O., Lutz, W., Popp, A., Cuaserna, J. C., Kc, S., Leimbach, M., Jiang, L., Kram, T., Rao, S., Emmerling, J.,  
 3615 Ebi, K., Hasegawa, T., Havlik, P., Humpenöder, F., Da Silva, L. A., Smith, S., Stehfest, E., Bosetti, V., Eom, J.,  
 3616 Gernaat, D., Masui, T., Rogelj, J., Strefler, J., Drouet, L., Krey, V., Luderer, G., Harmsen, M., Takahashi, K.,  
 3617 Baumstark, L., Doelman, J. C., Kainuma, M., Klimont, Z., Marangoni, G., Lotze-Campen, H., Obersteiner, M., Tabeau,  
 3618 A. and Tavoni, M.: The Shared Socioeconomic Pathways and their energy, land use, and greenhouse gas emissions  
 3619 implications: An overview, *Glob. Environ. Change*, 42, 153–168, doi:10.1016/j.gloenvcha.2016.05.009, 2017.  
 3620 Rice, A. L., Butenhoff, C. L., Shearer, M. J., Teama, D., Rosenstiel, T. N. and Khalil, M. A. K.: Emissions of anaerobically  
 3621 produced methane by trees, *Geophys. Res. Lett.*, 37, L03807, doi:10.1029/2009GL041565, 2010.  
 3622 Ridgwell, A. J., Marshall, S. J. and Gregson, K.: Consumption of atmospheric methane by soils: A process-based model,  
 3623 *Glob. Biogeochem. Cycles*, 13(1), 59–70, doi:10.1029/1998gb900004, 1999.  
 3624 Riedel, T. P., Wolfe, G. M., Danas, K. T., Gilman, J. B., Kuster, W. C., Bon, D. M., Vlasenko, A., Li, S. M., Williams, E.  
 3625 J., Lerner, B. M., Veres, P. R., Roberts, J. M., Holloway, J. S., Lefer, B., Brown, S. S. and Thornton, J. A.: An MCM  
 3626 modeling study of nitryl chloride (ClNO<sub>2</sub>) impacts on oxidation, ozone production and nitrogen oxide partitioning in  
 3627 polluted continental outflow, *Atmospheric Chem. Phys.*, 14(8), 3789–3800, doi:10.5194/acp-14-3789-2014, 2014.  
 3628 Rigby, M., Montzka, S. A., Prinn, R. G., White, J. W. C., Young, D., O'Doherty, S., Lunt, M. F., Ganesan, A. L., Manning,  
 3629 A. J., Simmonds, P. G., Salameh, P. K., Harth, C. M., Mühle, J., Weiss, R. F., Fraser, P. J., Steele, L. P., Krummel, P.  
 3630 B., McCulloch, A. and Park, S.: Role of atmospheric oxidation in recent methane growth, *Proc. Natl. Acad. Sci.*,  
 3631 114(21), 5373, 2017.  
 3632 Riley, W. J., Subin, Z. M., Lawrence, D. M., Swenson, S. C., Torn, M. S., Meng, L., Mahowald, N. M. and Hess, P.:  
 3633 Barriers to predicting changes in global terrestrial methane fluxes: analyses using CLM4Me, a methane  
 3634 biogeochemistry model integrated in CESM, *Biogeosciences*, 8(7), 1925–1953, doi:10.5194/bg-8-1925-2011, 2011.  
 3635 Ringeval, B., Friedlingstein, P., Koven, C., Ciais, P., de Noblet-Ducoudre, N., Decharme, B. and Cadule, P.: Climate-CH<sub>4</sub>  
 3636 feedback from wetlands and its interaction with the climate-CO<sub>2</sub> feedback, *Biogeosciences*, 8(8), 2137–2157,  
 3637 doi:10.5194/bg-8-2137-2011, 2011.  
 3638 Robison, A.L., W.M. Wollheim, B. Turek, C. Bova, C. Snay, and R.K. Varner, Spatial and temporal heterogeneity of  
 3639 methane ebullition in lowland headwater streams and the impact on sampling design, *Limnology and Oceanography*,

66(12): p. 4063-4076, 2021

Rocher-Ros, G., Stanley, E.H., Loken, L.C., Casson, N.J., Raymond, P.A., Liu, S., Amatulli, G. and Sponseller, R.A.,  
Global methane emissions from rivers and streams. *Nature*, pp.1-6.,621, 530–535, <https://doi.org/10.1038/s41586-023-06344-6>, 2023

Rosentreter, J. A., Maher, D. T., Erler, D. V., Murray, R. H. and Eyre, B. D.: Methane emissions partially offset “blue carbon” burial in mangroves, *Sci. Adv.*, 4(6), eaao4985, doi:10.1126/sciadv.aao4985, 2018.

Rosentreter, J. A., A. V Borges, B. R. Deemer, and others : Half of global methane emissions come from highly variable aquatic ecosystem sources. *Nat. Geosci.* **14**: 225–230. doi:10.1038/s41561-021-00715-2, 2021

Rosentreter, J.A., Laruelle, G.G., Bange, H.W., Bianchi, T.S., Busecke, J.J.M., Cai, W-J, Eyre, B.D., Forbrich, I., Kwon, E.Y., Mavara, T., Moosdorf, N., Van Dam, B. and Regnier, P. Coastal vegetation and estuaries are collectively a greenhouse gas sink. *Nature Climate Change*, 13, 579–587, doi: 10.1038/s41558-023-01682-9, 2023.

Rosentreter, J. A., Alcott, L., Maavara, T., Sun, X., Zhou, Y., Planavsky, N. J., and Raymond, P. A.: Revisiting the global methane cycle through expert opinion, *Earth's Future*, 12, e2023EF004234, <https://doi.org/10.1029/2023EF004234> , 2024

Rowlinson, M. J., Rap, A., Arnold, S. R., Pope, R. J., Chipperfield, M. P., McNorton, J., Forster, P., Gordon, H., Pringle, K. J., Feng, W., Kerridge, B. J., Latter, B. L., and Siddans, R.: Impact of El Niño–Southern Oscillation on the interannual variability of methane and tropospheric ozone, *Atmos. Chem. Phys.*, 19, 8669–8686, <https://doi.org/10.5194/acp-19-8669-2019>, 2019.

Ruppel, C. D., and J. D. Kessler (2017), The interaction of climate change and methane hydrates, *Rev. Geophys.*, 55, 126–168, doi:10.1002/2016RG000534, 2017

Saad, K. M., Wunch, D., Toon, G. C., Bernath, P., Boone, C., Connor, B., Deutscher, N. M., Griffith, D. W. T., Kivi, R., Notholt, J., Roehl, C., Schneider, M., Sherlock, V. and Wennberg, P. O.: Derivation of tropospheric methane from TCCON CH<sub>4</sub> and HF total column observations, *Atmospheric Meas. Technol.*, 7(9), 2907–2918, doi:10.5194/amt-7-2907-2014, 2014.

Sanderson, M. G.: Biomass of termites and their emissions of methane and carbon dioxide: A global database, *Glob. Biogeochem. Cycles*, 10(4), 543–557, doi:10.1029/96gb01893, 1996.

Sasakawa, M., Shimoyama, K., Machida, T., Tsuda, N., Suto, H., Arshinov, M., Davydov, D., Fofonov, A., Krasnov, O., Saeki, T., Koyama, Y. and Maksyutov, S.: Continuous measurements of methane from a tower network over Siberia, *Tellus B*, 62(5), 403–416, doi:10.1111/j.1600-0889.2010.00494.x, 2010.

Sasakawa, M., Machida, T., Ishijima, K., Arshinov, M., Patra, P. K., Ito, A., Aoki, S., and Petrov, V.: Temporal characteristics of CH<sub>4</sub> vertical profiles observed in the West Siberian Lowland over Surgut from 1993 to 2015 and Novosibirsk from 1997 to 2015. *Journal of Geophysical Research: Atmospheres*, 122, 11,261– 11,273. <https://doi.org/10.1002/2017JD026836>, 2017.



3673 Saunio, M., Bousquet, P., Poulter, B., Peregon, A., Ciais, P., Canadell, J. G., Dlugokencky, E. J., Etiope, G., Bastviken,  
 3674 D., Houweling, S., Janssens-Maenhout, G., Tubiello, F. N., Castaldi, S., Jackson, R. B., Alexe, M., Arora, V. K.,  
 3675 Beerling, D. J., Bergamaschi, P., Blake, D. R., Brailsford, G., Brovkin, V., Bruhwiler, L., Crevoisier, C., Crill, P.,  
 3676 Covey, K., Curry, C., Frankenberg, C., Gedney, N., Höglund-Isaksson, L., Ishizawa, M., Ito, A., Joos, F., Kim, H. S.,  
 3677 Kleinen, T., Krummel, P., Lamarque, J. F., Langenfelds, R., Locatelli, R., Machida, T., Maksyutov, S., McDonald, K.  
 3678 C., Marshall, J., Melton, J. R., Morino, I., Naik, V., O'Doherty, S., Parmentier, F. J. W., Patra, P. K., Peng, C., Peng,  
 3679 S., Peters, G. P., Pison, I., Prigent, C., Prinn, R., Ramonet, M., Riley, W. J., Saito, M., Santini, M., Schroeder, R.,  
 3680 Simpson, I. J., Spahni, R., Steele, P., Takizawa, A., Thornton, B. F., Tian, H., Tohjima, Y., Viovy, N., Voulgarakis,  
 3681 A., van Weele, M., van der Werf, G. R., Weiss, R., Wiedinmyer, C., Wilton, D. J., Wiltshire, A., Worthy, D., Wunch,  
 3682 D., Xu, X., Yoshida, Y., Zhang, B., Zhang, Z. and Zhu, Q.: The global methane budget 2000–2012, *Earth Syst Sci*  
 3683 *Data*, 8(2), 697–751, doi:10.5194/essd-8-697-2016, 2016.  
 3684 Saunio, M., Bousquet, P., Poulter, B., Peregon, A., Ciais, P., Canadell, J. G., Dlugokencky, E. J., Etiope, G., Bastviken,  
 3685 D., Houweling, S., Janssens-Maenhout, G., Tubiello, F. N., Castaldi, S., Jackson, R. B., Alexe, M., Arora, V. K.,  
 3686 Beerling, D. J., Bergamaschi, P., Blake, D. R., Brailsford, G., Bruhwiler, L., Crevoisier, C., Crill, P., Covey, K.,  
 3687 Frankenberg, C., Gedney, N., Höglund-Isaksson, L., Ishizawa, M., Ito, A., Joos, F., Kim, H. S., Kleinen, T., Krummel,  
 3688 P., Lamarque, J. F., Langenfelds, R., Locatelli, R., Machida, T., Maksyutov, S., Melton, J. R., Morino, I., Naik, V.,  
 3689 O'Doherty, S., Parmentier, F. J. W., Patra, P. K., Peng, C., Peng, S., Peters, G. P., Pison, I., Prinn, R., Ramonet, M.,  
 3690 Riley, W. J., Saito, M., Santini, M., Schroeder, R., Simpson, I. J., Spahni, R., Takizawa, A., Thornton, B. F., Tian, H.,  
 3691 Tohjima, Y., Viovy, N., Voulgarakis, A., Weiss, R., Wilton, D. J., Wiltshire, A., Worthy, D., Wunch, D., Xu, X.,  
 3692 Yoshida, Y., Zhang, B., Zhang, Z. and Zhu, Q.: Variability and quasi-decadal changes in the methane budget over the  
 3693 period 2000–2012, *Atmospheric Chem. Phys.*, 17(18), 11135–11161, doi:10.5194/acp-17-11135-2017, 2017.  
 3694 Saunio, M., Stavert, A. R., Poulter, B., Bousquet, P., Canadell, J. G., Jackson, R. B., Raymond, P. A., Dlugokencky, E.  
 3695 J., Houweling, S., Patra, P. K., Ciais, P., Arora, V. K., Bastviken, D., Bergamaschi, P., Blake, D. R., Brailsford, G.,  
 3696 Bruhwiler, L., Carlson, K. M., Carrol, M., Castaldi, S., Chandra, N., Crevoisier, C., Crill, P. M., Covey, K., Curry, C.  
 3697 L., Etiope, G., Frankenberg, C., Gedney, N., Hegglin, M. I., Höglund-Isaksson, L., Hugelius, G., Ishizawa, M., Ito, A.,  
 3698 Janssens-Maenhout, G., Jensen, K. M., Joos, F., Kleinen, T., Krummel, P. B., Langenfelds, R. L., Laruelle, G. G., Liu,  
 3699 L., Machida, T., Maksyutov, S., McDonald, K. C., McNorton, J., Miller, P. A., Melton, J. R., Morino, I., Müller, J.,  
 3700 Murguia-Flores, F., Naik, V., Niwa, Y., Noce, S., O'Doherty, S., Parker, R. J., Peng, C., Peng, S., Peters, G. P., Prigent,  
 3701 C., Prinn, R., Ramonet, M., Regnier, P., Riley, W. J., Rosentreter, J. A., Segers, A., Simpson, I. J., Shi, H., Smith, S.  
 3702 J., Steele, L. P., Thornton, B. F., Tian, H., Tohjima, Y., Tubiello, F. N., Tsuruta, A., Viovy, N., Voulgarakis, A., Weber,  
 3703 T. S., van Weele, M., van der Werf, G. R., Weiss, R. F., Worthy, D., Wunch, D., Yin, Y., Yoshida, Y., Zhang, W.,  
 3704 Zhang, Z., Zhao, Y., Zheng, B., Zhu, Q., Zhu, Q., and Zhuang, Q.: The Global Methane Budget 2000–2017, *Earth*  
 3705 *Syst. Sci. Data*, 12, 1561–1623, <https://doi.org/10.5194/essd-12-1561-2020>, 2020.

3706 Sayers, M.J., Grimm, A.G., Shuchman, R.A., Deines, A.M., Bunnell, D.B., Raymer, Z.B., Rogers, M.W., Woelmer, W.,  
 3707 Bennion, D.H., Brooks, C.N., Whitley, M.A.A., Warner, D.M., and J. Mychek-Londer: A new method to generate a  
 3708 high-resolution global distribution map of lake chlorophyll, *International Journal of Remote Sensing*, 36:7, 1942-1964,  
 3709 DOI: [10.1080/01431161.2015.1029099](https://doi.org/10.1080/01431161.2015.1029099), 2015  
 3710 Schepers, D., Guerlet, S., Butz, A., Landgraf, J., Frankenberg, C., Hasekamp, O., Blavier, J. F., Deutscher, N. M., Griffith,  
 3711 D. W. T., Hase, F., Kyro, E., Morino, I., Sherlock, V., Sussmann, R. and Aben, I.: Methane retrievals from Greenhouse  
 3712 Gases Observing Satellite (GOSAT) shortwave infrared measurements: Performance comparison of proxy and physics  
 3713 retrieval algorithms, *J. Geophys. Res. Atmospheres*, 117, D10, doi:10.1029/2012jd017549, 2012.  
 3714 Schmale O, Greinert J, Rehder G (2005) Methane emission from high-intensity marine gas seeps in the Black Sea into the  
 3715 atmosphere. *Geophys Res Lett* 32:L07609. doi:10.1029/2004GL021138, 2005  
 3716 Schmid, M., Batist, M.D., Granin, N.G., Kapitanov, V.A., McGinnis, D.F., Mizandrontsev, I.B., Obzhairov, A.I., and  
 3717 Wüest, A.. Sources and sinks of methane in Lake Baikal: A synthesis of measurements and modelling. *Limnol.*  
 3718 *Oceanogr.*, 52(5), 1824–1837. doi: 10.4319/lo.2007.52.5.1824, 2007  
 3719 Schneising, O., Buchwitz, M., Reuter, M., Vanselow, S., Bovensmann, H., and Burrows, J. P.: Remote sensing of  
 3720 methane leakage from natural gas and petroleum systems revisited, *Atmos. Chem. Phys.*, 20, 9169–9182,  
 3721 <https://doi.org/10.5194/acp-20-9169-2020>, 2020.  
 3722 Schorn, S., S. Ahmerkamp, E. Bullock, and others. : Diverse methylophilic methanogenic archaea cause high methane  
 3723 emissions from seagrass meadows. *Proc. Natl. Acad. Sci.* **119**: 1–12. doi:10.1073/pnas.2106628119, 2022  
 3724 Schuldt, K. N., Mund, J., Aalto, T., Arlyn Andrews, Apadula, F., Jgor Arduini, Arnold, S., Baier, B., Bani, L., Bartyzel,  
 3725 J., Bergamaschi, P., Biermann, T., Biraud, S. C., Pierre-Eric Blanc, Boenisch, H., Brailsford, G., Brand, W. A.,  
 3726 Brunner, D., Bui, T. P. V., ... Mirosław Zimnoch. : *Multi-laboratory compilation of atmospheric carbon dioxide data*  
 3727 *for the period 1983-2022; obspack\_ch4\_1\_GLOBALVIEWplus\_v6.0\_2023-12-01* [Data set]. NOAA Global  
 3728 Monitoring Laboratory. <https://doi.org/10.25925/20231001>, 2023  
 3729 Schuur, E.A., Abbott, B.W., Commancin, R., Ermakovich, J., Euskirchen, E., Hugelius, G., Grosse, G., Jones, M., Koven,  
 3730 C., Leshyk, V. and Lawrence, D. (2022) Permafrost and climate change: carbon cycle feedbacks from the warming  
 3731 Arctic. *Annual Review of Environment and Resources*, 47, pp.343-371. [https://doi.org/10.1146/annurev-environ-](https://doi.org/10.1146/annurev-environ-012220-011847)  
 3732 [012220-011847](https://doi.org/10.1146/annurev-environ-012220-011847), 2022  
 3733 Schwietzke, S., Sherwood, O. A., Bruhwiler, L. M. P., Miller, J. B., Etiope, G., Dlugokencky, E. J., Michel, S. E., Arling,  
 3734 V. A., Vaughn, B. H., White, J. W. C. and Tans, P. P.: Upward revision of global fossil fuel methane emissions based  
 3735 on isotope database, *Nature*, 538(7623), 88–91, doi:10.1038/nature19797, 2016.  
 3736 Segers, A., Steinke, T., and Houweling, S.: Description of the CH<sub>4</sub> Inversion Production Chain, CAMS (Copernicus  
 3737 Atmospheric Monitoring Service) Report.. [online] Available from:  
 3738 [https://atmosphere.copernicus.eu/sites/default/files/2022-10/CAMS255\\_2021SC1\\_D55.5.2.1-](https://atmosphere.copernicus.eu/sites/default/files/2022-10/CAMS255_2021SC1_D55.5.2.1-)

2021CH4\_202206\_production\_chain\_CH4\_v1.pdf (Accessed 1 février 2024), 2022.

Shaw, J. T., Allen, G., Barker, P., Pitt, J. R., Pasternak, D., Bauguitte, S. J.-B., Lee, J., Boewer, K. N., Daly, M. C., Lunt, M. F., Ganesan, A. L., Vaughan, A. R., Chibesakunda, F., Lambakasa, M., Fisher, R. E., France, J. L., Lowry, D., Palmer, P. I., Metzger, S., Parker, R. J., Gedney, N., Bateson, P., Cain, M., Lorente, A., Borsdorff, T., and Nisbet, E. G.: Large methane emission fluxes observed from tropical wetlands in Zambia, *Global Biogeochem. Cy.*, 36, e2021GB007261, <https://doi.org/10.1029/2021GB007261>, 2022.

Shen, L., Gautam, R., Omara, M., Zavala-Araiza, D., Maasakkers, J. D., Scarpelli, T. R., Lorente, A., Lyon, D., Sheng, J., Varon, D. J., Nesser, H., Qu, Z., Lu, X., Sulprizio, M. P., Hamburg, S. P., and Jacob, D. J.: Satellite quantification of oil and natural gas methane emissions in the US and Canada including contributions from individual basins, *Atmos. Chem. Phys.*, 22, 11203–11215, <https://doi.org/10.5194/acp-22-11203-2022>, 2022.

Shen, L., Jacob, D.J., Gautam, R. et al. National quantifications of methane emissions from fuel exploitation using high resolution inversions of satellite observations. *Nat Commun* 14, 4948 , <https://doi.org/10.1038/s41467-023-40671-6>, 2023

Sherwen, T., Schmidt, J. A., Evans, M. J., Carpenter, L. J., Großmann, K., Eastham, S. D., Jacob, D. J., Dix, B., Koenig, T. K., Sinreich, R., Ortega, I., Volkamer, R., Saiz-Lopez, A., Prados-Roman, C., Mahajan, A. S., and Ordóñez, C.: Global impacts of tropospheric halogens (Cl, Br, I) on oxidants and composition in GEOS-Chem, *Atmos. Chem. Phys.*, 16, 12239–12271, <https://doi.org/10.5194/acp-16-12239-2016>, 2016.

Sherwin, E. D., Rutherford, J. S., Zhang, Z., Chen, Y., Wetherley, E. B., Yakovlev, P. V., Berman, E. S. F., Jones, B. B., Cusworth, D. H., Thorpe, A. K., Ayasse, A. K., Duren, R. M., and Brandt, A. R.: US oil and gas system emissions from nearly one million aerial site measurements, *Nature*, 627(8003), 328–334, doi:10.1038/s41586-024-07117-5, 2024

Shindell, D, Sadavarte, P, Aben, I, Bredariol, TdO, Dreyfus, G, Höglund-Isaksson, L, Poulter, B, Sauniois, M, Schmidt, GA, Szopa, S, Rentz, K, Parsons, L, Qu, Z, Faluvegi, G and Maasakkers, JD. : The methane imperative, *Front Sci*, 2:1349770, doi: 10.3389/fsci.2024.1349770, 2024

Shindell, D., Kuylenstierna, J. C. I., Vignati, E., van Dingenen, R., Amann, M., Klimont, Z., Anenberg, S. C., Muller, N., Janssens-Maenhout, G., Raes, F., Schwartz, J., Faluvegi, G., Pozzoli, L., Kupiainen, K., Höglund-Isaksson, L., Emberson, L., Streets, D., Ramanathan, V., Hicks, K., Oanh, N. T. K., Milly, G., Williams, M., Demkine, V. and Fowler, D.: Simultaneously Mitigating Near-Term Climate Change and Improving Human Health and Food Security, *Science*, 335(6065), 183–189, doi:10.1126/science.1210026, 2012.

Shorter, J. H., Mcmanus, J. B., Kolb, C. E., Allwine, E. J., Lamb, B. K., Mosher, B. W., Harriss, R. C., Partchatka, U., Fischer, H., Harris, G. W., Crutzen, P. J. and Karbach, H.-J.: Methane emission measurements in urban areas in Eastern Germany, *J. Atmospheric Chem.*, 124(2), 121–140, 1996.

Shu, S., Jain, A.K. and Khesghi, H.S.: Investigating Wetland and Nonwetland Soil Methane Emissions and Sinks Across

Code de champ modifié

the Contiguous United States Using a Land Surface Model. *Global Biogeochem. Cycles*, 34: e2019GB006251. <https://doi-org.insu.bib.cnrs.fr/10.1029/2019GB006251>, 2020

Simpson, I. J., Thurtell, G. W., Kidd, G. E., Lin, M., Demetriades-Shah, T. H., Flitcroft, I. D., Kanemasu, E. T., Nie, D., Bronson, K. F. and Neue, H. U.: Tunable diode laser measurements of methane fluxes from an irrigated rice paddy field in the Philippines, *J. Geophys. Res. Atmospheres*, 100(D4), 7283–7290, doi:10.1029/94jd03326, 1995.

Simpson, I. J., Sulbaek Andersen, M. P., Meinardi, S., Bruhwiler, L., Blake, N. J., Helmig, D., Rowland, F. S. and Blake, D. R.: Long-term decline of global atmospheric ethane concentrations and implications for methane, *Nature*, 488(7412), 490–494, doi:10.1038/nature11342, 2012.

Smith I.R., Grasby S.E., Lane L.S.: An investigation of gas seeps and aquatic chemistry in Fisherman Lake, southwest Northwest Territories. Geological Survey of Canada, Current Research 2005-A3, 8 p., 2005

Solomon EA, Kastner M, MacDonald IR, Leifer I: Considerable methane fluxes to the atmosphere from hydrocarbon seeps in the Gulf of Mexico. *Nat Geosci* 2:561–565, 2009

Spahni, R., Wania, R., Neef, L., van Weele, M., Pison, I., Bousquet, P., Frankenberg, C., Foster, P. N., Joos, F., Prentice, I. C. and van Velthoven, P.: Constraining global methane emissions and uptake by ecosystems, *Biogeosciences*, 8(6), 1643–1665, doi:10.5194/bg-8-1643-2011, 2011.

Stanley, E. H., Casson, N. J., Christel, S. T., Crawford, J. T., Loken, L. C. and Oliver, S. K.: The ecology of methane in streams and rivers: patterns, controls, and global significance, *Ecol. Monogr.*, doi:10.1890/15-1027, 2016.

Stanley, K. M., Grant, A., O'Doherty, S., Young, D., Manning, A. J., Stavert, A. R., Spain, T. G., Salameh, P. K., Harth, C. M., Simmonds, P. G., Sturges, W. T., Oram, D. E. and Derwent, R. G.: Greenhouse gas measurements from a UK network of tall towers: technical description and first results, *Atmospheric Meas. Tech.*, 11(3), 1437–1458, doi:10.5194/amt-11-1437-2018, 2018.

Stanley, E. H., Loken, L. C., Casson, N. J., Oliver, S. K., Sponseller, R. A., Wallin, M. B., Zhang, L., and Rocher-Ros, G.: GRiMeDB: the Global River Methane Database of concentrations and fluxes, *Earth Syst. Sci. Data*, 15, 2879–2926, <https://doi.org/10.5194/essd-15-2879-2023>, 2023.

Stavert, A. R., Sauniois, M., Canadell, J. G., Poulter, B., Jackson, R. B., Regnier, P., Lauerwald, R., Raymond, P. A., Allen, G. H., Patra, P. K., Bergamaschi, P., Bousquet, P., Chandra, N., Ciais, P., Gustafson, A., Ishizawa, M., Ito, A., Kleinen, T., Maksyutov, S., Joe McNorton, Joe R. Melton, Jurek Müller, Yosuke Niwa, Shushi Peng, William J. Riley, Arjo Segers, Hanqin Tian, Aki Tsuruta, Yi Yin, Zhen Zhang, Bo Zheng, Zhuang, Q. Regional trends and drivers of the global methane budget. *Global Change Biology*, 28, 182–200. <https://doi.org/10.1111/gcb.15901>, 2021

Steele, L. P., Fraser, P. J., Rasmussen, R. A., Khalil, M. A. K., Conway, T. J., Crawford, A. J., Gammon, R. H., Masarie, K. A. and Thoning, K. W.: The global distribution of methane in the troposphere, *J. Atmospheric Chem.*, 5, 125–171, 1987.

3805 Stevenson, D. S., Zhao, A., Naik, V., O'Connor, F. M., Tilmes, S., Zeng, G., Murray, L. T., Collins, W. J., Griffiths, P. T.,  
3806 Shim, S., Horowitz, L. W., Sentman, L. T., and Emmons, L.: Trends in global tropospheric hydroxyl radical and  
3807 methane lifetime since 1850 from AerChemMIP, *Atmos. Chem. Phys.*, 20, 12905–12920, [https://doi.org/10.5194/acp-](https://doi.org/10.5194/acp-20-12905-2020)  
3808 20-12905-2020, 2020.

3809 Stevenson, D. S., Derwent, R. G., Wild, O., and Collins, W. J.: COVID-19 lockdown emission reductions have the  
3810 potential to explain over half of the coincident increase in global atmospheric methane, *Atmos. Chem. Phys.*, 22,  
3811 14243–14252, <https://doi.org/10.5194/acp-22-14243-2022>, 2022.

3812 Stocker, B. D., Spahni, R. and Joos, F.: DYPTOP: a cost-efficient TOPMODEL implementation to simulate sub-grid  
3813 spatio-temporal dynamics of global wetlands and peatlands, *Geosci. Model Dev.*, 7(6), 3089–3110, doi:10.5194/gmd-  
3814 7-3089-2014, 2014.

3815 Strauss, J., Abbott, B.W., Hugelius, G., Schuur, E., Treat, C., Fuchs, M., Schädel, C., Ulrich, M., Turetsky, M., Keuschnig,  
3816 M. and Biasi, C. (2021) Chapter 9. Permafrost. In *FAO Recarbonizing global soils—A technical manual of*  
3817 *recommended management practices: Volume 2—Hot spots and bright spots of soil organic carbon*, p.130, 2021

3818 Storde, S. A., Wang, J. S., Manyin, M., Duncan, B., Hossaini, R., Keller, C. A., Michel, S. E., and White, J. W. C.: Strong  
3819 sensitivity of the isotopic composition of methane to the plausible range of tropospheric chlorine, *Atmos. Chem. Phys.*,  
3820 20, 8405–8419, <https://doi.org/10.5194/acp-20-8405-2020>, 2020.

3821 Sugimoto, A., Inoue, T., Kitibutr, N., Abe, T: Methane oxidation by termite mounds estimate by the carbon isotope  
3822 composition of methane. *Glob. Biogeochem. Cy.* 12, 595-605. 1998.

3823 Sweeney, C., Karion, A., Wolter, S., Newberger, T., Guenther, D., Higgs, J. A., Andrews, A. E., Lang, P. M., Neff, D.,  
3824 Dlugokencky, E., Miller, J. B., Montzka, S. A., Miller, B. R., Masarie, K. A., Biraud, S. C., Novelli, P. C., Crotwell,  
3825 M., Crotwell, A. M., Thoning, K. and Tans, P. P.: Seasonal climatology of CO<sub>2</sub> across North America from aircraft  
3826 measurements in the NOAA/ESRL Global Greenhouse Gas Reference Network, *J. Geophys. Res. Atmospheres*,  
3827 120(10), 5155–5190, doi:10.1002/2014jd022591, 2015.

3828 Szopa, S., V. Naik, B. Adhikary, P. Artaxo, T. Bernsten, W.D. Collins, S. Fuzzi, L. Gallardo, A. Kiendler-Scharr, Z.  
3829 Klimont, H. Liao, N. Unger, and P. Zanis: Short-Lived Climate Forcers. In *Climate Change 2021: The Physical Science*  
3830 *Basis. Contribution of Working Group I to the Sixth Assessment Report of the Intergovernmental Panel on Climate*  
3831 *Change* [Masson-Delmotte, V., P. Zhai, A. Pirani, S.L. Connors, C. Péan, S. Berger, N. Caud, Y. Chen, L. Goldfarb,  
3832 M.I. Gomis, M. Huang, K. Leitzell, E. Lonnoy, J.B.R. Matthews, T.K. Maycock, T. Waterfield, O. Yelekçi, R. Yu,  
3833 and B. Zhou (eds.)]. Cambridge University Press, Cambridge, United Kingdom and New York, NY, USA, pp. 817–  
3834 922, doi:10.1017/9781009157896.008., 2021Tan, Z. and Zhuang, Q.: Methane emissions from pan-Arctic lakes during  
3835 the 21st century: An analysis with process-based models of lake evolution and biogeochemistry, *J. Geophys. Res.*  
3836 *Biogeosciences*, 120(12), 2641–2653, doi:10.1002/2015JG003184, 2015.

3837 Tans, P. and Zwellberg, C.: 17th WMO/IAEA Meeting on Carbon Dioxide, Other Greenhouse Gases and Related Tracers

Measurement Techniques (GGMT-2013), GAW Report, WMO, Geneva. [online] Available from: [https://library.wmo.int/index.php?lvl=notice\\_display&id=16373#.XnpBPW7jIq8](https://library.wmo.int/index.php?lvl=notice_display&id=16373#.XnpBPW7jIq8), 2014.

Taranu, Z.E., I. Gregory-Eaves, P.R. Leavitt, L. Bunting, T. Buchaca, J. Catalan, I. Domaizon, P. Guilizzoni, A. Lami, S. McGowan, H. Moorhouse, G. Morabito, F.R. Pick, M.A. Stevenson, P.L. Thompson, and R.D. Vinebrooke: Acceleration of cyanobacterial dominance in north temperate-subarctic lakes during the Anthropocene. *Ecology Letters*, 18(4): p. 375-384., 2015

Taylor, P. G., Bilinski, T. M., Fancher, H. R. F., Cleveland, C. C., Nemergut, D. R., Weintraub, S. R., Wieder, W. R. and Townsend, A. R.: Palm oil wastewater methane emissions and bioenergy potential, *Nat. Clim. Change*, 4(3), 151–152, doi:10.1038/nclimate2154, 2014.

le Texier, H., Solomon, S. and Garcia, R. R.: The role of molecular hydrogen and methane oxidation in the water vapour budget of the stratosphere, *Q. J. R. Meteorol. Soc.*, 114(480), 281–295, doi:10.1002/qj.49711448002, 1988.

Thanverdas, J., Saunois, M., Berchet, A., Pison, I., Vaughn, B. H., Michel, S. E., and Bousquet, P.: Variational inverse modeling within the Community Inversion Framework v1.1 to assimilate  $\delta^{13}\text{C}(\text{CH}_4)$  and  $\text{CH}_4$ : a case study with model LMDz-SACS, *Geosci. Model Dev.*, 15, 4831–4851, <https://doi.org/10.5194/gmd-15-4831-2022>, 2022a.

Thanverdas, J., Saunois, M., Pison, I., Hauglustaine, D., Berchet, A., Baier, B., Sweeney, C., and Bousquet, P.: How do  $\text{Cl}$  concentrations matter for the simulation of  $\text{CH}_4$  and  $\delta^{13}\text{C}(\text{CH}_4)$  and estimation of the  $\text{CH}_4$  budget through atmospheric inversions?, *Atmos. Chem. Phys.*, 22, 15489–15508, <https://doi.org/10.5194/acp-22-15489-2022>, 2022b.

Thanverdas, J., Saunois, M., Berchet, A., Pison, I., and Bousquet, P.: Investigation of the renewed methane growth post-2007 with high-resolution 3-D variational inverse modeling and isotopic constraints, *Atmos. Chem. Phys.*, 24, 2129–2167, <https://doi.org/10.5194/acp-24-2129-2024>, 2024.

Thompson, R. L., Montzka, S. A., Vollmer, M. K., Arduini, J., Crotwell, M., Krummel, P. B., Lunder, C., Mühle, J., O'Doherty, S., Prinn, R. G., Reimann, S., Vimont, I., Wang, H., Weiss, R. F., and Young, D.: Estimation of the atmospheric hydroxyl radical oxidative capacity using multiple hydrofluorocarbons (HFCs), *Atmos. Chem. Phys.*, 24, 1415–1427, <https://doi.org/10.5194/acp-24-1415-2024>, 2024.

Thoning, K. W., Tans, P. P. and Komhyr, W. D.: Atmospheric carbon dioxide at Mauna Loa Observatory. 2. Analysis of the NOAA GMCC data, 1974,1985, *J. Geophys. Res.*, 94(D6), 8549–8565, 1989.

Thorneloe, S. A., Barlaz, M. A., Peer, R., Huff, L. C., Davis, L. and Mangino, J.: Waste management, in *Atmospheric Methane: Its Role in the Global Environment*, edited by M. Khalil, pp. 234–262, Springer-Verlag, New York., 2000.

Thornton, B. F., Prytherch, J., Andersson, K., Brooks, I. M., Salisbury, D., Tjernström, M. and Crill, P. M.: Shipborne eddy covariance observations of methane fluxes constrain Arctic sea emissions, *Sci. Adv.*, 6(5), eaay7934, doi:10.1126/sciadv.aay7934, 2020.

Thornton B.F., Etiope G., Schwietzke S., Milkov A.V., Klusman R.W., Judd A., Oehler D.Z.: Conflicting estimates of natural geologic methane emissions. *Elem. Sci. Anth.*, 9, 1, doi:<https://doi.org/10.1525/elementa.2021.00031>, 2021

3871 Thornton, J. A., Kercher, J. P., Riedel, T. P., Wagner, N. L., Cozic, J., Holloway, J. S., Dubé, W. P., Wolfe, G. M., Quinn,  
3872 P. K., Middlebrook, A. M., Alexander, B. and Brown, S. S.: A large atomic chlorine source inferred from mid-  
3873 continental reactive nitrogen chemistry, *Nature*, 464(7286), 271–274, doi:10.1038/nature08905, 2010.

3874 Thorpe, A. K., Kort, E. A., Cusworth, D. H., Ayasse, A. K., Bue, B. D., Yadav, V., Thompson, D. R., Frankenberg, C.,  
3875 Hermer, J., Falk, M., Green, R. O., Miller, C. E., and Duren, R. M.: Methane emissions decline from reduced oil,  
3876 natural gas, and refinery production during COVID-19, *Environmental Research Communications*, 5, 021006, 2023

3877 Tian, H., Xu, X., Liu, M., Ren, W., Zhang, C., Chen, G. and Lu, C.: Spatial and temporal patterns of CH<sub>4</sub> and N<sub>2</sub>O fluxes  
3878 in terrestrial ecosystems of North America during 1979–2008: application of a global biogeochemistry model,  
3879 *Biogeosciences*, 7(9), 2673–2694, doi:10.5194/bg-7-2673-2010, 2010.

3880 Tian, H., Xu, X., Lu, C., Liu, M., Ren, W., Chen, G., Melillo, J. and Liu, J.: Net exchanges of CO<sub>2</sub>, CH<sub>4</sub>, and N<sub>2</sub>O between  
3881 China's terrestrial ecosystems and the atmosphere and their contributions to global climate warming, *J. Geophys. Res.*  
3882 *Biogeosciences*, 116, G2, doi:10.1029/2010jg001393, 2011.

3883 Tian, H., Chen, G., Lu, C., Xu, X., Ren, W., Zhang, B., Banger, K., Tao, B., Pan, S., Liu, M., Zhang, C., Bruhwiler, L.  
3884 and Wofsy, S.: Global methane and nitrous oxide emissions from terrestrial ecosystems due to multiple environmental  
3885 changes, *Ecosyst. Health Sustain.*, 1(1), 1–20, doi:10.1890/ehs14-0015.1, 2015.

3886 Tian, H., Lu, C., Ciais, P., Michalak, A. M., Canadell, J. G., Saikawa, E., Huntzinger, D. N., Gurney, K. R., Sitch, S.,  
3887 Zhang, B., Yang, J., Bousquet, P., Bruhwiler, L., Chen, G., Dlugokencky, E., Friedlingstein, P., Melillo, J., Pan, S.,  
3888 Poulter, B., Prinn, R., Saunio, M., Schwalm, C. R. and Wofsy, S. C.: The terrestrial biosphere as a net source of  
3889 greenhouse gases to the atmosphere, *Nature*, 531(7593), 225–228, doi:10.1038/nature16946, 2016.

3890 Tian, H., Xu, R., Canadell, J. G., Thompson, R. L., Winiwarter, W., Suntharalingam, P., Davidson, E. A., Ciais, P.,  
3891 Jackson, R. B., Janssens-Maenhout, G., Prather, M. J., Regnier, P., Pan, N., Pan, S., Peters, G. P., Shi, H., Tubiello, F.  
3892 N., Zaehle, S., Zhou, F., Arneeth, A., Battaglia, G., Berthet, S., Bopp, L., Bouwman, A. F., Buitenhuis, E. T., Chang,  
3893 J., Chipperfield, M. P., Dangal, S. R. S., Dlugokencky, E., Elkins, J. W., Eyre, B. D., Fu, B., Hall, B., Ito, A., Joos, F.,  
3894 Krummel, P. B., Landolfi, A., Laruelle, G. G., Lauerwald, R., Li, W., Lienert, S., Maavara, T., MacLeod, M., Millet,  
3895 D. B., Olin, S., Patra, P. K., Prinn, R. G., Raymond, P. A., Ruiz, D. J., van der Werf, G. R., Vuichard, N., Wang, J.,  
3896 Weiss, R. F., Wells, K. C., Wilson, C., Yang, J., and Yao, Y.: A comprehensive quantification of global nitrous oxide  
3897 sources and sinks, *Nature*, 586, 248–256, <https://doi.org/10.1038/s41586-020-2780-0>, 2020.

3898 Tian, H., Yao, Y., Li, Y., Shi, H., Pan, S., Najjar, R. G., et al. (2023). Increased terrestrial carbon export and CO<sub>2</sub> evasion  
3899 from global inland waters since the preindustrial era. *Global Biogeochemical Cycles*, 37, e2023GB007776.  
3900 <https://doi.org/10.1029/2023GB007776>, 2023

3901 Tibrewal, K., Ciais, P., Saunio, M., Martinez, A., Lin, X., Thanwerdas, J., Deng, Z., Chevallier, F., Giron, C., Albergel,  
3902 C., Tanaka, K., Patra, P., Tsuruta, A., Zheng, B., Belikov, D., Niwa, Y., Janardanan, R., Maksyutov, S., Segers, A.,  
3903 Tzompa-Sosa, Z. A., Bousquet, P., and Sciare, J.: Assessment of methane emissions from oil, gas and coal sectors

across inventories and atmospheric inversions, *Commun Earth Environ* 5, 26, <https://doi.org/10.1038/s43247-023-01190-w>, 2024

Tiwari, Y. K. and Kumar, K. R.: GHG observation programs in India, *Asian GAWgreenhouse Gases 3 Korea Meteorol. Adm. Chungnam South Korea*, 2012.

Tsuruta, A., Aalto, T., Backman, L., Hakkarainen, J., Laan-Luijkx, I. T. van der, Krol, M. C., Spahni, R., Houweling, S., Laine, M., Dlugokencky, E., Gomez-Pelaez, A. J., Schoot, M. van der, Langenfelds, R., Ellul, R., Arduini, J., Apadula, F., Gerbig, C., Feist, D. G., Kivi, R., Yoshida, Y. and Peters, W.: Global methane emission estimates for 2000–2012 from CarbonTracker Europe-CH<sub>4</sub> v1.0, *Geosci. Model Dev.*, 10(3), 1261–1289, doi:10.5194/gmd-10-1261-2017, 2017.

Tsuruta, A.; Kivimäki, E.; Lindqvist, H.; Karppinen, T.; Backman, L.; Hakkarainen, J.; Schneising, O.; Buchwitz, M.; Lan, X.; Kivi, R.; et al. CH<sub>4</sub> Fluxes Derived from Assimilation of TROPOMI XCH<sub>4</sub> in CarbonTracker Europe-CH<sub>4</sub>: Evaluation of Seasonality and Spatial Distribution in the Northern High Latitudes. *Remote Sens.* 2023, 15, 1620. <https://doi.org/10.3390/rs15061620>, 2023

Tubiello, F. N.: Greenhouse Gas Emissions Due to Agriculture, in *Elsevier Encyclopedia of Food Systems.*, 2019.

Tubiello, F. N., Salvatore, M., Rossi, S., Ferrara, A., Fitton, N. and Smith, P.: The FAOSTAT database of greenhouse gas emissions from agriculture, *Environ. Res. Lett.*, 8(1), 015009, doi:10.1088/1748-9326/8/1/015009, 2013.

Tubiello, F. N., Karl, K., Flammini, A., Gütschow, J., Obli-Laryea, G., Conchedda, G., Pan, X., Qi, S. Y., Halldórudóttir Heiðarsdóttir, H., Wanner, N., Quadrelli, R., Rocha Souza, L., Benoit, P., Hayek, M., Sandalow, D., Mencos Contreras, E., Rosenzweig, C., Rosero Moncayo, J., Conforti, P., and Torero, M.: Pre- and post-production processes increasingly dominate greenhouse gas emissions from agri-food systems, *Earth Syst. Sci. Data*, 14, 1795–1809, <https://doi.org/10.5194/essd-14-1795-2022>, 2022.

Turetsky, M. R., Kotowska, A., Bubier, J., Dise, N. B., Crill, P., Hornibrook, E. R. C., Minkinen, K., Moore, T. R., Myers-Smith, I. H., Nykänen, H., Olefeldt, D., Rinne, J., Saarnio, S., Shurpali, N., Tuittila, E.-S., Waddington, J. M., White, J. R., Wickland, K. P. and Wilkening, M.: A synthesis of methane emissions from 71 northern, temperate, and subtropical wetlands, *Glob. Change Biol.*, 20(7), 2183–2197, doi:10.1111/gcb.12580, 2014.

Turetsky, M. R., Abbott, B. W., Jones, M. C., Anthony, K. W., Olefeldt, D., Schuur, E. A. G., et al.: Carbon release through abrupt permafrost thaw. *Nature Geoscience*, 13(2), 138–143. <https://doi.org/10.1038/s41561-019-0526-0>, 2020

Turner, A. J., Fung, I., Naik, V., Horowitz, L. W. and Cohen, R. C.: Modulation of hydroxyl variability by ENSO in the absence of external forcing, *Proc. Natl. Acad. Sci.*, 115(36), 8931–8936, doi:10.1073/pnas.1807532115, 2018.

Turner, A. J., Frankenberg, C. and Kort, E. A.: Interpreting contemporary trends in atmospheric methane, *Proc. Natl. Acad. Sci.*, 116(8), 2805, doi:10.1073/pnas.1814297116, 2019.

UNEP, United Nations Environment Programme and Climate and Clean Air Coalition. Global Methane Assessment:



3937 Benefits and Costs of Mitigating Methane Emissions. Nairobi: United Nations Environment Programme., 2021

3938 UNEP, United Nations Environment Programme/Climate and Clean Air Coalition. Global Methane Assessment: 2030

3939 Baseline Report. Nairobi, 2022

3940 USEPA: Greenhouse Gas Emissions Estimation Methodologies for Biogenic Emissions from Selected Source Categories:

3941 Solid Waste Disposal Wastewater Treatment Ethanol Fermentation, Measurement Policy Group, US EPA. [online]

3942 Available from: [https://www3.epa.gov/ttnchie1/efpac/ghg/GHG\\_Biogenic\\_Report\\_draft\\_Dec1410.pdf](https://www3.epa.gov/ttnchie1/efpac/ghg/GHG_Biogenic_Report_draft_Dec1410.pdf) (Accessed 11

3943 March 2020a), 2010a.

3944 USEPA: Office of Atmospheric Programs (6207J), Methane and Nitrous Oxide Emissions From Natural Sources, U.S.

3945 Environmental Protection Agency, EPA 430-R-10-001. Available online at <http://nepis.epa.gov/>, Washington, DC

3946 20460., 2010b.

3947 USEPA: Draft: Global Anthropogenic Non-CO<sub>2</sub> Greenhouse Gas Emissions: 1990-2030. EPA 430-R-03-002, United

3948 States Environmental Protection Agency, Washington D.C., 2011.

3949 USEPA: Global Anthropogenic Non-CO<sub>2</sub> Greenhouse Gas Emissions 1990-2030, EPA 430-R-12-006, US Environmental

3950 Protection Agency, Washington DC., 2012.

3951 USEPA: Draft Inventory of U.S. Greenhouse gas Emissions and Sinks: 1990-2014. EPA 430-R-16-002. February 2016.

3952 U.S. Environmental protection Agency, Washington, DC, USA., 2016.

3953 USEPA: Global Non-CO<sub>2</sub> Greenhouse Gas Emission Projections & Mitigation Potential: 2015-2050, EPA-430-R-19-010,

3954 U.S. Environmental protection Agency, Washington, DC, USA., 2019

3955 Valentine, D. W., Holland, E. A. and Schimel, D. S.: Ecosystem and physiological controls over methane production in

3956 northern wetlands, *J. Geophys. Res.*, 99(D1), 1563–1571, 1994.

3957 Vardag, S. N., Hammer, S., O'Doherty, S., Spain, T. G., Wastine, B., Jordan, A. and Levin, I.: Comparisons of continuous

3958 atmospheric CH<sub>4</sub>, CO<sub>2</sub> and N<sub>2</sub>O measurements &ndash; results from a travelling instrument campaign at Mace Head,

3959 *Atmospheric Chem. Phys.*, 14(16), 8403–8418, doi:10.5194/acp-14-8403-2014, 2014.

3960 Varon, D. J., Jacob, D. J., Hmiel, B., Gautam, R., Lyon, D. R., Omara, M., Sulprizio, M., Shen, L., Pendergrass, D., Nesser,

3961 H., Qu, Z., Barkley, Z. R., Miles, N. L., Richardson, S. J., Davis, K. J., Pandey, S., Lu, X., Lorente, A., Borsdorff, T.,

3962 Maasackers, J. D., and Aben, I.: Continuous weekly monitoring of methane emissions from the Permian Basin by

3963 inversion of TROPOMI satellite observations, *Atmos. Chem. Phys.*, 23, 7503–7520, [https://doi.org/10.5194/acp-23-](https://doi.org/10.5194/acp-23-7503-2023)

3964 7503-2023, 2023.

3965 VODCA2GPP – a new, global, long-term (1988–2020) gross primary production dataset from microwave remote sensing,

3966 *Earth Syst. Sci. Data*, 14, 1063–1085, <https://doi.org/10.5194/essd-14-1063-2022>, 2022.

3967 Voulgarakis, A., Naik, V., Lamarque, J. F., Shindell, D. T., Young, P. J., Prather, M. J., Wild, O., Field, R. D., Bergmann,

3968 D., Cameron-Smith, P., Cionni, I., Collins, W. J., Dalsøren, S. B., Doherty, R. M., Eyring, V., Faluvegi, G., Folberth,

3969 G. A., Horowitz, L. W., Josse, B., MacKenzie, I. A., Nagashima, T., Plummer, D. A., Righi, M., Rumbold, S. T.,

3970 Stevenson, D. S., Strode, S. A., Sudo, K., Szopa, S. and Zeng, G.: Analysis of present day and future OH and methane  
 3971 lifetime in the ACCMIP simulations, *Atmospheric Chem. Phys.*, 13(5), 2563–2587, doi:10.5194/acp-13-2563-2013,  
 3972 2013.  
 3973 Voulgarakis, A., Marlier, M. E., Faluvegi, G., Shindell, D. T., Tsigaridis, K. and Mangeon, S.: Interannual variability of  
 3974 tropospheric trace gases and aerosols: The role of biomass burning emissions, *J. Geophys. Res. Atmospheres*, 120(14),  
 3975 7157–7173, doi:10.1002/2014jd022926, 2015.  
 3976 Wallmann, K., Pinero, E., Burwicz, E., Haeckel, M., Hensen, C., Dale, A. and Ruepke, L.: The Global Inventory of  
 3977 Methane Hydrate in Marine Sediments: A Theoretical Approach, *Energies*, 5(7), 2449, 2012.  
 3978 Walter Anthony, K.M., Anthony, P., Grosse, G. and Chanton, J.: Geologic methane seeps along boundaries of Arctic  
 3979 permafrost thaw and melting glaciers. *Nature Geoscience*, 5(6), pp.419–426., DOI: 10.1038/ngeo1480, 2012  
 3980 Wang, F., Maksyutov, S., Tsuruta, A., Janardanan, R., Ito, A., Sasakawa, M., Machida, T., Morino, I., Yoshida, Y., Kaiser,  
 3981 J. W., Janssens-Maenhout, G., Dlugokencky, E. J., Mammarella, I., Lavric, J. V. and Matsunaga, T.: Methane Emission  
 3982 Estimates by the Global High-Resolution Inverse Model Using National Inventories, *Remote Sens.*, 11(21), 2489,  
 3983 doi:10.3390/rs11212489, 2019a.  
 3984 Wang, G., X. Xia, S. Liu, L. Zhang, S. Zhang, J. Wang, N. Xi, and Q. Zhang, Intense methane ebullition from urban inland  
 3985 waters and its significant contribution to greenhouse gas emissions. *Water Research*, 189: p. 116654, 2021a  
 3986 Wang, X., Jacob, D. J., Eastham, S. D., Sulprizio, M. P., Zhu, L., Chen, Q., Alexander, B., Sherwen, T., Evans, M. J., Lee,  
 3987 B. H., Haskins, J. D., Lopez-Hilfiker, F. D., Thornton, J. A., Huey, G. L. and Liao, H.: The role of chlorine in global  
 3988 tropospheric chemistry, *Atmospheric Chem. Phys.*, 19(6), 3981–4003, doi:10.5194/acp-19-3981-2019, 2019b.  
 3989 Wang, X., Jacob, D. J., Downs, W., Zhai, S., Zhu, L., Shah, V., Holmes, C. D., Sherwen, T., Alexander, B., Evans, M. J.,  
 3990 Eastham, S. D., Neuman, J. A., Veres, P. R., Koenig, T. K., Volkamer, R., Huey, L. G., Bannan, T. J., Percival, C. J.,  
 3991 Lee, B. H., and Thornton, J. A.: Global tropospheric halogen (Cl, Br, I) chemistry and its impact on oxidants, *Atmos.*  
 3992 *Chem. Phys.*, 21, 13973–13996, <https://doi.org/10.5194/acp-21-13973-2021>, 2021b.  
 3993 Wang, Z., Deutscher, N. M., Warneke, T., Notholt, J., Dils, B., Griffith, D. W. T., Schmidt, M., Ramonet, M. and Gerbig,  
 3994 C.: Retrieval of tropospheric column-averaged CH<sub>4</sub> mole fraction by solar absorption FTIR-spectrometry using N<sub>2</sub>O  
 3995 as a proxy, *Atmospheric Meas. Tech.*, 7(10), 3295–3305, doi:10.5194/amt-7-3295-2014, 2014.  
 3996 Wang, Z.-P., Gu, Q., Deng, F.-D., Huang, J.-H., Megonigal, J. P., Yu, Q., Lü, X.-T., Li, L.-H., Chang, S., Zhang, Y.-H.,  
 3997 Feng, J.-C. and Han, X.-G.: Methane emissions from the trunks of living trees on upland soils, *New Phytol.*, 211(2),  
 3998 429–439, doi:10.1111/nph.13909, 2016.  
 3999 Wania, R., I. Ross and I. C. Prentice: Implementation and evaluation of a new methane model within a dynamic global  
 4000 vegetation model: LPJ-WHyMe v1.3, *Geosci. Model Dev. Discuss.*, 3, 1–59, 2010.  
 4001 Wania, R., Melton, J. R., Hodson, E. L., Poulter, B., Ringeval, B., Spahni, R., Bohn, T., Avis, C. A., Chen, G., Eliseev, A.  
 4002 V., Hopcroft, P. O., Riley, W. J., Subin, Z. M., Tian, H., van Bodegom, P. M., Kleinen, T., Yu, Z. C., Singarayer, J.

4003 S., Zurcher, S., Lettenmaier, D. P., Beerling, D. J., Denisov, S. N., Prigent, C., Papa, F. and Kaplan, J. O.: Present state  
 4004 of global wetland extent and wetland methane modelling: Methodology of a model inter-comparison project  
 4005 (WETCHIMP), *Geosci. Model Dev.*, 6(3), 617–641, 2013.

4006 Wassmann, R., Lantin, R. S., Neue, H. U., Buendia, L. V., Corton, T. M. and Lu, Y.: Characterization of methane emissions  
 4007 in Asia III: Mitigation options and future research needs, *Nutr. Cycl. Agroecosystems*, 58, 23–36, 2000.

4008 Weber, T., Wiseman, N. A. and Kock, A.: Global ocean methane emissions dominated by shallow coastal waters, *Nat.*  
 4009 *Commun.*, 10(1), 1–10, doi:10.1038/s41467-019-12541-7, 2019.

4010 Wells, N. S., J. J. Chen, D. T. Maher, P. Huang, D. V. Erler, M. Hipsey, and B. D. Eyre: Changing sediment and surface  
 4011 water processes increase CH<sub>4</sub> emissions from human-impacted estuaries. *Geochim. Cosmochim. Acta* **280**: 130–147.  
 4012 doi:10.1016/j.gca.2020.04.020, 2020

4013 van der Werf, G. R., Randerson, J. T., Giglio, L., Collatz, G. J., Mu, M., Kasibhatla, P. S., Morton, D. C., DeFries, R. S.,  
 4014 Jin, Y. and van Leeuwen, T. T.: Global fire emissions and the contribution of deforestation, savanna, forest,  
 4015 agricultural, and peat fires (1997-2009), *Atmospheric Chem. Phys.*, 10(23), 11,707-11,735, 2010.

4016 van der Werf, G. R., Randerson, J. T., Giglio, L., Leeuwen, T. T. van, Chen, Y., Rogers, B. M., Mu, M., Marle, M. J. E.  
 4017 van, Morton, D. C., Collatz, G. J., Yokelson, R. J. and Kasibhatla, P. S.: Global fire emissions estimates during 1997–  
 4018 2016, *Earth Syst. Sci. Data*, 9(2), 697–720, doi:10.5194/essd-9-697-2017, 2017.

4019 Westbrook, G. K., Thatcher, K. E., Rohling, E. J., Piotrowski, A. M., Pálke, H., Osborne, A. H., Nisbet, E. G., Minshull,  
 4020 T. A., Lanoisellé, M., James, R. H., Hühnerbach, V., Green, D., Fisher, R. E., Crocker, A. J., Chabert, A., Bolton, C.,  
 4021 Beszczynska-Möller, A., Berndt, C., and Aquilina, A.: Escape of methane gas from the seabed along the West  
 4022 Spitsbergen continental margin, *Geophys. Res. Lett.*, 36, L15608, <https://doi.org/10.1029/2009GL039191>, 2009.

4023 Whalen, S. C.: Biogeochemistry of Methane Exchange between Natural Wetlands and the Atmosphere, *Environ. Eng.*  
 4024 *Sci.*, 22(1), 73–94, doi:10.1089/ees.2005.22.73, 2005.

4025 Wiedinmyer, C., Kimura, Y., McDonald-Buller, E. C., Emmons, L. K., Buchholz, R. R., Tang, W., Seto, K., Joseph, M.  
 4026 B., Barsanti, K. C., Carlton, A. G., and Yokelson, R.: The Fire Inventory from NCAR version 2.5: an updated global  
 4027 fire emissions model for climate and chemistry applications, *EGUsphere* [preprint], [https://doi.org/10.5194/egusphere-](https://doi.org/10.5194/egusphere-2023-124)  
 4028 2023-124, 2023.

4029 Wik, M., Thornton, B. F., Bastviken, D., Uhlbäck, J. and Crill, P. M.: Biased sampling of methane release from northern  
 4030 lakes: A problem for extrapolation, *Geophys. Res. Lett.*, 43(3), 1256–1262, doi:10.1002/2015gl066501, 2016a.

4031 Wik, M., Varner, R. K., Anthony, K. W., MacIntyre, S. and Bastviken, D.: Climate-sensitive northern lakes and ponds are  
 4032 critical components of methane release, *Nat. Geosci.*, 9(2), 99–105, doi:10.1038/ngeo2578, 2016b.

4033 Wild, B., Teubner, I., Moesinger, L., Zotta, R.-M., Forkel, M., van der Schalie, R., Sitch, S., and Dorigo, W.:  
 4034 VODCA2GPP – a new, global, long-term (1988–2020) gross primary production dataset from microwave remote  
 4035 sensing, *Earth Syst. Sci. Data*, 14, 1063–1085, <https://doi.org/10.5194/essd-14-1063-2022>, 2022.

Williams, J. P., Omara, M., Himmelberger, A., Zavala-Araiza, D., MacKay, K., Benmergui, J., Sargent, M., Wofsy, S. C., Hamburg, S. P., and Gautam, R.: Small emission sources disproportionately account for a large majority of total methane emissions from the US oil and gas sector, *EGUsphere* [preprint], <https://doi.org/10.5194/egusphere-2024-1402>, 2024.

Winderlich, J., Chen, H., Gerbig, C., Seifert, T., Kolle, O., Lavrič, J. V., Kaiser, C., Höfer, A. and Heimann, M.: Continuous low-maintenance CO<sub>2</sub>/CH<sub>4</sub>/H<sub>2</sub>O measurements at the Zotino Tall Tower Observatory (ZOTTO) in Central Siberia, *Atmospheric Meas. Tech.*, 3(4), 1113–1128, doi:10.5194/amt-3-1113-2010, 2010.

Wilson, C., Chipperfield, M. P., Gloor, M., Parker, R. J., Boesch, H., McNorton, J., Gatti, L. V., Miller, J. B., Basso, L. S., and Monks, S. A.: Large and increasing methane emissions from eastern Amazonia derived from satellite data, 2010–2018, *Atmos. Chem. Phys.*, 21, 10643–10669, <https://doi.org/10.5194/acp-21-10643-2021>, 2021.

Wood, T.G. and Sands, W.A. The role of termites in ecosystems. In: Brian, M.V. (Ed.), *Production Ecology of Ants and Termites*. Cambridge University Press, Cambridge, UK, 245–292, 1978.

Woodward G, Perkins D.M., and Brown L. E.: Climate change and freshwater ecosystems: impacts across multiple levels of organization, *Philos Trans R Soc Lond B Biol Sci.* ,365(1549), 2093-106, doi: 10.1098/rstb.2010.0055, 2010

Woodward, G., Gessner, M. O., Giller, P. S., Gulis, V., Hladysz, S., Lecerf, A., Malmqvist, B., McKie, B. G., Tiegs, S. D., Cariss, H., Dobson, M., Eloegi, A., Ferreira, V., Graça, M. A. S., Fleituch, T., Lacoursière, J. O., Nistorescu, M., Pozo, J., Risnoveanu, G., Schindler, M., Vadineanu, A., Vought, L. B.-M. and Chauvet, E.: Continental-Scale Effects of Nutrient Pollution on Stream Ecosystem Functioning, *Science*, 336(6087), 1438–1440, doi:10.1126/science.1219534, 2012.

Woolway RI, Jones ID, Maberly SC, French JR, Livingstone DM, Monteith DT, et al.: Diel Surface Temperature Range Scales with Lake Size, *PLoS ONE* 11(3): e0152466, [doi:10.1371/journal.pone.0152466](https://doi.org/10.1371/journal.pone.0152466), 2016

Worden, J. R., Bloom, A. A., Pandey, S., Jiang, Z., Worden, H. M., Walker, T. W., Houweling, S. and Röckmann, T.: Reduced biomass burning emissions reconcile conflicting estimates of the post-2006 atmospheric methane budget, *Nat. Commun.*, 8(1), 2227, doi:10.1038/s41467-017-02246-0, 2017.

Wu, Z., Li, J., Sun, Y. *et al.* : Imbalance of global nutrient cycles exacerbated by the greater retention of phosphorus over nitrogen in lakes. *Nat. Geosci.* 15, 464–468, <https://doi.org/10.1038/s41561-022-00958-7>, 2022

Wuebbles, D. J. and Hayhoe, K.: Atmospheric methane and global change, *Earth-Sci. Rev.*, 57(3–4), 177–210, 2002.

Wunch, D., Toon, G. C., Blavier, J.-F. L., Washenfelder, R. A., Notholt, J., Connor, B. J., Griffith, D. W. T., Sherlock, V. and Wennberg, P. O.: The Total Carbon Column Observing Network, *Philos. Trans. R. Soc. A*, 369(1943), doi:10.1098/rsta.2010.0240, 2011.

Wunch, D., Toon, G. C., Hedelius, J. K., Vizenor, N., Roehl, C. M., Saad, K. M., Blavier, J.-F. L., Blake, D. R. and Wennberg, P. O.: Quantifying the loss of processed natural gas within California’s South Coast Air Basin using long-term measurements of ethane and methane, *Atmospheric Chem. Phys.*, 16(22), 14091–14105, doi:10.5194/acp-16-



4102 Yuan, J., J. Xiang, D. Liu, and others: Rapid growth in greenhouse gas emissions from the adoption of industrial-scale  
 4103 aquaculture. *Nat. Clim. Chang.* **9**: 318–322. doi:10.1038/s41558-019-0425-9, 2019

4104 Yver Kwok, C. E., Müller, D., Caldow, C., Lebègue, B., Mønster, J. G., Rella, C. W., Scheutz, C., Schmidt, M., Ramonet,  
 4105 M., Warneke, T., Broquet, G. and Ciais, P.: Methane emission estimates using chamber and tracer release experiments  
 4106 for a municipal waste water treatment plant, *Atmospheric Meas. Tech.*, **8**(7), 2853–2867, doi:10.5194/amt-8-2853-  
 4107 2015, 2015.

4108 Zhang: Magnitude, spatio-temporal variability and environmental controls of methane emissions from global rice  
 4109 fields: Implications for water management and climate mitigation, *Glob. Change Biol.*, 2016.

4110 Zhang, B. and Chen, G. Q.: China's CH<sub>4</sub> and CO<sub>2</sub> Emissions: Bottom-Up Estimation and Comparative Analysis, *Ecol.*  
 4111 *Indic.*, **47**, 112–122, doi:10.1016/j.ecolind.2014.01.022, 2014.

4112 Zhang, L., X. Xia, S. Liu, S. Zhang, S. Li, J. Wang, G. Wang, H. Gao, Z. Zhang, Q. Wang, W. Wen, R. Liu, Z. Yang, E.H.  
 4113 Stanley, and P.A. Raymond: Significant methane ebullition from alpine permafrost rivers on the East Qinghai–Tibet  
 4114 Plateau. *Nature Geoscience*, **13**(5): p. 349-354, 2020

4115 Zhang, L., H. Tian, H. Shi, S. Pan, J. Chang, S. R. S. Dungal, X. Qin, S. Wang, F. N. Tubiello, J. G. Canadell, R. B.  
 4116 Jackson: A 130-year global inventory of methane emissions from livestock: Trends, patterns, and drivers, *Global*  
 4117 *Change Biology*, **28** (17), 5142-5158. <https://doi.org/10.1111/gcb.16280>, 2022

4118 Zhang, P., Zhang, Y., Liang, R., Chen, W., and Xie, X. : Evaluation of the stratospheric contribution to the inter-annual  
 4119 variabilities of tropospheric methane growth rates, *Geophysical Research Letters*, **50**,  
 4120 e2023GL103350, <https://doi.org/10.1029/2023GL103350>, 2023.

4121 Zhang, Y., Xiao, X., Wu, X., Zhou, S., Zhang, G., Qin, Y., and Dong, J.: A global moderate resolution dataset of gross  
 4122 primary production of vegetation for 2000–2016, *Sci. Data*, **4**, 1–13, <https://doi.org/10.1038/sdata.2017.165>, 2017.

4123 Zhang, Y., Jacob, D. J., Maasakkers, J. D., Sulprizio, M. P., Sheng, J.-X., Gautam, R., and Worden, J.: Monitoring global  
 4124 tropospheric OH concentrations using satellite observations of atmospheric methane, *Atmos. Chem. Phys.*, **18**, 15959–  
 4125 15973, <https://doi.org/10.5194/acp-18-15959-2018>, 2018.

4126 Zhang, Y., Gautam, R., Pandey, S., Omara, M., Maasakkers, J. D., Sadavarte, P., Lyon, D., Nesser, H., Sulprizio, M. P.,  
 4127 Varon, D. J., Zhang, R., Houweling, S., Zavala-Araiza, D., Alvarez, R. A., Lorente, A., Hamburg, S. P., Aben, I., and  
 4128 Jacob, D. J.: Quantifying Methane Emissions from the Largest Oil-Producing Basin in the United States from Space,  
 4129 *Sci. Adv.*, **6**, eaaz5120, <https://doi.org/10.1126/sciadv.aaz5120>, 2020.

4130 Zhang, Z., Zimmermann, N. E., Kaplan, J. O. and Poulter, B.: Modeling spatiotemporal dynamics of global wetlands:  
 4131 comprehensive evaluation of a new sub-grid TOPMODEL parameterization and uncertainties, *Biogeosciences*, **13**(5),  
 4132 1387–1408, doi:10.5194/bg-13-1387-2016, 2016.

4133 Zhang, Z., Fluet-Chouinard, E., Jensen, K., McDonald, K., Hugelius, G., Gumbrecht, T., et al. Development of the global  
 4134 dataset of Wetland Area and Dynamics for Methane Modeling (WAD2M), Earth System Science Data, 13(5), 2001–  
 4135 2023. <https://doi.org/10.5194/essd-13-2001-2021>, 2021a.

4136 Zhang, Z., Poulter, B., Knox, S., Stavert, A., McNicol, G., Fluet-Chouinard, E., Feinberg, A., Zhao, Y., Bousquet, P.,  
 4137 Canadell, J. G., Ganesan, A., Hugelius, G., Hurtt, G., Jackson, R. B., Patra, P. K., Saunio, M., Höglund-Isaksson, L.,  
 4138 Huang, C., Chatterjee, A., and Li, X.: Anthropogenic emission is the main contributor to the rise of atmospheric  
 4139 methane during 1993-2017, National science review, 9(5), nwab200, doi:10.1093/nsr/nwab200, 2021b

4140 Zhang, Z., Poulter, B., Feldman, A.F., Ying, Q., Ciais, P., Peng, S. and Li, X.: Recent intensification of wetland methane  
 4141 feedback, Nat. Clim. Chang. 13, 430–433, <https://doi.org/10.1038/s41558-023-01629-0>, 2023

4142 Zhang, Z., Poulter, B., Melton, J. R., Riley, W. J., Allen, G. H., Beerling, D. J., Bousquet, P., Canadell, J. G., Fluet-  
 4143 Chouinard, E., Ciais, P., Gedney, N., Hopcroft, P. O., Ito, A., Jackson, R. B., Jain, A. K., Jensen, K., Joos, F., Kleinen,  
 4144 T., Knox, S., Li, T., Li, X., Liu, X., McDonald, K., McNicol, G., Miller, P. A., Müller, J., Patra, P. K., Peng, C., Peng,  
 4145 S., Qin, Z., Riggs, R. M., Saunio, M., Sun, Q., Tian, H., Xu, X., Yao, Y., Yi, X., Zhang, W., Zhu, Q., Zhu, Q., and  
 4146 Zhuang, Q.: Ensemble estimates of global wetland methane emissions over 2000–2020, EGU sphere [preprint],  
 4147 <https://doi.org/10.5194/egusphere-2024-1584>, 2024.

4148 Zhao, J., M. Zhang, W. Xiao, L. Jia, X. Zhang, J. Wang, Z. Zhang, Y. Xie, Y. Pu, S. Liu, Z. Feng, and X. Lee: Large  
 4149 methan emission from freshwater aquaculture ponds revealed by long-term eddy covariance observation.  
 4150 Agricultural and Forest Meteorology, 308-309: p. 108600, 2021

4151 Zhao, Y., Saunio, M., Bousquet, P., Lin, X., Berchet, A., Hegglin, M. I., Canadell, J. G., Jackson, R. B., Hauglustaine,  
 4152 D. A., Szopa, S., Stavert, A. R., Abraham, N. L., Archibald, A. T., Bekki, S., Deushi, M., Jöckel, P., Josse, B., Kinnison,  
 4153 D., Kirner, O., Marécal, V., O'Connor, F. M., Plummer, D. A., Revell, L. E., Rozanov, E., Stenke, A., Strode, S.,  
 4154 Tilmes, S., Dlugokencky, E. J. and Zheng, B.: Inter-model comparison of global hydroxyl radical (OH) distributions  
 4155 and their impact on atmospheric methane over the 2000–2016 period, Atmospheric Chem. Phys., 19(21), 13701–  
 4156 13723, doi:10.5194/acp-19-13701-2019, 2019.

4157 Zhao, Y., Saunio, M., Bousquet, P., Lin, X., Berchet, A., Hegglin, M. I., Canadell, J. G., Jackson, R. B., Dlugokencky,  
 4158 E. J., Langenfelds, R. L., Ramonet, M., Worthy, D., and Zheng, B.: Influences of hydroxyl radicals (OH) on top-down  
 4159 estimates of the global and regional methane budgets, Atmos. Chem. Phys., 20, 9525–9546,  
 4160 <https://doi.org/10.5194/acp-20-9525-2020>, 2020a.

4161 Zhao, Y., Saunio, M., Bousquet, P., Lin, X., Berchet, A., Hegglin, M. I., Canadell, J. G., Jackson, R. B., Deushi, M.,  
 4162 Jöckel, P., Kinnison, D., Kirner, O., Strode, S., Tilmes, S., Dlugokencky, E. J., and Zheng, B.: On the role of trend and  
 4163 variability in the hydroxyl radical (OH) in the global methane budget, Atmos. Chem. Phys., 20, 13011–13022,  
 4164 <https://doi.org/10.5194/acp-20-13011-2020>, 2020b.

4165 Zhao, Y., Saunio, M., Bousquet, P., Lin, X., Hegglin, M. I., Canadell, J. G., Jackson, R. B., and Zheng, B.: Reconciling

the bottom-up and top-down estimates of the methane chemical sink using multiple observations, *Atmos. Chem. Phys.*, 23, 789–807, <https://doi.org/10.5194/acp-23-789-2023>, 2023.

Zheng, B., Chevallier, F., Ciais, P., Yin, Y. and Wang, Y.: On the Role of the Flaming to Smoldering Transition in the Seasonal Cycle of African Fire Emissions, *Geophys. Res. Lett.*, 45(21), 11,998–12,007, doi:10.1029/2018GL079092, 2018a.

Zheng, B., Chevallier, F., Ciais, P., Yin, Y., Deeter, M. N., Worden, H. M., Wang, Y., Zhang, Q. and He, K.: Rapid decline in carbon monoxide emissions and export from East Asia between years 2005 and 2016, *Environ. Res. Lett.*, 13(4), 044007, doi:10.1088/1748-9326/aab2b3, 2018b.

Zheng, B., Chevallier, F., Yin, Y., Ciais, P., Fortems-Cheiney, A., Deeter, M. N., Parker, R. J., Wang, Y., Worden, H. M., and Zhao, Y.: Global atmospheric carbon monoxide budget 2000–2017 inferred from multi-species atmospheric inversions, *Earth Syst. Sci. Data*, 11, 1411–1436, doi: 10.5194/essd-11-1411-2019, 2019.

Zheng, B., Ciais, P., Chevallier, F., Yang, H., Canadell, J. G., Chen, Y., van der Velde, I. R., Aben, I., Chuvieco, E., Davis, S. J., Deeter, M., Hong, C., Kong, Y., Li, H., Li, H., Lin, X., He, K., and Zhang, Q.: Record-high CO<sub>2</sub> emissions from boreal fires in 2021, *Science*, 379, 912–917, doi: 10.1126/science.ade0805, 2023.

Zhu, Q., Liu, J., Peng, C., Chen, H., Fang, X., Jiang, H., Yang, G., Zhu, D., Wang, W. and Zhou, X.: Modelling methane emissions from natural wetlands by development and application of the TRIPLEX-GHG model, *Geosci. Model Dev.*, 7(3), 981–999, doi:10.5194/gmd-7-981-2014, 2014.

Zhu, Q., Peng, C., Chen, H., Fang, X., Liu, J., Jiang, H., Yang, Y. and Yang, G.: Estimating global natural wetland methane emissions using process modelling: spatio-temporal patterns and contributions to atmospheric methane fluctuations, *Glob. Ecol. Biogeogr.*, 24, 959–972, 2015.

Zhu, Q., Laughner, J.L., Cohen, R.C.: Combining Machine Learning and Satellite Observations to Predict Spatial and Temporal Variation of near Surface OH in North American Cities, *Environ. Sci. Technol.*, 56, 11, doi:10.1021/acs.est.1c05636, 2022

Zhu, Y., K.J. Purdy, Ö. Eyice, L. Shen, S.F. Harpenslager, G. Yvon-Durocher, A.J. Dumbrell, and M. Trimmer: Disproportionate increase in freshwater methane emissions induced by experimental warming. *Nature Climate Change*, 10(7): p. 685–690., 2020

Zhuang, Q., Melillo, J. M., Kicklighter, D. W., Prinn, R. G., McGuire, A. D., Steudler, P. A., Felzer, B. S. and Hu, S.: Methane fluxes between terrestrial ecosystems and the atmosphere at northern high latitudes during the past century: A retrospective analysis with a process-based biogeochemistry model, *Glob. Biogeochem Cycles*, 18(3), GB3010, doi:10.1029/2004gb002239, 2004.

Zhuang, Q., Chen, M., Xu, K., Tang, J., Saikawa, E., Lu, Y., Melillo, J. M., Prinn, R. G. and McGuire, A. D.: Response of global soil consumption of atmospheric methane to changes in atmospheric climate and nitrogen deposition, *Glob. Biogeochem. Cycles*, 27(3), 650–663, doi:10.1002/gbc.20057, 2013.



4199     Zhuang, Q., M. Guo, J.M. Melack, X. Lan, Z. Tan, Y. Oh, and L.R. Leung: Current and Future Global Lake Methane  
4200     Emissions: A Process-Based Modeling Analysis. *Journal of Geophysical Research: Biogeosciences*, 128(3): p.  
4201     e2022JG007137, 2023

12 **Table 1: Bottom-up (BU) models and inventories for anthropogenic and biomass burning used in this study. \*Due to its limited**  
13 **sectoral breakdown this dataset was not used in Table 3.**

B-U models and inventories	Contribution	Time period (resolution)	Gridded	References
CEDS (country based)	Fossil fuels, Agriculture and waste, Biofuel	1970-2019 (yearly)	no	Hoesly et al. (2018)
CEDS (gridded)*	Fossil fuels, Agriculture and waste, Biofuel	1970-2020 (monthly)	0.5x0.5°	Hoesly et al. (2018) O'Rourke et al (2021)
EDGARv6	Fossil fuels, Agriculture and waste, Biofuel	1990-2018^ (yearly, monthly for some sectors)	0.1x0.1°	Oreggioni et al. (2021), Crippa et al. (2021)
EDGARv7	Fossil fuels, Agriculture and waste, Biofuel	1990-2021 (yearly)	0.1x0.1°	Crippa et al. (2023)
IIASA GAINS v4.0	Fossil fuels, Agriculture and waste, Biofuel	1990-2020 (yearly)	0.5x0.5°	Höglund-Isaksson et al., (2020)
USEPA	Fossil fuels, Agriculture and waste, Biofuel, Biomass Burning	1990-2030 (10-yr interval, interpolated to yearly)	no	USEPA (2019)
FAO-CH4	Agriculture, Biomass Burning	1961-2020 1990-2020 (Yearly)	no	Federici et al. (2015) ; Tubiello et al. (2013); Tubiello (2019)
FINNv2.5	Biomass burning	2002-2020 (daily)	1km resolution	Wiedinmyer et al. (2023)
GFASv1.3	Biomass burning	2003-2020 (daily)	0.1x0.1°	Kaiser et al. (2012)
GFEDv4.1s	Biomass burning	1997-2020 (monthly)	0.25x0.25°	Giglio et al. (2013); van der Werf et al (2017)
QFEDv2.5	Biomass burning	2000-2020 (daily)	0.1x0.1°	Darmenov and da Silva (2015)

14

15

16 **Table 2: Biogeochemical models that computed wetland emissions used in this study. Model runs were performed with two climate**  
17 **inputs, CRU and GSWP3-W5E5. Models were run with prognostic (using their own calculation of wetland areas) and/or diagnostic**  
18 **(using WAD2M (Zhang et al., 2021b)) wetland surface areas (see Sect 3.2.1).**

Model	Institution	Prognostic		Diagnostic		References
		CRU	GSWP3-W5E5	CRU	GSWP3-W5E5	
CH4MOD <sub>wetland</sub>	Institute of Atmospheric Physics, CAS	n	n	y	y	Li et al. (2010)
CLASSIC	Environment and Climate Change Canada	y	y*	y	y*	Arora et al. (2018); Melton and Arora (2016)
DLEM	Boston College	y	y	y	y	Tian et al. (2015, 2023)
ELM-ECA	Lawrence Berkeley National Laboratory	y	y	y	y	Riley et al. (2011)
ISAM	University of Illinois, Urbana-Champaign	y	y	y	y	Shu et al. (2020) Xu et al. (2021)
JSBACH	MPI	y	y	y	y	Kleinen et al. (2020, 2021, 2023)
JULES	UKMO	y	y	y	y	Gedney et al. (2019)
LPJ-GUESS	Lund University	n	n	y	y	McGuire et al. (2012)
LPJ-MPI	MPI	y	y	y	y	Kleinen et al. (2012)
LPJ-WSL	NASA GSFC	y	y	y	y	Zhang et al. (2016)
LPX-Bern	University of Bern	y	y	y	y	Spahni et al. (2011), Stocker et al. (2014)
ORCHIDEE	LSCE	y	y	y	y	Ringeval et al. (2011)

SDGVM	University of Birmingham/ University of Sheffield	y	y	y	y	Beerling & Woodward (2001), Hopcroft et al. (2011, 2020)
TEM-MDM	Purdue University	n	n	y	y	Zhuang et al. (2004)
TRIPLEX-GHG	UQAM	n	n	y	y	Zhu et al. (2014, 2015)
VISIT	NIES	y	y	y	y	Ito and Inatomi (2012)

9) \*CLASSIC uses GSWP3-W5E version 2 that covers the time period till 2016. All other models use GSWP-W5E5 version 3.

Table 3: Global methane emissions by source type in Tg CH<sub>4</sub> yr<sup>-1</sup> from Saunois et al. (2020) (left column pair) and from this work using bottom-up and top-down approaches. Because top-down models cannot fully separate individual processes, only five categories of emissions are provided (see text). Uncertainties are reported as [min-max] range of reported studies. The mean, minimum and maximum values are calculated while discarding outliers, for each category of source and sink. As a result, discrepancies may occur when comparing the sum of categories and their corresponding total due to differences in outlier detections. Differences of 1 Tg CH<sub>4</sub> yr<sup>-1</sup> in the totals can also occur due to rounding errors. Compared to Saunois et al. (2020), emissions are split between “direct anthropogenic” emissions and “natural and indirect anthropogenic” sources. We also propose an estimate of the double-counting between bottom-up wetland and inland freshwater ecosystems emissions.

	Saunois et al. (2020)		This work					
Period of time	2000-2009		2000-2009		2010-2019		2020	
Approaches	bottom-up	top-down	bottom-up	top-down	bottom-up	top-down	bottom-up	top-down
<b>NATURAL &amp; indirect anthropogenic SOURCES</b>								
<b>Combined wetlands and inland freshwaters</b>	<b>306</b> [229-391]	<b>180</b> [153-196]	<b>242</b> [156-355]	<b>158</b> [145-172]	<b>248</b> [159-369]	<b>165</b> [145-214]	<b>251</b> [171-364]	<b>175</b> [151-229]
<b>Wetlands</b>	<b>147</b> [102-179]	<b>180</b> [153-196]	<b>153</b> [116-189] (***)	<b>158</b> [145-172]	<b>159</b> [119-203] (***)	<b>165</b> [145-214]	<b>161</b> [131-198] (***)	<b>175</b> [151-229]
<b>Inland freshwaters<sup>a</sup></b>	<b>159</b> [117-212]		<b>112</b> [49-202]		<b>112</b> [49-202]		<b>112</b> [49-202]	
<b>Double counting<sup>b</sup></b>	NA		-23 [-9 - -36]		-23 [-9 - -36]		-23 [-9 - -36]	
<b>Other natural sources</b>	<b>63</b> [26-94]	<b>35</b> [21-47]	<b>63</b> [24-93]	<b>44</b> [40-46]	<b>63</b> [24-93]	<b>43</b> [40-46]	<b>63</b> [24-93]	<b>44</b> [40-47]
<b>Land sources</b>	<b>50</b> [17-72]		<b>51</b> [18-73]					
Geological (onshore)	38 [13-53]		38 [13-53]					
Wild animals	2 [1-3]		2 [1-3]					
Termites	9 [3-15]		10 [4-16]					
Wildfires	(**)		(**)					
Permafrost soils (direct)	1 [0-1]		1 [0-1]					
Vegetation	(*)		(*)					
<b>Coastal and Oceanic sources<sup>c</sup></b>	<b>13</b> [9-22]		<b>12</b> [6-20]					
Biogenic	6 [4-10]		5 [3-10]					
Geological (offshore)	7 [5-12]		7 [5-12]					
<b>TOTAL NATURAL &amp; INDIRECT SOURCES</b>	<b>369</b> [245-485]	<b>215</b> [176-243]	<b>305</b> [180-448]	<b>204</b> [189-223]	<b>311</b> [183-462]	<b>206</b> [188-225]	<b>314</b> [195-457]	<b>216</b> [193-241]
<b>DIRECT ANTHROPOGENIC SOURCES</b>								
<b>Agriculture and waste</b>	<b>192</b> [178-206]	<b>202</b> [198-219]	<b>194</b> [181-208]	<b>210</b> [197-223]	<b>211</b> [195-231]	<b>228</b> [213-242]	<b>211</b> [204-216]	<b>245</b> [232-259]
<b>Agriculture</b>	<b>132</b> [NA]		<b>134</b> [125-142]		<b>143</b> [132-155]		<b>147</b> [143-149]	
Enteric ferm. & manure	104 [93-109]		104 [100 -110]		112 [107 -118]		117 [114 -124]	
Rice cultivation	28 [23-34]		30 [24-34]		32 [25-37]		32 [29-37]	
<b>Landfills and waste</b>	<b>60</b> [55-63]		<b>61</b> [52-71]		<b>69</b> [56-80]		<b>71</b> [60-84]	
<b>Fossil fuels</b>	<b>110</b> [94-129]	<b>101</b> [71-151]	<b>105</b> [97-123] (****)	<b>105</b> [88-115]	<b>120</b> [117-125] (****)	<b>115</b> [100-124]	<b>128</b> [120-133] (****)	<b>122</b> [101-133]
Coal mining	32 [24-42]							

	Saunois et al. (2020)		This work					
Period of time	2000-2009		2000-2009		2010-2019		2020	
Oil & Gas	73 [60-85]		30 [26-32]		40 [37-44]		41 [38-43]	
Industry	2 [0-6]		65 [63-71]		67 [57-74]		74 [67-80]	
Transport	4 [1-11]		4 [1-8]		5 [1-9]		5 [1-8]	
			3 [1-8]		2 [1-3]		2 [1-3]	
Biomass & biof. burn.	31 [26-46]	29 [23-35]	30 [22-44]	26 [22-29]	28 [21-39]	27 [26-27]	27 [20-41]	26 [22-27]
Biomass burning	19 [15-32]		19 [14-29]		17 [12-24]		17 [13-27]	
Biofuel burning	12 [9-14]		11 [8-14]		11 [8-14]		10 [7-14]	
TOTAL DIRECT ANTHROPOGENIC SOURCES	334 <sup>d</sup> [321-358]	332 [312-347]	333 <sup>d</sup> [305-365]	341 [319-355]	358 <sup>d</sup> [329-387]	369 [350-391]	372 <sup>d</sup> [345-409]	392 [368-409]
SINKS								
Total chemical loss	595 [489-749]	505 [459-516]	585 [481-716]	504 <sup>e</sup> [496-511]	602 [496-747]	521 <sup>e</sup> [485-532]	602 [496-747]	538 <sup>e</sup> [503-554]
Tropospheric OH	553 [476-677]		546 [446-663]		563 [462-663]		563 [462-663]	
Stratospheric loss	31 [12-37]		37 [27-51]		37 [28-43]		37 [28-43]	
Tropospheric Cl	11 [1-35]		6 [1-13]		6 [1-13]		6 [1-13]	
Soil uptake	30 [11-49]	34 [27-41]	30 [11-49]	34 [34-34]	31 [11-49]	35 [35-35]	31 [11-49]	36 [35-36]
TOTAL SINKS	625 [500-798]	540 [486-556]	615 [492-765]	538 [530-545] <sup>e</sup>	633 [507-796]	554 [520-567] <sup>e</sup>	633 [507-796]	575 [566-589] <sup>e</sup>
SOURCES – SINKS IMBALANCE								
TOTAL SOURCES	703 [566-842]	547 [524-560]	638 [485-813]	543 [526-558]	669 [512-849]	575 [553-586]	685 [540-865]	608 [581-627]
TOTAL SINKS	625 [500-798]	540 [486-556]	615 [492-765]	538 [530-545] <sup>e</sup>	633 [507-796]	554 [550-567] <sup>e</sup>	633 [507-796]	575 [566-589] <sup>e</sup>
IMBALANCE	78	3 [-10-38]	23	5 [-4-13] <sup>e</sup>	36	21 [19-33] <sup>e</sup>	52	32 [15-38] <sup>e</sup>
ATMOSPHERIC GROWTH <sup>f</sup>		5.8 [4.9-6.6] <sup>f</sup>		6.1 [5.2-6.9] <sup>f</sup>		20.9 [20.1-21.7] <sup>f</sup>		41.8 [40.7-42.9] <sup>f</sup>

(\*) uncertain but likely small for upland forest and aerobic emissions, potentially large for forested wetland, but likely included elsewhere

(\*\*) We stop reporting this value to avoid potential double counting with satellite-based products of biomass burning (see Sect. 3.1.5)

(\*\*\*) Here the numbers are from prognostic runs. To ensure a fair comparison with previous budgets (Saunois et al., 2020), the numbers are 163[117-195] for 2000-2009 from diagnostic runs with CRU/CRU-JRA-55 climate inputs (see Sect. 3.2.1).

(\*\*\*\*) Up to 8 Tg of additional emissions could account for ultra emitters (Lauvaux et al., 2022), as in Tibrewal et al. (2024), that are fully or partly missed in regular anthropogenic inventories

a: Freshwater includes lakes, ponds, reservoirs, streams and rivers, part of it is due to anthropogenic disturbances estimated in Sect.3.2.2

b: The double counting estimate is discussed in Sect. 3.2.2

c: includes flux from hydrates considered at 0 for this study, includes estuaries

d: Total anthropogenic emissions are based on estimates of full anthropogenic inventory and not on the sum of “Agriculture and Waste”, “Fossil fuels” and “Biofuel and biomass burning” categories (see Sect. 3.1.2)

e: Some inversions did not provide the chemical sink. These values are derived from a subset of the inversion ensemble.

f: Atmospheric growth rates are given in the same unit Tg CH<sub>4</sub> yr<sup>-1</sup>, based on the conversion factor of 2.75 Tg CH<sub>4</sub> ppb<sup>-1</sup> given by Prather et al. (2012) and the atmospheric growth rates provided in the text in ppb yr<sup>-1</sup>.

11 **Table 4: Top-down studies used here with their contribution to the decadal and yearly estimates noted. For decadal means, top down**  
12 **studies must provide at least 8 years of data over the decade to contribute to the estimate. Details on each inverse system and inversions**  
13 **are provided in Table S8 to S11 in the Supplementary Material.**

Model	Institution	Observation used	Time period	Number of inversions	2000-2009	2010-2019	2020	References
Carbon Tracker-Europe CH <sub>4</sub>	FMI	Surface stations	2000-2020	4	y	y	y	Tsuruta et al. (2017)
LMDz-CIF	LSCE/CE A	Surface stations	2000-2020	4	y	y	y	Thanwerdas et al. (2022a)
LMDz-PYVAR	LSCE/CE A/THU	GOSAT Leicester v9.0	2010-2020	4	n	y	y	Zheng et al. (2018a, 2018b, 2019)
MIROC4-ACTM	JAMSTEC	Surface stations	2000-2020	5	y	y	y	Patra et al. (2018); Chandra et al. (2021)
NISMON-CH <sub>4</sub>	NIES/MRI	Surface stations	2000-2020	2	y	y	y	Niwa et al. (2022; 2024)
NIES-TM-FLEXPART (NTFVAR)	NIES	Surface stations	2000-2020	2	y	y	y	Maksyutov et al. (2020); Wang et al. (2019a)
NIES-TM-FLEXPART (NTFVAR)	NIES	GOSAT NIES L2 v02.95	2010-2020	1	n	y	y	Maksyutov et al. (2020); Wang et al. (2019a)
TM5-CAMS	TNO/VU	Surface stations	2000-2020	1	y	y	y	Segers et al. (2022)
TM5-CAMS	TNO/VU	GOSAT ESA/CCI v2.3.8 (combined with surface observations)	2010-2020	1	n	y	y	Segers et al. (2022)
Total number of runs				24	18	24	24	

14

45 Table 5: Global and latitudinal total methane emissions in Tg CH<sub>4</sub> yr<sup>-1</sup>, as decadal means (2000-2009 and 2010-2019) and for the  
 46 year 2020 from this work using bottom-up and top-down approaches. Global and latitudinal emissions for 2000-2009 are also  
 47 compared with Saunois et al. (2016, 2020) for top-down and bottom-up approaches when available. Uncertainties are reported as  
 48 [min-max] range. The mean, minimum and maximum values are calculated while discarding outliers, for each category of source  
 49 and sink. As a result, discrepancies may occur when comparing the sum of categories and their corresponding total due to differences  
 50 in outlier detections. Differences of 1 Tg CH<sub>4</sub> yr<sup>-1</sup> in the totals can also occur due to rounding errors. For the latitudinal breakdown,  
 51 bottom-up anthropogenic estimates are based only on the gridded products (see Table 1). As a result, the total from the latitudinal  
 52 breakdown (line called “This work (gridded BU products only)”) is slightly different from the values provided in Table 3 and recalled  
 53 in the line “This work (all BU products)”. BU stands for bottom-up.

Period	2000-2009		2010-2019		2020	
Approach	Bottom-up	Top-down	Bottom-up	Top-down	Bottom-up	Top-down
Global						
This work (all BU products)	638 [485-813]	543 [526-558]	669 [512-849]	575 [553-586]	685 [540-865]	608 [581-627]
This work (gridded BU products only)	642 [501-809]		676 [526-845]		691 [565-862]	
<i>S2020</i>	703 [566-842]	547 [524-560]	-	-	-	-
<i>S2016</i>	719[583-861]	552[535-566]	-	-	-	-
90°S-30°N						
This work	367 [254-487]	337 [311-361]	388 [275-503]	364 [337-390]	395 [292-521]	386 [353-425]
<i>S2020</i>	408 [322-532]	346 [320-379]	-	-	-	-
<i>S2016</i>	-	356 [334-381]	-	-	-	-
30°N-60°N						
This work	234 [169-335]	182 [162-197]	250 [184-345]	187 [160-204]	256 [186-356]	197 [170-215]
<i>S2020</i>	252 [202-342]	178 [159-199]	-	-	-	-
<i>S2016</i>	-	176[159-195]	-	-	-	-
60°N-90°N						
This work	42 [22-79]	26 [22-33]	38[17-73]	24 [18-29]	39 [17-74]	25 [20-32]
<i>S2020</i>	42 [28-70]	23 [17- 32]	-	-	-	-
<i>S2016</i>	-	20 [15-25]	-	-	-	-



.55  
 .56 **Table 6: Latitudinal methane emissions in Tg CH<sub>4</sub> yr<sup>-1</sup> for the last decade 2010-2019, based on top-down and bottom-up approaches.**  
 .57 **Uncertainties are reported as [min-max] range of reported studies. The mean, minimum, and maximum values are calculated while**  
 .58 **discarding outliers, for each category of source and sink. As a result, discrepancies may occur when comparing the sum of categories**  
 .59 **and their corresponding total due to differences in outlier detections. Differences of 1 Tg CH<sub>4</sub> yr<sup>-1</sup> in the totals can also occur due to**  
 .60 **rounding errors. For bottom-up approaches, natural and indirect anthropogenic sources are estimated based on available gridded**  
 .61 **data sets (see text Sect 5.2). As some emissions are missing gridded products (wild animals, permafrost, and hydrates), discrepancies**  
 .62 **may occur in terms of totals proposed in Table 3. Bottom-up direct anthropogenic estimates are based only on the gridded products**  
 .63 **(see Table 1).**

.64

Latitudinal band	90°S- 30°N		30°N-60°N		60°-90°N	
Approach	Bottom-up	Top-Down	Bottom-up	Top-Down	Bottom-up	Top-Down
<b>Natural and indirect anthropogenic Sources</b>	<b>178</b> [95-276]	<b>148</b> [133-164]	<b>100</b> [43-188]	<b>42</b> [36-50]	<b>28</b> [9-53]	<b>14</b> [10-21]
Combined wetland and Inland freshwaters	151 [85-234]	128 [112-155]	73 [32-147]	27 [20-42]	24 [9-53]	9 [7-17]
Other natural	27 [11-42]	22 [20-29]	27 [10-41]	19 [16-22]	4 [2-6]	3 [1-5]
<b>Anthropogenic direct sources</b>	<b>210</b> [180-227]	<b>215</b> [191-238]	<b>151</b> [142-157]	<b>144</b> [121-162]	<b>10</b> [6-14]	<b>10</b> [6-16]
Agriculture & Waste	140 [121-150]	150 [135-168]	81 [77-84]	77 [56-88]	1 [1-2]	2 [2-2]
Fossil Fuels	52 [44-65]	46 [36-62]	65 [61-71]	61 [50-69]	7 [4-10]	7 [3-13]
Biomass & biofuel burning	22 [18-30]	19 [16-21]	7 [4-10]	6 [2-7]	1 [0-1]	1 [1-2]
<b>Sum of sources</b>	<b>388</b> [275-503]	<b>364</b> [337-390]	<b>250</b> [184-345]	<b>187</b> [160-204]	<b>38</b> [7-73]	<b>24</b> [18- 29]

.65  
 .66  
 .67

68 Table 7: Regional methane emissions (regions ranked by continent) in Tg CH<sub>4</sub> yr<sup>-1</sup> for the last decade 2010-2019, based on top-down  
 69 and bottom-up approaches. Uncertainties are reported as [min-max] range of reported studies. Differences of 1 Tg CH<sub>4</sub> yr<sup>-1</sup> in the  
 70 totals can occur due to rounding errors. For bottom-up approaches, natural and indirect anthropogenic sources are estimated based  
 71 on available gridded data sets (see text Sect 5.2). As some emissions are missing gridded products (wild animals, permafrost, and  
 72 hydrates), discrepancies may occur in terms of totals proposed in Table 3. Bottom-up direct anthropogenic estimates are based on  
 73 all products (gridded and per country).  
 74

Region	Total emissions		Natural and indirect anthropogenic emissions		Direct anthropogenic emissions	
	Bottom-up	Top-down	Bottom-up	Top-down	Bottom-up	Top-down
USA	49 [27-77]	38 [32-46]	24 [7-43]	12 [7-22]	26 [19-34]	25 [16-31]
Canada	38 [14-71]	20 [17-24]	32 [11-63]	14 [11-22]	6 [3-8]	7[5-9]
Central America	18 [10-28]	17 [14-19]	8 [3-17]	5 [2-6]	10 [8-12]	12 [11-13]
Northern South America	19 [9-35]	16 [13-20]	10 [3-17]	9 [7-11]	9 [6-17]	7 [6-8]
Brazil	51 [26-79]	47 [41-58]	32 [11-57]	26 [22-36]	19 [16-22]	21 [17-26]
Southwest South America	34 [16-51]	38 [30-48]	21 [6-35]	24 [16-34]	13 [10-16]	14 [12-17]
Europe	42 [29-57]	31 [24-36]	17 [6-30]	7 [5-9]	25 [22-27]	24 [20-31]
Northern Africa	24 [18-33]	25 [23-29]	7 [2-13]	6 [6-8]	18 [16-20]	19 [17-21]
Equatorial Africa	47 [28-83]	47 [39-59]	23 [10-49]	24 [20-30]	24 [19-34]	23 [19-29]
Southern Africa	21 [5-43]	19 [16-24]	11 [2-29]	8 [7-10]	10 [3-14]	11 [10-12]
Russia	48 [24-83]	36 [27-45]	25 [9-47]	14 [11-18]	23 [15-36]	21 [14-29]
Central Asia	15 [6-29]	10 [8-13]	8 [2-19]	1 [0-2]	8 [4-10]	9 [7-11]
Middle East	35 [21-47]	31 [24-39]	9 [3-15]	4 [1-6]	26 [18-31]	28 [20-34]
China	71 [55-99]	57 [37-72]	15 [4-33]	4 [3-7]	57 [51-66]	53 [34-66]
Korean-Japan	6 [4-12]	5 [4-6]	3 [1-7]	1 [1-1]	4 [3-5]	4 [3-5]
South Asia	58 [49-72]	52 [43-60]	13 [5-25]	6 [5-6]	45 [44-47]	45[37-49]
Southeast Asia	64 [42-93]	63 [52-71]	32 [19-54]	27 [20-34]	32 [23-39]	35 [31-46]
Australasia	16 [9-26]	13 [10-17]	10 [4-19]	6 [4-7]	7 [6-7]	7 [6-7]

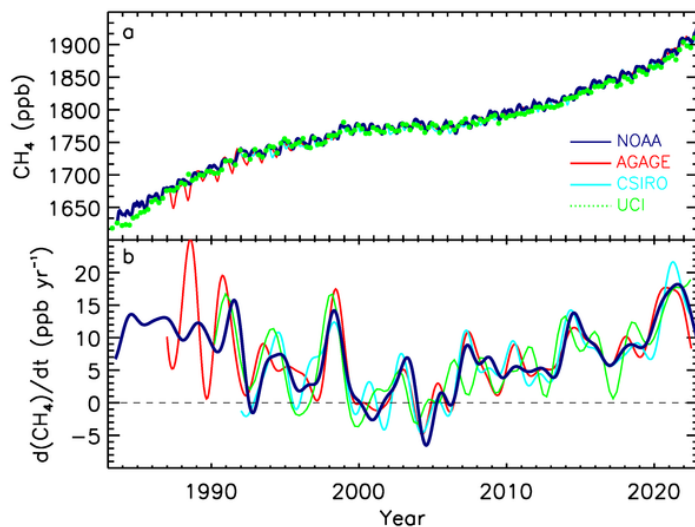
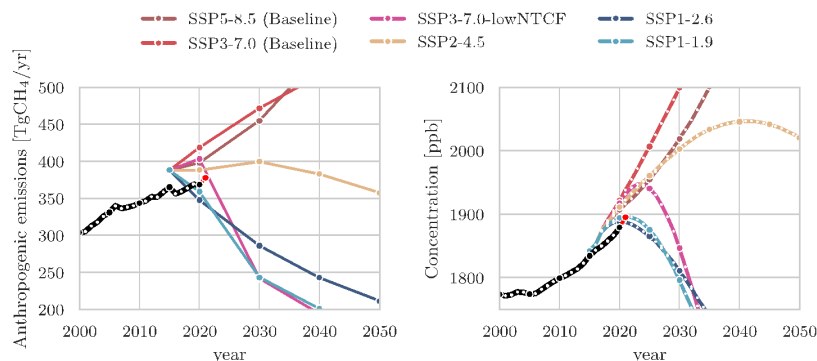


Figure 1: Globally averaged atmospheric  $\text{CH}_4$  concentrations (ppb) (a) and annual growth rates  $G_{\text{ATM}}$  ( $\text{ppb yr}^{-1}$ ) (b) between 1983 and 2022, from four measurement programs, National Oceanic and Atmospheric Administration (NOAA), Advanced Global Atmospheric Gases Experiment (AGAGE), Commonwealth Scientific and Industrial Research Organisation (CSIRO), and University of California, Irvine (UCI). Detailed descriptions of methods are given in the supplementary material of Kirschke et al. (2013).



**Figure 2:** Left: Global anthropogenic methane emissions (including biomass burning) over 2000-2050 from historical inventories (black line and grey shaded area) and future projections (colored lines) (in Tg CH<sub>4</sub> yr<sup>-1</sup>) from selected scenarios harmonized with historical emissions (CEDS) for CMIP6 activities (Gidden et al., 2019). Historical mean emissions correspond to the average of anthropogenic inventories listed in Table 1 added to the GFEDv4.1s (van der Werf et al., 2017) biomass burning historical emissions. Right: Global atmospheric methane concentrations for NOAA surface site observations (black) and projections based on SSPs (Riahi et al., 2017) with concentrations estimated using MAGICC (Meinshausen et al., 2017, 2020). Red dots show the last year available (2022 for observations).

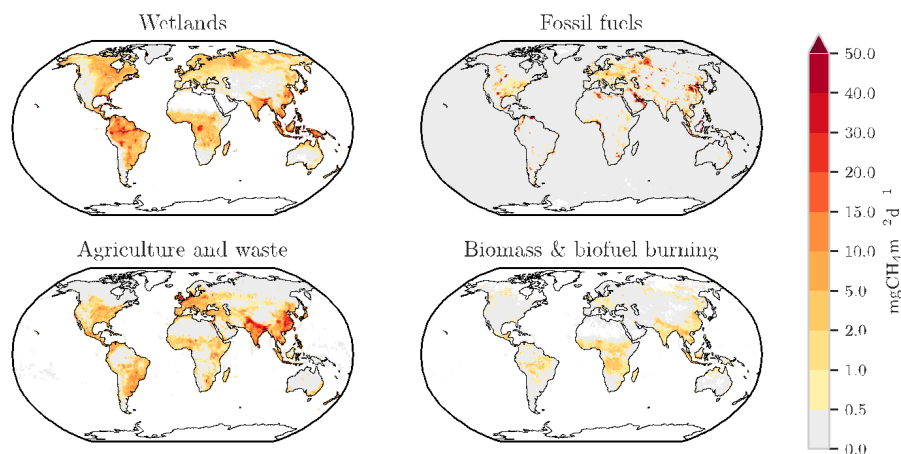


Figure 3: Methane emissions from four source categories: natural wetlands (excluding lakes, ponds, and rivers), biomass and biofuel burning, agriculture and waste, and fossil fuels for the 2010-2019 decade in  $\text{mg CH}_4 \text{ m}^{-2} \text{ day}^{-1}$ . The wetland emission map represents the mean daily emission average over the 16 biogeochemical models listed in Table 2 and over the 2010-2019 decade. Fossil fuel and Agriculture and Waste emission maps are derived from the mean estimates of gridded CEDS, EGDARv6, EDGARv7 and GAINS models. The biomass and biofuel burning map results from the mean of the biomass burning inventories listed in Table 1 added to the mean of the biofuel estimate from CEDS (O'Rourke et al., 2021), EDGARv6 (Crippa et al., 2021), EDGARv7 (Crippa et al., 2023) and GAINS (Höglund-Isaksson et al., (2020)) models.

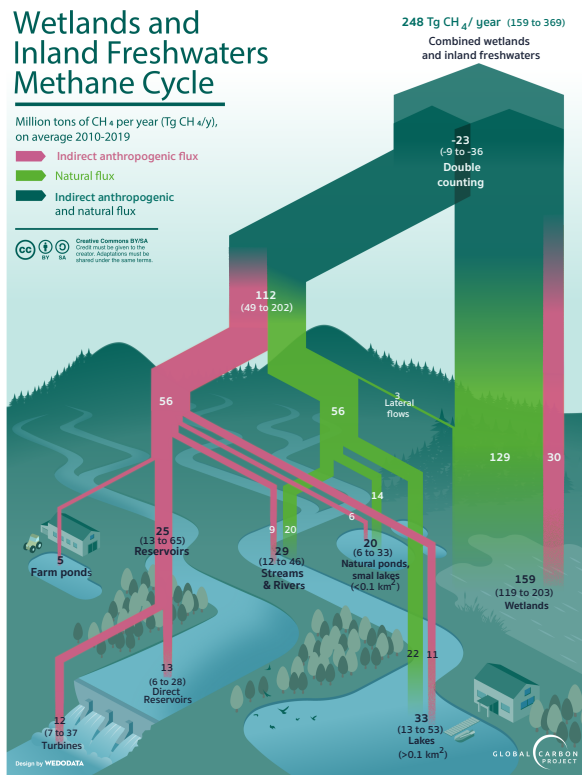


Figure 4: Estimation of wetland and inland freshwater emissions over the 2010-2019 decade in Tg CH<sub>4</sub> yr<sup>-1</sup>. The fluxes related to voluntary (such as through reservoirs or farm ponds) or involuntary (land use or eutrophication-related) perturbations of the methane cycle are shown here in pink. They are accounted for into the “natural and indirect anthropogenic” sources in the Table 3 budget and depicted as “natural and indirect anthropogenic” sources (darker green and pink hatches) in Fig. 7.

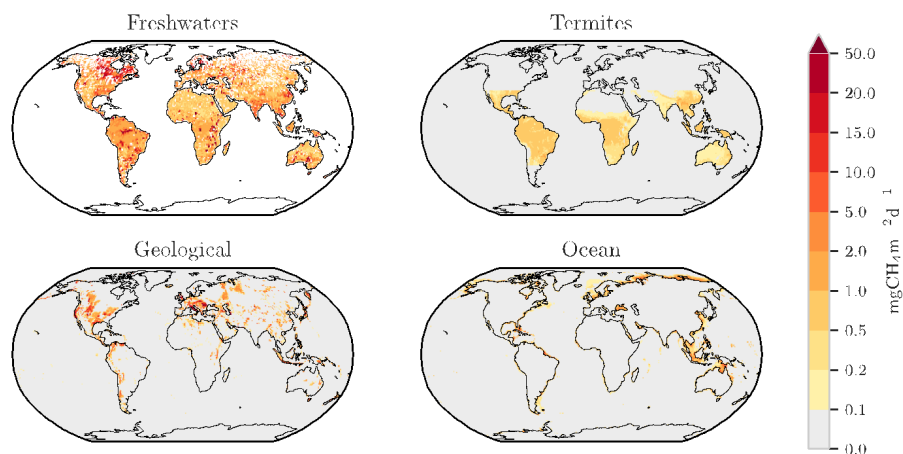


Figure 5: Methane emissions ( $\text{mg CH}_4 \text{m}^{-2} \text{day}^{-1}$ ) from four natural and indirect anthropogenic sources: inland freshwaters (includes lakes, ponds (Johnson et al., 2022.), reservoirs (Johnson et al., 2021) and stream and rivers (Rocher-Ros et al., 2023) with a global total scaled to  $89 \text{ Tg yr}^{-1}$ ), geological (Etiope et al., 2019), termites (this study) and oceans (Weber et al., 2019).

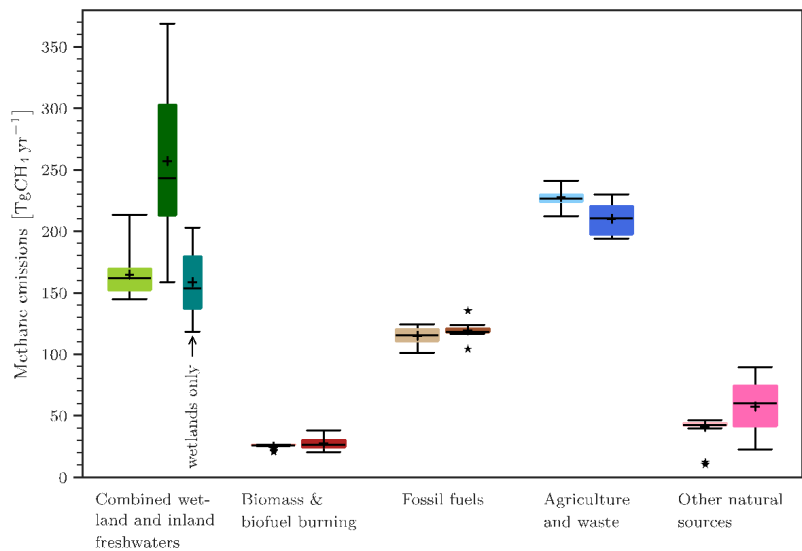
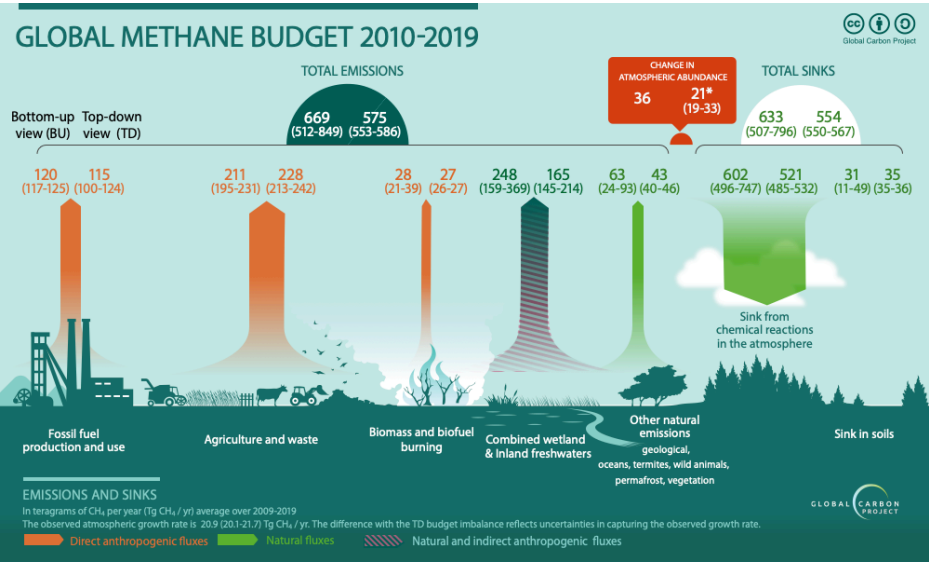


Figure 6: Methane global emissions from five broad categories (see Sect. 2.3) for the 2010-2019 decade for top-down inversion models (left light coloured boxplots) in  $\text{Tg CH}_4 \text{ yr}^{-1}$  and for bottom-up models and inventories (right dark coloured boxplots). For combined wetland and inland freshwaters three estimates are given: left = top-down estimates, middle = bottom-up estimates, right = bottom-up estimates for wetlands only. Median value, first and third quartiles are presented in the boxes. The whiskers represent the minimum and maximum values when suspected outliers are removed (see Sect. 2.2). Suspected outliers are marked with stars. Bottom-up quartiles are not available for bottom-up estimates, except for wetland emissions. Mean values are represented with “+” symbols, these are the values reported in Table 3.



27



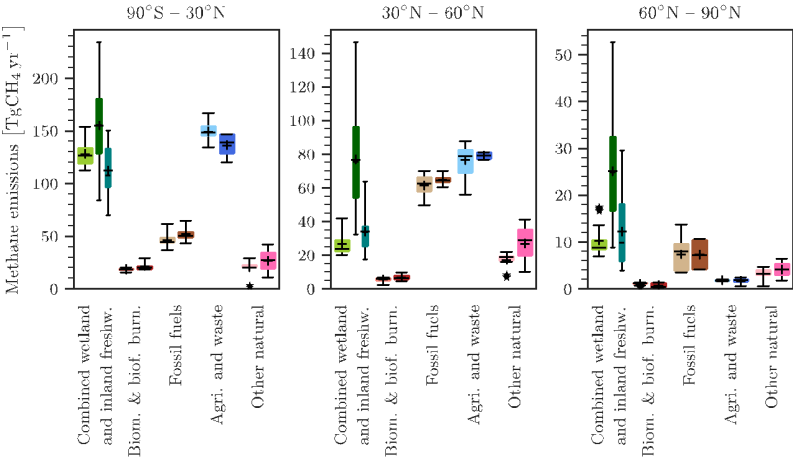
28

29

30 **Figure 7: Global Methane Budget for the 2010-2019 decade. Both bottom-up (left) and top-down (right) estimates are provided for**  
31 **each emission and sink category in Tg CH<sub>4</sub> yr<sup>-1</sup>, as well as for total emissions and total sinks. Combined wetland and inland**  
32 **freshwaters are depicted as natural and indirect anthropogenic sources (darker green and pink hatches) to recall Figure 4 (Sect.**  
33 **3.2.2 ).**

34

35



36

37 **Figure 8: Methane latitudinal emissions from five broad categories (see Sect. 2.3) for the 2010-2019 decade for top-down inversion**  
38 **models (left light coloured boxplots) in Tg CH<sub>4</sub> yr<sup>-1</sup> and for bottom-up models and inventories (right dark coloured boxplots). For**  
39 **combined wetland and inland freshwaters three estimates are given: left = top-down estimates, middle = bottom-up estimates, right**  
40 **= bottom-up estimates for wetlands only. Median value, first and third quartiles are presented in the boxes. The whiskers represent**  
41 **the minimum and maximum values when suspected outliers are removed (see Sect. 2.2). Suspected outliers are marked with stars.**  
42 **Bottom-up quartiles are not available for bottom-up estimates, except wetland emissions. Mean values are represented with “+”**  
43 **symbols, these are the values reported in Table 6.**

44

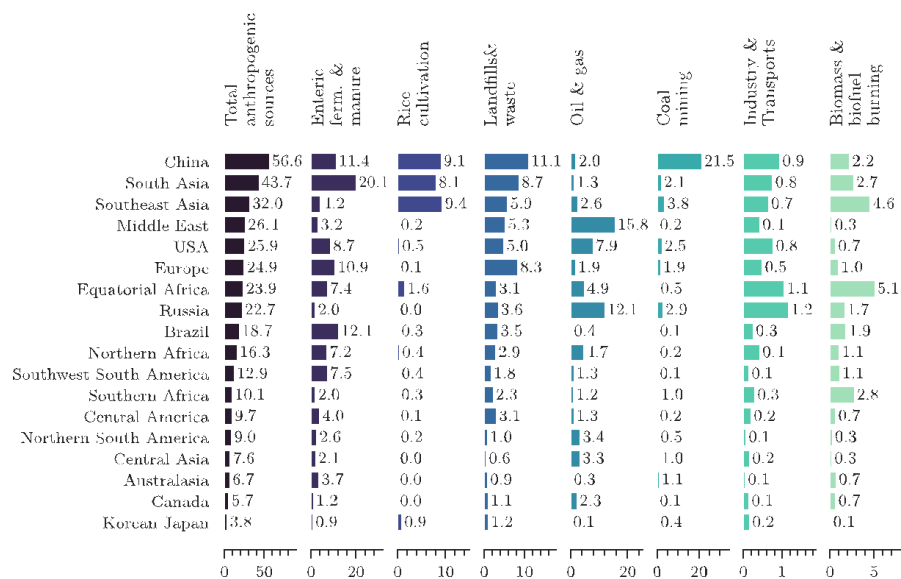


Figure 9: Regional anthropogenic emissions for the 2010-2019 decade from bottom-up estimates in Tg CH<sub>4</sub> yr<sup>-1</sup>. Regions are ranked by their total anthropogenic emissions. Note that each category has its own emission scale.

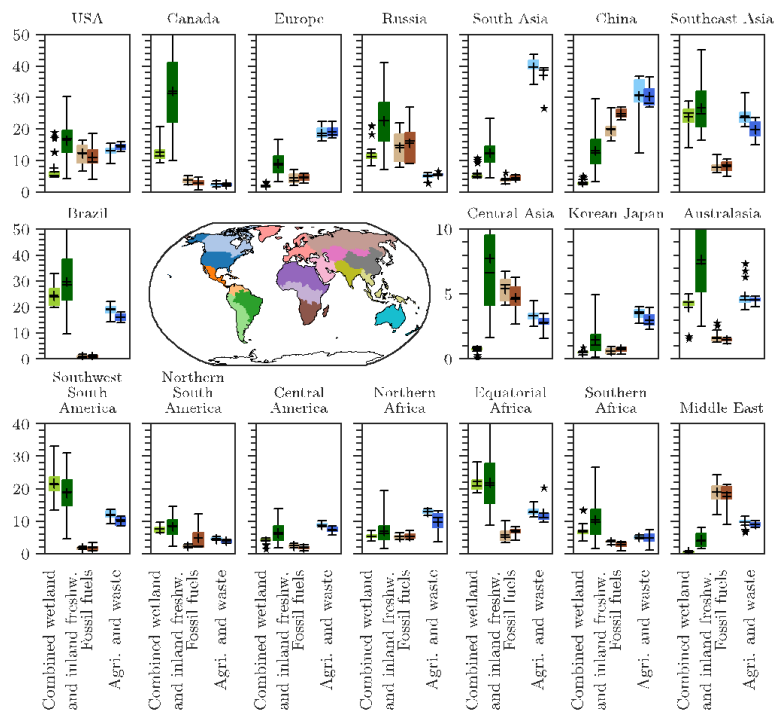


Figure 10: Regional emissions in  $\text{Tg CH}_4 \text{ yr}^{-1}$  for three broad main emissions categories for the 2010-2019 decade: Combined wetland and inland freshwaters, fossil fuel and agriculture & waste from top-down estimates (left box-plots- and bottom-up estimates (right boxplots). The inner map shows the region's distribution (see also Supplementary material, Table S1 and Fig. S3). More categories are presented in the Supplementary Material in Figure S6.

54 **Table A1.** Comparison of terminologies used in this study and previous reports for methane sources.

GCP terminology (This study)		IPCC AR6 (Canadell et al., 2021)	National GHG inventories (used by UNFCCC according to IPCC (2006) and IPCC (2019))	IPCC (2006, 2019) Source sector numbering
<i>Anthropogenic Sources</i>				
Fossil fuels	Coal Mining	Coal Mining	Fugitive emissions from Fuels / Solid fuels	1B1
	Oil and gas	Oil and gas	Fugitive emissions from Fuels / Oil and natural gas	1B2
	Transport	Transport	Transport	1A3
	Industry	Industry	Mineral, chemical, metal industry and others	2A, 2B, 2C, 2D, 2E
			Energy/fuel Combustion activities	1A except 1A3 + 1B3
Agriculture	Enteric fermentation and manure management	Enteric fermentation and manure management	Livestock	3A
	Rice cultivation	Rice cultivation	Rice cultivation	3C7
Waste	Landfills and waste	Landfills and waste	Waste	4
Biofuel and biomass burning	Biofuel burning	Biofuel burning	Biofuel burning	1A4b
	Biomass burning	Biomass burning	Biomass burning	3C1
<i>Natural and indirect sources</i>				
Wetlands	Wetlands	Wetlands	--	--
Inland freshwaters	Reservoirs	included in Inland freshwaters	Land (incl Reservoirs)	in 3B
	Lakes, ponds, and rivers	incl in Inland freshwaters	only canal, ditches and ponds for human uses	in 3B
Other natural sources	Oceans	Oceans	--	--
	Termites	Termites	--	--

.55  
.56

	Geological sources	Geological sources	--	--
--	--------------------	--------------------	----	----

57 **Table A2.** Summary of methodological changes since the previous budget (Saunois et al., 2020). No significant changes have been  
58 applied to the vegetation (Sect. 3.2.8), wild animal (Sect. 3.2.5) and terrestrial permafrost and hydrates (Sect 3.2.7) estimates, though  
59 literature has been expanded and/or updated.  
60

	Saunois et al. (2020)	This study
Regions definition (Table S1, Fig S3)	18 continental regions + ocean	same regions except the last region including only Australia and New-Zealand and called Australasia
Anthropogenic global inventories (See Table 1, Sect 3.1.1)	CEDS, EDGARv4.3.2, USEPA (2012), FAO and GAINS ECLIPSE v6	CEDS, EDGARv6 and v7, USEPA (2019), FAO, IIASA GAINS v4 Add estimate of ultra emitters from Lauvaux et al. (2022)
Biomass burning data sets	FINNV1.5, GFASv1.3, GFEDv4.1s, QFEDv2.5	FINNV2.5, GFASv1.3, GFEDv4.1s, QFEDv2.5
Estimate of wetland emissions (See Tables 2 and S3 and Section 3.2.1)	13 land surface models involved, runs with either prescribed areas or based on Hydrological scheme, single meteorological forcing	16 land surface models involved, runs with either prescribed areas or based on Hydrological scheme, two sets of meteorological forcings
Estimate of reservoirs emissions (Sect.3.2.2)	based on Deemer et al. (2016)	based on Johnson et al. (2021), Rosentreter et al. (2021) and Harrison et al. (2021)
Estimate of lakes and ponds emissions (Sect.3.2.2)	based on Bastviken et al. (2011), Wik et al. (2016b) and Tan and Zhuang (2015)	lakes > .1km <sup>2</sup> : based on Rosentreter et al. (2021), Zhuang et al. (2023) and Johnson et al. (2022) lakes and ponds < 0.1 km <sup>2</sup> : based on Rosentreter et al. (2021), and Johnson et al. (2022)
Estimates of stream and river emissions (Sect.3.2.2)	From Stanley et al. (2016)	based on Rosentreter et al. (2021) and Rocher-Ros et al. (2023)
Estimates of the anthropogenic perturbation component of inland freshwater emissions (Sect.3.2.2)	- -	based on several individual studies on the effect of eutrophication on emissions from lakes, and ponds (See text in Sect. 3.2.2)
Estimate of the double counting in the aquatic systems (Sect.3.2.2)	--	due to the accounting of small lakes and ponds (<0.1km <sup>2</sup> ) in the vegetated wetlands areas used in land surface models and to lateral transport from vegetated wetland to rivers.

Geological sources (Sect 3.2.3) - onshore and offshore	based on Etiope and Schwietzke et al. (2019)	same as in Saunio et al. (2020)
Termite emissions (Sect. 3.2.4)	GPP : Zhang et al. (2017) termite biomass: Jung et al. (2011) EF : Kirshke et al. (2013) and Fraser et al., 1986)	GPP: Wild et al. (2022) termite biomass: based on different studies depending on regions (see text) EF: Sugimoto et al. (1998) Applied a correction factor for mound from Nauer et al. (2018)
Oceanic sources (Sect 3.2.6)	modern biogenic: based on Wuebbles and Hayhoe (2002), Laruelle et al. (2013) and Rosentreter et al. (2018); geological: based on Etiope (2019)	modern biogenic: based on Rosentreter et al. (2021;2023) and Laruelle et al. (2025 ) geological: based on Etiope (2019)
Tropospheric OH oxidation (Sect 3.3.2) and stratospheric loss (Sect 3.3.3) (See Supplementary Table S4)	based on results from 11 models contributing to the Chemistry Climate Model Initiative (Morgenstern et al., 2017)	based on results from 11 models contributing to the Chemistry Climate Model Initiative 2022 (Plummer et al., 2021) and the CMIP6 simulations (Collins et al., 2017)
Tropospheric reaction with Cl	based on Hossaini et al. (2016), Wang et al. (2019b) and Gromov (2018)	based on Hossaini et al (2016), Sherwenn et al. (2016), Wang et al (2019b, 2021b) and Gromov (2018)
Soil uptake (See Table S6)	based on Tian et al. (2016)	based on VISIT, JSBACH en MeMo surface models.
Estimates through top-down approaches (See table S7 and S8 to S11)	9 inverse systems contributing, prior fluxes based on EDGARv4.2 or v4.3.2 for most inversions. Most inversion used constant OH.	7 inverse systems contributing, runs with constant and varying OH, prior fluxes based on either EDGARv6 or GAINS



62 **Table A3.** Funding supporting the production of the various components of the global methane budget in addition to the authors’  
63 supporting institutions (see also acknowledgements).  
64

Funder and grant number (where relevant)	Authors/Simulations/Observations
Director, Office of Science, Office of Biological and Environmental Research of the US Department of Energy under Contract No. DE-AC02-05CH11231 to Lawrence Berkeley National Laboratory as part of the RUBISCO Scientific Focus Area.	WJR, QZ, E3SM/ELM simulations
Funded by NASA's Interdisciplinary Research in Earth Science (IDS) Program and the NASA Terrestrial Ecology and Tropospheric Composition Programs	MSJ; lake and reservoir bottom-up methane emission data sets
Funded by Agence National de la Recherche through the project Advanced Methane Budget through Multi-constraints and Multi-data streams Modelling (AMB-M <sup>3</sup> ) - (ANR-21-CE01-0030)	AM, MS
The Environment Research and Technology Development Fund (JPMEERF21S20800) of the Environmental Restoration and Conservation Agency provided by Ministry of the Environment of Japan	YN, NISMON-CH <sub>4</sub>
Funded by the German Federal Ministry of Education and Research (BMBF) via the “PalMod” project, grant No. 01LP1921A	TK; CH <sub>4</sub> emission modelling with JSBACH and LPJ-MPI
Funded by the Swedish Research Council VR (2020-05338) and Swedish National Space Agency (209/19)	WZ; LPJ-GUESS simulations
Funded by BELSPO (project FedTwin ReCAP), EU Horizon 2020 project ESM2025 (nr. 101003536) and FRNS PDR project CH4-lake (T.0191.23)	PR; inland water, coastal and oceanic CH <sub>4</sub> emission synthesis
EU H2020 (725546 ERC METLAKE and 101015825 TRIAGE) , Swedish Research Councils VR (2022-03841) and Formas (2018-01794)	DB; inland waters - data and bottom up estimation.
Supported by the Newton Fund through the Met Office Climate Science for Service Partnership Brazil (CSSP Brazil)	NG; JULES simulations
Funded by United Nations Environment Programme, Stanford University DTIE21-EN3143	RBJ; inversions and general budget support
the Joint Fund for Regional Innovation and Development of the National Natural Science Foundation (Grant No. U22A20570); the Natural Sciences and Engineering Research Council of Canada (NSERC, #371706)	Changhui Peng/TRIPLEX-GHG
<b>Computing Resources</b>	
LSCE computing resources	Marielle Saunois, Philippe Bousquet, Joël Thanwerdas and Adrien Martinez
NASA High-End Computing (HEC) Program through the NASA Advanced Supercomputing (NAS) Division at NASA Ames Research Center	Matthew S. Johnson (MSJ)
Deutsches Klimarechenzentrum (DKRZ), Hamburg, Germany	Thomas Kleinen (TK)

ALICE High Performance Computing Facility at the University of Leicester	GOSAT retrievals
FUJITSU PRIMERGY CX2550M5 at MRI and NEC SX-Aurora TSUBASA at NIES	Yosuke Niwa (YN)
<b>Support for atmospheric observations</b>	
Australian Antarctic Division	CSIRO flask network
Australian Institute of Marine Science	CSIRO flask network
Bureau of Meteorology (Australia)	Kennaook/Cape Grim AGAGE, CSIRO flask network
Commonwealth Scientific and Industrial Research Organisation (CSIRO, Australia)	Kennaook/Cape Grim AGAGE, CSIRO flask network
Department of Climate Change, Energy, the Environment and Water (DCCEEW, Australia)	Kennaook/Cape Grim AGAGE
Meteorological Service of Canada	CSIRO flask network
NASA: grants NAG5-12669, NNX07AE89G, NNX11AF17G, NNX16AC98G and 80NSSC21K1369 to MIT with subawards to the University of Bristol (for Barbados and Mace Head) and CSIRO (for Kennaook/Cape Grim); grants NAG5-4023, NNX07AE87G, NNX07AF09G, NNX11AF15G, NNX11AF16G, NNX16AC96G, NNX16AC97G, 80NSSC21K1210 and 80NSSC21K1201 to SIO.	AGAGE calibrations and measurements at SIO, La Jolla and AGAGE station operations at Trinidad Head, Mace Head, Barbados, American Samoa, and Kennaook/Cape Grim
National Oceanic and Atmospheric Administration (NOAA, USA) contract RA133R15CN0008 to the University of Bristol	Barbados
NOAA USA	CSIRO flask network
Refrigerant Reclaim Australia	Kennaook/Cape Grim AGAGE
UK Department for Business, Energy & Industrial Strategy (BEIS) contract TRN1537/06/2018 and TRN 5488/11/2021 to the University of Bristol	Mace Head
National Oceanic and Atmospheric Administration (NOAA, USA)	Cape Matatula
Japanese Ministry of Environment	GOSAT data, Robert Parker
Japanese Aerospace Exploration Agency, National Institute for Environmental Studies	GOSAT data, Robert Parker
UKRI UK: grants NE/W004895/1, NE/R016518/1, NE/X019071/1 and MR/X033139/1	GOSAT data, Robert Parker
The Swedish Research Council VR (2022-04839), European Space Agency projects AMPAC-Net and CCI+ permafrost, European Union's Horizon 2020 Research and Innovation Programme to the Nunataryuk project (no. 773421)	Permafrost region, Gustaf Hugelius